IMPERIAL COLLEDGE OF SCIENCE, TECHNOLOGY AND MEDICINE

University of London

HIGH QUALITY MODAL TESTING METHODS

by

Mohammad Reza Ashory

A thesis submitted to the University of London
for the degree of Doctor of Philosophy

Dynamics Section
Department of Mechanical Engineering
Imperial College of Science, Technology and Medicine
London, SW7 2BX

March 1999

ABSTRACT

Modal Analysis has been a developing science in the experimental evaluation of the dynamic properties of the structures. In practice, the models produced by modal testing often have poor quality due to factors inherent in the measurement. One of the sources of a lack of precision in modal testing is the errors caused by mechanical devices such as accelerometers, suspension springs and stingers.

The aim of this thesis is to improve the current methods of modal testing for dealing with mechanical errors and to develop new ones which permit the acquisition of modal test data of high quality. To achieve this end, the work initially focuses on reviewing existing methods. The research, then, focuses on developing methods for assessing the quality of the measurement; and for cancelling the effects of mechanical devices on the measured FRFs in the cases that the quality of the measurement is not acceptable.

A new method has been developed for the correction of mass-loading effects of accelerometers on measured FRFs. It is shown that the non-driving point FRFs can be corrected if the measurement is repeated with an accelerometer with different mass. It is also shown that the driving point FRF of the response point can be obtained by the same procedure without actually having to measure it. Moreover, this method is used for assessing the quality of the measurement due to mass-loading effects of transducers in a conventional modal test. A similar method is developed for assessing the quality of measurement and for the correction of the effects of suspension springs on the measured FRFs.

The problem of the interaction between the test structure and the shaker through stinger is discussed and the practical ways to avoid the effects of the stinger on the measured FRFs has been investigated. Particular attention is given to the problem of the misalignment of the stinger and its effect on the measured FRFs. Moreover, a method for assessing the effects of the stinger on the measured FRFs is presented.

The correction method is further developed for the cases that the test structure is affected by mechanical elements in more than one DOF. Moreover, it is shown that nonlinearity of the structure or the attached elements affects the results of the correction of the measured FRFs.

Although a new trend has been developed for the initial aim of dealing with mechanical errors in modal testing, it has been shown that this new trend is applicable in other fields of modal testing such as generation of rotational FRFs. On this basis a method is developed to eliminate the need for producing the rotational excitations and measuring them.

It is also shown that the whole matrix of translational FRFs can be generated from measurements of one column using one accelerometer and one dummy mass. This procedure can eliminate the problem of residual effects of out-of-range modes. Finally, a recommended test strategy for acquisition of modal test data of high quality related to the mechanical errors is presented.

Acknowledgements

I would like to express my gratitude to my supervisor, Prof. D. J. Ewins, for his valuable advice, interest, and encouragement throughout this project. I also thank Mr. D. A. Robb for his advice and discussions.

I would like to thank my past and present colleagues of Imperial College Dynamics Section who by their enthusiasm, encouragement and their useful discussions provided insight into related fields of interest and enjoyable working environment.

I am grateful to the ministry of culture and higher education of Iran for the financial support provided for this project.

Special thanks are due to my mother, my wife and my daughter for all their love, patience and support during the course of this work, especially during the last few months. Without them this thesis would not have been completed.

Nomenclature

Basic Terms and Dimensions

x, y, z　　　　　translational DOFs (time domain)

θ_x, θ_y, θ_z　　　　rotational DOFs (time domain)

X, Y, Z　　　displacements (frequency domain)

X''　　　　　　acceleration (frequency domain)

ω, f　　　　　frequency of vibration (in rad/sec; Hz)

P, F　　　　　forces (frequency domain)

R, R'　　　　reaction forces (frequency domain)

M　　　　　　moment (frequency domain)

m, m_1, m_2, …　　mass of an object/accelerometer

k, k_1, k_2, …　　stiffness of the spring

c, c_1, c_2, …　　damping value

ρ　　　　　　mass density

A　　　　　　cross section area

I　　　　　　area moment of inertia

i, j, k, l　　points on the structure

$\varepsilon, \varepsilon_1, \varepsilon_2$　　　values of the noise error

TR　　　　　transmissiblity ratio

k_{sh}　　　　　translational stiffness of the shaker suspension

kr_{sh}　　　　rotational stiffness of the shaker suspension

m_{sh}　　　　mass of the shaker

m_{cl}　　　　mass of the shaker coil

m_{st}　　　　mass of the structure

W_{st}　　　　weight of the structure

k_{st}　　　　stiffness of the structure suspension

k_{ver}　　　　elastic cord (suspension spring) axial stiffness

k_{lat}　　　　elastic cord (suspension spring) lateral stiffness

l_o　　　　　zero-load elastic cord (suspension spring) length

l_f　　　　　elastic cord (suspension spring) length under load

E_{sp}	elastic modulus of the elastic cord
A_{sp}	cross sectional area of the elastic cord
l_s	length of the stinger
l_{max}	maximum allowable length of the stinger
d_s	diameter of the stinger
d_{min}	minimum allowable diameter of the stinger
σ_s	material endurance stress of the stinger
E_s	Young's modulus of the stinger
I_s	area moment of inertia of the stinger
G_s	shear modulus of the stinger
A_s	shear area of the stinger
f_{min}	minimum desirable measurement frequency
f_{max}	maximum desirable measurement frequency
k_{sx}	stinger's axial stiffness
m_{sxt}	total mass of the shaker coil, the force transducer and the mounting hardware
m_a	mass of the accelerometer
m_d	mass of the dummy mass
$\ddot{x}$	acceleration (time domain)
f_e	effective force (time domain)
f_{meas}	measured force (time domain)
m_{ext}	total extra mass attached to the structure
k_{ext}	total extra stiffness attached to the structure
β	coefficient of the nonlinear term in Duffing's equation
β_{ext}	coefficient of the nonlinear term of a nonlinear spring attached to the structure
G_{xy}	cross spectrum between signals x and y
G_{xx}	auto spectrum of signal x
H	estimator
j	imaginary value ($\sqrt{-1}$)
n	number of modification DOFs

n_c	number of different configurations
r	number of unknowns
s	spacing between accelerometers

Matrices and Vectors

$[\ ]$	matrix
$\{\ \}$	column vector
$\|\ \|$	determinant of a matrix
$\|\ \|$	norm of a matrix/vector
$[\ ]^T$; $\{\ \}^T$	transpose of a matrix; vector
$[I]$	identity matrix
$[\ ]^{-1}$	inverse of a matrix
$[\ ]^+$	generalised/pseudo inverse of a matrix
$[\ ]^H$	complex conjugate transpose of a matrix
$[U], [V]$	matrices of left and right singular vectors
$[\Sigma]$	rectangular matrix of singular values
σ_i	singular value i
$c_{11}, c_{12}, ...$	the elements of the inverse of a matrix

Spatial Properties

$\left[\omega_r^2\right]$	diagonal natural frequencies matrix
$\left[\omega_{or}^2\right]$	diagonal natural frequencies matrix of the modified system
$[M]$	mass matrix
$[K]$	stiffness matrix
$[C]$	damping matrix
$[\Delta M]$	mass modification matrix
$[\Delta K]$	stiffness modification matrix
ΔM_i	the mass attached to the structure at DOF i
ΔK_i	the stiffness attached to the structure at DOF i
$\{x\}$	displacement vector (time domain)
$\{\ddot{x}\}$	acceleration vector (time domain)

$\{f\}$ force vector (time domain)

Modal and Frequency Response Properties

ω_r natural frequency of rth mode (rad/sec)

ω_{or} natural frequency of rth mode of the modified system

(rad/sec)

$[\lambda_r]$ eigenvalue matrix

$[\phi]$ mass-normalised mode shape/eigenvector matrix

λ_r r^{th} eigenvalue

$\{\phi\}_r$ r^{th} mode shape/eigenvector

ϕ_{ir} i^{th} element of rth mode shape/eigenvector

$_r\mathbf{A}_{ij} = \phi_{ir}\phi_{jr}$ the modal constant for mode r and DOFs i and j

$[\alpha(\omega)]$ receptance matrix

$[D(\omega)]$ dynamic stiffness matrix

$[D(\omega)]^{md}$ dynamic stiffness matrix of the modified structure

$[A(\omega)]$ accelerance matrix

α_{ij} individual receptance element for DOFs i and j

(response at DOF i and excitation at DOF j)

A_{ij} individual accelerance element for DOFs i and j

$A_{iR,jR}$ accelerance of points i and j and in rotational DOF , here i

and j refer to the points and R refers to the rotational DOF

$\alpha_{ij}^{(l)}$ measured receptance when a mechanical element is attached

to the structure at DOF l

$A_{ij}^{(l)}$ measured accelerance when a mechanical element is attached

to the structure at DOF l

$A_{ij}^{(l,k)}$ measured accelerance when two mechanical elements are

attached to the structure at DOFs l and k

$A_{ij}^{(l,\bar{k})}$ measured accelerance when an accelerometer is attached

at DOF k and a dummy mass is attached at DOF l

α_{ij}^* measured receptance of a modified structure

(more than 2 DOFs)

A_{ij}^{*}	measured acceleration of a modified structure (more than 2 DOFs)
$A_{ij}^{(l)}$, $\overline{A}_{ij}^{(l)}$, $\overline{\overline{A}}_{ij}^{(l)}$	measured accelerances for different configurations
$^{(p)}A_{ij}^{(l)}$	measured acceleration for p^{th} configuration
α_{mm} , α_{nn} , α_{rr}	the receptances of the attached mechanical elements
α_{ii}'	the receptance of the attached mechanical element at DOF i
$^{(p)}\alpha_{ii}'$	the receptance of the attached mechanical element at DOF i for p^{th} configuration
$\left[\alpha_{ii}'\right]$	the matrix of the receptances of the attached mechanical elements for different configurations
α_{ij}^{g}	receptance of the grounded structure
$\tilde{A}_{ij}$	computed FRF using uncolibrated data
$\hat{A}_{ij}$	computed FRF of a nonlinear system
$\breve{A}_{ij}$	noisy FRF
$E_{A}(\omega)$	measured accelerance error

Abbreviations

FEM	Finite Element Method
FRF(s)	Frequency Response Function(s)
DOF(s)	Degree(s)-of-Freedom
RDOF(s)	Rotational Degree(s)-of-Freedom
FFT	Fast Fourier Transform
SVD	Singular Value Decomposition
dB	decibel
SMURF	<u>S</u>tructural <u>M</u>odifications <u>U</u>sing experimental frequency <u>R</u>esponse <u>F</u>unctions
PBC	Perturbed Boundary Condition
ARMA	Auto-Regressive Moving-Average (method/model)
UMPA	Unified Matrix Polynomial Approach (method/model)
LDV	Laser Doppler Vibrometer

Table of contents

Chapter 1. Introduction

Chapter 2. Literature survey

Chapter 3. Correction of mass-loading effects of   transducers in modal testing

Chapter 4. Correction of suspension effects in modal testing

Chapter 5. The effects of stingers on measured FRFs

Chapter 6. Correction of mechanical effects in more than one DOF

Chapter 7. The effect of nonlinearity on the correction methods of mechanical devices

Chapter 8. Generation of the whole matrix of translational FRFs from measurements on one column

Chapter 9. Generation of RDOFs by modifying of the test structure

Chapter 10. Conclusions and suggestion for future work

Appendices

Chapter 1

Introduction

1.1 Background

The understanding of the physical nature of vibration phenomena has always been important for researchers and engineers in industry, even more so today as structures are becoming lighter and more flexible due to increased demands for efficiency, speed, safety and comfort. When any structure vibrates, it makes major problems and operating limitations ranging from discomfort (including noise), malfunction, reduced performance and early breakdown or structural failure. Two approaches may be considered to resolve the vibration problem: first, prevention, through proper design, and second, cure, by modification of structure or a vibration control design. In any case, a thorough understanding of vibration of the structure is essential. Hence, accurate mathematical models are required to describe the vibration characteristics of the structure.

For simple structures, such as beams and plates, good analytical predictions using closed form solutions can be easily found in various reference books and tables (Such as Blevins **[1]**) or lumped parameter systems can be used to model the dynamic behaviour of the structure. However, for more complex structures more powerful tools are needed. Today, two separate tools are used to model the dynamic behaviour of the structures, namely analytical tools and experimental ones. The most widely-used analytical tool is the Finite Element (FE) method, while the experimental counterparts are largely based on modal testing and analysis. Due to different built-in limitations, assumptions and choices, each approach has its own advantages and disadvantages.

1.2 Finite Element Method (FEM)

The main assumption in Finite Element Method (FEM) is that a continuous structure can be discretised by describing it as an assembly of finite (discrete) elements, each with a number of boundary points which are commonly referred to as nodes. For structural dynamic analysis, element mass, stiffness and damping matrices are generated first and then assembled in to global system matrices. Dynamic analysis of the produced model gives the modal properties; the natural frequencies and corresponding eigenvectors. The modal solution can subsequently be used to calculate forced vibration response levels for the structure under study.

Element system matrices have been developed for many simple structures, such as beams, plates, shells and bricks. Most general-purpose FE programs have a wide range of choice of element types, and the user must select the appropriate elements for the structure under investigation and its particular application. Further theoretical background and practical implementation of the FE method are given in various text books, such as those by Cook **[2]**, Bathe **[3]** and Zienkiewicz **[4]**.

The FE method is extensively used in industry as it can produce a good representation of a true structure. However, for complicated structures, due to limitations in the method, an FE model can lead to errors. The sources of errors in Finite Element models are :

1. inaccuracy in estimation of the physical properties of the structure;

2. poor quality of mesh generation and selection of individual shape functions;

3. poor approximation of boundary conditions;

4. omission or poor modelling of damping properties of the system;

5. computational errors which are mainly due to rounding off.

The result of a Finite Element analysis is mainly dependent on the judgement and experience of the operator and the package used.

1.3 Modal testing method

The experimental approach to modelling the dynamic behaviour of structures (modal testing) relies mostly on extracting the vibration characteristics of a structure from measurements. The procedure consists of three steps :

1. taking the measurements .

2. analysing the measured data .

3. constructing the model by combining the results of analysing the data.

Vibration measurements are taken directly from a physical structure, without any assumptions about the structure, and that is the reason that modal testing models are considered to be more reliable than Finite Element models. However, due to limitations and errors in the measurement process, the model created from the measured data may not represent the real behaviour of the structure as actually as desired.

In general, limitations and errors of these three stages of modal testing are :

- random errors due to noise.

- systematic errors due to attachment of the structure to the mechanical devices like springs, transducers and stingers.

- non-linear behaviour of the structure or attached mechanical devices

- systematic errors due to signal processing of the measured data.

- poor modal analysis of experimental data.

- limited number of measured degrees of freedom.

- not all modes being excited due to excitation at a node.

- difficulty in measuring rotational degrees of freedom.

The theoretical background of modal testing and practical aspects of vibration measurement techniques are discussed by Ewins [5].

1.4 Applications of modal test models

It is generally believed that more confidence can be placed in experimental data as measurements are taken on the true structure. Therefore, the mathematical models which have been created as a result of modal testing can be used in various ways to avoid or to cure the problems encountered in structural dynamics. In this section we shall consider the applications of modal testing methods for improving the structural dynamics.

1.4.1 Updating of the analytical models

One of the applications of the result of a modal test is the updating of an analytical model (usually a model derived using finite element method). Model updating can be defined as adjustment of an existing analytical model which represents the structure under study, using experimental data, so that it more accurately reflects the dynamic behaviour of that structure. Model updating can be divided into three steps :

1. comparison and correlation of two sets of data;

2. locating the errors;

3. correcting the errors.

Correlation can be defined as the initial step to assess the quality of the analytical model. If the difference between analytical and experimental data is within some preset tolerances, the analytical model can be judged to be accurate and no updating is necessary.

Most difficulties are encountered in the second step. The difficulties in locating the errors in a theoretical model are mostly due to measurement process and can be summarised as :

1. insufficient experimental modes;

2. insufficient experimental coordinates;

3. size and mesh incompatibility of the experimental and FE models;

4. experimental random and systematic errors.

5. absence of damping in the FE model

In spite of extensive research over the last two decades, model updating is still far from mature and no reliable and general applicable procedures have been formulated so far.

1.4.2 Structural dynamic modification

Structural Dynamic Modification can be defined as the study of changes (in natural frequencies and mode shapes) of measured dynamic properties of the test structure due to specified mass or stiffness (or damping) modifications introduced to the structure. In principle, the modification process is a form of optimisation of the structure to bring the dynamic properties of the structures to some desired condition. This method saves large amounts of redesign time as it reduces the cycle time in the test, analysis, redesign, shop drawings, install redesign, and retest cycle.

In practice, if a mass is added at a point on a structure, it is inevitable that this will change the elements in the mass matrix which relate to the *x, y* and *z* displacement in the translational directions and θ_x, θ_y and θ_z in rotational directions at the point of interest. This means that it is practically impossible to consider changing elements individually, and also it is necessary to include rotational coordinates in the modal model. Similar comments apply when a stiffener, such as a beam or truss, will influence the structure in several directions simultaneously, including rotational ones. However, translational accelerometers result in mode shape vectors that are deficient in rotational degrees of freedom. This means that any modification methodology applied to the experimental modal space model is deficient in rotational degrees of freedom. So the method has problems dealing with real-world modifications such as addition of plates, beams, rotors, or other structural elements with bending resistance.

Moreover, there is a need for sufficient modal vector information to carry out real-world structural modification. This demands that more data be taken, but the number of data points is limited by the time available from the highly-trained modal staff. Generally, most modal tests are limited to 200-400 *x-y-z* degrees of freedom. This is

usually too few for the structural modification to be implemented without excessive retesting.

Sometimes it is desired to construct a mathematical model of a complete structural assembly formed by the assembly of several individual substructures. There are a number of methods for assembling such a model which are extensions of modification methods and called structural assembly methods. The essential difference is that here the modifications are themselves dynamic systems, rather than simple mass or stiffness elements. It is possible to combine subsystem or component models derived from different sources or analyses for example from a mixture of analytical and experimental studies. Again the same problems encountered with modification methods also arise here.

There are other quantitative applications of the modal test models which demand a high degree of both accuracy and completeness of the test data (enough points and enough DOFs on the test structure). These applications are :

- response predictions for the test structure if it is subjected to other excitations;

- force determination, from measured responses;

- damage detection.

1.5 Sources of a lack of precision in modal testing

Laboratory experiments and practical measurements serve several purposes, some of which do not demand high accuracy. Some experiments are exploratory in the sense of looking for the existence and direction of some effect before trying to establish its magnitude; others are chiefly instructional, to demonstrate theoretical principles. Some industrial measurements are needed only to control and repeat a process in accordance with previously established values. Errors in such cases may be harmless. However, engineering applications of some experiments demand test data of high quality. In these cases, large errors may arise if test data with poor quality are used. In recent years there has been a strong demand for modal testing with high quality

suitable for advanced applications such as structural modification and model updating.

In the last section, we have explained in general terms how the mathematical models which have been created as a result of modal tests can be used in various ways to apply in vibration-related problems encountered in theory and practice and how these applications are hindered from a lack of precision in modal testing. In this section the problem of the sources of the lack of precision in modal testing will be studied more systematically. In the following paragraphs attention is drawn to the reasons why the experimental modal test data can depart from the true values it purports to measure.

The sources of a lack of precision in modal testing procedure can be categorised in three groups : (*i*) experimental data acquisition errors (*ii*) signal processing errors and (*iii*) modal analysis errors (Figure 1-1), each of them has been categorised itself in below :

```
┌──────────────────┐      ┌──────────────────┐      ┌──────────────────┐
│ Experimental Data│─────▶│ Signal Processing│─────▶│  Modal analysis  │
│   Acquisition    │      │                  │      │                  │
└──────────────────┘      └──────────────────┘      └──────────────────┘

            Experimental  Modal  Analysis
```
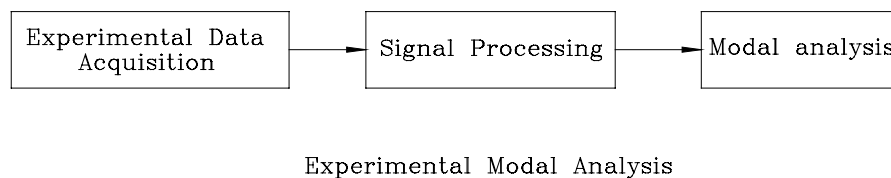
Figure 1-1. Three stages of the modal testing

(*i*) Experimental data acquisition errors :

    a) **Quality :**

        1) Mechanical errors :

- Mass loading effect of transducers

- Shaker-structure interaction

- Supporting of the structure

2) Measurement noise

3) Nonlinearity

b) **Quantity :**

- Measuring enough points on the structure

- Measuring enough Degrees of Freedom (i.e.Rotational DOFs)

(*ii*) signal processing errors :

- Leakage

- Aliasing

- Effect of window functions

- Effect of Discrete Fourier Transform

- Effect of averaging

(*iii)* modal analysis errors :

- Circle-Fit Modal Analysis

- Line-Fit Modal Analysis

- Global Modal Analysis

The main concern of this research is the first category of the sources of a lack of precision, namely experimental data acquisition errors and especially mechanical errors which demand particular attention in order to provide input data of high-quality which are required for the next stages.

1.6 Nature of the errors

In general, the nature of the experimental errors are different. In most cases, we have a situation under control with repeatable results. When we cannot repeat a result we must suspect that part of the system is not under control and some type of errors contaminate test results. Sometimes natural variation between individuals and fluctuating natural conditions demand a statistical approach. These types of the error

are called random errors and can be treated statistically. In these cases, repeatability is a strong weapon to reveal the errors. However, statistical methods can not reveal systematic errors. In one sense systematic error is a true observation not of the basic phenomenon but of the system phenomenon plus instrumentation. References to systematic errors are relatively brief and although they are very important, they cannot be easily treated

The nature of the errors introduced in the first category (experimental data acquisition errors) is completely different. The nature of the measurement noise is random. On the other hand, mechanical errors typically are systematic and cannot be treated statistically. Nonlinearty arises from the assumption of linear behaviour of the structures while most engineering structures exhibit some degree of deviation from linear behaviour. On the other hand, the difficulty in measuring enough points and enough degrees of freedom, or incompleteness of test data, lies in the problem of instrumentation and know-how of criteria which decide what to measure

1.7 Current approach to deal with mechanical errors in modal testing

The current approach used to resolve the problems which the mechanical errors cause is basically "*avoidance*" through proper design of the test equipment. By "*avoidance*" we mean choosing a strategy in the preparation of the test structure in which the probable errors become minimum. Some of these methods are given in below:

In the free-free condition the test structure is freely-supported in space and is not attached at any of its coordinates. In practice it is not possible to provide a truly free-free support but it is feasible to approximate to this condition by supporting the test structure on very soft springs such as light elastic cords.

In the grounded condition the selected points of the structure are fixed . However, it is very difficult to implement the grounded condition in the practical case. It is not possible to provide a base or foundation which is sufficiently rigid to provide truly grounded condition. Moreover, the coordinates involved for grounding will often

include rotations and these are still difficult to measure. As a result, test structures are better to be tested in free-free condition.

In shaker testing, it is necessary to connect the driving platform of the shaker to the structure. There is a stipulation that the axial force should be the only excitation of the structure. However, the excited structure responds not only in the axial direction but also in the other directions including rotational directions. To prevent the excitation of structure in other directions, the shaker attached to the structure through a slim rod which is called a stinger or a pushrod. A stinger is stiff in the axial direction and flexible in the other directions.

The input force excitation is partly spent on accelerating of the force transducer mass and also the accelerometer mass. This causes mass-loading effects of transducers. The current approach to resolve this problem is to use small accelerometers or force transducers and to employ mass-cancellation correction.

These examples of the current strategies in dealing with the mechanical errors in modal testing show that there is no general method to correct the effects of these errors on measured FRFs but it is preferred to minimise them by proper design of the test set up.

1.8 What is still not available

Although a lot of difficulties encountered during applications of modal testing have been reported from the *"experimental data acquisition"* stage, a logical strategy to deal with this problem is still unavailable. Development of a smoothing technique to reduce the effect of the mechanical errors on the measured FRFs and a method which is able to indicate the accuracy of the measured FRF are both required.

What is still not available and is needed for improvement of modal testing procedure can be summarised as :

1. an extensive method for correction of mass-loading effects of transducers, especially for transfer FRFs;

2. dealing with the effects of stingers on the test structure;

3. investigation and correction of the effects of supporting the test structure;

4. obtaining rotational degrees of freedom;

5. dealing with nonlinear behaviour of the structures in routine tests;

6. dealing with noise in the test procedure;

7. assessment of the quality of the measured FRFs.

Here are several areas of concern, all of which combine to make conventional modal testing methods of limited quality.

1.9   New approach to deal with mechanical errors in modal testing

In section 1.7 it was explained that the current approach to deal with mechanical errors in modal testing is "*avoidance*" by using proper equipment such as soft suspensions, flexible stingers and small accelerometers to minimise the errors. However, the effect of these errors on measured FRFs cannot be removed completely due to the fact that the structure cannot be tested without interaction with other structures such as accelerometers, springs and stingers. Moreover, there is no reference to data on the effects of mechanical devices on measured FRFs and means to assess the quality of measurement. This situation arises from the contradiction which is encountered when trying to find the optimum equipment and procedure for measurement. This contradiction is "the information about the dynamic behaviour of the test structure is required to choose the optimum equipment for the test while the purpose of modal testing itself is to find this information". Consequently, the approximate methods for selection of appropriate stingers, accelerometers and suspensions are not very effective in practice.

Another approach to dealing with the problem of experimental data acquisition errors is computing the exact values of the FRFs by systematically changing the physical source of the errors. We explain this approach by a simple example : suppose that the mass of structure X needs to be measured (Figure 1-2) and the process of measurement is in such a way that cylinder C can not be detached from structure X.
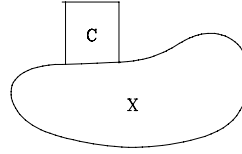
Figure 1-2. Cancellation of the effect of an extra mass on the weight measurement

The total mass can be computed as :

$$m_t = m_X + m_C \qquad\qquad\qquad \textbf{(1-1)}$$

or :

$$m_t = m_X + \rho A l \qquad\qquad\qquad \textbf{(1-2)}$$

where m_t is the total mass, m_X is the mass of structure X , m_C is the mass of the cylinder, ρ is the mass density of the cylinder, A is the cross section area of the cylinder and l is the length of the cylinder.

The total mass can be measured with two different cylinders with different lengths (l_1 and l_2). For two different lengths of cylinder C we have :

$$\begin{cases} m_{t1} = m_X + \rho A l_1 \\ m_{t2} = m_X + \rho A l_2 \end{cases} \qquad\qquad \textbf{(1-3)}$$

where m_{t1} and m_{t2} are total masses corresponding to l_1 and l_2 respectively. From which m_X can be computed :

$$m_X = m_{t1} - \frac{m_{t2} - m_{t1}}{l_2 - l_1}.l_1 \qquad\qquad \textbf{(1-4)}$$

By using this approach without physically moving the cylinder $C,$ the exact mass of structure X could be obtained. Moreover, the mass of the cylinder can be found from equation (1-1).

This simple example can be used to deal with mechanical errors in modal testing. This is the main idea to deal with mechanical errors in this thesis which will be developed in the following next chapters.

1.10 Scope and structure of thesis

This work is an attempt :

* to carry out a literature survey of previous work, on the subject of the quality of measurement related to experimental data acquisition errors (see section 5.1), in order to review critically the existing methods of modal testing to deal with these kind of errors ;

* to improve the current methods of modal testing for dealing with mechanical errors and to develop new ones which permit the acquisition of modal test data of high quality ;

* to devise methods to assess the quality of the measured data related to mechanical errors in a modal test; and

* to propose a test strategy based on the experience gained in the previous stages.

Although a new trend was developed using the idea suggested above in section 1-9 to deal with mechanical errors in modal testing, further investigation showed that this new trend is applicable in other fields of modal testing such as the generation of rotational FRFs. Chapter 2 of this thesis contains an extensive literature review of previous work in a consistent format and notation. Chapter 3 presents a method for the assessment of the quality and the correction of the mass-loading effects of transducers. Chapter 4 investigates the application of the correction method for suspension effects. Chapter 5 focuses on the practical ways to avoid the effects of stingers on the measured FRFs. In chapter 6 a general solution for the correction of the effects of the mechanical devices on the measured FRFs is suggested. Chapter 7 considers the effect of the nonlinearity on the correction methods of the mechanical devices. In chapter 8 a method is developed to generate the whole matrix of translational FRFs using one accelerometer and one dummy mass. The application of the results of chapters 6 and 7 is in chapter 9 where a method is presented for the generation of the rotational FRFs by modifying the test structure. Finally, a

recommended test strategy is proposed and the main conclusions of this research are presented in chapter 10. Figure 1-3 shows the road map of the thesis.
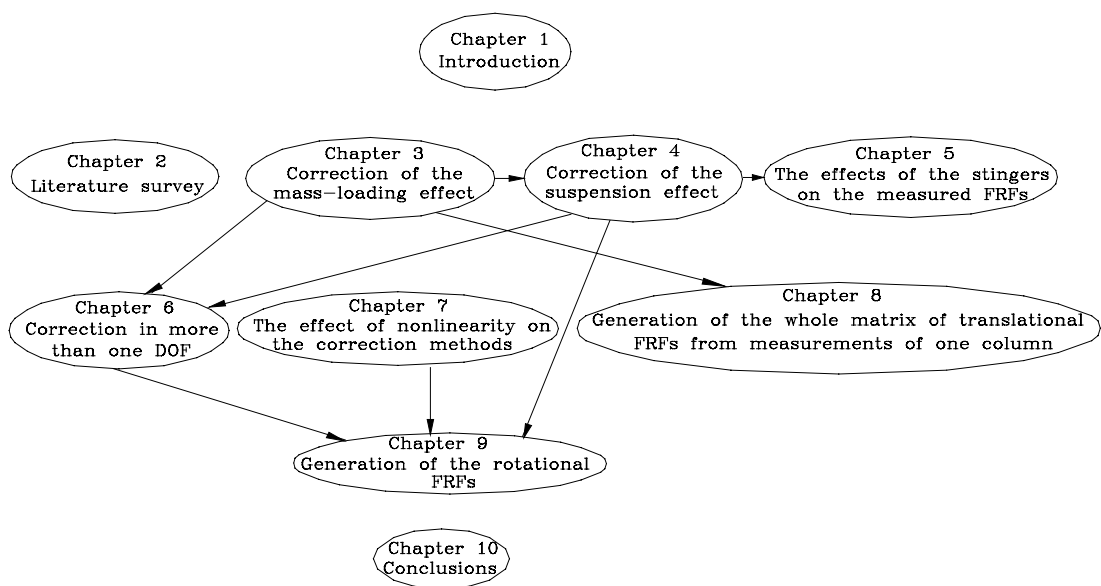
Figure 1-3. Road map of the thesis

Chapter 2

Literature Survey

2.1 Introduction

Modal testing has become an increasingly indispensable tool in the design and development of cost-competitive, safe and reliable engineering structures and components. In recent years, a major effort has been made to correlate and combine modal testing with analytical methods in the area of structural dynamics modelling. Since modal testing deals with the real structure directly, the models produced by modal testing are invariably used to identify analytical modelling problems and consequently to update analytical models.

In practice, the models produced by modal testing often have poor quality due to factors inherent in the measurement and identification processes. This lack of precision detracts from the confidence and reliability of the experimental results. However, the expanding interest in, and importance of, modal testing means that it is now opportune to take a strategic initiative to improve the quality of experimental methods.

Given the extensive list of publications in the area of the quality of measurements related to experimental data acquisition errors (see section 1.5) in modal testing, the aim of this chapter is to review critically the existing methods and to present the latest developments in a consistent and unified notation.

2.2 Quality of measurement

The SAMM survey, which was initiated some years ago to test for consistency in modal testing practice, revealed an unacceptably wide range of results measured on a single structure, [6]. The results from that exercise were very illuminating from a quality assurance point of view, as was the outcome of the more recent DYNAS survey for consistency in application of the FEM to dynamic analysis, [7]. The results from such

surveys imply that it is imperative that a quality assurance initiative be undertaken to improve the general competence of practitioners.

In 1990 Harwood [8] presented the aims and philosophy of the DTA (Dynamic Testing Agency) and the importance of the use of reliable experimental data in structural dynamics. The fundamental aim of the DTA is to establish an organisation which would maintain independent quality assurance standards in the field of modal testing.

Usually, in modal testing, errors are introduced by contaminating the FRFs with random noise but, in practice, the characteristics of measurement errors are not random. Jung and Ewins [9] categorised the systematic errors involved in modal testing as :

1. measurement errors

1.1 nonlinearity of structure

1.2 mass loading effect of transducers

1.3 useful frequency range of transducer

1.4 transverse sensitivity

1.5 mounting effect

    1.6 shaker/structure interaction

2. signal processing errors

    2.1 leakage

    2.2 effect of window functions

    2.3 effect of averaging

3. modal analysis errors

    3.1 circle fit modal analysis

    3.2 line fit modal analysis

Marudachalam and Wicks [10] studied sources of systematic errors in modal testing from a qualitative perspective. A simple system, a free-free beam, was chosen as the structure to be measured. Using the FE model as a reference, attempts were made to

study the systematic errors which arise in deriving an experimental modal model. The effect of accelerometer mass, shaker-structure interaction, the parameter extraction process resolution, influence of rigid body modes and the effects of higher modes were investigated. It was shown that the modal testing techniques are very sensitive to even small changes in the system, such as accelerometer mass and shaker-structure interaction that are usually assumed to have a negligible influence on a structure's dynamic behaviour.

Mitchell and Randolph [11] discussed the current thinking and trends in the improvement of experimental methods to be used in updating of numerical models of structural systems and in the building of experimentally-based models for use in experimental structural modification efforts. In their opinion, modal test methods are affected by :

1. **Quality** of the FRFs

2. **Quantity** of the FRFs

3. **Unobtainable** modal parameters

'Quality of the FRFs' refers to the effects of the measurement errors on the measured FRFs. The methods based on experimental models, need quality in the FRF measurement; otherwise, the output of the computations based on these methods will not be reliable. Noise is the main problem which affects the quality of the FRFs.

'Quantity of the FRFs' refers to the measurement of enough points on the structure and enough DOFs at the point of measurement. Most modal tests are limited to 200-450 *x-y-z* DOFs. This is usually too few for a structural modification to be implemented without excessive retesting. Therefore, building modal models from experimental data has been hampered by a lack of test data points [12], [13], [14]. More important than the number of points is the measurement of the rotational DOFs and producing rotational FRFs. Unfortunately, there are neither reliable rotational transducers available nor practical means of applying and measuring moment excitations.

The 'unobtainable modal parameters' refers to structures with high modal density (too many modes in a specific range of frequency) and/or high damping. In some cases, the FRFs are relatively flat because the damping brings the resonance amplitudes down and the anti-resonance amplitudes up. For years the modal analysis community has attempted to develop methods that would allow experimentally-based mathematical modelling of structures with high modal density and high damping but without much success.

On a more philosophical note, the expectations from a high quality modal test have not been formulated so far. The maximum allowable changes in the measured FRFs due to the effects of the measurement errors and their relation to measurement accuracy need to be defined further.

2.3 The mechanical devices errors

2.3.1 Shaker-structure interaction

When using a shaker to conduct a modal test, the dynamic characteristics of the shaker become combined with those of the test structure. In general, when a structure under test undergoes high levels of rotational response at the point where the shaker is attached, the shaker becomes an active portion of the test structure and forces (or moments) other than the intended axial force component may also be included and act on the structure. These unwanted forces (or moments) have multiple input effects and may bias test results, [15]. It is common practice to install a long slender element between the test structure and the shaker to minimise such undesired excitation components. This is called a stinger, pushrod or drive rod. A stinger must be axially stiff, buckling resistant, and very flexible in other DOFs than the axial direction. The low flexural stiffness is used to isolate the structure from the rotary inertia of the shaker system.

The selection of stingers are generally made by trial-and-error, by chance or by experience. Ewins [5] recommended by experience that the size of the slender portion of a stinger is 5~10 mm in length and 1 mm in diameter.

Mitchell and Elliot [16], [17] developed a systematic but approximate method for the selection of the stinger dimensions. Figure 2-1 shows the model that they used for the selection of stingers.

a) Shaker–stinger–structure system   *b) Model*
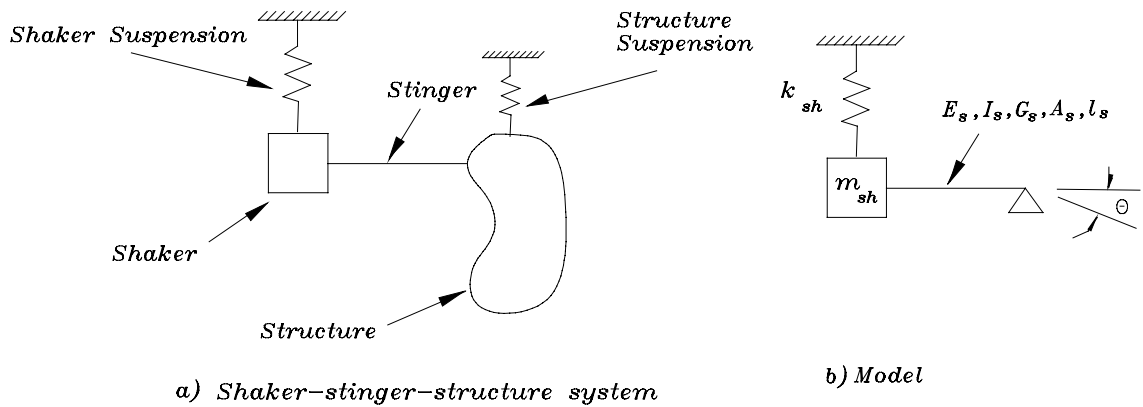
Figure 2-1. The model used by Mitchell and Elliot

They defined the transmissibility ratio as the ratio of the moment imposed to the structure when a stinger is used to the moment imposed on the structure when the shaker is rigidly connected to the structure. The resulting equation is :

$$TR = \frac{1}{1 + \gamma(1 - \beta^2)}$$ (2-1)

where β is the frequency ratio and is defined as :

$$\beta^2 = (\frac{\omega}{\omega_r})^2 \; ;$$ (2-2)

$$\omega_r^2 = \frac{k_{sh}}{m_{sh}}$$

γ is the stiffness ratio and is defined as :

$$\gamma = \frac{k_{sh}}{k_B} \quad ;$$

$$k_B = \frac{1}{(\frac{l_s^{\,3}}{3E_s I_s} + \frac{1}{G_s A_s})}$$

(2-3)

Then, the values for β and γ are chosen in such a way that the transmissibility ratio, defined in equation (2-1), be minimised.

Two guidelines for the selection of the stinger and the shaker support stiffness were suggested in [16]. It was shown that for heavy structures, for 5 percent or less of the maximum transmissibility, the conditions are :

$\beta \leq 0.5$ and $\gamma \geq 25$

where β is calculated using the highest measurable frequency in the modal test.

For light structures and for a maximum transmissibility of 5 percent, the conditions are :

$\beta \geq 2.25$ and $\gamma \geq 25$

where β is calculated using the lowest measurable frequency in the modal test. Although it was a promising analysis, many parameters are not considered in this model of the stinger.

Hieber [18] made a more detailed study of the design of stingers and gave interesting recommendations. He considered the rotary inertia of the shaker and the rotational stiffness of the shaker suspension in his model (Figure 2-2) and showed that the shaker-stinger system causes three notches and peaks in the measured FRFs of the test specimen. He recommended the following steps to design the appropriate stinger:

- find the <u>minimum allowable diameter</u> of the stinger based on the maximum shaker force and the appropriate material endurance limit;

- find the <u>maximum allowable length</u> of the stinger to prevent buckling based on the minimum diameter and the maximum force;

- find the <u>lateral stiffness and bending stiffness</u> of the stinger

- consider the <u>sensitivity of the force transducer</u> to lateral forces and moments by choosing the maximum possible length of the stinger;

- find the <u>coupled frequency of the shaker-stinger assembly,</u> using the characteristics of the shaker and the bending stiffness of the stinger. On this basis find the minimum measurable frequency;

- find the <u>first bending resonance</u> and <u>the axial resonance of the stinger-armature/actuator system</u>. The maximum measurable frequency should be below these resonance frequencies.

The essential step in this design procedure is choosing the appropriate length of the stinger. The designer should make a compromise between the minimum and maximum measurable frequencies and the length of the stinger.
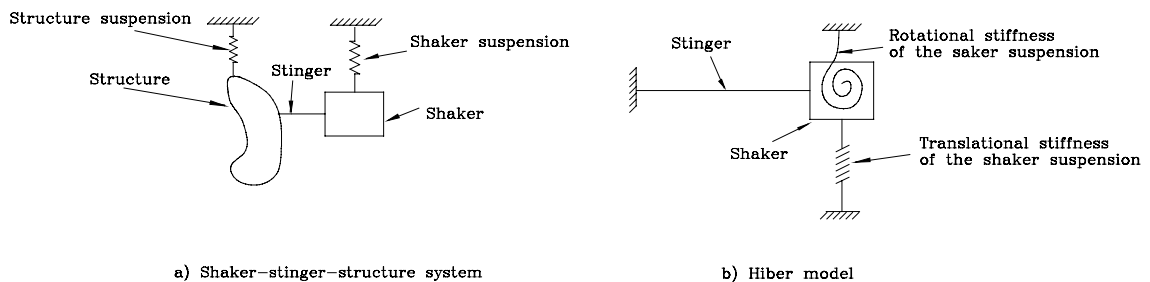
Figure 2-2. The model used by Hiber

Mitchell and Elliot [16], [17] and Hieber [18] did not account for the dynamic characteristics of the structure and assumed that the structure-side condition of the stinger is simply pinned or clamped (Figures 2-1 and 2-2). Jyh-Chiang Lee and Yuan-Fang Chou [19], [20] used a substructure synthesis algorithm to predict the effects of

stingers on the FRF measurements, treating both the excitation system and the test structure as substructures.

They showed that a properly-designed stinger can have a small effect on measured FRFs. Based on this analysis, they suggested to compute the error using the FEM results of the structure and the excitation system. Although this analysis gives a complete formulation of the problem but their suggestion to rely on FEM results is not practical for engineering cases.

Recently, McConnell and Zander [21] used a different point of view to attack the problem of the effect of the stinger bending stiffness on the measured FRFs. The principles of substructuring were used to determine the measured FRFs with respect to exact driving point and transfer FRFs. The governing equation is :

$$A_{11}^{(2)} = A_{11} - \frac{A_{12}A_{21}}{A_{22} + A_{ss}} \tag{2-4}$$

in which 1 refers to a DOF on the structure and 2 refers to the rotational DOF of the attachment of the stinger. A_{ss} is the stinger rotational accelerance. What we want to measure is A_{11}, but what we get is a combination of A_{11} and other FRFs. Thus, equation (2-4) shows how the measured driving point accelerance is influenced by the connecting point accelerances, A_{11}, A_{12}, A_{21}, A_{22}, and the stinger angular accelerance, A_{ss}. They defined corresponding measured accelerance error, $E_A(\omega)$,as :

$$E_A(\omega) = 100 \times \left| \frac{A_{11}(\omega) - A^{(2)}{}_{11}(\omega)}{A_{11}(\omega)} \right| \tag{2-5}$$

A detailed study was made to investigate the influence of the rotational stiffness of the stinger on two elementary structures, one a cantilever beam and the other a simply-supported beam. It was found that the fundamental natural frequency measurement had the largest errors. A surprising result was obtained when the stinger's driving point accelerance had a sharp notch between stinger resonances for the longest and most compliant stingers. For this case, a single peak became two peaks in the measured FRF

where only one should exist. Hence a flexible stinger may be the cause of considerable misinformation. However, they did not present a procedure to design stingers based on this analysis.

Anderson [22] considered techniques for avoiding the effects of shaker-stinger interaction in modal tests on small structures. He concluded that mounting a force transducer or impedance head on the shaker armature instead of on the structure can overcome problems to do with physically loading the structure. Based on his experience, he suggested to apply soft polyurethane foam to the rod to damp simply the resonant behaviour of the stinger.

Brillhart, Hunt and Pierre [23] discussed the material of the stinger. Historically, metal stingers have been used to transfer an input force from shaker to the load cell in order to excite a structure during a modal test. However, plastic stingers can provide a consistent axial force to the structure and minimise side loads. The deflection of a cantilevered beam due to a concentrated transverse load, *P*, at its free end is :

$$\delta = \frac{Pl_s^{\,3}}{3E_s I_s} \qquad\qquad \textbf{(2-6)}$$

in which δ is the deflection of the tip of the cantilever beam. Typical modulus values for steel are in the order of 100 times greater than those for plastic. Therefore, with a constant diameter, in order to allow the same deflection of the test structure to occur, the length of a steel stinger would have to be on the order of 5 times greater than a plastic one. So, plastic stingers can provide adequate transmission of the axial force to the test structure without buckling, while their weaker bending stiffness reduces the moment being applied to the force transducer. This provides a more accurate measurement of the force being applied.

Han [24] investigated the influence of the shaker on natural frequencies when extracting the FRFs of the test structure. He showed that the amount of distortion of natural frequencies due to the attachment of the shaker depended not only on the generalised

mass and shape of the particular mode of the test structure under excitation, but also on the mass and stiffness of the coil of the shaker and the bending stiffness of the stinger.

In 1997 Vandepitte and Olbrechts [25] discussed the dynamic loading effects that different excitation methods have on the dynamic behaviour of the test structures. Comparison of modal tests with different types of excitation systems was made. Three tests were performed with hammer excitation, shaker-with-stinger excitation and inertial shaker excitation. All tests gave different results, proving that loading effects can be important. It was also shown that inertial shakers not only add mass to the structure, but can also increase the stiffness of the complete system.

Several research workers [26], [27], [22] mentioned stinger axial resonance but defined the axial resonance frequency and its effects in different ways. Ewins [5] mentioned that it is always necessary to check for the existence of an internal resonance of the stinger either axially or in flexure because this can introduce spurious effects on the measured mobility properties. Furthermore, in the case of an axial resonance, very little excitation force will be delivered to the test structure at frequencies above the first mode. Hieber [18] suggested that the stinger axial resonant frequency is :

$$\omega_r = \sqrt{k_{sx}/m_{cl}} \qquad\qquad \textbf{(2-7)}$$

$$k_{sx} = \frac{A_s E_s}{l_s}$$ **(2-8)**

k_{sx} is the stinger's axial stiffness and m_{cl} is the mass of the shaker coil. He also declared that if this axial resonance is too low, there may be difficulty transferring enough force to the specimen at higher frequencies. Anderson [22] gave the same expression for the fundamental longitudinal resonance frequency as Hieber [18] but suggested that in the case that the force transducer is mounted in the stinger's shaker side m_{sxt}, the total mass of the force transducer's seismic mass, mounting hardware mass at the stinger's shaker end and the mass of the shaker coil, should be used instead of m_{cl} in equation (2-7).

In the resonant frequency calculation, both references [18] and [22] assumed that the structure's accelerance is zero. Unfortunately, this is true only when the structure is near an antiresonance. Generally, the structure's accelerance cannot be neglected compared to that of the stinger's shaker end. So equation (2-7) may cause misinformation.

Hu and McConnell [26], [27] studied extensively the axial resonance effects of the stinger on test results. They treated the stinger as a distributed-mass elastic system represented as a longitudinal bar. Stinger motion and force transmissibility, axial resonance, and excitation energy transfer problems were discussed. The results showed that the peaks of the force and motion transmissibility are closely related to the resonances and antiresonances of the test structure and the stinger-structure systems. Moreover, the stinger mass compensation problem when the force transducer is mounted on the stinger's exciter end were investigated theoretically, numerically and experimentally. It was found that the measured FRF can be underestimated if the mass compensation is based on the stinger exciter-end acceleration and can be overestimated if the mass compensation is based on the structure-end acceleration because of the stinger's acceleration. The mass compensation that is based on two accelarations was seen to improve the accuracy considerably.

Another problem in the axial direction is the drop of the input force at natural frequencies due to the axial interaction between the excitation system and the structure.

This drop in force causes noise and low coherence at natural frequencies. This problem has been studied in [28], [29], [30] and [31]. It was shown that proper choice of the shaker characteristics and an amplifier using current feedback instead of voltage feedback can reduce the force drop-off problem.

While interesting guidelines have been given to the design of stingers so far, there are some parameters such as misalignment of the stinger which should be considered in the behaviour of stingers. Moreover, a technique is needed to assess the performance of the stinger in practice.

2.3.2 Mass-loading effects of transducers

The measurement of the dynamic force and response of a structure, in terms of FRFs, often involves the use of accelerometers and force transducers, thus introducing changes to the structure due to the addition of extraneous masses. Figure 2-3 shows a beam which is excited by a shaker. The shaded zone represents the total extra mass, m_{ext}. Only about half of the force transducer mass contributes to the force signal, because the terminal is nearly at the half height of the transducer.
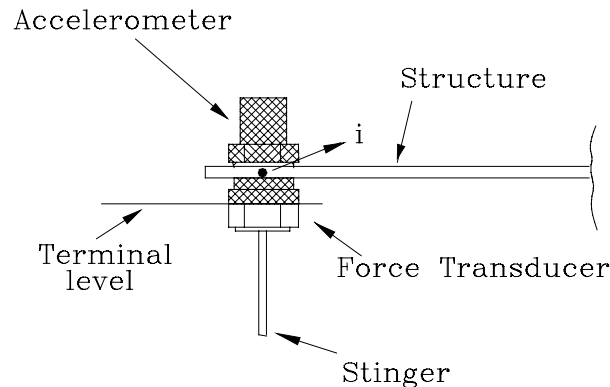
Figure 2-3. Mass-loading effect of transducers

As the objective is to obtain the effective force, f_e, going into the beam, the inertia force corresponding to the total extra mass, m_{ext}, should be subtracted from the measured force f_{meas}, i.e.:

$$f_e = f_{meas} - m_{ext}\ddot{x}_i \tag{2-9}$$

From equation (2-9), the desired acceleration FRF can be obtained in the frequency domain from:

$$A_{ii} = \frac{A^{(i)}_{ii}}{1 - m_{ext}A^{(i)}_{ii}} \tag{2-10}$$

This process is known as mass cancellation [5]. In general, some of the resonances will always be somewhat affected by the masses of the transducers, so a mass cancellation procedure is usually desirable, especially if the accelerometer position is to be changed around the structure, as which is often the case. As shown above, the mass cancellation procedure is quite straightforward for driving point FRFs. However, for transfer FRFs the problem is much more difficult.

The effect of mass-loading was studied via the modal formulation of structural dynamics, and in particular, by the modification theory formulated in modal space, as explained by Synder [32] and further discussed by Avitabile & O'Callahan [33]. Based on this study, Dossing [34] introduced the driving point residue method to predict shifts of natural frequencies due to mass-loading effects. The equation of motion in modal space for the mass modified structure is :

$$\left[[\phi]^T[\Delta M][\phi] + [I]\right]\{\ddot{x}\} + [\omega_{or}^2]\{x\} = 0 \tag{2-11}$$

The eigensolution to equation (2-11) is :

$$\left| -[[I] + [\phi]^T[\Delta M][\phi]][\lambda_r^2] + [\omega_{or}^2] \right| = 0 \tag{2-12}$$

Dossing simplified the problem further by solving for one mode at a time, assuming the influence from other modes to be negligible. This assumption seems numerically reasonable because the mode shape components are generally smaller than 1 and ΔM_i is

small too. Therefore the off-diagonal elements in the characteristic matrix are very small compared to the ω_{or}^2 elements. The equation then reduces to :

$$-\left[1 + \{\phi\}_r^T [\Delta M] \{\phi\}_r \right] \lambda_r^2 + \omega_{or}^2 = 0 \qquad \textbf{(2-13)}$$

and if mass is added to only one DOF (point/coordinate) at a time, the problem reduces to the scalar equation :

$$-\left[1 + \phi_{ir} \Delta m_i \phi_{ir} \right] \lambda_r^2 + \omega_{or}^2 = 0 \qquad \textbf{(2-14)}$$

Thus the relation between the natural frequency of the modified structure and the exact natural frequency of the structure in terms of the added mass and the mode shape component is :

$$\frac{\omega_r^2}{\omega_{or}^2} = \frac{\dfrac{1}{\phi_{ir}^2}}{\dfrac{1}{\phi_{ir}^2} + \Delta M_i} \qquad \textbf{(2-15)}$$

$1/\phi_{ir}^2$ represents the mass in this model which can be defined as "Apparent Dynamic Mass" in DOF *i* associated with mode *r*. Using this method, it can be determined how much the natural frequencies will change due to a mass-loading in a point. Or it can be determined what the natural frequencies were before the accelerometer was attached to the structure and modified its dynamics.

Decker and Witfeld [35] used the FRF substructuring technique, Structural Modification Using experimental frequency Response Function (SMURF) to correct mass-loading effects of transducers. The method of SMURF avoids the difficult and time-consuming development of a modal model. For a structure modified by mass, *m*, the accelerance FRF can be computed as :

$$A_{lk}(\omega) = A_{lk}^{(j)}(\omega) - \frac{A_{lk}^{(j)}(\omega)A_{ll}^{(j)}(\omega)}{\dfrac{1}{m} + A_{ll}^{(j)}(\omega)} \tag{2-16}$$

in which m is negative. This equation has to be applied to every frequency value. In equation (2-16) if $A_{ll}^{(j)}$ is known the correct FRF can be computed. However, measuring the driving-point FRFs at all measurement points is a very time-consuming process and sometimes impossible. The authors suggested two techniques to approximate A_{ll}. In spite of some pitfalls the methods improve the measured FRFs. However, noise was the main problem in the computations. To eliminate the effect of noise in the computation, a weighted FRF method was introduced. The method is successful in elimination of the effect of noise but causes discontinuity in the corrected FRFs.

Silva, Maia and Ribeiro, [36] used coupling/uncoupling techniques to correct the mass-loading effects of transducers for transfer FRFs which seems the most effective method suggested so far. They showed that by coupling the structure with a lumped mass and by mean of a series of relatively straightforward calculations the measured FRFs can be corrected. The structure shown in Figure 2-4 is coupled with the mass m_1 at point 1. Using FRF coupling of substructures, the equation governing the new system is :

$$\begin{bmatrix} A_{22}^{(1)} & A_{21}^{(1)} \\ A_{12}^{(1)} & A_{11}^{(1)} \end{bmatrix} = \begin{bmatrix} A_{22} & A_{21} \\ 0 & 0 \end{bmatrix} + \begin{Bmatrix} -A_{21} \\ 1/m_1 \end{Bmatrix}(A_{11} + 1/m_1)^{-1}\begin{Bmatrix} A_{12} & A_{11} \end{Bmatrix} \tag{2-17}$$

from which we have :

$$A_{11}^{(1)} = \frac{A_{11}}{1 + m_1 A_{11}} \tag{2-18}$$

and

$$A_{12}^{(1)} = \frac{A_{12}}{1 + m_1 A_{11}} \tag{2-19}$$

and

$$A_{22}^{(1)} = A_{22} - \frac{m_1 A_{12}^2}{1 + m_1 A_{11}} \qquad \textbf{(2-20)}$$

Using equations (2-18), (2-19) and (2-20), three FRFs A_{11}, A_{12} and A_{22}, can be obtained. Only three measurements are needed :

1 - Attach the accelerometer at point 1 and measure driving point FRF, $A_{11}^{(1)}$;

2- Add another accelerometer at point 2 and measure transfer FRF, $A_{12}^{(1,2)}$;

3- At the same condition measure again driving point FRF, $A_{11}^{(1,2)}$.
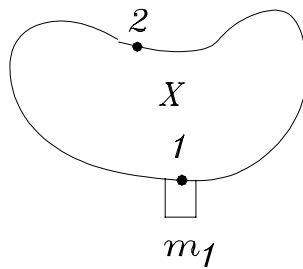
Figure 2-4. Modification of a structure by a mass

The interesting point is that it is possible to obtain the driving point FRF at point 2, A_{22} , without having to measure it. However, measurement problems of this method such as the effect of noise on the computations were not studied by the authors. The same technique was used by the authors for the evaluation of the complete FRF matrix, based on measurements taken along a single column of the FRF matrix using different accelerometers and dummy masses [37]. The technique inherently cancels the effects of the extra masses of the transducers. This result is especially important to deal with residual terms: It should be noted that there has not been found (so far) a way of relating the residual terms of the measured curves to the residual terms of the unmeasured ones.

There is still no general applicable procedure to deal with the mass-loading effects of transducers at non-driving points. Moreover, a method is needed to assess the quality of the measurement due to the mass-loading effects of transducers.

2.3.3   Suspension effects on test structures

In modal testing, test structures are often suspended using soft springs to approximate a free-free state of the structure. Free-free modal tests are popular because it is felt that the effect of soft springs on the test structure is negligible. In free-free state of the structure, the six rigid body modes no longer have zero natural frequencies, but they have values which are significantly lower than that of the first elastic mode of the structure. However, for flexible structures, the lowest elastic mode may interfere with the rigid body modes. Therefore the support system is needed to be designed to avoid interference of the rigid body modes on the lowest elastic mode of the test structure.

 On the other hand, even soft springs introduce stiffness and damping into the system. This added stiffness and damping of the suspension may significantly alter the modal parameters of the elastic modes of the test structure.

Historically, there has been concern for suspension stiffness and its effect on measured modal parameters of the test structure. Bisplinghoff, Ashley and Halfman [38] discussed the effects of support stiffness and mass on the modal frequencies, based on the results of Rayleigh [39]. Wolf [40] discussed the effects of support stiffness with regard to modal testing of a car. Initially, he analytically studied the effects of a spring to ground on a simple 2 DOF system. He then analysed data from a modal test of a car. He concluded that to minimise the influence of the suspension system, the support system should be attached to the most massive portion of the test system. He also reported that the rule of thumb to simulate free-free boundary conditions is to design the support system so that the rigid body modes are no more than one-tenth of the frequency of the lowest elastic mode. But, for the case of vehicle tests, it is seldom possible to achieve such a separation. He stated that test engineers frequently use 1:3 to 1:5 separation ratios between rigid body modes and lowest elastic mode. He showed that such stiff supports can lead to significant errors in the measured modal parameters.

Carne and Dohrmann [41] studied the effects of the support stiffness and damping on measured modal frequencies and damping ratios. They developed the model used by Wolf by including damping in the supporting system of the model. It was shown that for

a ligtly-damped structure even when the rigid body modes are no more than one-tenth of the frequency of the lowest elastic mode, the measured damping can be far from the true damping.

Lindholm and West [42] investigated the effects of suspension stiffness on a beam using different shock cord lengths and thickness. A perturbation study was done to determine what effects suspension stiffness would have on the mode shapes of the beam. In order to update the analytical model of the beam, optimisation routines were used to achieve a minimal difference between the analytical mode shapes and the experimental mode shapes. This study is especially important because the updating routine was done using several experimental mode shapes at once to find the optimum one.

It can be concluded that although suspension springs may have serious effects on the measurement, there is still no method to correct the effects of the suspension springs on the measured FRFs. Moreover, a method is needed to assess the quality of the measurement due to the effects of the suspension springs on the measurement.

2.4 Perturbation of Boundary Condition (PBC)

In a standard modal testing method, a modal model is normally based upon a single testing configuration (i.e.: free-free, fixed boundary condition, etc). The number of modes which can be extracted by this method consists typically of 10 to 40 lowest frequency modes for the given test configuration. This data base is far too small to completely update an FE model, and , in general, is still too small to develop an accurate modal model for dynamic modification. As a result, a new testing procedure has been developed which is referred to as the Perturbed Boundary Condition (PBC) testing method. In the PBC method, the system is tested in a number of different configurations; each configuration consists of the system with one or more of its boundary conditions perturbed. The different boundary conditions change the original modal space of the system. (Figure 2-5).
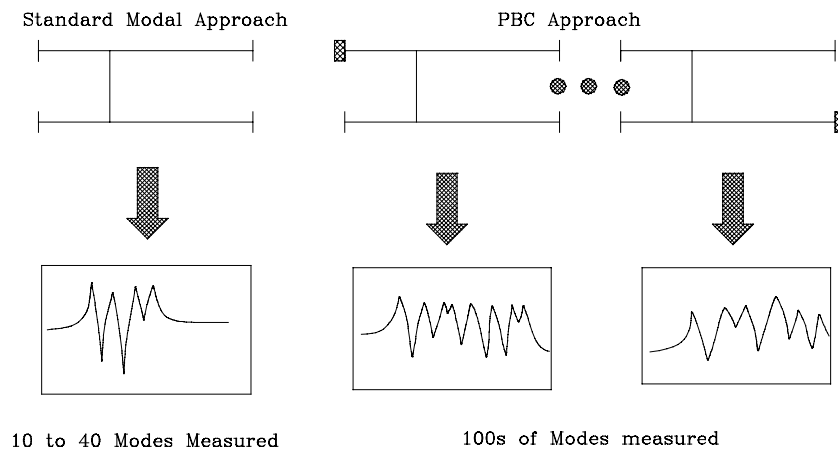
Figure 2-5. Perturbation of boundary condition (PBC)

Basically, two boundary condition perturbations are being examined. The first is a stiffness change; the second is a mass addition at the boundary point. The mass addition technique is specially targeted at stiffer structures while stiffness modification testing is targeted towards low frequency flexible structures tested in a free-free configuration where the test support system interferes with the accuracy of the resulting modal model.

The use of PBC allows for :

1. Estimation of rotational degrees-of-freedom.

2. Elimination of support effects.

3. Simple boundary simulation

4. Mode enhancement

Simley and Brinkman [43] employed the mass additive testing approach to show the importance of rotational degrees of freedom and to estimate them. For a simple beam the rotational mode shape was computed from a set of translational data. However, it was not possible to achieve the necessary resolution in the areas where it is needed.

One of the first PBC methods applied to Finite Element modelling verification was applied to large flexible structures by constraining to ground the interior points of the structure and verifying the constrained structure against an FEM model [44], [45], [46], [47].These large flexible structures were difficult to test free-free because the

frequencies of the elastic modes were too close to the rigid body modes of the structure. Constraining the structure eliminated the support problem.

Coleman and Anderson [48] used mass additive testing for a simple boundary simulation to approximate an in-situ configuration for a space shuttle flight pay-load. Traditionally a fixed-base modal test has been performed as a means of verifying the coupled-load mathematical model. An alternative method, a free-free configured payload using mass loaded boundary conditions , was presented as a means of verifying the coupled loads model. The method is cost-effective in that an expensive test fixture with unknown boundary conditions is replaced by a relatively inexpensive, reusable suspension system that produces a known boundary condition which does not contaminate the modal test results with fixture-coupled modes or boundary condition uncertainties.

Mode enhancement utilises certain modifications to a structure to allow for the measurement of a mode which is normally outside the measurement bandwidth, thereby allowing verification of potentially important system modes. Mode enhancement has been examined as a method for incremental updating an FE model using the various system models for each configurations. Gwinn, Lauffer and Miller [49] used a technique for synthesis of mathematical models of structural systems using experimentally-measured component modes that have been enhanced by mass interface loading. With this technique, individual components were tested with arbitrary discrete masses added to interface points. The effect of the interface mass was then analytically removed before the component was assembled into the global system. Results from this study indicated significant improvement in the assembled system property.

Recently, procedures for utilising a PBC database for updating of finite element models were being developed [50], [51]. These techniques are currently at an early stage of development.

Brown, Pierre and Barney [52] introduced a procedure for estimating the free-free modal characteristics of a system by testing multiple constrained states. The procedure utilises PBC to decouple the effective forces from the true excitation forces and reduces the influences of the constraints on the modal parameters. A frequency domain Auto Regressive Moving Average (ARMA) model was used to calculate the system's free-free

characteristics and to provide additional system model information for Finite Element (FE) correlation.

Structural modifications in the form of mass and stiffness additions are usually applied to the basic equation for describing the dynamics of a lumped parameter system as small additions to the respective free-free mass and stiffness matrices.

$$([M + \Delta M]s^2 + [C]s + [K + \Delta K])\{X\} = \{F\} \tag{2-21}$$

Equation (2-21) can be rearranged to allow for a direct solution of the free-free system characteristics :

$$([M]s^2 + [C]s + [K])\{X\} = \{F\} + \{-[\Delta M]s^2 - [\Delta K])\{X\} \tag{2-22}$$

$$= \{F\} + \{F_e\} = \left\{F_{total}\right\}$$

where $\{F_e\}$ is the matrix of the effective forces. It can be seen that by measuring the displacements of the system, as well as input forces, all of the terms on the right hand side of the equation (2-22) are known (given that the modification matrices are known) and the free-free system parameters are obtainable.

By using the ARMA model the effective forces, the unmodified system's characteristics may be obtained without the need for an FRF calculation. The equation for describing the dynamics of a lumped parameter system is shown as :

$$([M]s^2 + [C]s + [K])\{X\} = \left\{F_{total}\right\} \tag{2-23}$$

or :

$$([M]^{-1}[C])s\{X\} + ([M]^{-1}[K])\{X\} - [M]^{-1}\{F_{total}\} = -[I]s^2\{X\} \tag{2-24}$$

or :

$$[A_1]s\{X\} + [A_0]\{X\} + [B_0]\{F_{total}\} = -[I]s^2\{X\} \tag{2-25}$$

The above equation is a standard Auto-Regressive Moving-Average (ARMA) model. Or in matrix form:

$$[A_1 \quad A_0 \quad B] \begin{Bmatrix} sX \\ X \\ F \end{Bmatrix} = -[I]s^2 X \tag{2-26}$$

To solve the above equation there must be at least as many measured vectors as active modes. These measured vectors can consist of the various test configurations at several frequencies. By condensation of different configurations, the resulting matrix of equation (2-26) takes on the form of :

$$[A_1 \quad A_0 \quad B] \begin{Bmatrix} j\omega_1\{X_{1P}\} & j\omega_1\{X_{1Q}\} & . & j\omega_2\{X_{2P}\} & . & . \\ \{X_{1P}\} & \{X_{1Q}\} & . & \{X_{2P}\} & . & . \\ \{F_{1P}\} & \{F_{1Q}\} & . & \{F_{2P}\} & . & . \end{Bmatrix} = $$
$$\begin{bmatrix} -\omega_1^2\{X_{1P}\} & -\omega_1^2\{X_{1Q}\} & . & -\omega_2^2\{X_{2P}\} & . & . \end{bmatrix} \tag{2-27}$$

in which P and Q refer to different configurations. The ARMA coefficients , the $[A_i]s$ and $[B_i]s$, can be solved by using the pseudo-inverse of the measurement matrix in equation (2-27).The averaging property of this procedure uncorrelate the effective forces and allow for a solution.

Equation (2-23) can be arranged in the form of :

$$([A_2]s^2 + [A_1]s + [A_0])\{X(s)\} = [B_0]\{F_{total}\} \tag{2-28}$$

Equation (2-28) is the Laplace domain UMPA model for PBC test data. The same procedure which was explained for the ARMA model is applied here to find the unknown UMPA coefficient matrices, $[A_i]$ and $[B_i]$ in equation (2-28).

Brown, Vold and Shumin Li [53] used the scaled least square method with an UMPA model to find the free-free parameters. They showed that the unknown coefficient can be estimated from solving the following equation :

$$
[\tilde{A}_1 \quad \tilde{A}_0 \quad \tilde{B}]
\begin{bmatrix}
(j\omega_1)^2\{X_{1P}\} & (j\omega_1)^2\{X_{1Q}\} & . & (j\omega_2)^2\{X_{2P}\} & . & . \\
j\omega_1\{X_{1P}\} & j\omega_1\{X_{1Q}\} & . & j\omega_2\{X_{2P}\} & . & . \\
\{F_{1P}\} & \{F_{1Q}\} & . & \{F_{2P}\} & . & .
\end{bmatrix} =
\tag{2-29}
$$

$$
\begin{bmatrix}
\{X_{1P}(\omega_1)\} & \{X_{1Q}(\omega_1)\} & . & \{X_{2P}(\omega_2)\} & . & .
\end{bmatrix}
$$

in which P and Q refer to different configurations. Since both $X(\omega)$ and $F(\omega)$ normally contain measurement errors, a more accurate estimate of the UMPA coefficients can be obtained by using the total least-square method. This method allows for the cancellation of the effect of noise and provides unbiased estimates of the modal parameters. The procedure is reported in [53].

It seems that the PBC method can provide an effective tool to deal with measurement problems such as mechanical errors which are not possible using conventional modal testing. However, so far the PBC concept has been applied only for spatial models (mass and stiffness models) and not for response models (FRFs) which is the subject of this thesis.

2.5 Measurement of rotational DOFs

Rotational DOFs are present, in most cases, in 75% of the complete FRF matrix. Knowledge of them can therefore be of extreme importance to obtain reliable results when doing calculations related to coupling, structural modification, Finite Element model updating, joint identification, etc. However, there are neither reliable angular transducers available, nor a practical means of applying moment excitations.

For this reason most of modal analysis techniques tend to be developed by avoiding as much as possible the measurement of rotational FRFs, or by minimising the effects of not knowing them. Condensation and expansion techniques, mainly when addressing FE updating methods, are sometimes used to circumvent the problem.

Kistler's 8832 TAP system simultaneously measures one translational and one rotational acceleration. The system uses the dynamic deformation of piezoelectric cantilever beams as the transduction principle [54]. However, this system could not adequately solve the problem of measurement of the rotation. Aside from rotational accelerometers, several other methods have been used for rotational measurements and obtaining rotational FRFs which are discussed below.

2.5.1 The exciting block technique

This technique is based on the measurement of accelerometers properly placed on an additional block which is attached to the point of interest on the structure. The theory of exciting block is fully developed in references [55] and [56]. An engineering application of this technique is presented in [57]. However, the cross-sensitivity of accelerometers and additional mass and local stiffening of the block could cause problem in this technique. These are explained in references [58] and [59]. It was shown in [60] that it is possible to estimate accurate rotational response/force FRFs but the more difficult FRFs to estimate are those related to moment excitations.

2.5.2 The finite difference technique

This technique is based on the estimation of the rotational properties from spatial derivatives of translational data which in turn are gathered by accelerometers placed on the structure at convenient distances from each other [61] , [62]. This approach presents an advantage over the exciting block technique since the mass and stiffness properties of the structure are not altered so much in the measurement region. The distance between measurement points is critical for the correct estimation of rotational FRFs [59] .

The derivation of the translational data can be accomplished using either first-order [61] or second-order [62] finite difference formulas. The derivative approaches, however , proved to be effective only for simple structures [63] ,[64]. The fitting function is an alternate approach to cover either simple or complicated structures. The fitting function approach is divided into two groups : polynomials [65], [66] and splines [64], [67], [68] fitted to translational data. These techniques have shown considerable potential. The

polynomials are ideal for representing uncomplicated relationships. The main disadvantage, however, is the inability of polynomial fits to produce acceptable results for the higher frequency modes. Splines, on the other hand, are more suitable for representing very complex surfaces. On the other hand, splines are computationally efficient and more stable numerically than polynomials.

2.5.3 Laser interferometry

Laser interferometry is a technique in which by analysing the difference in phase between a measurement beam, reflected off the object of interest, and a reference beam, displacement can be detected with a resolution on the order of nanometers. Coupling two or more measurement beams, offset laterally by a fixed distance, allows rotation about one axis to be measured. While offering a very accurate means for sensing simultaneous rotations and translations, laser interferometry requires expensive, unwieldy analysis equipment.

Several application-specific devices capable of multi-axis measurement systems have been reported. Automotive researchers have developed a laser-based system for piston measurement [69]. In this system a collimated light beam is aimed through an optical port machined into the cylinder head at the piston surface and receives the reflected beam on to two position sensing photodetectors. The detector outputs are then used to determine the axial position and tilt angle of the piston. However, the hardware limits on resolution and the position and rotational angle of the piston were not effectively established.

Another system developed for positioning of a magnetically levitated micro-manipulator relies on three light sources and three photodetectors [70]. Opaque wings with a single pinhole in each are attached symmetrically to the manipulator. The wings are positioned so that a light source and a detector are on opposite sides of each pinhole. As the wings move, the light spots sensed by the detectors move, and the corresponding output information can be processed to determine the manipulator's new position. Since the wings are all coplanar, this system is only capable of measuring four degrees of freedom, two translational and two rotational.

Sommer, Trthewey, Caefo and Rieker [71] used Laser interferometry for a noncontacting measurement approach, capable of simultaneously sensing one dynamic translation and two dynamic angular rotations. The transducer system is based on the positional measurement of two laser beams reflected from a planar target. Using the geometric orientation between the incident light beams and the corresponding reflections onto two position sensing photodetector, the translation, pitch angle and roll angle of a planar target can be determined. The reported resolution is 40 μm for translation and 0.02 degrees for rotation with a working range of 2×3 mm and ± 5.0 degrees. Bokelberg, Sommer, Trethewey and Chu [72] developed the technique for simultaneous measurement of three translational and three rotational displacements of a vibrating object. The system is based on sensing the positions of three collimated light beams reflected from a tetrahedral target attached to the vibrating object. The dynamic position of the target is determined by using the system geometry , coordinate transformations and kinematics closure procedure.

This method offers accurate results but it is vulnerable to noise in the computations and the mass and stiffness properties of the structure altered by the attachment of tetrahedral target.

2.5.4   Laser-based 3D structural dynamics modelling

Modelling the laser-based experimental 3-D (3 dimensional) structural dynamics response of structures under test is one aspect of a larger body of research defined as structural imaging. Structural imaging includes shape and dynamic response modelling from laser measurements, and it then culminates with the visual display and analysis of the complete shape and dynamic response models. This method consists of taking three single-dimension measurements from different vantage points and then transforming them into an orthogonal triad of velocities. The measurements do not need to be in an orthogonal orientation. This method has evolved from the work of R. M. Huffaker [73]. Huffaker used a Laser Doppler system to measure the three-dimensional velocity of a gas. To measure the velocity he had one laser shooting into the gas and three laser

detectors measuring the velocities. The velocities were then transformed into an orthogonal coordinate system. His method would not work for the measurement of the dynamic behaviour of a structure because it depends upon the transparency of the gas. Most structures are opaque, thus blocking the laser light. However, Huffaker's method was modified by Donavan [74] for use on structures. Donavan used a Laser Doppler velocimeter that had the laser and detector all in the same unit. The unit actually measures velocity in the same direction as the laser beam and makes measuring dynamic response of a structure possible. Donavan's approach used one laser that took all three velocity measurements in three different positions. The laser had to be physically moved to each defined location separately. In many measurement situations it is difficult to position the laser accurately.

Mitchell and Abel [75] used a computer algorithm called the Four Point Registration Method to accomplish the locating of the laser in space. The method requires that the structure have four points marked with their exact coordinates known, in the reference coordinate system. These four points are called registration points. At each new laser position the laser beam needs to be moved, or scanned, to the first registration point. This is done by electronically moving the two internal scanning mirrors.

Mitchell and Galaitisis [76] developed a theoretical technique to extract drilling-angular velocities (θ_z) from translational velocities using high spatial density data from a scanning Laser Doppler Vibrometer (LDV). where z is the out of plane direction.

Kochersberger [77] and Sun [78] developed a method for angular velocity of in-plane velocities using a DFT-IDF technique (Discrete Fourier Transform-Inverse Discrete Fourier Transform). Their effort resulted on measurement of two more DOFs; rotation about x and y axes where x and y are in-plane directions (θ_x and θ_y).

Lindholm [79] used a registration procedure in which the laser is "manually" aimed at several points of known location on the structure. Three translation coordinates and three rotation angles are then estimated using a weighted non-linear least-squares procedure in which differences between predicted scanning angles and measured scanning angles (used to hit the registration points) are minimised.

Although laser-based 3D techniques are expensive and time-consuming processes, they do give a general and continuous data about the dynamic behaviour of the most of the points of the structure. However, this is not an easy task using other methods of measurement.

2.5.5 Scanning Laser Doppler Vibrometer (LDV)

An LDV beam can be scanned continuously along a line on a vibrating surface giving a modulated output which can be used in a number of ways to analyse structural vibration. Stanbridge and Ewins [80], [81], [82] used a continuously-scanning LDV to measure rotational response of the structure. They found that the response signal contains three components : one at the excitation frequency, giving the translational response, the others with an equal distance from the excitation frequency, giving the rotational responses. Two linear sine scans along orthogonal in-plane axes are sufficient to find the in-plane rotational vibration. However, by using a circular scan it is possible to obtain this information with just one measurement.

Stanbridge and Ewins [83] developed a new conical-scanning technique which gives an easily-quantifiable measure of the magnitude and direction of the vibration of a point, even if the vibration is in-plane. It has been shown that the total state of translational vibration and rotational vibration except drilling angular velocity can be derived using a short-focus lens to produce a conical scan. This method, however, is in its early stage and needs to be developed for practical cases.

2.6 Noise

Measured FRFs contain a certain amount of noise, a feature inherently present in all measured data. The success of the methods based on modal testing depends on the quality of data and, especially on the level of the experimental noise. Estimators are used to deal with the problem of noise. Bendat and Piersol defined H_1 [84] estimator as:

$$H_1 = \frac{G_{xy}}{G_{xx}} = \frac{G_{uv}}{G_{uu} + G_{mm}} \tag{2-30}$$

where G_{xy} is the cross spectrum between the measured force signal and the measured response signal, G_{uv} is the cross spectrum between the true force signal and the true response signal, G_{xx} is the auto spectrum of the measured force signal, and G_{mm} is the auto spectrum of the noise from the force transduction system. The H_1 estimator underestimates the magnitude of the FRF near resonance. At resonance the structure looks like a short circuit (low impedance) to the shaker. This results in large losses within the power amplifier-shaker itself and a low-force input. The low-force input reduces the level of signal-to-noise ratio and allows the force transducer output signal to approach the transducer noise. In this case, the result is biased. However, the bias is caused only by the noise from the force transduction system. Transducer noise has no influence on such bias provided the estimates are sufficiently averaged.

This is the worst place to have erroneous estimates of an FRF. The reduction of the magnitude in this resonance area can effectively influence the estimation of the modal parameters. The first alternate estimator H_2 [85] was proposed in the early 80's. This estimator was designed to yield an upper bound estimator on the FRF. The H_2 estimator is defined as :

$$H_2 = \frac{G_{yy}}{G_{yx}} = \frac{G_{vv} + G_{nn}}{G_{uv}} \tag{2-31}$$

where G_{yy} is the auto spectrum of the measured response signal, G_{vv} is the auto spectrum of the true response signal, and G_{nn} is the auto spectrum of the output transducer noise. The H_2 estimator is a good estimator of the FRF at resonance even in the presence of the noise from the force transduction system. At resonance the response signal is very large with respect to the system noise. Thus, the numerator approaches the true auto spectrum of the response. The denominator of equation (2-31) approaches the true cross spectrum with appropriate averages. The problem with this estimator is that it has a poor quality at the anti-resonances within the FRF.

After estimator H_2, a series of other FRF estimators were proposed [86], [87], [88]. The H_s [86] and the H_v [89] estimator were the closest to an optimal estimator over the full range of the FRF. However, these estimators required another estimator for the various levels of uncorrelated content entering the estimation process.

In 1985 Goyder [90] presented an idea for the improvement of the FRF estimation process. He suggested :

$$\hat{H}^c = \frac{G_{ys}}{G_{xs}} = \frac{G_{vs}}{G_{us}}$$

(**2-32**)

where G_{ys} is the cross spectrum between the excitation source signal and the measured response signal, G_{vs} is the cross spectrum between the source signal and the true noiseless response signal, and similar definition between the measured force signal and the excitation source signal. The details of this methodology (Equation (2-32)) were delineated by Cobb [91], [92]. He explained the unbiased estimator properties of the $\hat{H}^c$ estimator and defined the finite sample size bias error effect. Moreover, he defined a technique for estimating the confidence bounds on the FRF for the first time and proposed a method for the determination of the source of and the quantity of noise associated with each transducer and shaker in the system. This new FRF estimator provides one of the best methods for the unbiased estimation of the FRF.

2.7 Conclusions

- Modal testing techniques can be very sensitive to even small changes in the structure's dynamic behaviour, such as those that are usually considered negligible in the measurement. So there is a need to investigate the effect of the small changes in the system relating to the mechanical devices such as accelerometers, suspension springs and stingers.

- On a more philosophical note, the expectations from a high quality modal test are not formulated very clearly. The maximum allowable changes in the measured FRFs due

to the effects of the measurement errors and their relation to measurement accuracy need to be defined further.

- There is still no general applicable procedure to deal with the mass-loading effects of transducers at non-driving points. Moreover, a method is needed to assess the quality of the measurement due to the mass-loading effects of transducers.

- Suspension springs may have serious effects on the measurement but there is still no method to correct the effects of the suspension springs on measured FRFs. Moreover, a method is needed to assess the quality of the measurement due to the effects of the suspension springs on the measurement.

- While some researchers have given interesting guidelines to the design of stingers, there are some parameters such as misalignment of the stinger which should be considered in the behaviour of stingers. Moreover, a technique is needed to assess the performance of the stinger in practice.

- The PBC method seems quite promising for the assessment of the quality of the modal testing in the sense that different configurations for an identical test structure allow for the detection of the measurement errors and obtain the exact FRFs.

- In spite of extensive research for the measurement of rotational DOFs, no generally applicable procedure has been found so far. The more difficult FRFs to obtain are those related to moment excitations.

- Noise is the main problem in the computations of the methods based on the modal testing results.

CHAPTER 3

Correction of mass-loading effects

of transducers in modal testing

3.1 Introduction

The mass-loading effect of transducers is one of the sources of error in modal testing. A transducer mounted on a vibrating system changes the dynamics of the structure and introduces errors into measured FRFs. One problem with this is the production of unrealistic results, which cause the measured resonant frequencies to be less than the correct values. A further problem is the inconsistency of the data base when using a series of measurements with roving transducers in order to acquire data for modal analysis. Data inconsistency can cause severe problems in the curve-fitting process, particularly when applying a modern global parameter estimation algorithm.

It is desirable to cancel the effect of the extra masses on a measured FRF. The mass cancellation technique for transducers at the driving points has been explained by Ewins [5]. However, there are few publications about quantification of the mass-loading effects, caused by a measuring transducer, at the non-driving points [34], [94].

The method of Structural Modifications Using experimental frequency Response Functions (SMURF) was investigated first to avoid the difficulties of developing a modal model for structural modification proposes. This method was introduced by Klosterman [95].

In this chapter, the SMURF method is used to revisit the problem of mass-loading effect of transducers. Based on this analysis, a general solution for correction of the mass-loading effects of transducers is proposed.

This work was done prior to and independently of the work published in [36] and then revised and published in IMAC 1998 [93].

3.2 Theory

3.2.1 Mass modification

Changes in the FRF of a system due to mounting a mass can be estimated using direct substructuring technique SMURF as follows :

Figure 3-1(a) indicates a structure which has been rigidly connected to the second system of a mass. The connection is at point *j* and in *x* direction. The force excites the structure at point *i* and the response is measured at point *l*. Figure 3-1(b) indicates the free body diagram of the system.

Figure 3-1. Mass modification

As is usually the case in modal testing, the system is presumed to be linear. The equations governing the coupled system are:

$$X_l = \alpha_{li} F_i + \alpha_{lj} R_j \tag{3-1}$$

$$X_j = \alpha_{ji} F_i + \alpha_{jj} R_j \tag{3-2}$$

$$X_m = \alpha_{mm} R_m \qquad \text{(3-3)}$$

where :

$$\alpha_{mm} = -\frac{1}{m\omega^2} \qquad \text{(3-4)}$$

and the constraining equations are :

$$X_j = X_m \qquad \text{(3-5)}$$

$$R_j + R_m = 0 \qquad \text{(3-6)}$$

Elimination of the reaction forces and displacements at the connection point results in :

$$X_l = (\alpha_{li} - \frac{\alpha_{ji}\alpha_{lj}}{\alpha_{mm} + \alpha_{jj}})F_i = \alpha_{li}^{(j)}.F_i \qquad \text{(3-7)}$$

in which $\alpha_{li}^{(j)}$ is the modified receptance function between points l and i when the second system is a mass with the amount of m and connected rigidly to the original system at point j. From equation (3-7) one can immediately relate $\alpha_{li}^{(j)}$ and the original receptances, thus :

$$\alpha_{li}^{(j)} = \alpha_{li} - \frac{\alpha_{ji}\alpha_{lj}}{\alpha_{mm} + \alpha_{jj}} \qquad \text{(3-8)}$$

in which $\alpha_{li}, \alpha_{ji}, \alpha_{lj}, \alpha_{jj}$ are the original receptances, namely for the system without the accelerometer. Multiplying both sides by $-\omega^2$, the relation between accelerances is :

$$A_{li}^{(j)} = A_{li} - \frac{A_{ji}A_{lj}}{A_{mm} + A_{jj}} \qquad \text{(3-9)}$$

Equations (3-8) and (3-9) are general equations for modifying a system by the connection of a mass, m.

One can develop three special cases which are applicable in the mass cancellation technique suggested in this work.

(a) For the special case of an attached accelerometer, the point of response measurement is the same as the point of connection $(j=l\,,\,l\neq i)$ (Figure 3-2) .

Equation (3-9) can then be rewritten as :

$$A_{li}^{(l)} = A_{li} - \frac{A_{li}A_{ll}}{A_{mm} + A_{ll}} \tag{3-10}$$

where A_{mm} is :

$$A_{mm} = \frac{1}{m} \tag{3-11}$$
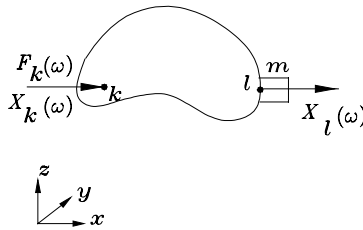
Figure 3-2. Mass modification of an accelerometer

Inserting equation (3-11), equation (3-10) can be simplified as :

$$A_{li}^{(l)} = \frac{A_{li}}{1 + mA_{ll}} \tag{3-12}$$

Equation (3-12) shows how the measured FRF $A_{li}^{(l)}$ is related to the correct accelerances, A_{li} and A_{ll} .

(b) For the driving point accelerance *(j=l=i)*, equation (3-12) can be summarised as:

$$A_{ll}^{(l)} = \frac{A_{ll}}{1 + mA_{ll}} \tag{3-13}$$

which is nothing other than the standard mass modification at the driving point.

(c) For the case that there are two accelerometers attached at points *i* and *j* (*i=l*) (Figure 3-3(a)), one can consider mass m_j is attached at point *j* to the system consisting of mass m_i and the structure *B* (Figure 3-3(b)).
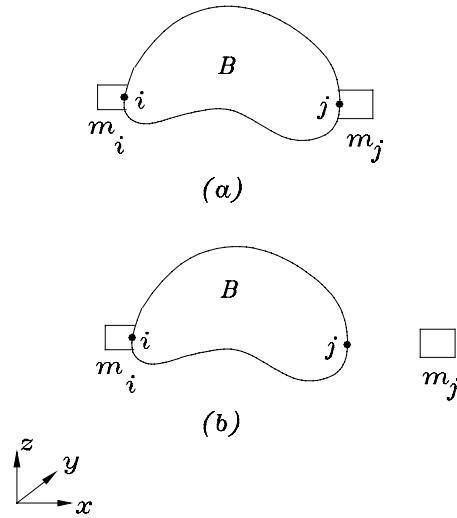
Figure 3-3. Uncoupling of one mass

In this case equation (3-9) can be summarised as :

$$A_{ii}^{(i,j)} = A_{ii}^{(i)} - \frac{(A_{ji}^{(i)})^2}{\frac{1}{m_j} + A_{jj}^{(i)}} \tag{3-14}$$

Equations (3-12) , (3-13) and (3-14) can be derived using the FRF coupling technique which is the same idea suggested by Maia, Silva and Riberio [36].

3.2.2 Correction of the mass-loading effects of transducers

Equation (3-12) shows how the measured accelerance $A_{li}^{(l)}$ is related to the correct accelerances, A_{li} and A_{ll}. In equation (3-12), If $A_{li}^{(l)}$ and A_{ll} are known, A_{li}, the correct transfer FRF, can be computed. $A_{li}^{(l)}$ is obtained by measurement. If $A_{ll}^{(l)}$ could be measured, A_{ll} would be obtainable using equation (3-13) . However,

measuring FRFs at all driving points is a time-consuming process. Furthermore in most cases the excitation and response measurement at some points on the test structure is impossible. To overcome the problem of obtaining A_{ll}, one may consider two measurements with two different accelerometers with different masses (Figure 3-4).

Here the magnitude of m_1 is different to that of m_2. The equations governing the systems are :

$$\begin{cases} A_{li}^{(l)} = \dfrac{A_{li}}{1 + m_1 A_{ll}} \\ \overline{A}_{li}^{(l)} = \dfrac{A_{li}}{1 + m_2 A_{ll}} \end{cases} \tag{3-15}$$
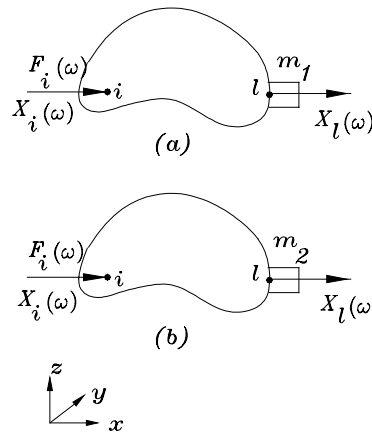
Figure 3-4. Measurement using two different accelerometers

in which $A_{li}^{(l)}$ is different from $\overline{A}_{li}^{(l)}$. In matrix form, equation (3-15) can be written as :

$$\begin{bmatrix} \dfrac{1}{A_{li}^{(l)}} & -m_1 \\ \dfrac{1}{\overline{A}_{li}^{(l)}} & -m_2 \end{bmatrix} \begin{Bmatrix} A_{li} \\ A_{ll} \end{Bmatrix} = \begin{Bmatrix} 1 \\ 1 \end{Bmatrix} \tag{3-16}$$

Equation (3-16) is a combination of two linear equations and can be solved for A_{li} and A_{ll} :

$$\left\{ \begin{array}{c} A_{li} \\ A_{ll} \end{array} \right\} = \left(\left[\begin{array}{cc} \dfrac{1}{A_{li}^{(l)}} & -m_1 \\ \dfrac{1}{\overline{A}_{li}^{(l)}} & -m_2 \end{array} \right] \right)^{-1} \left\{ \begin{array}{c} 1 \\ 1 \end{array} \right\}$$

(3-17)

With this procedure one can obtain two correct FRFs (A_{li} and A_{ll}) by undertaking two different measurements ($A_{li}^{(l)}$ and $\overline{A}_{li}^{(l)}$). So the mass cancellation has been accomplished for transfer FRFs. Moreover, the driving point FRF at point *l* has been found without having to measure it. This method is basically the same as that suggested in [36]. However, the present computational procedure is more systematic and is especially helpful in dealing with noise, as discussed below.

3.3 Demonstration and verification of the method

3.3.1 Validation of the method

To prove the validity of the method presented in section 3.2.2, a 12 DOF system of masses, springs and dampers has been considered in a simulated test (Figure 3-5). Table 3-1 shows the specifications of the system.

Table 3-1 . Parameters of the 12 DOF system

DOF	Mass (Kg)	Stiffness (N/m)	Damping (Ns/m)
1	3	7000	0.3
2	1.3	10000	0.2
3	1.5	5000	0.1
4	1	2000	0.8
5	1	10000	0.5
6	2.5	5000	1.6
7	1.5	10000	1
8	1	3000	0.3
9	1	5000	0.8

10	2.5	10000	0.3
11	1.2	4000	0.5
12	1	8000	0.9
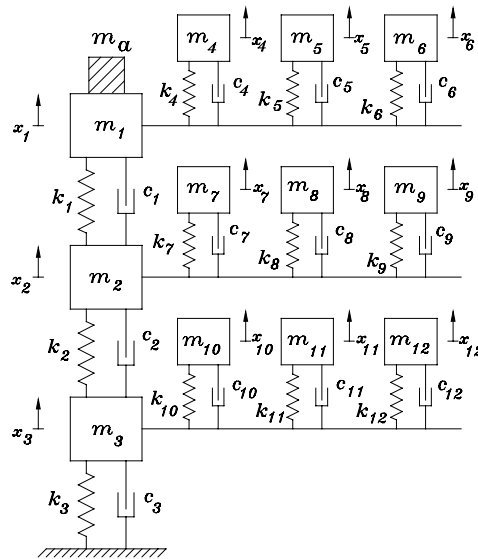
Figure 3-5. A numerical example of 12 DOF system

The system is excited at point 2. An accelerometer has been attached to the system at point 1 to measure transfer FRF, A_{12}, in the simulated test (Figure 3-5). In order to show the difference in graphical representations clearly, the mass of the accelerometer has been exaggerated (m_a = 1.5 Kg). Figure 3-6 shows the comparison of the accelerances , A_{12}, of the system without accelerometer (solid line) and with accelerometer (dashed line).

For correction of the measured FRF, another accelerometer with the mass of 1.2 Kg was used at point 1 in the simulated measurement . Using equation (3-17) the correct values of A_{11} and A_{12} were calculated. Figure 3-7 shows the comparison of the true FRF, A_{12}, and the measured FRF, $A_{12}^{(1)}$, after correction. As can be seen, the measured FRF, $A_{12}^{(1)}$, coincides with the true FRF after correction.
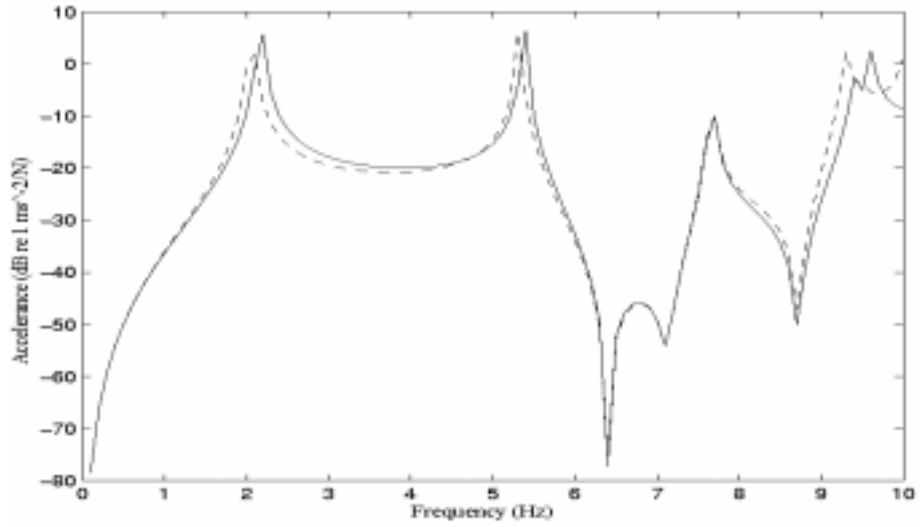
Figure 3-6. Comparison of the accelerances, A_{12}, of the system without accelerometer (solid line) and with accelerometer (dashed line)
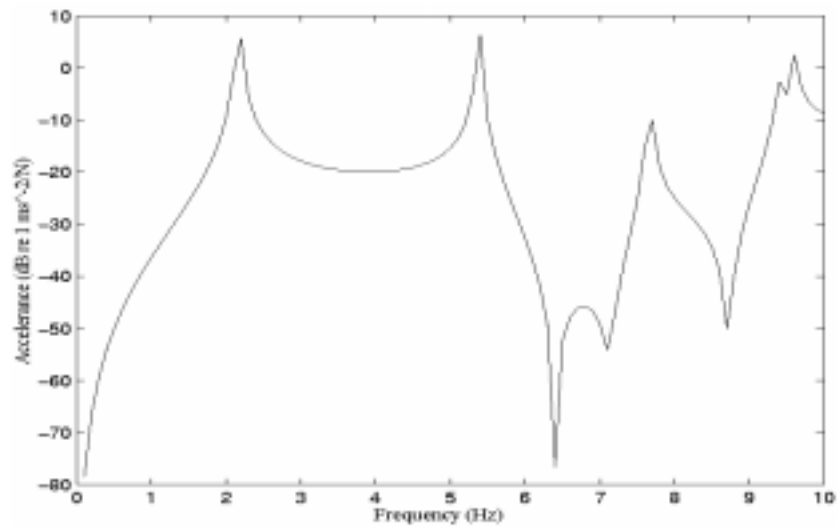
Figure 3-7. Comparison of the accelerances, A_{12}, of the system without accelerometer (solid line) and with accelerometer (dashed line) after correction

The same coincidence was obtained for A_{11}, (not shown here)

3.3.2 Practical considerations

The method suggested in this article is exact, but in practical situations may be vulnerable to measurement errors such as noise. To understand the scale of the problem, two further simulated tests were conducted. The specifications of these tests are given in Table 3-2.

Table 3-2. The effect of accelerometer mass on the computations

FRF	A_{12}
The mass of the first accelerometer	0.1 (Kg)
The mass of the second accelerometer (1st example)	0.11 (Kg)
The mass of the second accelerometer (2nd example)	0.2 (Kg)
Percentage of noise	5%
Frequency Range	1-10 (Hz)

The FRFs of the system were polluted by adding random noise using the following relation:

$$\breve{A}_{li} = [1 + \alpha \times (2 \times RAN - 1)] \times A_{li} \qquad \textbf{(3-18)}$$

where $\breve{A}_{li}$ is the noisy accelerance, α is the percentage of noise, *RAN* is a random value between 0 and 1 and A_{li} is the accelerance without noise. The percentage of noise in this example is 5%.

Two different masses were used for the second accelerometer. The mass of one of them was close to the mass of the first accelerometer (0.11 Kg) while the mass of the other one was quite different (0.2 Kg). Figure 3-8 shows the result of the correction with the 0.11 Kg mass. Figure 3-9 shows the result of the correction with 0.2 Kg mass. It is clear that this calculation is sensitive to noise when the two masses are

close in size. However, if the two masses are different enough from each other, the result is quite satisfactory.
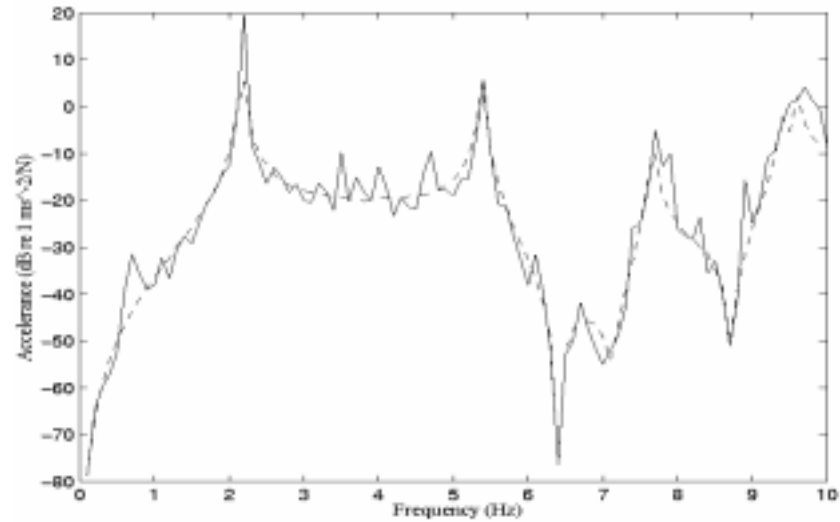
Figure 3-8.   Comparison of the accelerances, A_{12}, of the system without accelerometer (dashed line) and with accelerometer (solid line) after correction using noisy data
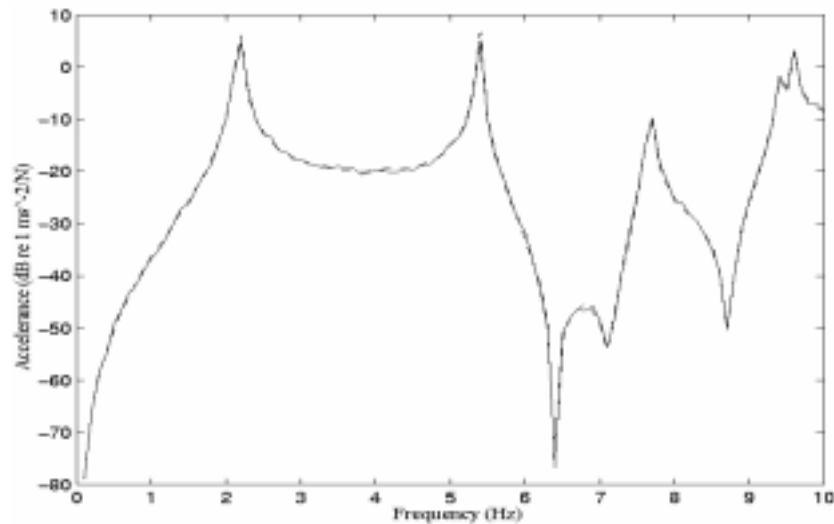
Figure 3-9.   Comparison of the accelerances, A_{12}, of the system without accelerometer (dashed line) and with accelerometer (solid line) after correction using noisy data

The reason for this can be found by looking carefully at equation (3-17). The matrix :

$$\begin{bmatrix} \dfrac{1}{A_{li}^{(l)}} & -m_1 \\ \dfrac{1}{\overline{A}_{li}^{(l)}} & -m_2 \end{bmatrix} \qquad \textbf{(3-19)}$$

will be ill-conditioned if two rows of the matrix are highly correlated. As m_1 becomes closer to m_2, $A_{li}^{(l)}$ becomes closer to $\overline{A}_{li}^{(l)}$. Consequently, two rows become more dependent on each other and in the presence of noise, the inverse of the matrix is unrealistic. Therefore, it is important to choose suitable masses to avoid unrealistic results.

3.3.3 Experimental case study

A simple beam was used for the experimental validation of the method presented in this chapter. The beam was made of mild steel, and had dimensions $20 \times 0.6 \times 44 cm$ and a weight of 0.412 Kg. Figure 3-10 shows the set-up of the equipment for a hammer test of the beam. Although 6 directions must be considered, the motion of the beam was considered in only two directions: one axial direction (z) and one rotational direction (θ_y). The experimental model of beam was divided in to 6 equal elements and was tested in a free-free configuration, suspended by soft elastic cords attached to the beam at points 2 and 6 (see Figure 3-10).The excitation was applied at its neutral axis at point 5 and the response was measured at point 4 using a light accelerometer with a mass of 0.004 Kg. To conduct a genuine test, it was assumed that the structure consisted of the beam and the accelerometer. Then, two different extra masses are added to the accelerometer on two different tests and the beam was measured. These extra masses were assumed to be two different accelerometers with different masses. There are two benefits in this assumption. First, an exact result (without any extra mass) of the structure can be obtained. Second, one accelerometer is used for all of the measurements. Therefore, this procedure allows us to eliminate all the other possible sources of the error (except for mass-loading effect) in the measurements.

 The extra mass for the first test was 0.029 Kg (7% of the mass of the structure) and for the second test was 0.048 Kg (11.5% of the mass of the structure). The structure was tested once without extra masses installed to obtain exact transfer and point FRFs for comparison purposes. Figure 3-11 shows the comparison of the exact receptance function (α_{45}) and the measured receptance function around one of the resonances of the beam using two extra masses to represent the accelerometers. In this case the measured recptance was affected by the extra masses and the resonance was shifted to the left. Using the method suggested in this chapter for the correction of the mass-loading effects of transducers, the FRFs were corrected. Figures 3-12 and 3-13 show the comparison of the computed FRFs and the exact FRFs for the transfer and point FRFs, respectively. An interesting point is that the driving point FRF(α_{44}) was obtained without measurement. Figure 3-13 shows that the corrected FRF and the exact FRF match around resonance while at other points the computed FRF is more noisy. Fortunately, most of the information from modal testing is from the resonance areas.
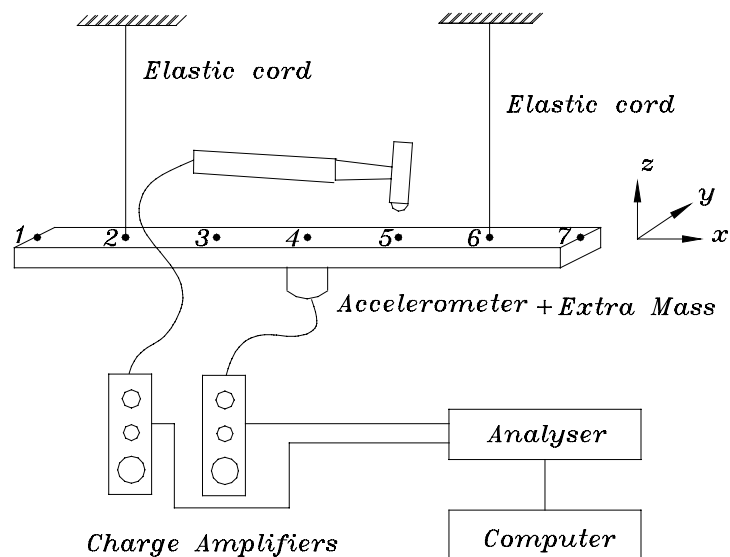
Figure 3-10. Experimental set-up for hammer testing of the beam
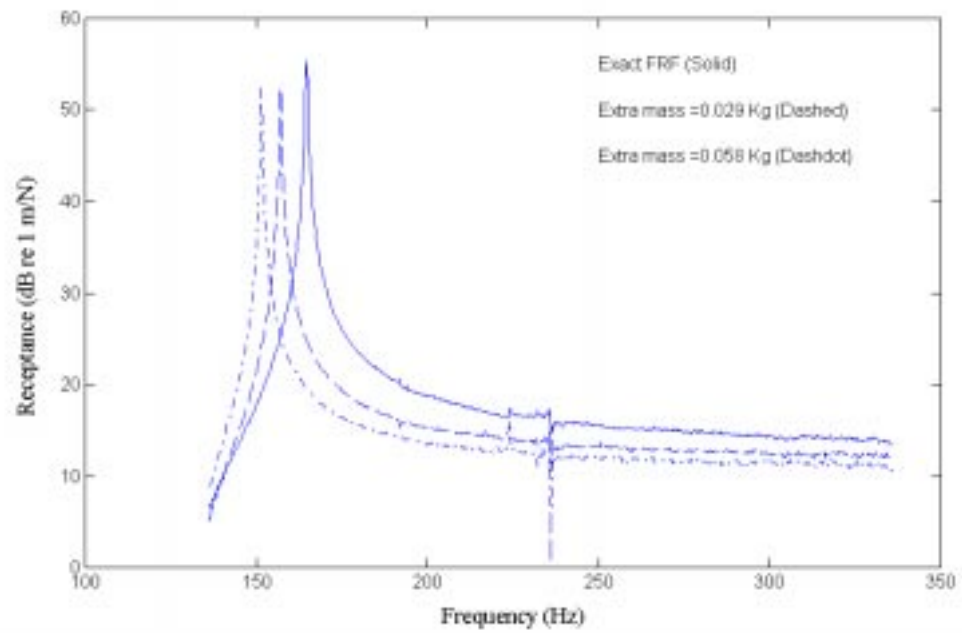
Figure 3-11. Measurement of the structure affected by extra masses (α_{45})
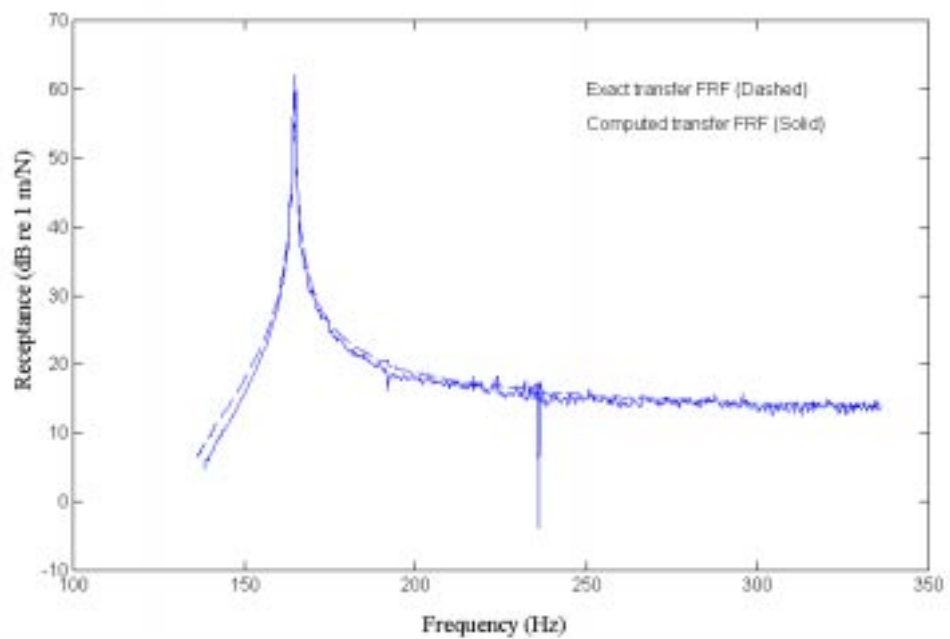
Figure 3-12. The comparison of the computed transfer FRF and the excat FRF (α_{45})
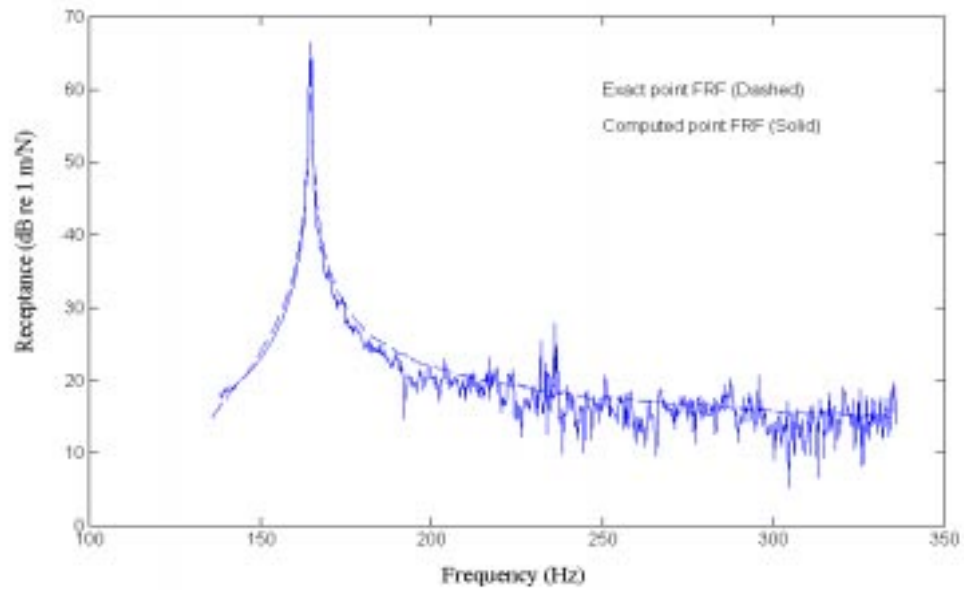
Figure 3-13. The comparison of the computed point FRF and the exact FRF (α_{44})

3.4 Calibration of the test set-up using the correction method

One of the interesting applications of the method suggested in section 3.2.2 is checking the calibration of the test set up. As with all measurement process, it is necessary to calibrate the equipment which is used in modal testing during each test. It is customary to use a simple rigid mass-like structure to calibrate the equipment. If the accelerance of this rigid mass is measured, then the FRF obtained should be equal to (1/mass) over the entire frequency range, and this is a quantity which can be accurately determined by weighing.

In this section an alternative method is presented to calibrate the test set up by modifying the test structure. It was shown that the measured FRFs can be corrected if the measurement is repeated with an accelerometer of different mass. The answers to equation (3-17) can be simplified as :

$$A_{li} = \frac{-m_2 + m_1}{\dfrac{-m_2}{\overline{A}_{li}^{(l)}} + \dfrac{m_1}{A_{li}^{(l)}}} \qquad\qquad (\textbf{3-20})$$

and

$$A_{ll} = \frac{-\dfrac{1}{\overline{A}_{li}^{(l)}} + \dfrac{1}{A_{li}^{(l)}}}{\dfrac{-m_2}{\overline{A}_{li}^{(l)}} + \dfrac{m_1}{A_{li}^{(l)}}} \tag{3-21}$$

Now suppose that the test set up is uncalibrated. Then the measured FRFs shift upwards or downwards by a factor like α with respect to the calibrated FRF. Therefore, the measured uncalibrated FRFs are equal to calibrated FRFs multiplied by α . For uncalibrated FRFs, equations (3-20) and (3-21) are changed as:

$$\tilde{A}_{li} = \frac{-m_2 + m_1}{\dfrac{-m_2}{\alpha \overline{A}_{li}^{(l)}} + \dfrac{m_1}{\alpha A_{li}^{(l)}}} = \alpha A_{li} \tag{3-22}$$

and :

$$\tilde{A}_{ll} = \frac{-\dfrac{1}{\alpha \overline{A}_{li}^{(l)}} + \dfrac{1}{\alpha A_{li}^{(l)}}}{\dfrac{-m_2}{\alpha \overline{A}_{li}^{(l)}} + \dfrac{m_1}{\alpha A_{li}^{(l)}}} = A_{ll} \tag{3-23}$$

As can be seen from equation (3-23) the driving point FRF is automatically calibrated through this process while equation (3-22) shows that the transfer FRF has not been calibrated yet. Therefore the measured FRFs , $A_{li}^{(l)}$ and $\overline{A}_{li}^{(l)}$, and the corrected transfer FRF, $\tilde{A}_{li}$, are all uncalibrated and at the same level although at a wrong level while the corrected driving point FRF is now calibrated and shifts to the right level.

Figure 3-14 shows the result of the correction process for the calibrated measured FRFs and Figure 3-15 shows the result of the correction process for the uncalibrated FRFs. As can be seen, the corrected point FRF shifts to the correct level through this process while the corrected transfer FRF is at the same level as the measured FRFs.
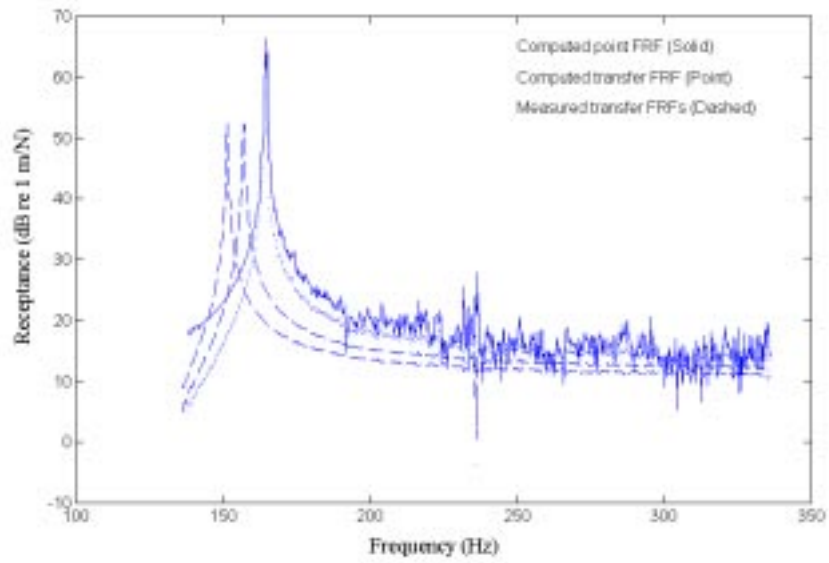
Figure 3-14. Correction of the calibrated measured FRFs
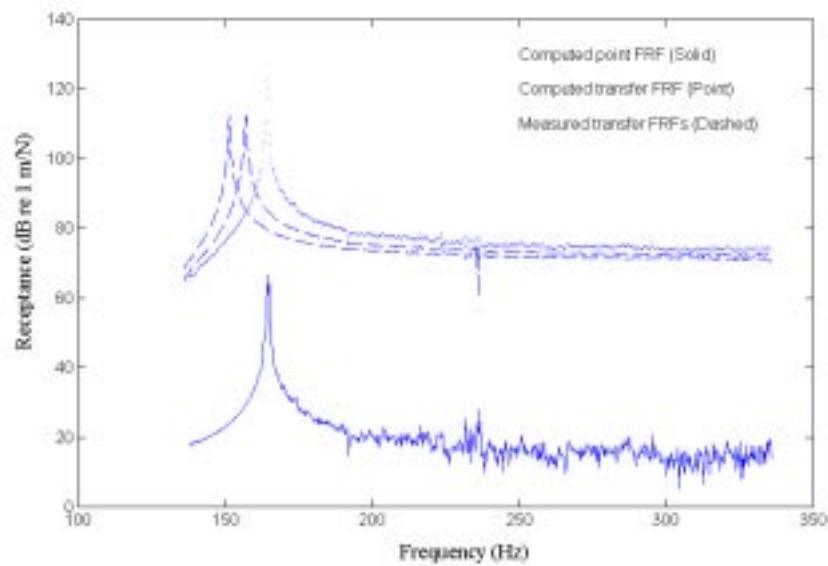
Figure 3-15. Correction of the uncalibrated measured FRFs

This procedure can be used to check the calibration of the measurement set-up. Because this calibration method is on the structure, instead of a rigid calibration mass, it is more reliable and more convenient than existing calibration methods.

3.5 Assessment of the quality of the measurement

Traditionally, the mass-loading effects of accelerometers are avoided by using small accelerometers and, as a result, the effects of these mechanical devices on the measured FRFs are often considered to be negligible. There is no known proof to this belief and no criterion to quantify the quality of the measurement. In this section a method will be suggested for assessing the quality of the measurements in conventional modal testing related to the mass-loading effects of accelerometers. Here the emphasis is to use the theory which was presented earlier in this chapter for the correction of the mass-loading effects of accelerometers.

3.5.1 Assessment of the quality of the measurement based on the changes in the natural frequencies of the structure

From a practical point of view, comparison between the natural frequencies of the measured FRFs and those of the exact FRFs is a suitable way of assessing the quality of the measurement. When there is no discernible change in the natural frequency of the structure due to the attachment of an accelerometer, the measured FRFs can be judged to have a good quality; otherwise, the results are not reliable and there is a need to cancel the mass-loading effect of the accelerometer. Even though, there is no access to the exact natural frequencies of the structure in the test, they should be obtained in some way. If the driving point FRF at the point of the attachment of the accelerometer, $A_{ll}^{(l)}$ in Figure 3-2, could be measured then the exact driving point FRF, A_{ll}, would be computed using equation (3-13). A comparison between $A_{ll}^{(l)}$ and A_{ll} shows the difference between the natural frequencies of the structure and those of the modified structure. However, sometimes measurement of $A_{ll}^{(l)}$ is not practical. In these cases the following method is suggested for obtaining the exact natural frequencies of the structure:

If an extra mass is added to the accelerometer and the structure is measured again, the exact FRF can be obtained using the method presented in section 3.2.2 In equation (3-17), the frequencies that make the determinant of the matrix

$$\begin{bmatrix} \dfrac{1}{A_{li}^{(l)}} & -m_1 \\[2ex] \dfrac{1}{\overline{A}_{li}^{(l)}} & -m_2 \end{bmatrix}$$ **(3-24)**

equal to zero are the exact natural frequencies of the structure. This means that the exact natural frequencies of the structure are at the frequencies where:

$$\frac{A_{li}^{(l)}}{\overline{A}_{li}^{(l)}} = \frac{m_2}{m_1}$$ **(3-25)**

on a logarithmic scale, we have:

$$20\log A_{li}^{(l)} - 20\log \overline{A}_{li}^{(l)} = 20\log \frac{m_2}{m_1}$$ **(3-26)**

If the magnitude of m_2 is twice that of m_1, then the right hand side of equation (3-26) is equal to 6.02. In this case we have:

$$A_{li}^{(l)} = 2\overline{A}_{li}^{(l)}$$ **(3-27)**

This means that if $\overline{A}_{li}^{(l)}$ is doubled and drawn on a graph together with $A_{li}^{(l)}$, the point of intersection of $2\overline{A}_{li}^{(l)}$ and $A_{li}^{(l)}$ represents the exact natural frequency of the structure. Figure 3-16 shows the graphical representation of this method. Therefore the exact natural frequency of the structure can be estimated either by the addition to the structure of an extra mass, with the same mass as that of the accelerometer, and using the graphical method shown in Figure 3-16 or by solving equation 3-27. If, by doubling the mass of the accelerometer, a major difference is not discerned between $A_{li}^{(l)}$ and $\overline{A}_{li}^{(l)}$, it can be concluded that the natural frequency of the structure has not been changed by the addition of the accelerometer. In this case the quality of the original measurement is acceptable.
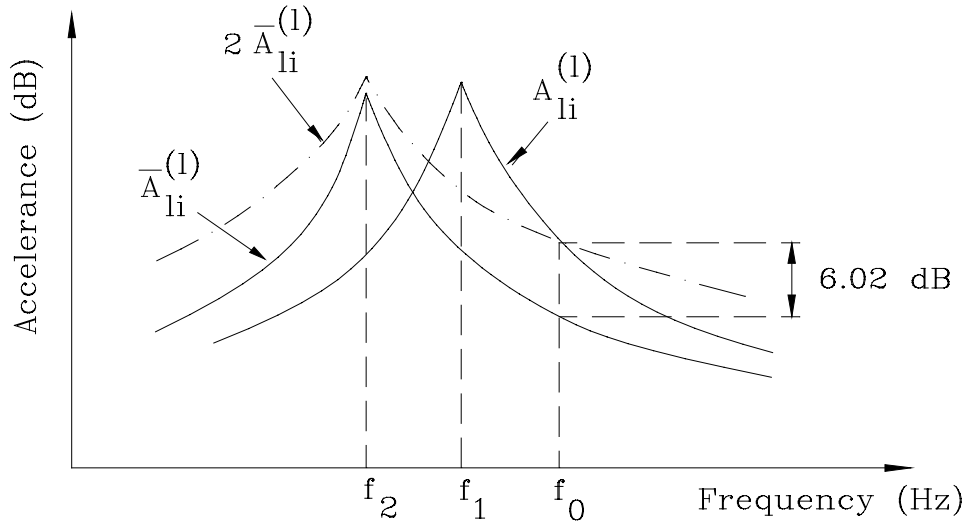
Figure 3-16. Estimation of the changes in the natural frequency of the structure by doubling the mass of the accelerometer

f_0 = Natural frequency of the structure

f_1 = Natural frequency of the structure and the accelerometer

f_2 = Natural frequency of the structure and the accelerometer and an extra mass with the same mass as that of the accelerometer.

3.5.2 Numerical case study

To examine the validity of the method presented in the previous section for assessing the quality of the measurement related to the mass-loading effect of transducers, a simulated measurement of a beam was considered. The dimensions of the beam were $20 \times 0.6 \times 44 cm$ and its material was steel. The theoretical model of the beam was built using the concept of coupling of the free-free beam elements. Figure 3-17 shows the coupling of two free-free beam elements. The receptance matrix of the element A is [96]:

$$[\alpha_A] = \begin{bmatrix} \alpha_{q_o q_o} & \alpha_{q_o r_o} & \alpha_{q_o q_l} & \alpha_{q_o r_l} \\ \alpha_{r_o q_o} & \alpha_{r_o r_o} & \alpha_{r_o q_l} & \alpha_{r_o r_l} \\ \alpha_{q_l q_o} & \alpha_{q_l r_o} & \alpha_{q_l q_l} & \alpha_{q_l r_l} \\ \alpha_{r_l q_o} & \alpha_{r_l r_o} & \alpha_{r_l q_l} & \alpha_{r_l r_l} \end{bmatrix} \tag{3-28}$$

in which q_o, q_1 and r_o, r_l are the vertical and rotational displacements of two sides of the beam element.

The elements of $[\alpha_A]$ can be computed using the beam properties given in [96]. In the same manner, the elements of $[\alpha_B]$ can be generated .

The dynamic stiffness matrix of the coupled structure can be computed from :

$$[D_{A+B}]_{6\times6} = \begin{bmatrix} [D_A]_{4\times4} & 0 & 0 \\ 0 & 0 & 0 \\ 0 & 0 & 0 \end{bmatrix}_{6\times6} + \begin{bmatrix} 0 & 0 & 0 \\ 0 & 0 & 0 \\ 0 & 0 & [D_B]_{4\times4} \end{bmatrix}_{6\times6} \tag{3-29}$$

in which $[D_A]$ and $[D_B]$ are the dynamic stiffness matrices of element *A* and element *B.*

The complete coupling procedure is explained in [5]. In the same manner as the coupling of two elements, based on the number of the elements all the beam elements can be coupled to obtain the dynamic stiffness matrix of the beam. In this numerical example the beam was divided into four elements (see Figure 3-18).
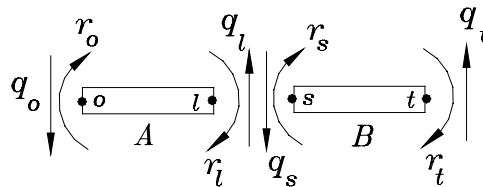
Figure 3-17. Modelling of a free-free beam
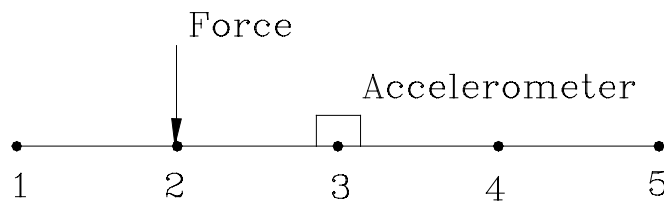
Figure 3-18. Simulated measurement on a beam

An accelerometer with a mass of 0.02 kg was added to the beam at point 3 using the following equation:

$$D^{md}(3,3) = D(3,3) - m_a\omega^2 \qquad\qquad (\textbf{3-30})$$

Here 3 refers to the translational DOF at point 3. In the simulated test the beam was excited at point 2 and the response was measured at point 3. An extra mass of 0.02 kg was then added to the accelerometer and the simulated   measurement computed. Figure 3-19 shows the FRF in the region of the third mode of the beam. As can be seen, the predicted natural frequency (the intersection of the two dashed lines) is the same as the exact natural frequency of the beam. The results of this simulated measurement confirm the validity of the method.
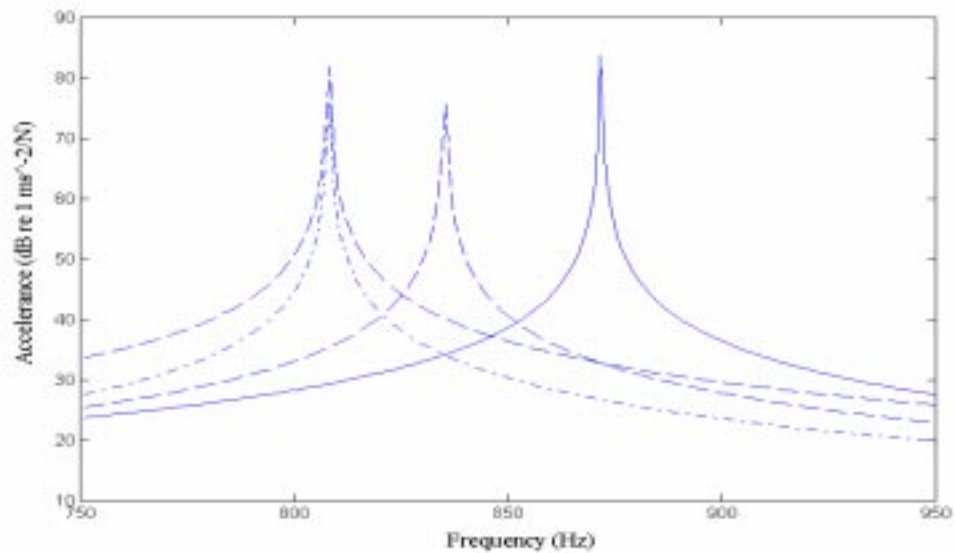
Figure 3-19. Prediction of the exact natural frequency of a beam in a numerical example

A_{32} (Solid), $A_{32}^{(3)}$ (Dashed), $\overline{A}_{32}^{(3)}$ (Dashdot), $2\times\overline{A}_{32}^{(3)}$ (Dashed)

A_{32} Accelerance of the structure

$A_{32}^{(3)}$ Accelerance of the structure and the accelerometer

$\overline{A}_{32}^{(3)}$ Accelerance of the structure and the accelerometer and an extra mass with the same mass as that of the accelerometer

3.5.3 Experimental case study

A simple beam was used for the experimental validation of the method presented in section 3.5.1. The beam was made of mild steel and had dimensions of $2 \times 0.6 \times 44 cm$ and a weight of 0.412 Kg. The experimental model of the beam was divided in to 6 equal elements and was tested in a free-free configuration, suspended by a soft elastic cord attached to the beam at point 1 as shown in Figure 3-20.
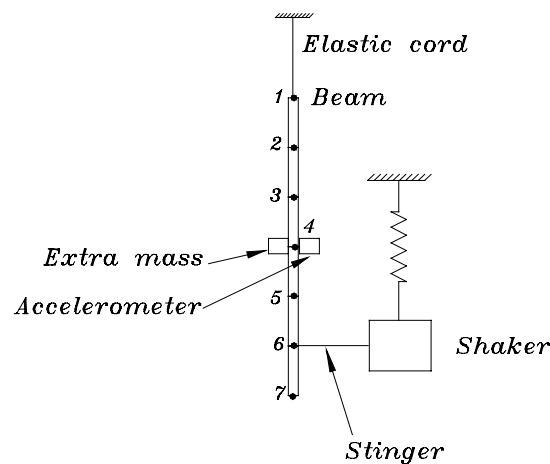
Figure 3-20. Assessment of the mass-loading effect of an accelerometer

The beam was excited at point 6 by a shaker and the response was measured at point 4 using an accelerometer with a mass of 0.03 Kg. After testing the structure, an extra mass with the same mass of the accelerometer (0.03 Kg) was added to the beam at point 4 on the other side of the beam (Figure 3-20) and the beam was remeasured. Figure 3-21 shows the result of the measurement in the frequency range of 0-1200 Hz. A comparison between $A_{46}^{(4)}$ and $\overline{A}_{46}^{(4)}$ in Figure 3-21 shows that there is no considerable change in the first and second natural frequencies of the beam relating to the mass-loading effect of the accelerometer. However, for the third natural frequency of the beam, the difference between $A_{46}^{(4)}$ and $\overline{A}_{46}^{(4)}$ is not negligible. The exact resonance of the beam is at 883 Hz (The intersection of $A_{46}^{(4)}$ and $2 \times \overline{A}_{46}^{(4)}$, the solid and dashdot lines, in Figure 3-21) while the measured FRF, $A_{46}^{(4)}$, shows this to be at 834 Hz. It should be noted that the difference between $A_{46}^{(4)}$ and $\overline{A}_{46}^{(4)}$ at 883 Hz is 6 dB which was predicted in the theoretical part of the method. A 49 Hz error for the

third resonance of the beam is not acceptable. In this test we used a heavy accelerometer to demonstrate the method for assessing the quality of the measurement. In principle, we have to use the lightest available accelerometer in order to decrease the mass-loading effect of the accelerometer as much as possible. In the next section a test strategy will be suggested to deal with the mass-loading effects of accelerometers.
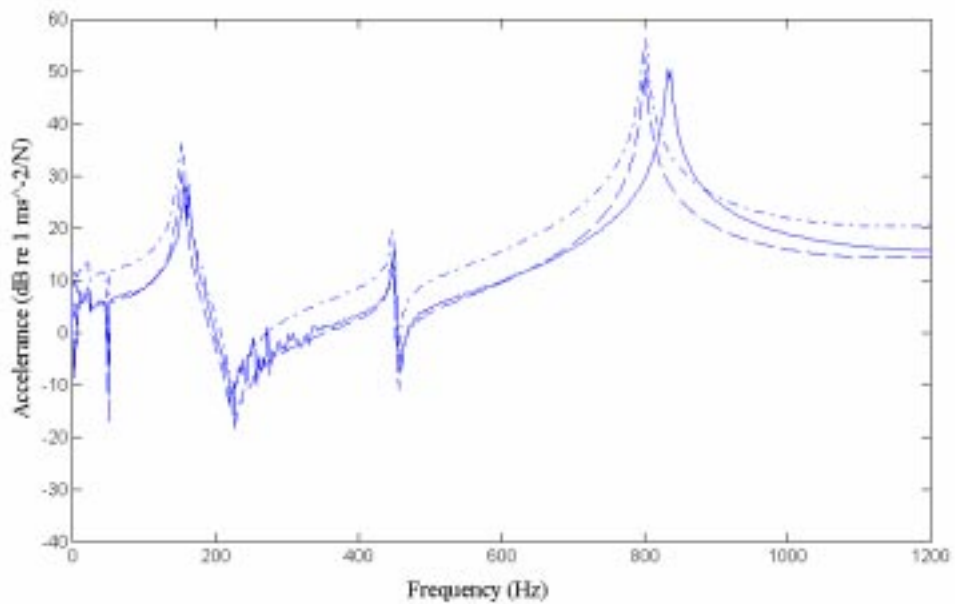
Figure 3-21. Estimation of the error relating to mass-loading effect

$$A_{46}^{(4)} \text{ (Solid)}, \ \overline{A}_{46}^{(4)} \text{ (Dashed)}, \ 2 \times \overline{A}_{46}^{(4)} \text{ (Dashdot)}$$

$A_{46}^{(4)}$ Accelerance of the structure and the accelerometer

$\overline{A}_{46}^{(4)}$ Accelerance of the structure and the accelerometer and an extra mass with the same

          mass as that of the accelerometer

3.5.4 Recommended test strategy

Clearly, a light accelerometer has the least mass-loading effect on the test structure. However, light accelerometers have low sensitivity. Moreover, light accelerometers are expensive and are not always available. Among the available accelerometers, the one which can measure the responses of the structure in the desired frequency range

and has the least mass, is the best choice. After choosing a suitable accelerometer, the following procedure is suggested for dealing with the mass-loading effect of the accelerometer in the test:

1- Test the structure using the selected accelerometer.

2- Add an extra mass with the same mass as that of the accelerometer to the structure at the point of the measurement of the response and repeat the measurement.

3- Estimate the exact natural frequencies of the structure using the method suggested in section 3.5.1.

4- If the changes in the natural frequency due to the mass-loading effect of the structure can not be ignored for a mode of the structure then use the correction method presented in this chapter to cancel the mass-loading effect of the accelerometer.

It should be noted that an accelerometer may affect some of the modes of a structure while other modes remain unchanged. If the accelerometer is attached to the structure near a node of a particular mode of the structure that mode remains unchanged. In this case the mass cancellation correction is less urgent. However, if we now move to another position near the antinode of that same mode, mass cancellation may well be important.

3.6 Conclusions

- In this chapter a SMURF method was presented for the correction of the mass-loading effects of transducers based on two tests with two different masses of accelerometer.

- The method improves the quality of measured FRFs. However, there are some pitfalls in the method when we use noisy data. In this case the correction should be made with caution.

- The calibration of the test set up can be checked by the method suggested in this chapter.

- The quality of the measurement relating to the mass-loading effect of the accelerometer can be assessed by estimating the exact natural frequency of the structure using the method presented in this chapter.

References

Chapter 4

Correction of suspension effects in modal testing

4.1 Introduction

In modal testing, test structures are usually suspended using soft springs to approximate free-free boundary conditions. Although sometimes the addition of springs is presumed to be negligible, they introduce stiffness to the structure and can change the structure's natural frequencies and mode shapes. Moreover, for flexible structures, the lowest elastic mode may be influenced by the rigid body modes of the structure which no longer have zero natural frequencies.

Although the problem of the suspension effects on the test structure is a basic problem in modal testing, there is no specific technique to quantify and to correct it. In this chapter a method will be presented for the correction of the suspension effects of the springs.

4.2 Theory

4.2.1 Modification of the structure by a suspension spring

For the simplest case, in laboratory-based modal analysis, the structure can be suspended from one spring. The gravity load of the structure exerts a tension on the spring and stretches it to a point where the gravity force is balanced by the reaction force of the spring.

As is usually the case in modal testing, the system is presumed to be linear. The linearity assumption is especially necessary for the suspension springs and throughout this chapter the springs are presumed to move in the linear range.

Changes in the FRF of a system due to the addition of a spring can be computed using direct substructuring technique SMURF as follows :

Figure 4-1(a) indicates a structure which has been connected to the second system of a spring. The connection is at point j and in vertical direction (z). The force excites the structure at point i and the response is measured at point l. Figure 4-1(b) indicates the free body diagram of the system.

The equations governing the coupled system are :

$$Z_l = \alpha_{li} F_i + \alpha_{lj} R_j \qquad (4\text{-}1)$$

$$Z_j = \alpha_{ji} F_i + \alpha_{jj} R_j \qquad (4\text{-}2)$$

$$Z_m = \alpha_{mm} R_m \qquad (4\text{-}3)$$

where :

$$\alpha_{mm} = \frac{1}{k_1} \qquad (4\text{-}4)$$

and the constraining equations are :

$$Z_j = Z_m \qquad (4\text{-}5)$$

$$R_j + R_m = 0 \qquad (4\text{-}6)$$

Elimination of the reaction forces and displacements at the connection point results in:

$$Z_l = (\alpha_{li} - \frac{\alpha_{ji} \alpha_{lj}}{\alpha_{mm} + \alpha_{jj}}) F_i = \alpha_{li}^{(j)} . F_i \qquad (4\text{-}7)$$

in which $\alpha_{li}^{(j)}$ is the coupled receptance function between points i and l when the second system is a spring with the stiffness of k_1 and is connected to the original system at point j. Inserting equation (4-4) into (4-7), the relation between $\alpha_{li}^{(j)}$ and original system receptances is :
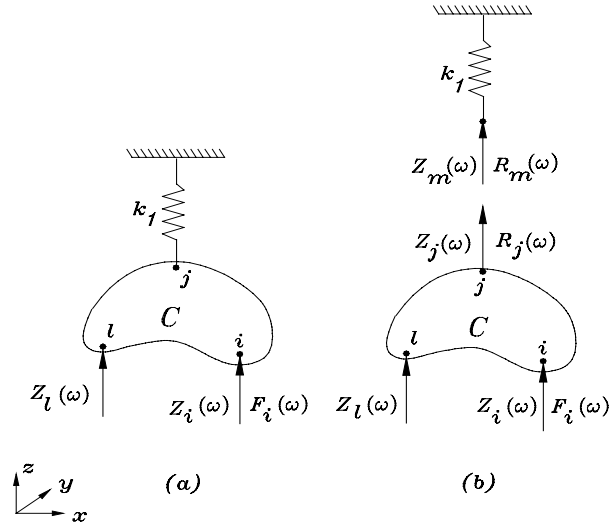
Figure 4-1. Suspension of a structure using a spring and its free body diagram

$$\alpha_{li}^{(j)} = \alpha_{li} - \frac{\alpha_{ji}\alpha_{lj}}{\dfrac{1}{k_1} + \alpha_{jj}} \tag{4-8}$$

in which α_{li}, α_{ji}, α_{lj}, α_{jj} are the exact receptances, namely for the system without the connected spring. Multiplying both sides by $(-\omega^2)$ and the numerator and denominator of the fraction on the right hand side of equation (4-8) by $(-\omega^2)$, the relation between accelerances is :

$$A_{li}^{(j)} = A_{li} - \frac{A_{ji}A_{lj}}{\dfrac{-\omega^2}{k_1} + A_{jj}} \tag{4-9}$$

There are two special cases of the equation (4-9) which are needed for the calculations of the next sections. For the driving point accelerance ($i=l$) of the excitation point, equation (4-9) can be written as :

$$A_{ll}^{(j)} = A_{ll} - \frac{(A_{jl})^2}{\dfrac{-\omega^2}{k_1} + A_{jj}} \tag{4-10}$$

and for the driving point accelerance of the response point (*l=i*), equation (4-9) can be written as :

$$A_{ii}^{(j)} = A_{ii} - \frac{(A_{ji})^2}{\dfrac{-\omega^2}{k_1} + A_{jj}}$$

(4-11)

It will be shown in the next chapters that the equations governing the case of springs are similar to those of the stingers and inertia property of an attached object. Therefore the results for the spring case can be applied for those cases as well.

4.2.2 Application of the theory to the correction of FRFs

Correction of FRFs in the case of springs is different from that of accelerometers because the point at which response is measured (*l*) differs from the point at which the spring is attached (*j*). Moreover, practically, measurement or excitation at the point of attachment of the spring is not always possible, in other words usually accelerances such as $A_{jl}^{(j)}$, $A_{jj}^{(j)}$ are not available. The following method is the development of the method expressed previously in chapter 3 to correct the mass-loading effects of accelerometers.

Equation (4-9) shows how the measured accelerance $A_{li}^{(j)}$ is related to the correct accelerances, A_{li}, $A_{jl}A_{li}$, A_{jj}. To find the correct FRFs, measurement of $A_{li}^{(j)}$ can be considered with three different springs of different stiffnesses (Figure 4-2).
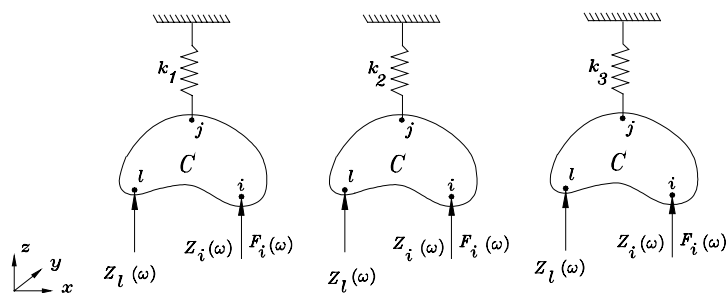
Figure 4-2. Measurement using three different springs

Where k_1, k_2, k_3 are different in amount. The equations governing the systems are :

$$\begin{cases} A_{li}^{(j)} = A_{li} - \dfrac{A_{jl}A_{ji}}{\dfrac{-\omega^2}{k_1} + A_{jj}} \\[3em] \overline{A}_{li}^{(j)} = A_{li} - \dfrac{A_{jl}A_{ji}}{\dfrac{-\omega^2}{k_2} + A_{jj}} \\[3em] \overline{\overline{A}}_{li}^{(j)} = A_{li} - \dfrac{A_{jl}A_{ji}}{\dfrac{-\omega^2}{k_3} + A_{jj}} \end{cases} \qquad (4\text{-}12)$$

in which $A_{ll}^{(j)}$, $\overline{A}_{ll}^{(j)}$, $\overline{\overline{A}}_{ll}^{(j)}$ are different in amount. The general form of the equations (4-12) can be written as :

$$\begin{cases} b_1 = \gamma - \dfrac{\lambda}{a_1 + \beta} \\[2em] b_2 = \gamma - \dfrac{\lambda}{a_2 + \beta} \\[2em] b_3 = \gamma - \dfrac{\lambda}{a_3 + \beta} \end{cases} \qquad (4\text{-}13)$$

in which γ, λ, β are unknown values and a_1, a_2, a_3, b_1, b_2, b_3 are known values. Equations (4-13) can be rewritten as :

$$\begin{cases} a_1\gamma - b_1\beta + \gamma\beta - \lambda = a_1 b_1 \\ a_2\gamma - b_2\beta + \gamma\beta - \lambda = a_2 b_2 \\ a_3\gamma - b_3\beta + \gamma\beta - \lambda = a_3 b_3 \end{cases} \qquad (4\text{-}14)$$

Equations (4-14) are nonlinear equations. However, if the first equation is subtracted from the second equation and the third equation, we have two linear equations instead. Thus :

$$\begin{cases} (a_2 - a_1)\gamma - (b_2 - b_1)\beta = a_2 b_2 - a_1 b_1 \\ (a_3 - a_1)\gamma - (b_3 - b_1)\beta = a_3 b_3 - a_1 b_1 \end{cases} \tag{4-15}$$

or in matrix form :

$$\begin{bmatrix} a_2 - a_1 & b_1 - b_2 \\ a_3 - a_1 & b_1 - b_3 \end{bmatrix} \begin{Bmatrix} \gamma \\ \beta \end{Bmatrix} = \begin{Bmatrix} a_2 b_2 - a_1 b_1 \\ a_3 b_3 - a_1 b_1 \end{Bmatrix} \tag{4-16}$$

Equation (4-16) can be solved for γ , β :

$$\begin{Bmatrix} \gamma \\ \beta \end{Bmatrix} = \left(\begin{bmatrix} a_2 - a_1 & b_1 - b_2 \\ a_3 - a_1 & b_1 - b_3 \end{bmatrix} \right)^{-1} \begin{Bmatrix} a_2 b_2 - a_1 b_1 \\ a_3 b_3 - a_1 b_1 \end{Bmatrix} \tag{4-17}$$

From equation (4-13), λ can be found :

$$\lambda = (\gamma - b_1)(a_1 + \beta) \tag{4-18}$$

Using equations (4-17) and (4-18), equations (4-12) can be solved for A_{li}, $A_{jl} A_{ji}$ and A_{jj} .

$$\begin{Bmatrix} A_{li} \\ A_{jj} \end{Bmatrix} = \left(\begin{bmatrix} -\omega^2 (\dfrac{1}{k_2} - \dfrac{1}{k_1}) & A_{li}^{(j)} - \overline{A}_{li}^{(j)} \\ -\omega^2 (\dfrac{1}{k_3} - \dfrac{1}{k_1}) & A_{li}^{(j)} - \overline{\overline{A}}_{li}^{(j)} \end{bmatrix} \right)^{-1} \begin{Bmatrix} -\omega^2 (\dfrac{\overline{A}_{li}^{(j)}}{k_2} - \dfrac{A_{li}^{(j)}}{k_1}) \\ -\omega^2 (\dfrac{\overline{\overline{A}}_{li}^{(j)}}{k_3} - \dfrac{A_{li}^{(j)}}{k_1}) \end{Bmatrix} \tag{4-19}$$

and :

$$A_{jl} A_{ji} = (A_{li} - A_{li}^{(j)})(\dfrac{-\omega^2}{k_1} + A_{jj}) \tag{4-20}$$

Therefore using equations (4-19) and (4-20), the measured FRF is corrected and the driving point FRF of the point of the attachment of the spring has been obtained. However, one question remains and is whether other transfer FRFs like A_{ji} and A_{jl} are obtainable using this method or not. If $A_{ll}^{(j)}$ is measured twice with two different springs k_1 and k_2, from equation (4-10) the governing equations of the systems are :

$$\left\{ \begin{array}{l} A_{ll}{}^{(j)} = A_{ll} - \dfrac{(A_{jl})^2}{\dfrac{-\omega^2}{k_1} + A_{jj}} \\[4em] \overline{A}_{ll}{}^{(j)} = A_{ll} - \dfrac{(A_{jl})^2}{\dfrac{-\omega^2}{k_2} + A_{jj}} \end{array} \right. \tag{4-21}$$

in which $A_{ll}{}^{(j)}$ is different from $\overline{A}_{ll}{}^{(j)}$. There are only two unknown values and just two measurements are needed because A_{jj} is known from the last stage. In this case, the general form of the equations are :

$$\left\{ \begin{array}{l} b_1 = \gamma - \dfrac{\lambda}{a_1} \\[1.5em] b_2 = \gamma - \dfrac{\lambda}{a_2} \end{array} \right. \tag{4-22}$$

or, in matrix form:

$$\begin{bmatrix} a_1 & -1 \\ a_2 & -1 \end{bmatrix} \begin{Bmatrix} \gamma \\ \lambda \end{Bmatrix} = \begin{Bmatrix} a_1 b_1 \\ a_2 b_2 \end{Bmatrix} \tag{4-23}$$

from which one can compute for γ, λ :

$$\begin{Bmatrix} \gamma \\ \lambda \end{Bmatrix} = \left(\begin{bmatrix} a_1 & -1 \\ a_2 & -1 \end{bmatrix} \right)^{-1} \begin{Bmatrix} a_1 b_1 \\ a_2 b_2 \end{Bmatrix} \tag{4-24}$$

From equation (4-24) one can compute A_{ll} and $(A_{jl})^2$:

$$\begin{Bmatrix} A_{ll} \\ (A_{jl})^2 \end{Bmatrix} = \left(\begin{bmatrix} \dfrac{-\omega^2}{k_1} + A_{jj} & -1 \\[1.5em] \dfrac{-\omega^2}{k_2} + A_{jj} & -1 \end{bmatrix} \right)^{-1} \begin{Bmatrix} (\dfrac{-\omega^2}{k_1} + A_{jj}) A_{ll}^{(j)} \\[1.5em] (\dfrac{-\omega^2}{k_2} + A_{jj}) \overline{A}_{ll}^{(j)} \end{Bmatrix} \tag{4-25}$$

Now if $A_{ii}{}^{(j)}$ is measured once, equation (4-11) is the governing equation. From the last stages $A_{jl} A_{ji}$ and $(A_{jl})^2$ are known, from which $(A_{ji})^2$ can be computed:

$$(A_{ji})^2 = \frac{(A_{jl}A_{ji})^2}{(A_{jl})^2} \tag{4-26}$$

So from equation (4-11), A_{ii} can be computed:

$$A_{ii} = A_{ii}^{(j)} - \frac{(A_{ji})^2}{\dfrac{-\omega^2}{k_1} + A_{jj}} \tag{4-27}$$

Using this technique, the correct values of A_{ll}, A_{ii} and A_{li} can be computed. Although $(A_{ji})^2$, $A_{jl}A_{ji}$ and $(A_{jl})^2$ are known, the correct phases of A_{ji} and A_{jl} are not available from these known values. However, the correct magnitudes of A_{ji} and A_{jl} are obtainable. If $A_{jl}^{(j)}$ or $A_{ji}^{(j)}$ could be measured, the correct amount of A_{ji} and A_{jl} would be obtainable.

4.2.3 Correction of FRFs for two springs

Usually in modal testing, test objects are suspended using at least two springs. The effects of two springs on the test structure can be corrected using a step by step correction. Figure 4-3 indicates a structure which is suspended by two springs. Table 4-1 shows a procedure for correction of the FRFs using four springs k_1, k_2, k_3, k_4 with different stiffnesses. The correction has been done in two steps. The first step is the elimination of the effect of the spring k_s, and the second step is the elimination of the effect of the spring, k_j. Nine measurements are made to obtain the FRFs A_{li}, A_{ss}, A_{jj}. This is not the most efficient way to correct the FRFs but the purpose of this section is to show the feasibility of the correction of the FRFs in a systematic step by step procedure when the structure is suspended using two springs (this will be discussed in detail in chapter 6 of this thesis). What is available through this procedure is the exact measured FRF and two driving point FRFs for the point of the attachment of the springs. None of the other transfer FRFs are available, as explained in the last section.
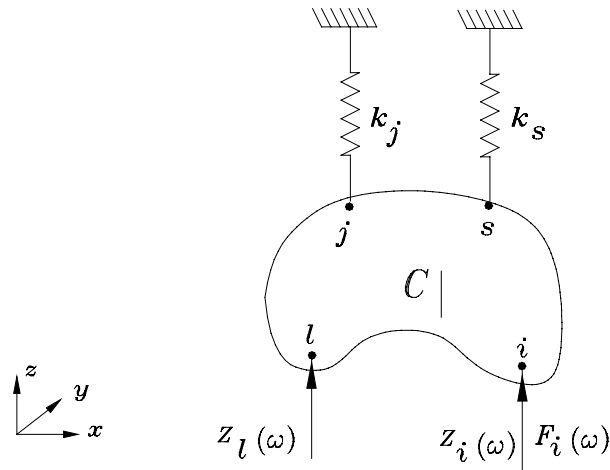
Figure 4-3. Suspension using two springs

Table 4-1. Correction of the effects of two suspension springs

k_{j}	k_s	measurements	computed terms from measurements	
k_1	k_2	$^{(1)}A_{li}^{(j,s)}$		
k_1	k_3	$^{(2)}A_{li}^{(j,s)}\quad\rightarrow$	$^{(1)}A_{li}^{(j)}$	$^{(1)}A_{ss}^{(j)}$
k_1	k_4	$^{(3)}A_{li}^{(j,s)}$		
k_2	k_1	$^{(4)}A_{li}^{(j,s)}$		
k_2	k_3	$^{(5)}A_{li}^{(j,s)}\quad\rightarrow$	$^{(2)}A_{li}^{(j)}$	$^{(2)}A_{ss}^{(j)}$
k_2	k_4	$^{(6)}A_{li}^{(j,s)}$		
k_3	k_1	$^{(7)}A_{li}^{(j,s)}$		
k_3	k_2	$^{(8)}A_{li}^{(j,s)}\quad\rightarrow$	$^{(3)}A_{li}^{(j)}$	$^{(3)}A_{ss}^{(j)}$
k_3	k_4	$^{(9)}A_{li}^{(j,s)}$		
			$\downarrow$	$\downarrow$
computed correct			A_{li}	A_{ss}
FRFs			A_{jj}	

4.3 Demonstration and verification of the method

To demonstrate the validity of the method, a simulated test of a 3 degrees-of-freedom system of masses, springs and dampers is considered (Figure 4-4).
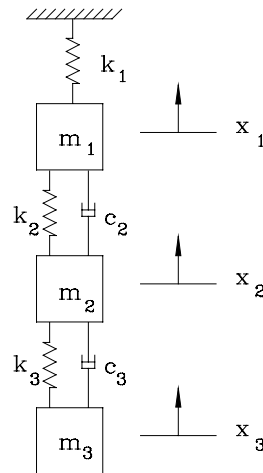
Figure 4-4. A simulated test of a 3 DOFs system

Spring k_1 is considered as the suspension spring. The rest of the system is considered as the structure (masses m_1, m_2, m_3 , springs k_2, k_3 and dampers c_2, c_3). The suspension spring, k_1, is attached to point 1. The system is excited at point 2 and the response is measured at point 3. The specifications of the system are :

$m_1 = 1$ kg , $k_1 = 2824.9$ N/m;

$m_2 = 1.3$ kg , $k_2 = 7200$ N/m , $c_2 = 0.6$ Ns/m ;

$m_3 = 2$ kg , $k_3 = 3500$ N/m , $c_3 = 0.4$ Ns/m ;

In order to cancel the effect of the spring k_1 on the measured FRF this spring was replaced with two other springs with different stiffnesses (3138.81 N/m, 3452.7 N/m) and the simulated test was repeated. Figure 4-5 shows the coincidence of the computed FRF and the exact FRF. It should be noted that noise has not been considered in the computations.
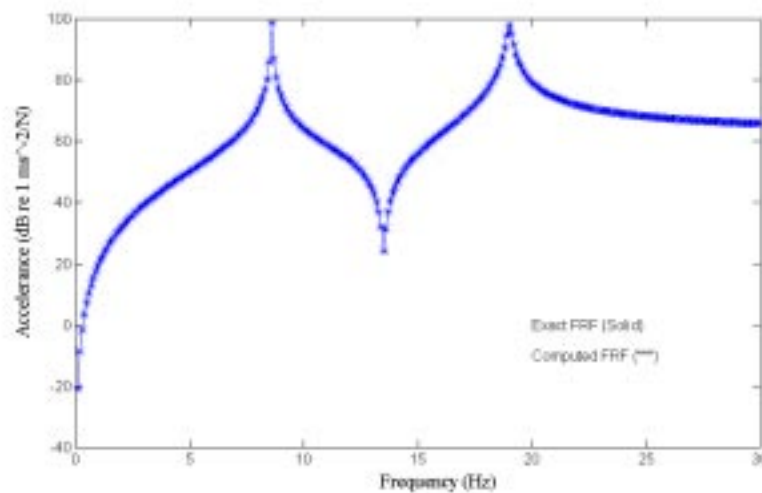
Figure 4-5. Correction of the suspension effect

4.3.1 The effect of the rigid body modes on the measured FRFs

In conventional modal testing, test structures are suspended using soft springs to prevent interference of the rigid body modes, which no longer have zero natural frequencies, with the lowest elastic mode of the structure. Wolf[40] used a system of 2 DOFs of masses and springs to investigate the effect of the rigid body modes on the measured FRFs. He suggested that the rule of thumb in simulating free-free boundary conditions is to design the support system so that the rigid body modes are no more than one-tenth of the frequency of the lowest elastic mode.

Figure 4-6 shows the effect of the rigid body modes on the measured FRFs of the system shown in Figure 4-4 for different suspension springs (k_1). Table 4-2 indicates different stiffnesses for spring k_1, the rigid body mode frequency for the corresponding suspension stiffness and the corresponding ratio of the rigid body mode natural frequency to that of the first elastic mode. As is shown in Figure 4-6, the effect of the rigid body mode is a peak to the left hand side of the measured FRF. As the suspension stiffness increases, this peak moves to the right. For case 2, the elastic modes do not change noticeably with respect to the free-free condition. For case 3, the changes are considerable and for case 4, the difference between the measured FRF and the exact FRF is excessive. For the case specified in Table 4-2, the limit of 10%

for the ratio of the natural frequency of the rigid body mode to that of the first elastic mode is a reasonable value for the design of the suspension stiffness, as suggested by Wolf [40].

Table 4-2. Specifications of different suspensions

Case	Suspension stiffness (k_1) (N/m)	Rigid body mode NF (Hz)	% of NF of the first elastic mode (8.6 Hz)
1	0	0	0 %
2	125.55	0.86	10 %
3	501.21	1.72	20 %
4	3138.81	4.3	50 %

(NF= Natural Frequency)
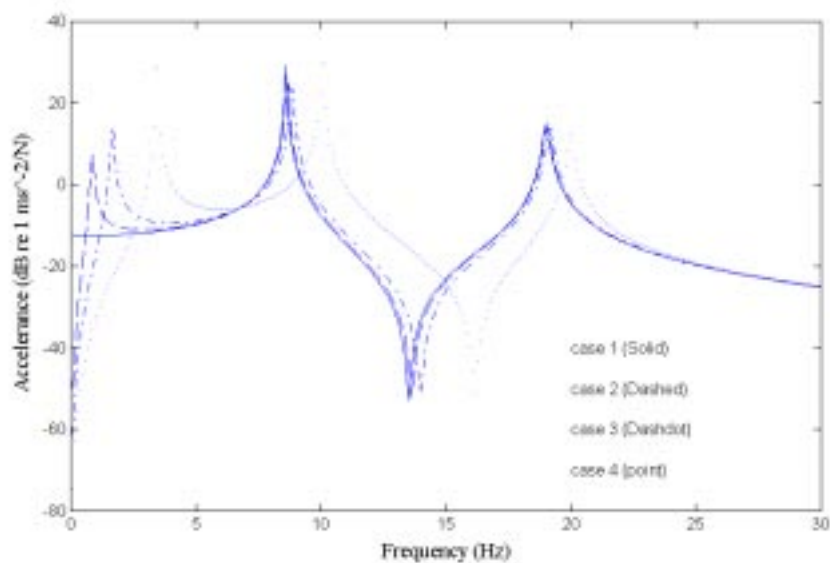
Figure 4-6. The effect of different suspension springs on the measured FRFs

4.3.2 The effect of noise on the computed FRF

In the method presented for the correction of suspension effects, computations are vulnerable to noisy FRFs. In this case, the selection of suitable values for the stiffness

of the suspension system is vital to reduce the effect of noise. Table 4-3 shows three different set of springs for the correction of noisy FRFs of the system shown in Figure 4-4. The ratio of the natural frequency of the rigid body mode to that of the first elastic mode for the first set is about 10 %, for the second set is about 20 % and for the third set is about 50 %. The FRFs of the system were polluted by adding random noise using the following relation:

$$\breve{A}_{li} = [1 + \alpha \times (2 \times RAN - 1)] \times A_{li} \tag{4-28}$$

where $\breve{A}_{li}$ is the noisy accelerance, α is the percentage of noise, *RAN* is a random value between 0 and 1 and A_{li} is the accelerance without noise. The percentage of noise in this example is 10%.

Table 4-3. Different ranges of stiffness for correction of FRFs

Set 1	Set 2	Set 3
$\frac{RGF}{FEF} \approx (10\ \%)$	$\frac{RGF}{FEF} \approx (20\ \%)$	$\frac{RGF}{FEF} \approx (50\ \%)$
113	451.089	2824.9
125.55	501.21	3138.81
138.1	551.3	3452.7

($\frac{RGF}{FEF}$ is the ratio of the natural frequency of the rigid body mode to that of the first elastic mode)

Figures 4-7, 4-8 and 4-9 show the results of the correction for the first set, second and third set of the springs, shown in Table 4-3, respectively. The result of the correction for the first set (Figure 4-7) is less noisy than the results of the other sets (Figures 4-8 and 4-9). For the third set of springs the result is dominated by noise. Moreover, these figures show that the effect of the rigid body modes is cancelled by the correction procedure.

In equation (4-19) when springs k_1, k_2 and k_3 are very stiff then the dynamic behaviour of the structure is dominated by the dynamics of the springs. So the

dynamics of the structure can hardly be monitored by the correction methods in the presence of noise. On the other hand, if springs k_1, k_2 and k_3 are very soft, the order of the changes in the FRFs of the structure will be close to the order of noise. In this case nothing can be monitored but noise.

Therefore, in order to apply the correction method presented in this chapter, suitable additive springs should be selected. If the order of changes of the measured FRFs is the same as the order of noise present in the experiment then nothing can be detected but the noisy results. On the other hand the additive springs should not make big changes in the measured FRFs. Based on the experience of this section, it is recommended that for a free-free structure, the additive springs are chosen in such a way that the ratio of the natural frequency of the rigid body mode to that of the first elastic mode of the structure is about 10% to 20%.

Although the method presented in this chapter has been presented to cancel the effect of a suspension spring on a free-free structure, it can be used to cancel the effect of springs on the structures with other boundary conditions. In the next section an application of the correction method presented in this chapter will be demonstrated for the case of a cantilever beam.
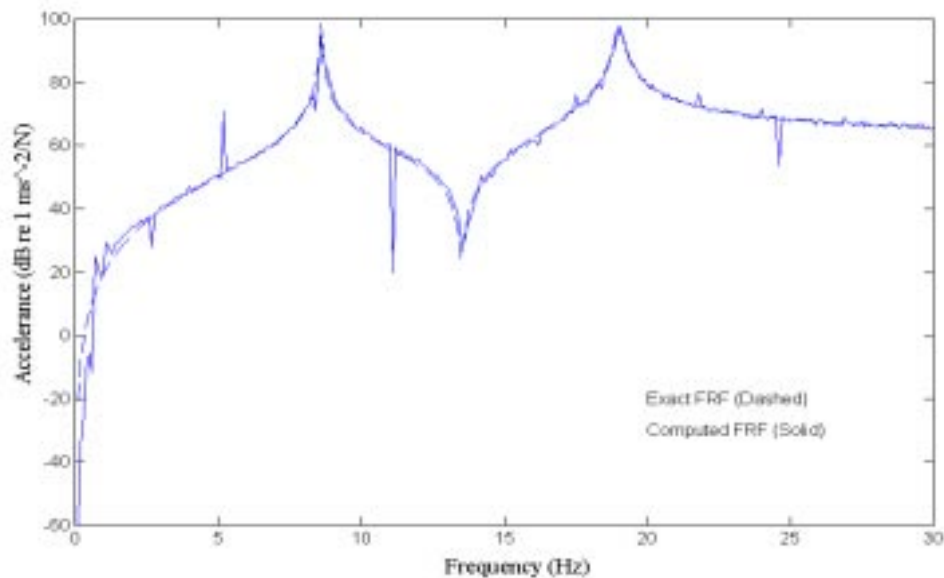
Figure 4-7. Correction of FRFs (Set 1)
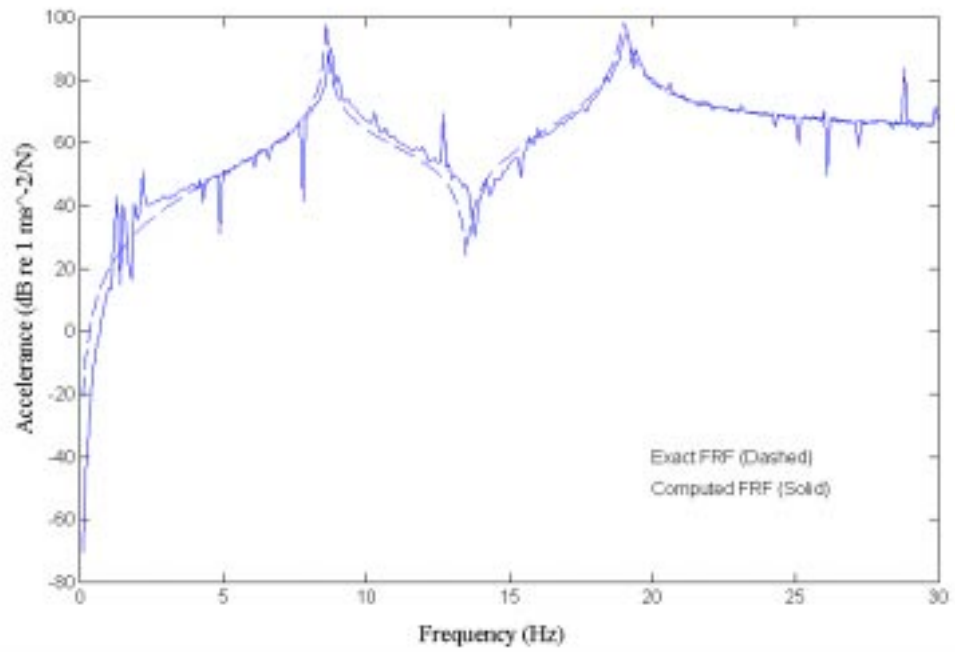
Figure 4-8. Correction of FRFs (Set 2)
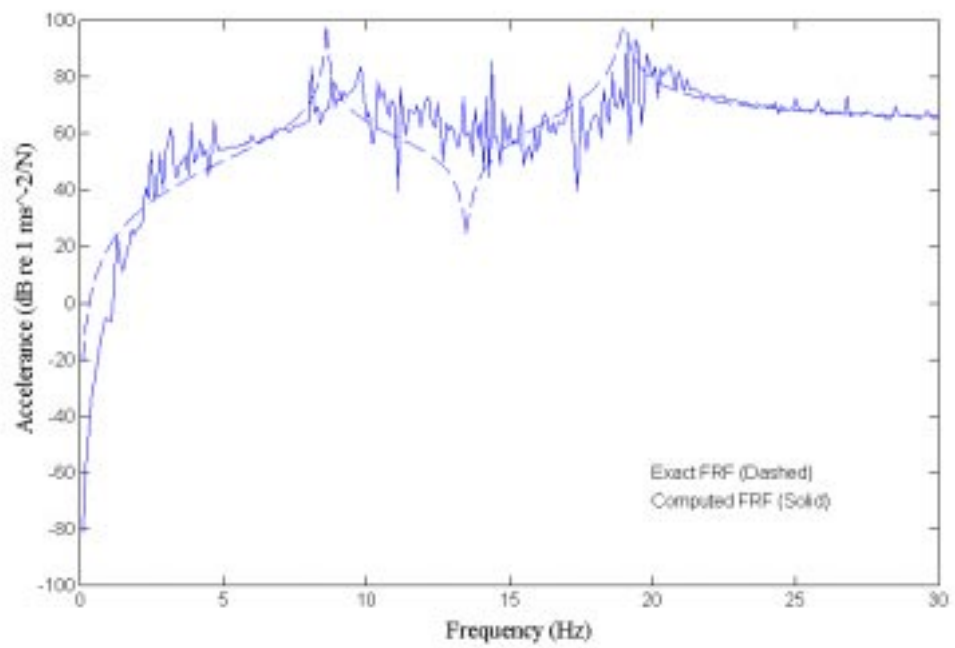
Figure 4-9. Correction of FRFs (Set 3)

4.3.3 Demonstration of the correction method

A cantilever (clamped-free) beam was used for demonstrating the correction method presented in this chapter in an actual test. The beam was made of steel and had dimensions $0.95 \times 0.024 \times 45 cm$. Figure 4-10 shows the experimental set up for the hammer test of the beam. The beam was clamped from one side using a massive fixture and was suspended from its middle point so that it remained straight. The beam was excited at its free end (point 3 in Figure 4-10) and the response was measured at the same point.
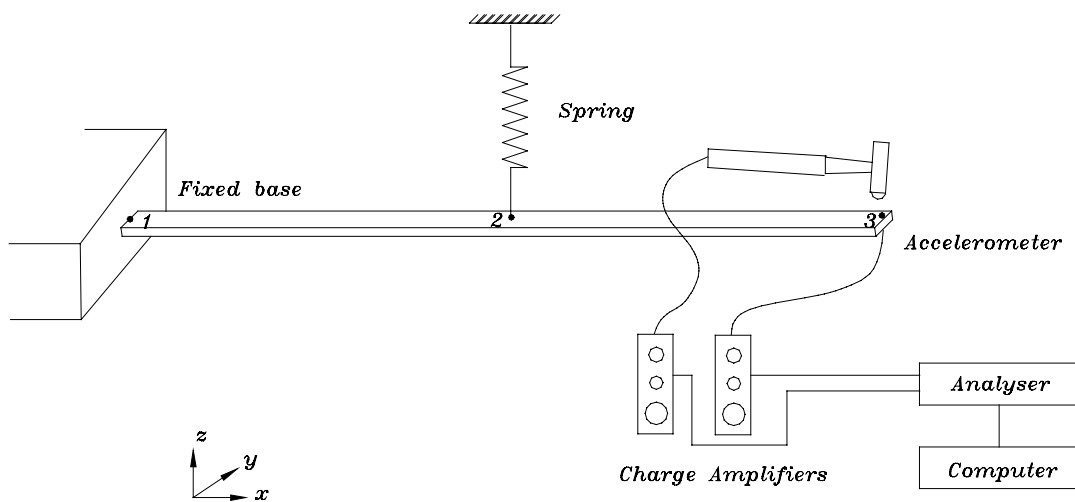
Figure 4-10. Experimental set-up for hammer testing of a cantilever beam

Addition of the suspension spring to the beam has three benefits. First, as the beam is a long beam, in the sense that the length of the beam is much longer than its width and thickness, due to its weight, the beam cannot remain straight without using a suspension spring. Second, because of the flexibility of the beam, the input force is low. The low-input force reduces the level of signal-to-noise ratio and as a result the measured FRFs are noisy. Addition of a spring makes the beam more stiff which allows us to obtain less noisy FRFs. Third, due to the large deflections, the beam may exhibit nonlinear behaviour. Addition of the spring reduces the amplitude of the vibration and this linearises the dynamic behaviour of the system (The effect of

nonlinearity on the correction methods of mechanical devices is the subject of chapter 7 of this thesis).

Three tests using three helical springs were conducted. The stiffness of springs were estimated experimentally to be 3000 N/m, 6000 N/m and 8700 N/m. Figure 4-11 shows the results of the measurements for the third mode of the beam. The additive springs make reasonable changes in the measured FRF. As the stiffness of the suspension spring increases, the natural frequency of the system shifts to the higher frequencies.

As noise pollutes the result of the computations, the three measured FRFs were regenerated using ICATS program. The result of the regeneration was carefully controlled to match the raw data. Using the method suggested in this chapter for the correction of suspension effects, the FRFs were corrected. Figures 4-12 and 4-13 show the computed FRFs. An interesting point is that the driving-point FRF (A_{22}) was obtained without measurement.
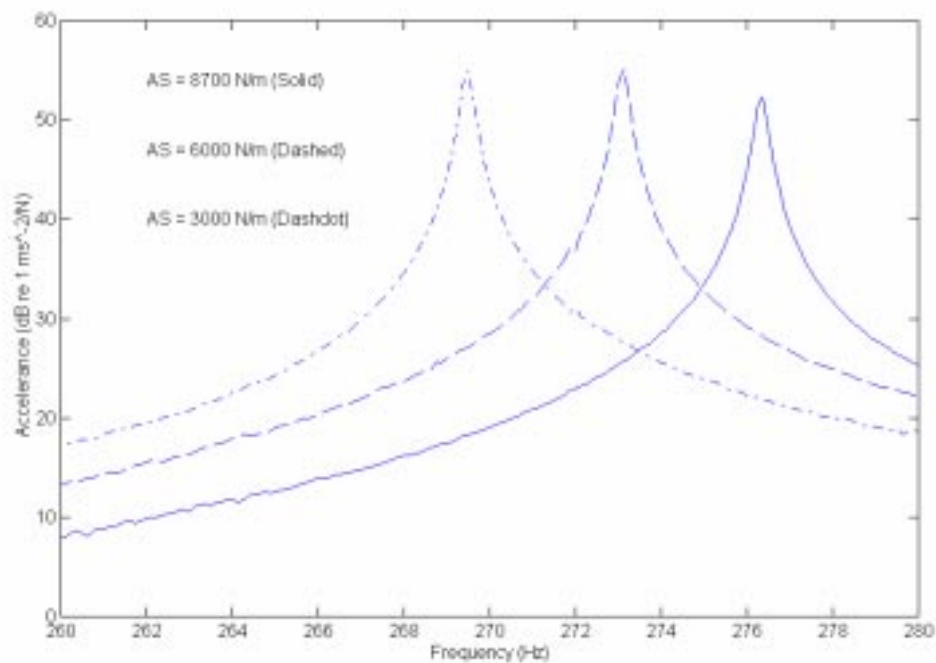
Figure 4-11. The effect of addition of a spring to the cantilever beam

(AS = Additive Stiffness)
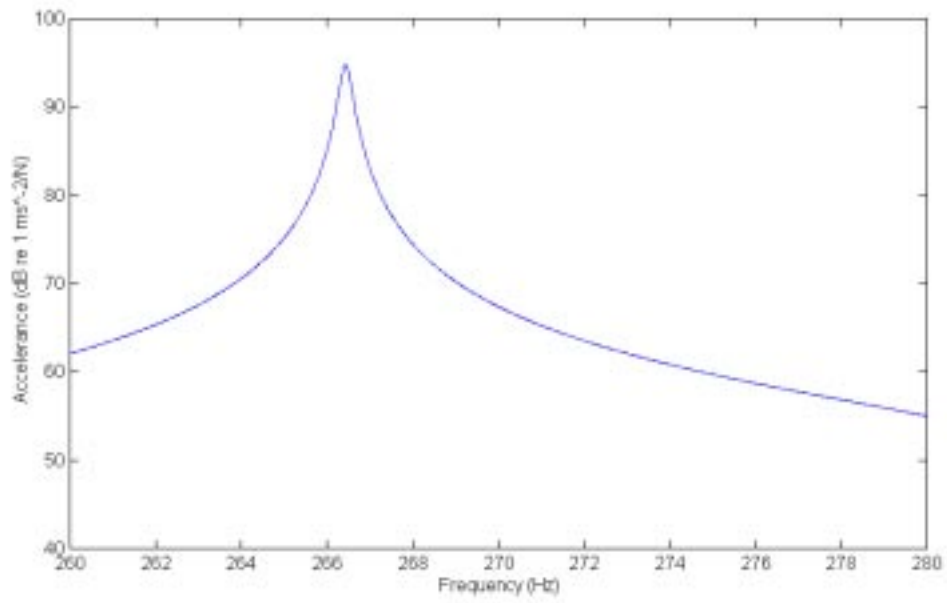
Figure 4-12. Computed FRF A_{33}
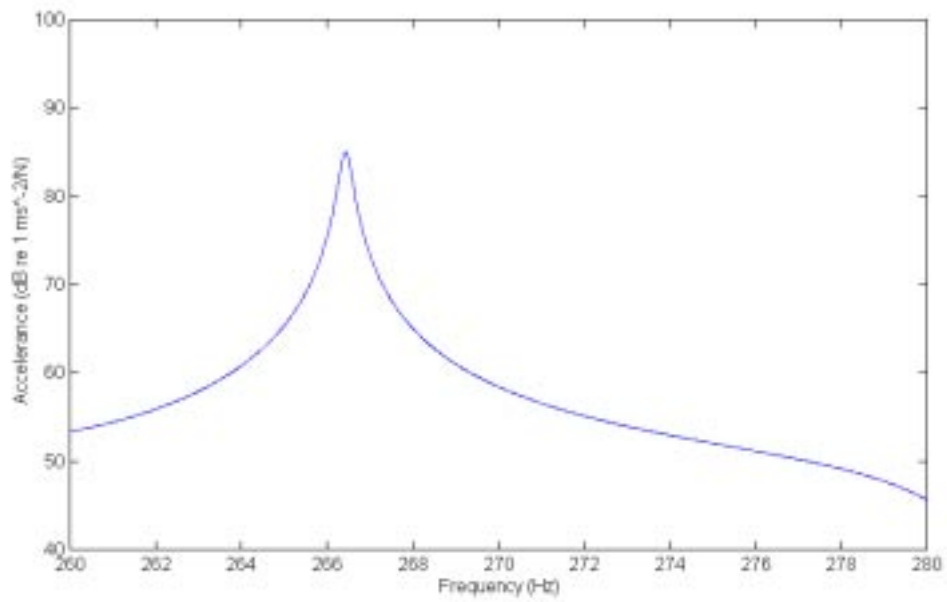
Figure 4-13. Computed FRF A_{22}

In the next stage we moved the accelerometer to point 2 (see Figure 4-10) and measured $A_{23}^{(2)}$ using the spring with the stiffness of 6000 N/m, the exact FRF A_{23} was computed from:

$$A_{23}^{(2)} = \frac{A_{23}}{A_{22} - \dfrac{\omega^2}{k}} \qquad \textbf{(4-29)}$$

As A_{22} was computed already, A_{23} could be obtained using only one measurement. One way of assessing the success of the method is to conduct an internal check of the computed FRFs using their modal constants. In principle, the following equation should hold between the modal constants of the measured FRFs of the beam:

$$_3\mathbf{A}_{33} = \frac{(_3\mathbf{A}_{23})^2}{_3\mathbf{A}_{22}} \qquad \textbf{(4-30)}$$

where $_r\mathbf{A}_{jk}$ is the modal constant for mode r and coordinates j and k. On this basis the required FRFs for equation (4-30) were regenerated and their modal constants derived using the ICATS program. The modal constant for A_{33} was obtained 62.78, for A_{22} was obtained 23.33 and for A_{23} was obtained 37.15. The result of the calculation for the right hand side of equation (4-30) is 59.16 which is close to 62.78 for the left hand side. The result of this experiment show that the two sides of equation (4-30) above are close together, demonstrating that the method is valid and applicable.

4.4 Assessment of the quality of the measurement of a free-free structure

In conventional modal testing, test structures are usually suspended using soft springs to approximate free-free boundary conditions and, as a result, the effects of these mechanical devices on the measured FRFs are considered negligible. In this section a method will be suggested for assessing the quality of the measurements related to the suspension effects. Here the emphasis is to use the theory presented earlier in this chapter for the correction of suspension effects on the measured FRFs.

4.4.1 Assessment of the quality of measurement based on the changes in the natural frequencies of the structure

As shown in section 4.2.2 when the structure is suspended from a point, the effect of the suspension spring on the measured FRFs can be corrected using equation (4-19). In this case the frequencies that make the determinant of the matrix:

$$
\begin{bmatrix}
-\omega^2(\dfrac{1}{k_2} - \dfrac{1}{k_1}) & A_{li}^{(j)} - \overline{A}_{li}^{(j)} \\
-\omega^2(\dfrac{1}{k_3} - \dfrac{1}{k_1}) & A_{li}^{(j)} - \overline{\overline{A}}_{li}^{(j)}
\end{bmatrix}
\tag{4-31}
$$

equal to zero are the exact natural frequencies of the structure. A comparison between the natural frequencies of the modified structure and the exact natural frequencies of the structure can show us the quality of the measurement. However, measurement of the structure three times using a different suspension spring in each test is a time-consuming process. In this case the following approximate method is suggested to reduce the number of required measurements for assessing the quality of the measurement:

In equation (4-8), the frequencies that make the denominator, $1/k_1 + \alpha_{jj}$, equal to zero give us the natural frequencies of the modified structure. This means that the natural frequencies of the modified structure are at the frequencies where:

$$
\frac{1}{\alpha_{jj}(\omega)} = -k_1
\tag{4-32}
$$

Figure 4-14 shows a typical linear graph of the inverse of the driving point receptance (or the dynamic stiffness) of a point on a beam in the region of one of the modes of the beam. At 871.6 Hz the dynamic stiffness of the beam is equal to zero which is the natural frequency of the beam. In the frequency range of 871.6-1600 Hz the dynamic stiffness of the beam is negative. Therefore, when a spring is attached to the beam at this point, according to equation (4-32), the new natural frequency of the modified

beam is a frequency point in the range of 871.6-1600 Hz where the magnitude of the dynamic stiffness of the beam is equal to the stiffness of the suspension spring.
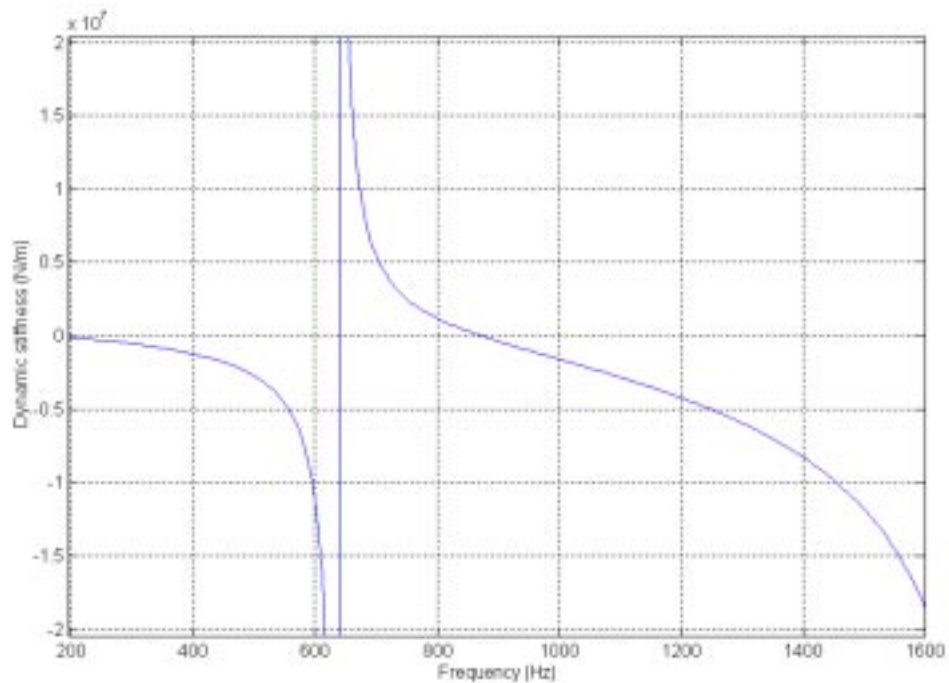
Figure 4-14. The linear graph of the inverse of the receptance around one of the natural frequencies of a beam

Figure 4-15 shows the change in the natural frequency of a structure when the structure is modified by a suspension spring with the stiffness of k_1. In this case the natural frequency of the structure shifts from f_0 to f_1. If the structure is suspended using another spring with the stiffness of k_2, where $k_2 = 2k_1$, the resonance of the structure shifts to f_2.

From the geometry of triangle *ABD* we have:

$$\frac{BC}{CD} = \frac{AF}{DF} = \frac{AE}{BE} = 1 \qquad\qquad \textbf{(4-33)}$$

or:

$$BC = CD \qquad\qquad \textbf{(4-34)}$$

We have:

$$BC = f_2 - f_1 \tag{4-35}$$

As we get closer to the natural frequency of the structure, the behaviour of the dynamic stiffness of the beam becomes more linear. This means that if the structure is suspended using very soft spring, point D (in figure 4-15) become closer to the natural frequency of the structure, f_0, and from relation (4-34) we have:

$$f_2 - f_1 \approx f_1 - f_0 \tag{4-36}$$

However, as the stiffness of the suspension spring increases two sides of equation (4-36) differ more. This can be seen from Figure 4-15.
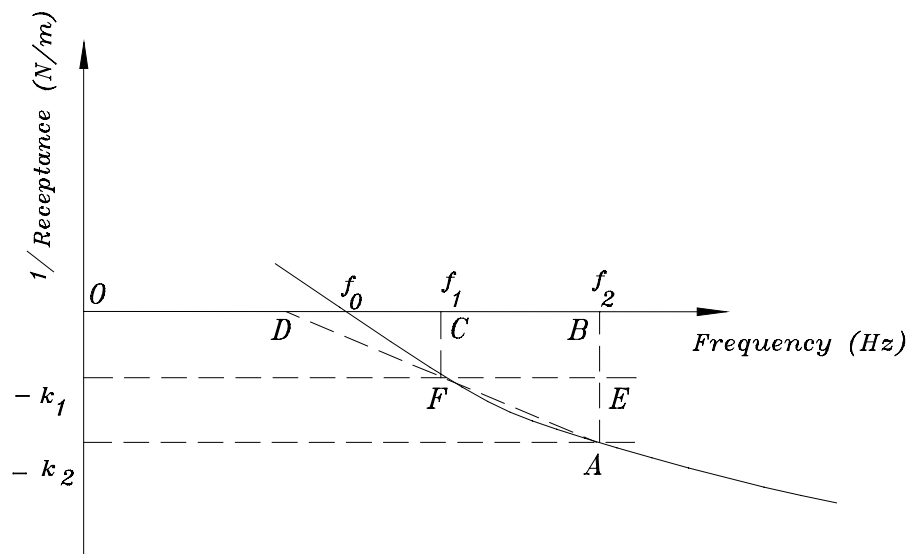
Figure 4-15. Estimation of the changes in the natural frequency of a suspended structure

This means if by doubling the stiffness of the suspension spring the natural frequency of the modified structure does not change discernibly, two sides of equation 4-36 are almost the same and the difference between f_2 and f_1 can monitor the quality of the measurement. Conversely, when by doubling the stiffness of the suspension spring the natural frequency of the structure has a discernible change, two sides of equation (4-36) are not the same but we can conclude that f_1 and f_0 differ considerably as well.

Therefore we can assess the quality of the measurement by doubling the stiffness of the suspension spring

4.4.2 Numerical example

The theoretical model of a beam was considered for the numerical validation of the method presented in the last section. The theoretical model of the beam was built by coupling of four free-free beam elements (Chapter 3). The beam was made of steel and had dimensions of $2 \times 0.6 \times 44 cm$. A suspension spring was attached to the middle of the beam by addition of a stiffness to the impedance matrix of the theoretical model of the beam (Figure 4-16). In the simulated test, the beam was excited at point 2 and the response was measured at point 4.
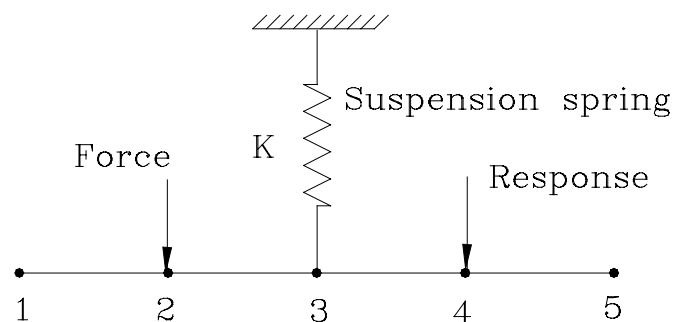
Figure 4-16. Assessment of the suspension effect by doubling the sttiffness of the spring

Table 4-4 shows the application of the method presented in the previous section for different suspension springs. As was proven when $f_2 - f_1$ is small, it is equal to $f_1 - f_0$. However, as the stiffness of the suspension spring increases $f_2 - f_1$ and $f_1 - f_0$ differ more. It can be concluded that for the first suspension spring (K=1000 N/m) $f_1 - f_0$ is negligible and the quality of the measurement is acceptable but for the second and third suspension springs (K= 10000 and 20000 N/m) $f_2 - f_1$ and $f_1 - f_0$

are not negligible and the quality of the measurement is not good. Therefore, $f_2 - f_1$ can monitor the quality of the measurement.

Table 4-4. Assessment of the suspension effect on the quality of the measurement

K (N/m)	f_1 (Hz)	f_2 (Hz)	$f_2 - f_1$ (Hz)	$f_1 - f_0$ (Hz)
1000	873.11	874.62	1.51	1.51
10000	886.65	903.77	17.09	15.08
20000	903.77	941.9	38.13	32.17

f_0 = Natural frequency of the structure (871.6 Hz)

f_1 = Natural frequency of the structure and a suspension spring with the stiffness of K

f_2 = Natural frequency of the structure and a suspension spring with the stiffness of   2K

K   =   Stiffness of the suspension spring

4.4.3 Experimental case study

Figure 3-20 shows an experimental set up of shaker testing of a beam which was used in chapter 3 for assessing of the mass-loading effect of an accelerometer. This way of suspending the test structure for shaker testing is quite popular. The beam was suspended using an elastic cord with the stiffness of 220 N/m and zero-load length of 10 cm. Although the elastic cord is used to offset the vertical load caused by the weight of the beam, it exhibits a stiffness effect as well when the tip of the beam is moved laterally. The equivalent lateral stiffness can be calculated in terms of the axial stiffness of the elastic cord if we assume:

1. The tip of the beam experiences only horizontal motion;

2. The elastic cord has no mass and remains in a straight line connecting the cord clamp and the tip of the beam;

3. The deflections of the tip of the beam are small enough such that the additional elongation does not significantly change the tension of the elastic cord; and

4. The elastic cord behaves as a linear spring.

As shown in [42], the equivalent lateral stiffness can be calculated from:

$$k_{lat} = \frac{W_{st}}{l_o + W_{st}/k_{ver}} = \frac{W_{st}}{l_f} \qquad \textbf{(4-37)}$$

where k_{lat} is the elastic cord lateral stiffness, k_{ver} is the elastic cord axial stiffness, W_{st} is the weight of the structure, l_o is the zero-load elastic cord length and l_f is the elastic cord length under load. Therefore in this way of suspending the structure not only the axial stiffness of the suspension spring is important but its length is also important. The axial stiffness of an elastic cord can be computed from:

$$k_{ver} = \frac{E_{sp} A_{sp}}{l_o} \qquad \textbf{(4-38)}$$

where E_{sp} is the elastic modulus of the elastic cord and A_{sp} is the cross sectional area of the elastic cord. Equation (4-38) shows that if we divide the zero-load length of the elastic cord in two, its axial stiffness becomes twice. Moreover, equation (4-37) shows that in the latter case the lateral stiffness of the elastic cord becomes twice as well because the zero-load length is half and the axial stiffness is twice. This suggests that in order to check the quality of the measurement related to suspension effects we have to remeasure the test structure using another suspension spring with the same parameters but half the length of the original suspension spring (Figure 4-17). This was done for the test case shown in Figure 3-20 and no discernible change was detected for the first four natural frequencies of the beam (167 Hz, 445 Hz, 880 Hz, 1445 Hz). The lateral stiffness of the elastic cord was calculated to be 59 N/m which is quite small. Therefore it was concluded that the measured FRF has a good quality with respect to the suspension effects.
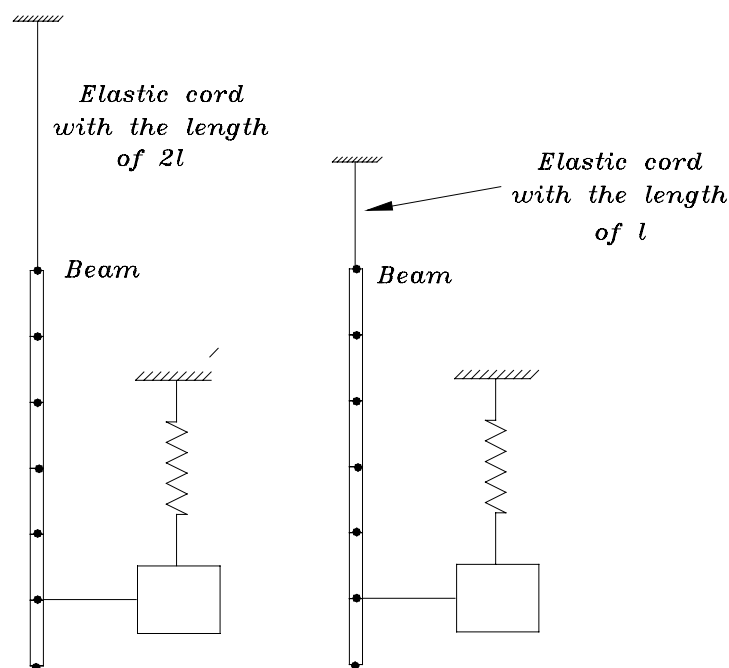
Figure 4-17. Assessment of the lateral stiffness of an elastic cord

4.4.4 Recommended test strategy

Clearly a softer suspension spring has less effect on the measurement. However, the suspension spring should be stiff enough to stand the gravity load of the test structure. After choosing a suitable suspension spring, the following procedure is suggested for dealing with the suspension effect in the test:

1- Suspend the structure with the chosen spring and measure an FRF.

2- Suspend the structure with another spring with twice the stiffness of the first spring and measure the same FRF.

3- If the difference between the natural frequencies of two measured FRFs in steps 1 and 2 are very small for a mode of the structure, the change of the natural frequency of the structure due to the suspension effect is negligible and the quality of the measurement is acceptable; if the difference is large the measured FRF is not acceptable.

When the quality of the measurement relating to the suspension effects is not acceptable two ways can be followed to improve the quality of the measurement:

1- Suspend the structure from another point of the structure. For a particular mode, if the structure is suspended from the nodal point of the structure, the effect of the spring on the test structure is eliminated in that mode.

2- Use the correction method presented in this chapter.

4.5 Conclusions

• In this chapter we have presented a method for the correction of the suspension effects on test structures. It has been shown that if three different modal tests are performed using a different suspension spring in each test, the FRFs can be corrected.

- Application of the method to a numerical example of a 3 DOFs system which is affected by suspension spring has also been examined. Moreover, the method was successfully applied to experimental data from testing a cantilever beam.

- The method has been developed for the case where the test structure is suspended with two springs. It has been shown that the measured FRFs can be corrected in a step by step procedure.

- The effects of the rigid body modes on the measured FRFs have been examined and it is shown that they are cancelled through the correction process.

- The method is vulnerable to noise and it is necessary that suitable springs are chosen to reduce the effect of the noise.

- The quality of the measurement of a free-free structure can be assessed by doubling the suspension stiffness and comparing the natural frequencies of the modified structure in each test. The method was applied to experimental data from testing on a beam which was suspended vertically using an elastic cord.

Chapter 5

The effects of stingers on measured FRFs

5.1 Introduction

When using a shaker to excite a structure and to measure Frequency Response Functions, it is customary to put a stinger (push rod or drive-rod) between the shaker and the force transducer which is attached to the test structure (Figure 5-1) . Ideally, the stinger should have high axial stiffness but low lateral or bending stiffness so as to excite the structure axially and to minimise excitations in all the other DOFs. However, forces and moments other than the axial excitation force component may also be introduced and act on the test structure and influence the force and/or response measurements. This will cause a systematic error in the measurement. There are relatively few publications which quantify the effects of stingers on the measured FRFs and the selection of stingers is usually made by trial and error or by experience.

In this chapter the effects of stingers on the measured FRFs will be investigated. The SMURF method is used to calculate the major influence of the stinger and the test structure on the measured results.
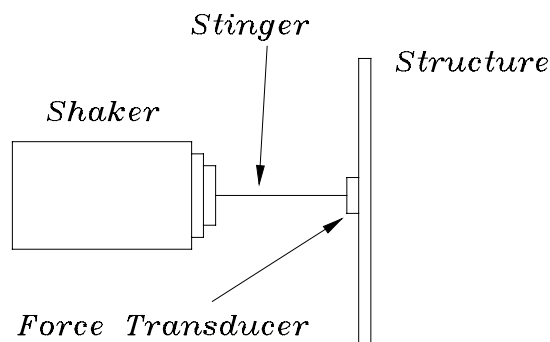
Figure 5-1. Shaker-structure Interaction

5.2 Theory

5.2.1 Modification of the test structure by stingers

Figure 5-2 (a) shows a structure which is excited by a shaker through a stinger. The excitation is in DOF i, which is in the axial x direction. The response is measured by an accelerometer at DOF l which is also in the x direction. However, the stinger excites the structure to respond not only in the axial direction but also in the rotational direction, θ_z. In Figure 5-2(a) the degree of freedom of axial excitation (x direction) has been shown by i and the rotational degree of freedom in θ_z direction by j. Figure 5-2(b) indicates the free-body diagram of the shaker-stinger-structure system. Except for the axial DOF (i), the shaker-stinger system is clamped rigidly to the structure at point P in DOF j and introduces a dynamic rotational stiffness on the structure.
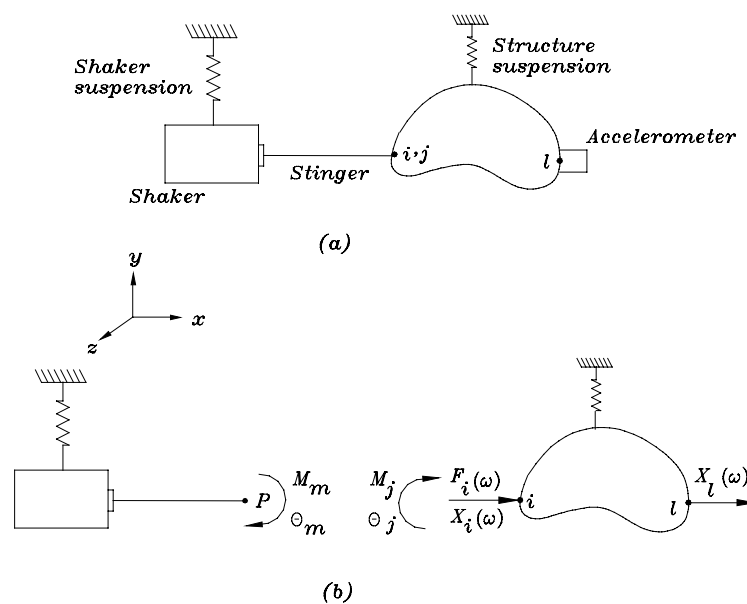
Figure 5-2. Dynamic model of the shaker-stinger-structure system

The special cases of the changes in the measured FRFs due to the attachment of the transducers and springs were investigated in chapters 3, 4. Comparing the results and the procedures it can be seen that the forms of the derived equations (equations (3-9) and (4-9)) are similar. Moreover, the procedure to analyse the problem is the same in

these cases. It seems that the same method can be used to analyse the general case in which the test structure is modified in more than one DOF (rotational or translational). Appendix A of this thesis investigates the general case of the changes in measured FRFs due to attachment of mechanical devices to the test structure. As shown at appendix A for the case of the stingers that the structure is modified in one DOF the relation between receptances is:

$$\alpha_{li}^{(j)} = \alpha_{li} - \frac{\alpha_{ji}\alpha_{lj}}{\alpha_{jj} + \alpha_{mm}}$$ (5-1)

Consequently, the relation between the accelerances is:

$$A_{li}^{(j)} = A_{li} - \frac{A_{ji}A_{lj}}{A_{jj} + A_{mm}}$$ (5-2)

in which j and m are rotational DOFs while i and l are translational DOFs. $A_{li}^{(j)}$ is the measured FRF when the stinger is rigidly connected to the test structure at rotational DOF j. A_{mm} is the rotational receptance of the tip of the stinger at point P in Figure 5-2.

What we want to measure is A_{li} , but what we get is a combination of A_{li} and the other FRFs. If the shaker is connected directly to the structure (without a stinger), A_{mm} is close to zero and we measure :

$$A_{li}^{(j)} = A_{li} - \frac{A_{ji}A_{lj}}{A_{jj}}$$ (5-3)

In this case the structure is coupled rigidly to the shaker at DOF j and the result is seriously contaminated.

In equation (5-2) when A_{mm} is large, the amount of the fraction on the right hand side is small and consequently the measured FRF is close to A_{li} . Conversely, when A_{mm} is small, the amount of error is large. In other words, when the stinger is dynamically stiff at any area of the frequency range, the measured results are more vulnerable to

error in that area.   Hence, this suggests that the antiresonances of the rotational driving point receptance of the tip of the stinger are responsible for the maximum error in measured FRFs. This question remains as to how we can deal with these undesirable effects and this will be discussed below.

5.2.2 Feasibility of correction of the stinger effects

Correction of FRFs for the case of stingers is similar to the case of springs discussed in chapter 4 because the form of the governing equation is the same for both cases (Equations (4-9) and (5-2)).   Equation (5-2) shows how the measured translational FRF, $A_{li}^{(j)}$, is related to the exact FRFs, A_{li} , A_{ji} , A_{jj} and A_{lj}. To find the exact FRF, measurement of $A_{li}^{(j)}$ can be considered with three different stingers with different lengths (Figure 5-3).   So there are three equations in the form of equation (5-2) corresponding to three different stingers.
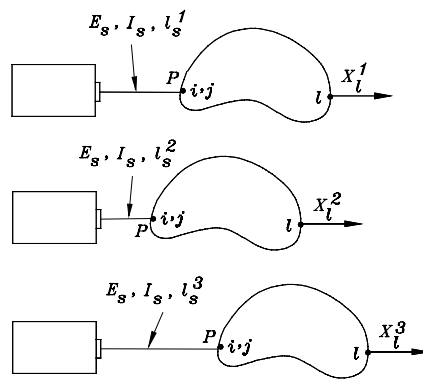
Figure 5-3. Measurement with three different stingers

$$\begin{cases} A_{li}^{(j)} = A_{li} - \dfrac{A_{ji}A_{lj}}{A_{jj} + A_{mm}} \\[2mm] \overline{A}_{li}^{(j)} = A_{li} - \dfrac{A_{ji}A_{lj}}{A_{jj} + \overline{A}_{mm}} \\[2mm] \overline{\overline{A}}_{li}^{(j)} = A_{li} - \dfrac{A_{ji}A_{lj}}{A_{jj} + \overline{\overline{A}}_{mm}} \end{cases} \qquad (5\text{-}4)$$

in which A_{mm}, $\overline{A}_{mm}$ and $\overline{\overline{A}}_{mm}$ are rotational FRFs of the stingers at point P. If A_{mm}, $\overline{A}_{mm}$ and $\overline{\overline{A}}_{mm}$ are known, the correct values of A_{li} and A_{jj} can be computed. The solution of the general form of these equations can be found in chapter 4. For the case of equations (5-4), the solutions are :

$$
\left\{ \begin{array}{c} A_{li} \\ A_{jj} \end{array} \right\} = \left(\left[\begin{array}{cc} \overline{A}_{mm} - A_{mm} & A_{li}^{(j)} - \overline{A}_{li}^{(j)} \\ \overline{\overline{A}}_{mm} - A_{mm} & A_{li}^{(j)} - \overline{\overline{A}}_{li}^{(j)} \end{array} \right] \right)^{-1} \left\{ \begin{array}{c} (\overline{A}_{li}^{(j)} \overline{A}_{mm} - A_{li}^{(j)} A_{mm}) \\ (\overline{\overline{A}}_{li}^{(j)} \overline{\overline{A}}_{mm} - A_{li}^{(j)} A_{mm}) \end{array} \right\} \qquad \textbf{(5-5)}
$$

Thus, the correct FRF, A_{li}, and the rotational driving point FRF at the point of attachment of the stinger, A_{jj}, have been computed with respect to measured FRFs and A_{mm}'s, namely the rotational point accelerances at point P of the stingers (Figure 5-2(b)). However, measurement of A_{mm} is not as straightforward as measuring the mass of the accelerometer in the mass cancellation procedure. Measurement of the rotations of such a small elements as stingers is not an easy task . Theoretical results to compute A_{mm} is not exact as well because the shaker-stinger assembly is a complicated structure some part of which (the coil) is moving in a magnetic field and any simplification in the theoretical model will lead to inaccurate results from the correction methods. Thus the correction method for the case of stingers is ineffective.

5.3 The effects of stingers on measured FRFs

In the previous section, it was explained that the correction of the rotational stiffness effect of stingers on the measured FRFs is an impractical task because measurement or exact simulation of the behaviour of stingers is impractical. However, the behaviour of stingers can be simulated approximately using simplified models of shaker-stinger assembly. On this basis stingers can be designed in a way that their effect on the measured FRFs is minimised. In this section practical ways to avoid the effects of stingers on the measured FRFs will be investigated.

5.3.1 Shaker-stinger-structure model

As was explained in chapter 2 different models were suggested in the past for the shaker-stinger-structure assembly (Figures 2-1 and 2-2) by different authors [17], [18], [19]. However, the dynamic characteristics of the test structure were not included in these models and it was simply assumed that the structure-side boundary condition of the stinger was pinned or clamped. Figure 5-4 indicates a more complete model of the shaker-stinger-structure system in which the test structure is considered as a rigid structure that moves in the transverse direction (relative to the excitation direction) . The stinger is modelled as a simple straight beam and the mass and suspension properties of the structure are coupled to the stinger in the transverse direction to illustrate the effect of the boundary conditions of the stinger on the structure side. This assumption for the transverse motion of the structure as a rigid body does not contradict with the axial vibration of the structure as a elastic body.
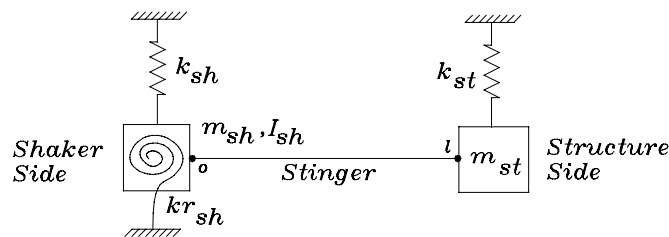
Figure 5-4. Shaker-stinger-structure model

The theoretical model of the shaker-stinger-structure system shown in Figure 5-4 is built on the concept of the coupling method. The shaker is modelled as a member with both a specified point mass and a point rotational inertia and the suspension of the shaker is modelled as a translational stiffness and a rotational stiffness. In reality, the stinger is coupled with the coil of the shaker which is moving in the magnetic field of the drive part of the shaker. However, this cannot be modelled by mechanical elements. The shaker can be modelled as shown in Figure 5-5. Because the coil has a slight axial motion, the rotational inertia properties of the shaker do not change

considerably. Hence, the shaker can be modelled as a lumped mass with rotational inertia as is shown in Figure 5-4.
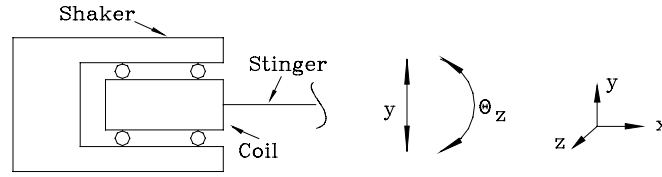
Figure 5-5. A model of the shaker

The separate stinger was assumed to be a free-free beam of constant cross-section which is modelled using the receptance function of a free-free beam introduced in [96]. The receptance matrix of the stinger (see Figure 5-6) is:

$$[\alpha] = \begin{bmatrix} \alpha_{q_{Sh}q_{Sh}} & \alpha_{q_{Sh}r_{Sh}} & \alpha_{q_{Sh}q_{St}} & \alpha_{q_{Sh}r_{St}} \\ \alpha_{r_{Sh}q_{Sh}} & \alpha_{r_{Sh}r_{Sh}} & \alpha_{r_{Sh}q_{St}} & \alpha_{r_{Sh}r_{St}} \\ \alpha_{q_{St}q_{Sh}} & \alpha_{q_{St}r_{Sh}} & \alpha_{q_{St}q_{St}} & \alpha_{q_{St}r_{St}} \\ \alpha_{r_{St}q_{Sh}} & \alpha_{r_{St}r_{Sh}} & \alpha_{r_{St}q_{St}} & \alpha_{r_{St}r_{St}} \end{bmatrix} \tag{5-6}$$

in which q_{Sh}, q_{St} and r_{Sh}, r_{St} are the vertical and rotational displacements of two sides of the stinger.
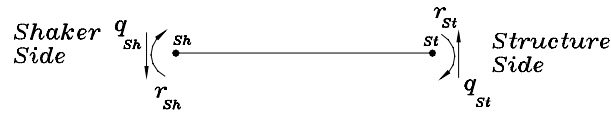
Figure 5-6. Modelling of a stinger as a free-free beam

The elements of $[\alpha]$ can be computed with respect to the beam properties as given in [96]. To complete the model of the shaker-stinger-structure system, the dynamic characteristics of the shaker and those of the structure should be added to the stinger as its two ends.

The mass of the shaker and the linear stiffness of the shaker suspension are added to the stinger as :

$$D^{md}(q_{Sh}, q_{Sh}) = D(q_{Sh}, q_{Sh}) - m_{sh}\omega^2 + k_{sh} \tag{5-7}$$

The rotary moment of inertia of the shaker and the rotational stiffness of the shaker suspension are added to the stinger as :

$$D^{md}(r_{Sh}, r_{Sh}) = D(r_{Sh}, r_{Sh}) - I_{sh}\omega^2 + kr_{sh} \qquad \text{(5-8)}$$

Moreover, the mass and suspension stiffness of the structure are added to the structure side of the stinger as:

$$D^{md}(q_{St}, q_{St}) = D(q_{St}, q_{St}) - m_{st}\omega^2 + k_{st} \qquad \text{(5-9)}$$

Thus the modified receptance matrix of the stinger is :

$$[\alpha]^{md} = ([D]^{md})^{-1} \qquad \text{(5-10)}$$

5.3.2 Comparison of different models of the stinger

The model shown in Figure 5-4 is not a simple model of the stinger and it has some of the parameters involved in the real test (this model is called real model from now on). However, for simplification purposes it is valuable to compare this model with the simpler models of stingers such as the ones shown in Figure 5-7.
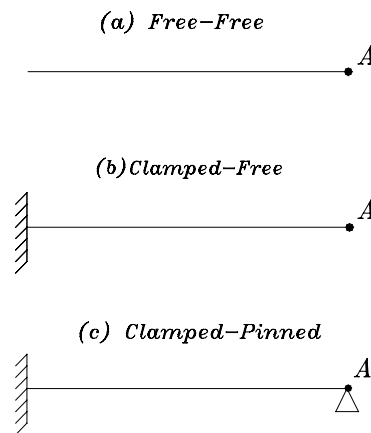
Figure 5-7. Three simple models for a stinger

To compare these models with the "real model", a numerical simulation was considered. The parameters of the shaker, stinger and the structure are :

<u>Shaker</u> : Mass : 8.3 *kg*; Rotary moment of inertia : 0.0256 kg/m^2 , Suspension: $k_{sh} =$ 1400 *N/m*, $kr_{sh} = 0.469$ *N-m/rad*.

<u>Stinger</u> : Diameter : 2 *mm*, Length : 100 *mm*, Material : steel

<u>Structure</u> : a beam with the mass of $m_{st} = 2.469$ *kg* and the suspension stiffness of $k_{st} = 850$ *N/m*.

Table 5-1 shows a comparison of the natural frequencies and antiresonance frequencies of the receptance function of point *l* of the model of the stinger shown in Figure 5-4 with those of the three simple models shown in Figure 5-7. The measurement points are specified as *A* in Figure 5-7. In this case, the resonances and antiresonances of the real model coincide with those of the clamped-pinned model. This means the stinger can be modelled using a clamped-pinned model.

Table 5-1. Comparison of different models of the stinger

Model of the beam	Natural Frequencies / Antiresonances (Hz)				
AR of the RM of beam		934	2574.9	5047.7	8344.2
AR of the CP beam		934	2574.9	5047.7	8344.2
NF of the FF beam		934	2574.9	5047.7	8344.2
NF of the CF beam	146.8	934	2574.9	5047.7	8344.2
NF of the RM of beam		643.7	2086	4352.4	7442.8
NF of the CP beam		643.7	2086	4352.4	7442.8

AR= AntiResonance, RM= Real Model, CP= Clamped-Pinned, NF= Natural Frequency, FF= Free-Free, CF= Clamped-Free.

Some researchers advise that to minimise the effect of stinger on the measured FRFs the resonance frequencies of the stinger should lie below or above the frequency range of measurement [17], [18], [19], [20], while others claim that this is the antiresonance of the stinger that is responsible for the maximum error [21]. It was shown in section 9-2 that in coupling the shaker-stinger assembly with the structure, it is the antiresonance of the stinger's angular driving point receptance which is responsible for the maximum error. However, as can be seen in Table 5-1, the antiresonances of the clamped-pinned stinger coincide with the natural frequencies of the free-free stinger and the natural frequencies of the clamped-free stinger (except for the first resonance). This coincidence can be proven as follows:

In Table 7.1*(c)* of [96] entries 1 and 3 it is shown that the rotational point receptance of the tip of a beam for the free-free and clamped-free boundary conditions respectively are $F_6/(EI\lambda F_3)$ and $F_3/(EI\lambda F_5)$, in which λ is a function of frequency, cross section area of the beam, mass density and flexural rigidity of the beam. F_3, F_5 and F_6 are functions of λ and the length of the beam. F_3 is in the denominator of the free-free condition and in the numerator of the clamped-pinned condition. It means that when the receptance of the clamped-pinned beam is zero (or in anti-resonance), the receptance of the free-free beam is ∞ (or in resonance). Moreover, As shown in [97] in Table 8-1, the natural frequencies of the free-free beam, clamped-clamped beam and clamped-free beam (except for the first one) are the same. It is a considerable result when we remember that most programs today are calculating natural frequencies and not antiresonances.

Table 5-2 indicates the antiresonances of the clamped-pinned stingers with different diameters and lengths. These are the lengths and diameters which usually are used in modal testing. The material of the stinger is steel. When using these stingers, the measurement may be affected around antiresonances of the stinger. The regions between these antiresonances are safe regions for the measurement.

Table 5-2. Antiresonances of the steel stingers for different length and diameter

Diameter(mm)↓	Length (mm)			
	50	70	100	150
0.5	930	464, 1293	231,633,1246	100,281,552,914,1366, 1909
1	1849	944	462, 1276	208,564,1110,1830
1.5	------	1418	697,1918	311,854,1668
2	------	1899	934	422,1140
2.5	------	--------	1176	532,1431
3	------	--------	1427	643,1728

Antiresonances are in Hz

In the previous example, the natural frequencies and the antiresonances of the real model coincided with the clamped-pinned model. However, this coincidence may not hold for other cases. To investigate the degree of coincidence of the clamped-pinned model with the real model another case is considered in which the shaker and the structure are small while the stinger is stiff. Therefore, in this case the boundaries of the stinger are not as rigid as in the previous case. The parameters of the shaker and those of the stinger and structure are :

<u>Shaker</u> : Mass : 2 *kg*; Rotary moment of inertia : 0.01 kg / m^2 ; Suspension: $k_{sh} = 400$ *N/m*; $kr_{sh} = 0.09$ *N-m/rad*.

<u>Stinger</u> : Diameter : 5 *mm*; Length : 10 *mm*, Material : steel

<u>Structure</u> : A beam with the mass of $m_{st} = 0.0156$ *kg* and the suspension stiffness of $k_{st} = 200$ *N/m*.

Figure 5-8 shows the comparison of the real model with the clamped-pinned and clamped-free models. In this case, the structure and shaker are not so massive while the stinger is not flexible but the real model is still close to the clamped-pinned model. It should be mentioned that the real model show the effect of the rigid body modes of the shaker-stinger-structure system in the frequency range of 0-500 Hz while the clamped-pinned model does not show this.
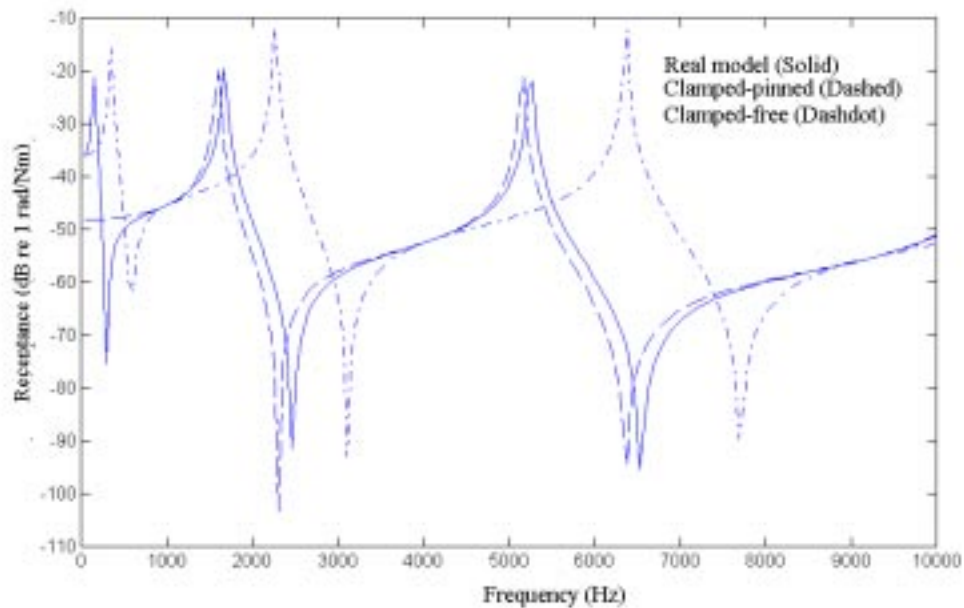
Figure 5-8. Measurement of a small structure using a small shaker and a stiff stinger

5.3.3 The effects of the stinger on the rigid body modes

The rigid body modes of the shaker-stinger-structure system have considerable effects on the measured FRFs in the low frequency range. By "low frequency range" we mean the frequency range in which the minimum frequency is zero and the maximum frequency is the first elastic mode of the shaker-stinger-structure system shown in Figure 5-4. The additional stiffness of the stinger (rotational and transverse) an raise the rigid body modes of the shaker and those of the structure in the low frequency range (like the effect of the suspension springs on the rigid body modes of a test structure). Figure 5-9 indicates the effects of different stingers on the rigid body

modes of the shaker-stinger-structure system. The parameters of the system used in this example are:

Shaker : Mass : 8.3 *kg*, Rotary moment of inertia : 0.0256 *kg / m²* , Suspension: $k_{sh}=$ 1400 *N/m*, $kr_{sh}=$ 0.469 *N-m/rad*.

Structure : is a beam with the mass of $m_{st}=2.469$ *kg* and its suspension stiffness is $k_{st}=850$ *N/m*.

Three different stingers were considered from steel:

Stinger 1 : Diameter : 2 *mm* ; Length : 100 *mm*.

Stinger 2 : Diameter : 0.5 *mm* ; Length : 100 *mm*.

Stinger 3 : Diameter : 2 *mm* ; Length : 50 *mm*.

Three resonances and three antiresonances are found in the angular receptance of the tip of the stinger (Point *P* in Figure 5-2) in the frequency range of 0 to 20 Hz for stinger 1. As was explained in section 5.2.1, the antiresonances of the stinger are responsible for the maximum error in the measured FRFs. For a shorter stinger with the same diameter (stinger 3), the antiresonances and resonances shift to the higher frequencies. This means that a shorter stinger raises the rigid body mode frequencies in the low frequency range. For stinger 2, which is thinner than stinger 1 but with the same length, the rigid body mode frequencies shift to the lower frequencies. Comparing these three stingers, stinger 2 has less effect on the rigid body modes in the low frequency range. Therefore, in order to measure the test structure at lower frequencies the stinger should be thinner and longer or, in other words, more flexible.

In design of stingers we usually ignore the results of the measurement in the frequency range from zero to the last antiresonance in the low frequency range. Therefore what is important in the low frequency range is the last antiresonance of the shaker-stinger-structure system. For the above-mentioned example, computations show that by changing the parameters of the shaker and the suspension stiffness of the structure, the location of the last antiresonance in the low frequency range does not

change considerably. In other words the important parameters in the design of stingers in the low frequency range are the parameters of the stinger and the mass of the structure.
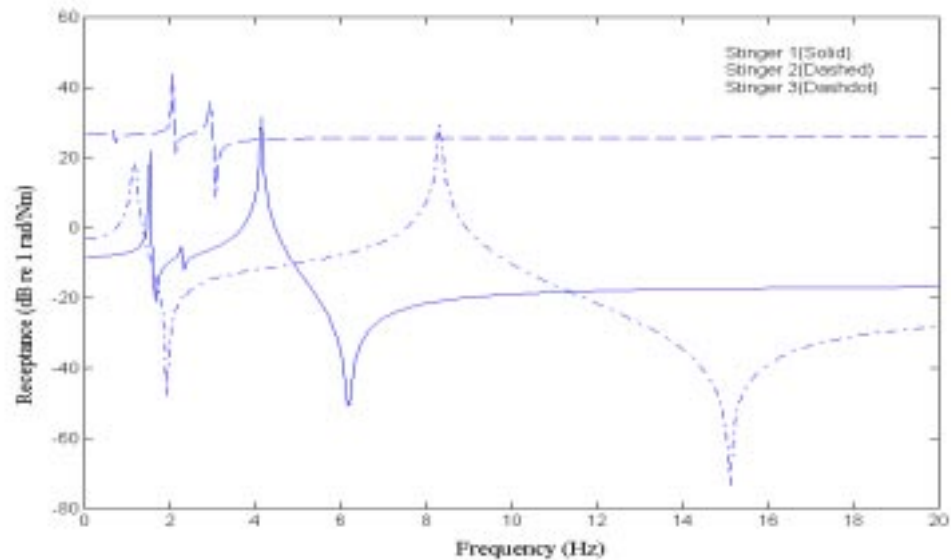
Figure 5-9. The effect of the stingers on the rigid body modes in the low frequency range

5.3.4 The effects of the flexibility of stinger on the measured FRFs

The rigid body modes of the shaker-stinger-structure system affect the measured FRFs in the low frequency range. A common problem that is encountered in the higher frequency region is the flexibility of the stinger. As was explained in section 5.2.1, at antiresonances of the rotational point receptance function of the tip of the stinger, the stinger is dynamically stiff and the measured FRFs will be more erroneous at these frequencies compared with other frequencies. Figure 5-10 indicates the rotational receptance of stingers for different diameters and different lengths. The parameters of the stingers are given in Table 5-3. The parameters of the shaker and those of the structure are :

<u>Shaker</u> :   Mass : 8.3 kg,   Rotary moment of inertia : 0.0256 kg / m^2 ,   Suspension: $k_{sh} = 1400$ *N/m*, $kr_{sh} = 0.469$ *N-m/rad*.

Structure : a beam with the mass of m_{st} =2.469 *kg* and its suspension stiffness is k_{st} =850 *N/m*.

Figure 5-10 (a) shows that by decreasing the diameter of the stinger, while its length is constant, the level of the receptance of the stinger shifts up while the resonances and antiresonances shift to the lower frequencies. On the other hand, by decreasing the length of the stinger, while its diameter is constant, the receptance of the stinger shifts slowly down to the lower levels and the resonances and antiresonances shift to the higher frequencies (Figure 5-10 (b)). Therefore, with the same diameter, a shorter stinger is safer in the areas that a long stinger is not. However, the problem with a shorter stinger is that in the low frequency range the effects of the rigid body modes of the shaker-stinger-structure system appear at higher frequencies than those of a longer stinger. This can be seen from the changes in the low frequency range of the stingers shown in Figure 5-9. Therefore, by using a shorter stinger we increase the allowable maximum and minimum frequencies at the same time. As a result, the best way to design a stinger is to determine the minimum diameter of the stinger and then to determine its length based on the minimum and maximum desired frequencies.
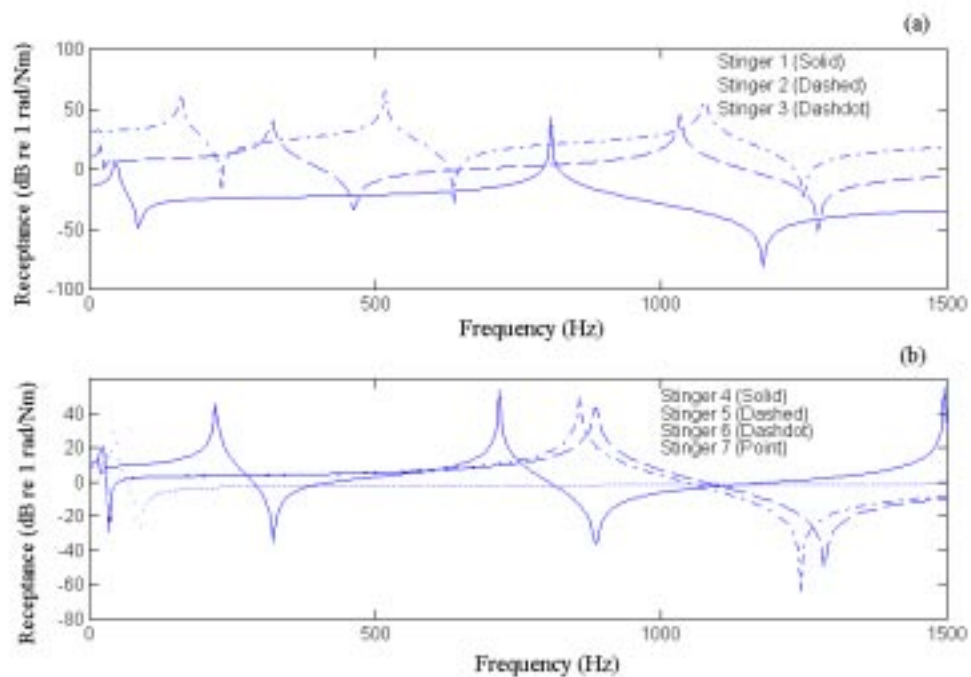
Figure 5-10. Angular receptance of different stingers

Table 5-3. The parameters of different stingers

Stinger	No.1	No.2	No.3	No.4	No.5	No.6	No.7
Diameter (mm)	2.5	1	0.6	1	1	1	1
Length (mm)	100	100	100	120	60	61	30

5.3.5 The effect of the shaker-stinger-structure system on the measured FRFs

In section 5-2 it was shown that the effect of the stinger on the measured FRFs can be computed from equation (5-2). Moreover, using the model shown in Figure 5-4, it was shown that how the rotational FRF of the tip of the beam (A_{mm} in equation (5-2)) varies and where are the most erroneous areas in the frequency range of a stinger. In this section the effects of the shaker-stinger-structure system on the measured FRFs of a beam as a test structure are investigated. Here, the effect of the structure as a rigid body on the boundary conditions of the stinger in the transverse direction should not be confused with the measurement of the elastic behaviour of the structure in the axial direction.

As a test structure, a theoretical model of a beam is built using the concept of coupling of the free-free beam elements. The procedure of building a model of the beam by coupling the beam elements is explained in Chapter 3. The model of the beam was built by coupling 10 beam elements and was used in a numerical simulation to illustrate the effects of the shaker-stinger-structure system on the measured FRFs (Figure 5-11). The shaker-stinger-structure system is coupled with the beam at point 4 (Figure 5-11) using equation (5-2). The response of the beam is measured at point 8. The parameters of the beam and those of the shaker and stinger are :

<u>Beam</u> : Length : 106 *mm*, Width : 20 *mm*, Thickness : 1*mm*, Material: steel, Modulus of elasticity : 2.1×10^{11} N/m^2 , Mass of density : 7800 kg/m^3 , Mass : 0.0156 *kg*, Suspension : k_{st} =200 *N/m*.

<u>Shaker</u> : Mass : 2 *kg*, Rotary moment of inertia : 0.01 kg / m^2 , Suspension: k_{sh} = 400 *N/m*, kr_{sh} = 0.09 *N-m/rad*.

<u>Stinger1</u> : Diameter : 1.5 *mm* , Length : 73.5 *mm*, Material : Steel.

<u>Stinger 2</u> : Diameter: 0.5 *mm*, Legth: 50 *mm*, Material : Steel.

<u>Measurement Set up</u> : Excitation : at point 4, Response: at point 8.

<u>Frequency range</u> : 0-2000 Hz.

Figure 5-12(b) indicates the rotational point receptance of the structure-side end of the stinger 1. The behaviour of the real model (the real mode was introduced in section 5.3.1) is compared with the behaviour of the clamped-pinned stinger. Figure 5-12(a) shows the effects of the stinger on the measurement of the beam. A "glitch" occurs in the computed FRF in the low frequency range. At higher frequencies, a notch has been made by the antiresonance of the shaker-stinger-structure system in the measured FRF and thus instead of one peak a double peak has been indicated. Moreover, because of the high angular stiffness of the stinger , around 450 Hz , the FRF has moved to the higher frequencies.
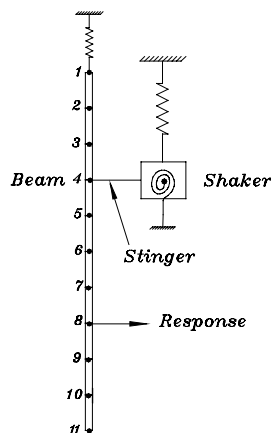
Figure 5-11. Measurement of a beam in a simulated test
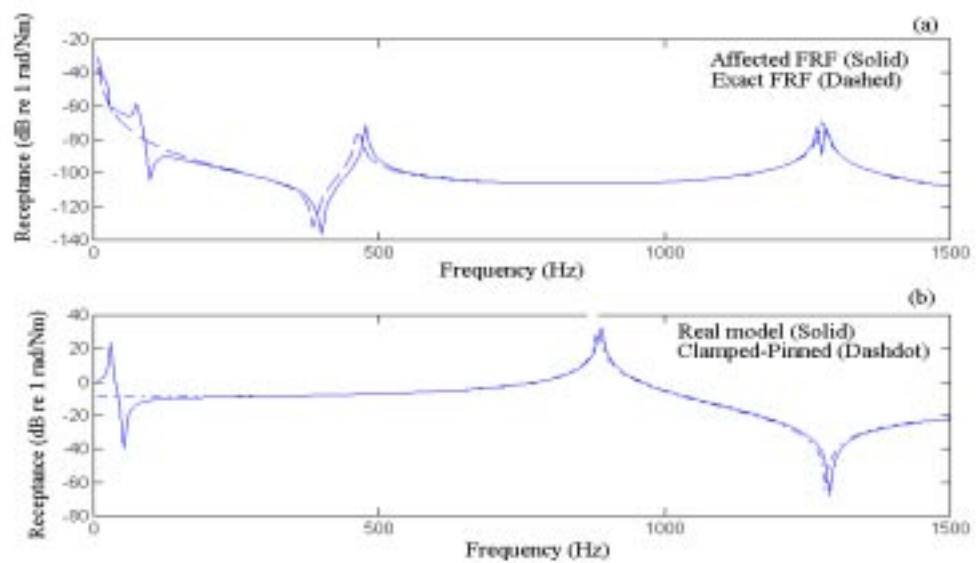
Figure 5-12. Measurement using stinger 1 : d_s=0.0015 m, l_s=0.0735 m.

Figure 5-13 (b) indicates the angular receptance of the structure-side end of stinger 2. Figure 5-13 (a) shows the effects of stinger 2 on the measured FRF. This stinger has a small effect on the resonances of the structure. Besides, in the low frequency range the stinger has a small effect on the structure.
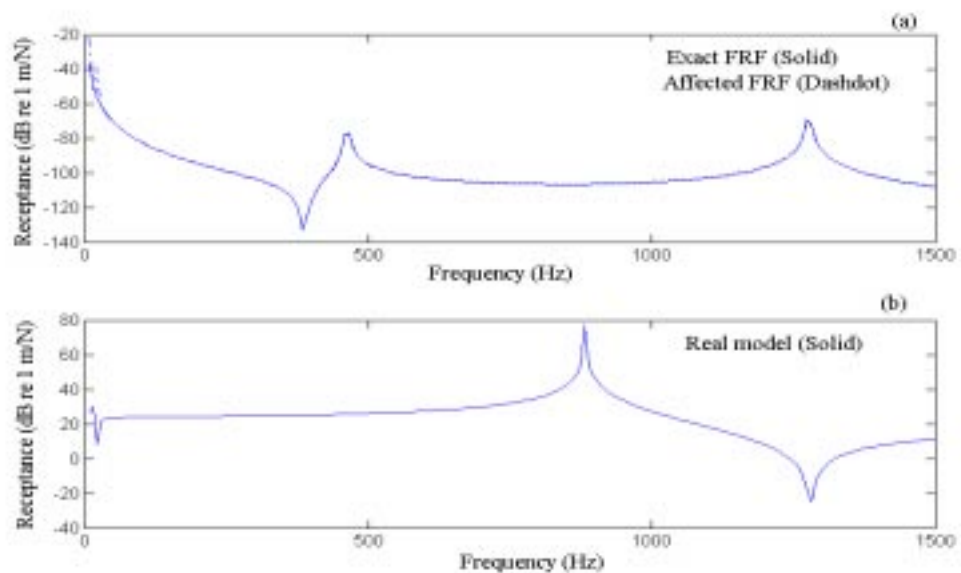
Figure 5-13. Measurement using stinger 2 : d_s=0.0005 m, l_s=0.05 m

From this study it can be concluded that the measured FRFs:

1. are affected by the rigid body modes of the shaker-stinger-structure system at low frequency region;

2. are affected by the antiresonances of the stinger at higher frequencies;

3. may be affected by the rotational stiffness of the stinger at all the other frequencies if the stinger is not flexible.

5.3.6 The effect of the misalignment on the performance of the stinger

The main assumption of building the model shown in Figure 5-4 was that after assembling the shaker-stinger-structure system the stinger remains straight. On this basis the model of the stinger was assumed to be a straight beam. However, in practice when the gravity load of the structure and that of the shaker exert tension on the suspension springs and stretch them, in equilibrium, the stinger may not remain straight. This causes misalignment of the stinger. Usually, the suspension springs are chosen to be very soft to fulfil the free-free boundary condition, consequently even with a slight force the suspension springs have a considerable displacement. This makes it difficult to assemble the test structure and exciter accurately so that the stinger remains straight. To examine the effect of the misalignment on the performance of the stinger Finite Element Method (FEM) was used. Figure 5-14 shows the model which was made in ANSYS program (see Appendix D). This model is similar to the model shown in Figure 5-4 and has the capability of assessing the misalignment effect of stingers. The stinger was modelled by assembling 100 BEAM3 elements from ANSYS element library. BEAM3 is a uniaxial element with tension, compression and bending capabilities. The element has three degrees of freedom at each node: translations in the nodal x and y directions and rotation about the nodal z-axis. The shaker is modelled as a nodal mass with rotary inertia property which is attached to the shaker-side of the stinger. The shaker is suspended using a longitudinal spring in y direction and a rotary spring in θ_z direction. On the structure

side, the structure is modelled as a lumped mass which is suspended using a longitudinal spring. If the axis of the gravity force of the structure does not pass through the point of the attachment of the stinger and the structure, the gravity force of the structure exerts a specific moment on the stinger in the structure-side. It is assumed that this moment can be estimated from the static properties of the structure.

Appendix D of this thesis shows the program which was used to build the ANSYS model of the shaker-stinger-structure system. To examine this model a test with the following parameters was considered:

Shaker : Mass : 8.3 *kg*; Rotary moment of inertia : 0.0256 *kg.m²* , Suspension: $k_{sh}=$ 1400 *N/m*, $kr_{sh}=$ 0.469 *N-m/rad*; Mass of the coil = 0.06 *kg*.

Stinger : Diameter : 2 *mm* , Length : 100 *mm*, Material : steel

Structure : Mass: $m_{st}=$10.5 *kg* and the suspension stiffness of $k_{st}=$850 *N/m*. The structure exerts a moment of 1.25 *kg.m²* on the stinger.
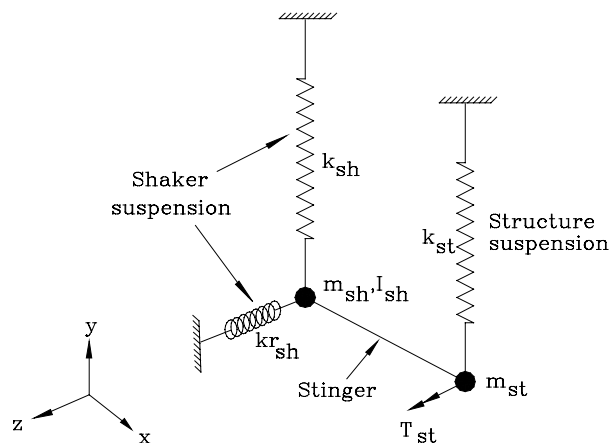
Figure 5-14. The ANSYS model of shaker-stinger-structure system

After building the model a prestressed modal analysis (this analysis is defined in the ANSYS program) was conducted to calculate the natural frequencies and mode shapes of the system. The procedure to do a prestressed modal analysis is essentially the same as a regular modal analysis except that we first need to prestress the

structure by exerting gravity forces and doing a static analysis. Figure 5-15 shows the result of the static analysis. In this case the stinger is deformed and is not straight any more.
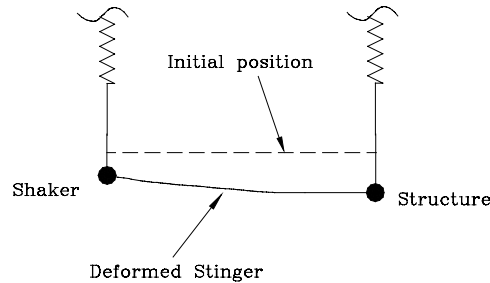
Figure 5-15. Misalignment of the stinger

In the second stage, modal analysis of the deformed system was performed by re-entering the solution of the static analysis and obtaining the modal solution, also with prestress effects turned on. The modal solution without performing the static analysis was also obtained in order to compare the results. Table 5-4 compares the natural frequencies and the mode shapes for the first fifteen modes of these two cases. The mode shape is related to the rotation of the structure-end of the stinger. Figure 5-16 shows the mode shapes of the shaker-stinger-structure system. It was shown earlier in section 5-2 that antiresonances of the stinger are responsible for the maximum error in the measured FRFs, therefore the point rotational receptance of the stinger in the structure side needs to be computed to obtain the antiresonances of the stinger. This can be achieved using the following equation:

$$\alpha_{ll} = \sum_{r=1}^{N} \frac{(\varphi_{lr})^2}{\overline{\omega}_r^2 - \omega^2} \tag{5-11}$$

in which φ_{lr} is the mass-normalised mode shape of the point rotational receptance of the stinger in the structure-side corresponding to mode *r*. Figure 5-17 shows first two anti-resonances of the stinger using the first twenty modes of the system (Table 5-4 shows data of the first 15 modes of the system). The first antiresonance for the

deformed stinger is 943 Hz while for the straight stinger is 953 Hz. The second anti-resonance for the deformed stinger is 2605 Hz while for the straight stinger is 2631 Hz. Consequently, if we do not consider the misalignment of the stinger there is a 10 Hz difference for the first anti-resonance and 26 Hz for the second anti-resonance which is a considerable amount in the design of stingers.

Table 5-4. Comparison of the mode shapes of the straight and deformed stingers

	Straight stinger		Deformed Stinger	
modes	f (Hz)	$(\theta_z)_l$	f (Hz)	$(\theta_z)_l$
1	0.0000	-0.29686E-5	0.90965	-0.11226E-8
2	1.1845	2.2958	1.842	2.2958
3	1.7978	0.26471E-1	1.7979	0.26147E-01
4	3.0326	7.2411	3.0326	7.2411
5	188.7	0.8684E-9	188.7	-0.19439E-13
6	636.58	1153.4	637.04	1155.1
7	2062.0	2015.9	2064.5	-2020.9
8	4299.4	2913.7	4335.8	-2948.4
9	7345.8	3806.6	7425.8	3864.4
10	11197	4697.0	11405	4843.6
11	15847	5584.0	16382	-5949.5
12	21289	6467.1	22255	-6506.2
13	25946	0.87009E-8	28932	8672.0
14	27516	7345.4	29327	0.94278E-8
15	34519	8218.8	39050	-9884.1

f = Natural Frequency , $(\theta_z)_l$ = rotation of the structure-side end of the stinger
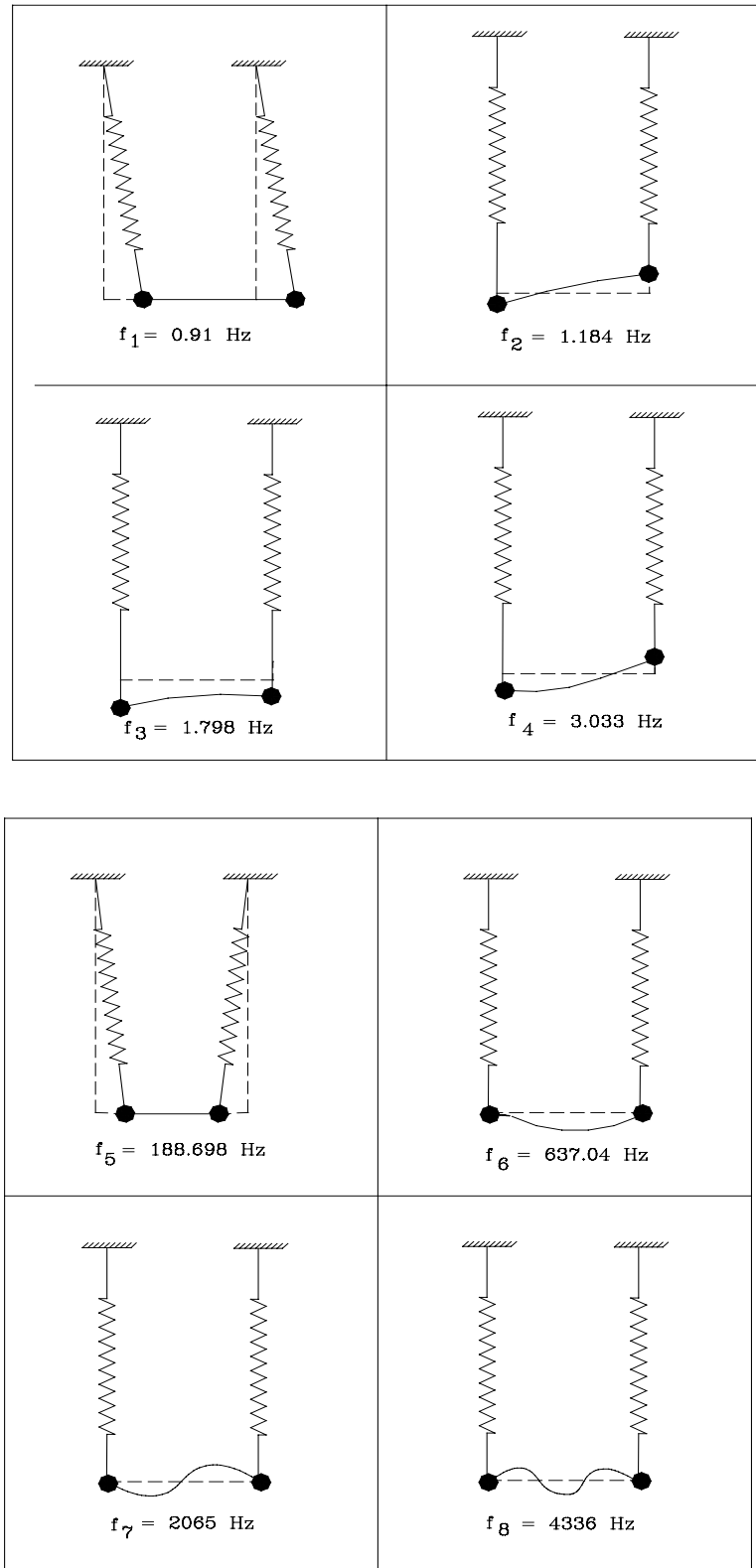
Figure 5-16. Mode shapes of the shaker-stinger-structure system
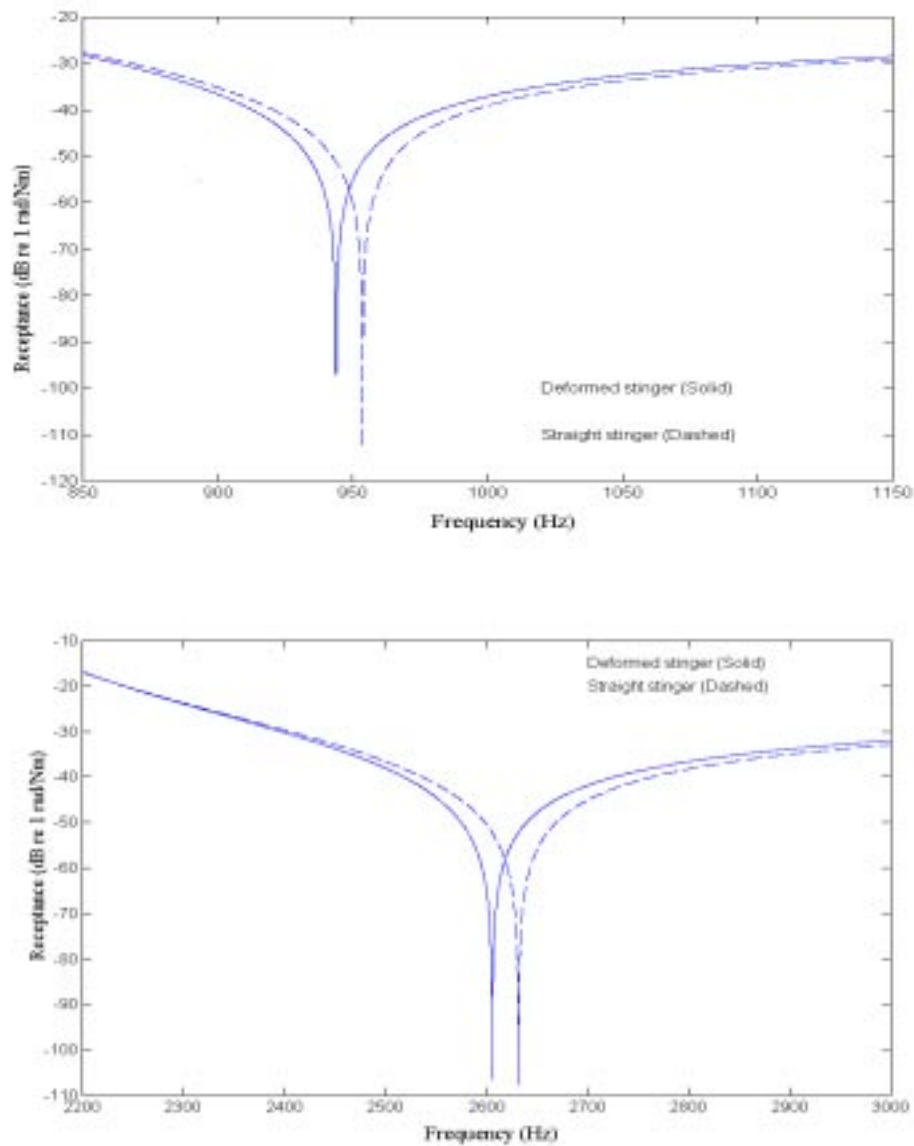
Figure 5-17. The effect of the misalignment of the stinger on its anti-resonances

5.3.7 The effect of the stinger on the measured FRFs in other DOFs

Figure 5-18 (a) indicates a structure which is coupled with the shaker-stinger system in three DOFs. The degree of freedom of axial excitation (x direction) has been shown by i, the rotational degree of freedom in θ_z direction by j and the transverse degree of freedom (y direction) by k. Except for the axial DOF (i), the shaker-stinger system is coupled rigidly to the structure at point P in DOFs j and k and introduces a dynamic stiffness on the structure.
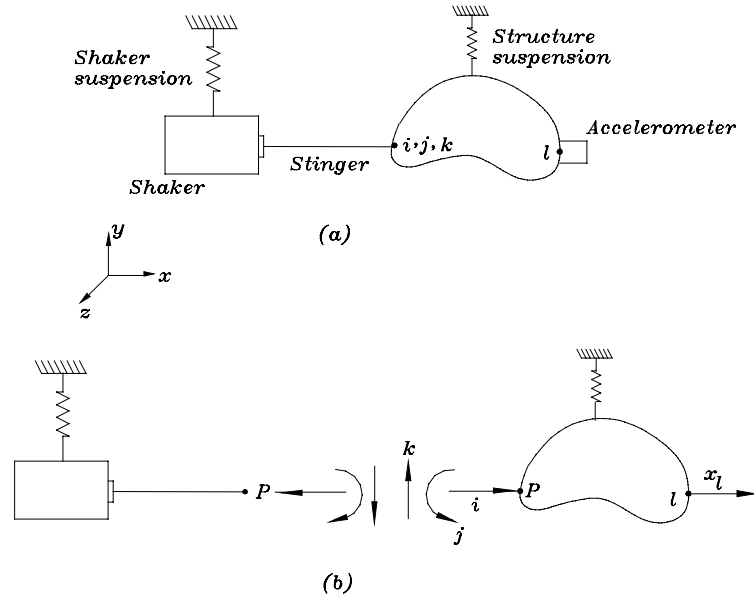
Figure 5-18. Coupling of the shaker-stinger system and the structure in three DOFs

The structure and the shaker-stinger system are coupled in three DOFs. In this case coupling can be done in a step by step procedure. In this approach two structures are coupled in one of the coupling DOFs in each step. If it is assumed that just the effect of the shaker-stinger system in axial direction (DOF *i*) is added to the structure, then from appendix A we have:

$$A_{li}^{(i,j,k)} = A_{li}^{(j,k)} - \frac{A_{ii}^{(j,k)} A_{li}^{(j,k)}}{A_{ii}^{(j,k)} + A_{nn}}$$ (5-12)

In equation (5-1), $A_{li}^{(j,k)}$ and $A_{ii}^{(j,k)}$ can be written in terms of the accelerances of the structure when the effect of the shaker-stinger system in θ_z direction (DOF *j*) is considered. For instance for $A_{li}^{(j,k)}$ we have:

$$A_{li}^{(j,k)} = A_{li}^{(k)} - \frac{A_{ji}^{(k)} A_{lj}^{(k)}}{A_{jj}^{(k)} + A_{mm}}$$ (5-13)

In equation (5-1), $A_{li}^{(k)}$, $A_{ji}^{(k)}$, $A_{lj}^{(k)}$ and $A_{jj}^{(k)}$ can be written in terms of the accelerances of the structure when the effect of the shaker-stinger system in y direction (DOF k) is considered. For instance for $A_{li}^{(k)}$ we have:

$$A_{li}^{(k)} = A_{li} - \frac{A_{ki} \, A_{lk}}{A_{kk} + A_{rr}} \qquad\qquad \textbf{(5-14)}$$

What we want to measure is A_{li}, but what we get is a combination of A_{li} and the other FRFs. If the shaker is connected directly to the structure (without a stinger), A_{nn}, A_{mm} and A_{rr} are close to zero and the result is seriously contaminated.

In equation (5-1), when A_{nn} is large, the amount of the fraction on the right hand side is small and consequently the measured FRF is closed to A_{li}. Conversely, when A_{nn} is small, the amount of error is large. In other words, when the stinger is dynamically stiff in the x direction at any area of the frequency range, the measured results are more vulnerable to error in that area. This fact holds for A_{mm} and A_{rr} in equations (5-13) and (5-14) as well. Hence, this suggests that the antiresonances of the driving point FRFs of the tip of the stinger are responsible for the maximum error in measured FRFs. It was assumed that the structure behaved as a rigid body in the transverse direction (k DOF). Thus, we shall not consider the effect of the structure in the transverse direction.

5.3.8 The effect of the stinger on the measured FRFs in the axial direction

The stinger which was modelled in ANSYS by assembling BEAM3 elements has tension and compression capability, therefore it can be used to estimate the axial behaviour of the stinger. However, as shown in Figure 5-5, in the axial direction the coil of the shaker slides on the drive part of the shaker. Therefore, assuming that whole of the shaker can be modelled as a lumped mass is not valid in the axial direction. In the previous section, Figure 5-16 shows that the fifth mode of the shaker-stinger-structure system is in the axial direction. This is not a true axial mode because

the whole mass of the shaker is considered in the axial direction. However, it should be mentioned that this mode does not have any influence in our calculation of the rotational antiresonances in the last section because, as shown in Table 5-4, in this mode the stinger has no rotation. In order to analyse the axial motion of the stinger, the same model can be used but the mass of the coil of shaker should be considered as the lumped mass which is attached to the stinger in the shaker-side. The example of section 5.3.6 is considered here again. The mass of the coil is 0.06 Kg. Figure 5-19 shows the receptances of the tip of the stinger on the structure-side in the axial direction for the cases of the straight stinger and the deformed stinger. Table 5-5 compares the resonances and anti-resonances of these two stingers. The first anti-resonances show 60 Hz difference which is considerable in the design of the stinger.

Table 5-5. Comparison of a deformed stinger and a straight stinger in axial direction

Mode	AR of the DS	AR of the SS	AAR of the DS	AAR of the SS
1	0.00	0.04915	2880	2940
2	13717	13586	26982	28170
3	40957	39133	57640	56300
4	68502	65006		

Axial Resonance = AR, Axial Antiresonance = AAR, Deformed Stinger = DS, Straight Stinger= SS
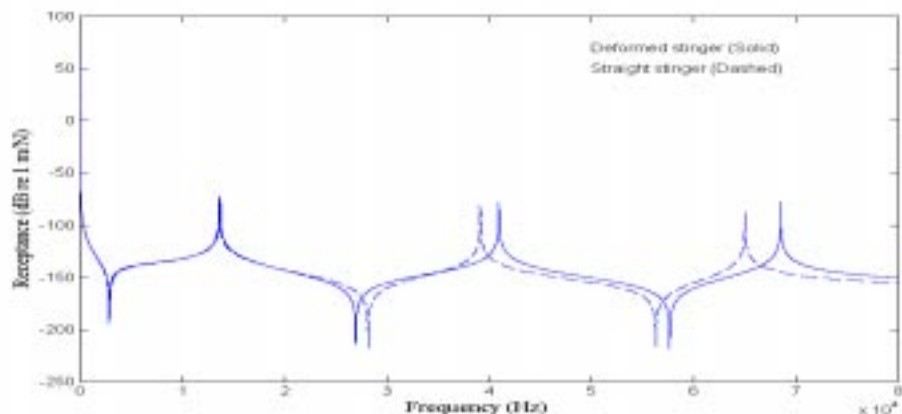
Figure 5-19. Axial receptance of the stinger

5.3.9 Computation of the rigid body modes using FEM model

It was shown in section 5.3.1 that the additional stiffness of the stinger raises the rigid body mode frequencies of the shaker and those of the structure. The ANSYS model which was introduced in the previous section can be used to estimate the rigid body modes of the shaker-stinger-structure system for a deformed stinger. If the structure is assumed to behave as a rigid body then derivation of the rigid body modes is possible. This can be done by considering a lumped mass in the structure end of the stinger which has three DOFs in the axial, transverse and rotational directions. The mass of the structure can easily be measured. However, the moment of inertia of the structure is usually unknown and needs to be estimated using approximate methods. The example of section 5.3.6 is considered here again. Table 5-6 indicates the rigid body modes for the straight stinger and the deformed stinger. The moment of inertia of the structure was estimated to be 0.03 $kg.m^2$. It should be mentioned that for the axial rigid body mode the mass of the coil should be considered on the shaker side. The results of the straight stinger and the deformed stinger cases do not show too much difference (see Table 5-6). Usually the highest rigid body mode is important to choose the minimum allowable measurement frequency. Therefore we can use a straight stinger model with enough accuracy for predicting the behaviour of the stinger in the low frequency range even there is a misalignment.

Table 5-6. Rigid body modes of the shaker-stinger-structure system

No. of mode	Straight stinger	Deformed stinger
axial mode (1)	0.049147	0.00000
2	1.0573	1.0573
3	1.7317	1.7319
4	1.8052	1.7815
5	4.6752	4.6753
6	0.42653	0.27282

5.4 Experimental case study

A beam was tested in the laboratory to validate the shaker-stinger-structure model presented in this chapter. The beam was made of mild steel, and had dimensions $0.2 \times 0.006 \times 0.44m$ and its weight was $0.412\ kg$. The experimental model of the beam was divided into 6 equal elements and was tested in a free-free configuration, suspended vertically by a soft elastic cord attached to the beam at point 1 (see Figure 5-20). The beam was excited by a shaker at point 6 and the response was measured at point 5 using an accelerometer with the weight of $0.004\ kg$. The input signal to the power amplifier was random and Hanning windows were used in both input and output channels to reduce the effects of the leakage. The weight of the shaker was $10.5\ kg$ and its moment of inertia, with respect to the horizontal axis which passes through the centre of gravity of the shaker, was estimated to be $0.03\ kg.m^2$. The weight of the accelerometer was 0.015 kg. The stiffness of the suspension spring of the shaker was estimated experimentally to be 5400 N/m and that of the structure was estimated to be 1200 N/m. No rotary spring was considered for the shaker because just one spring was used to suspend it. Four different stingers were used to transfer the excitation force of the shaker to the structure. Table 5-7 shows the parameters of the stingers. The diameters of the stingers are the same while their lengths are different.

Figure 5-21 shows the predicted rotational receptance of each stinger at the structure end in the frequency range of 0-1600 Hz, computed using the model shown in Figure 5-4. Figure 5-22 shows this receptance in the frequency range of 0-500 Hz. Table 5-8 shows the first bending anti-reonance, the first axial anti-resonance and the last anti-resonance in the low frequency range of each stinger. Stinger 1, which is shorter than the others, is dynamically stiffer and has raised the rigid body modes of the structure and those of the structure unacceptably. On the other hand, stinger 4, which is longer than the other stingers, has an elastic anti-resonance at 1110 Hz which can affect the measured FRFs.
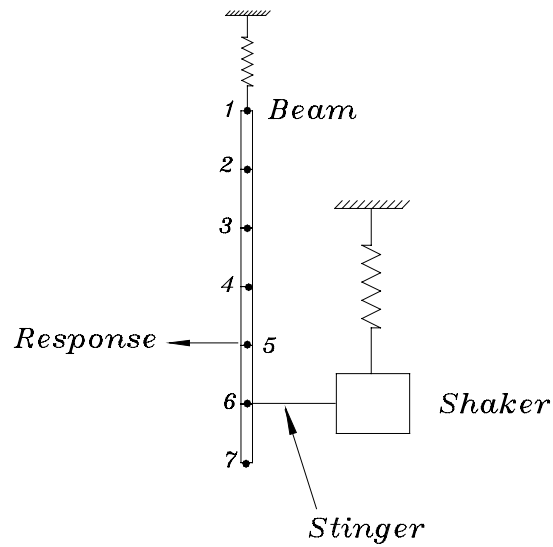
Figure 5-20. Measurement using different stingers

Table 5-7. The parameters of different stingers

No. of Stinger	Length (mm)	Diameter (mm)
1	7	1.5
2	20	1.5
3	25	1.5
4	79	1.5

Table 5-8. Dynamic properties of different stingers

No. of stinger	First bending anti-resonance	First axial anti-resonance	Last anti-resonance in the low frequency area
1	14400 Hz	8188 Hz	341 Hz
2	17320 Hz	4963 Hz	71.5Hz
3	11080 Hz	4239 Hz	51.3 Hz
4	1110 Hz	2389 Hz	12.55 Hz
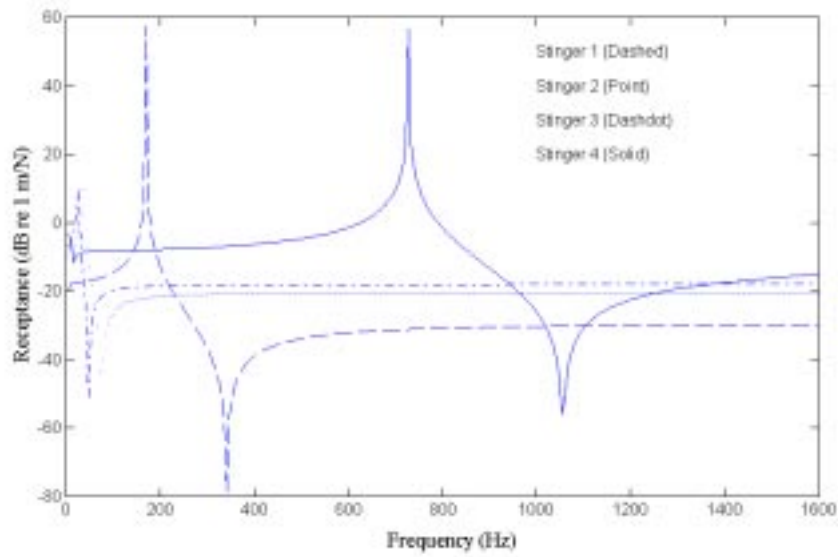
Figure 5-21. Predicted input rotational receptance of the shaker-stinger-structure system to the structure
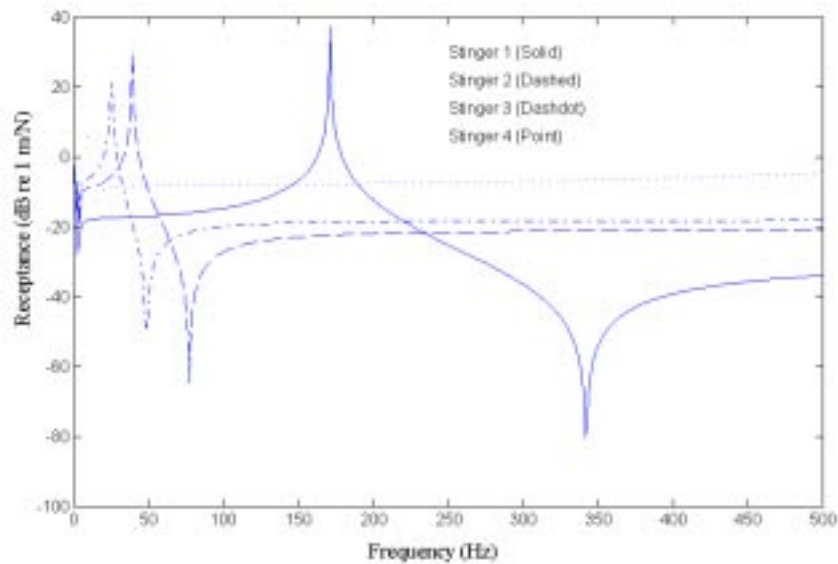
Figure 5-22. Predicted input rotational receptance of the shaker-stinger-structure system to the structure in the low frequency region

Figures 5-24 and 5-25 show the effects of the stingers on the measured FRFs in the actual test. Stinger 1, which is stiffer than the others, has affected the measured FRF unacceptably. In this case, the connection of the shaker and structure is so stiff that the dynamics of the shaker affects the measured FRFs seriously. The first bending anti-resonance of stinger 4 has introduced a glitch into the measured FRF around 1064 Hz. The prediction of the first bending antiresonance of the theoretical model of stinger 4 was 1110 Hz which shows a 46 Hz (4%) difference. The last anti-resonance in the low frequency area of stinger 3 was predicted to be at 51.3 Hz while the measured FRF show this at 45 Hz, a 6.3 Hz (12%) difference. The last anti-resonance in the low frequency range for stinger 2 was predicted to be at 71.5 Hz while the measured FRF is affected at 58 Hz, a 13.5 Hz (or 23%) difference.

The difference between the prediction and the result of the measurements for stingers 2 and 3 in the low frequency range is not acceptable. It was shown in section 5.3.3 that the parameters of the stinger and the mass of the structure are the most important factors in the determination of location of the last antiresonance in the low frequency range. In an actual test the stinger is attached to the structure using a mounting hardware. Moreover, a force transducer is attached to the stinger at the structure end (Figure 5-23). Therefore it is important to consider the mass of force transducer and that of mounting hardware in the model. Moreover, the extra length of the mounting hardware and that of the force transducer should be compensated in the model by adding an extra length to the stinger. If we add the mass of the force transducer and that of the mounting hardware (0.025 Kg) to the mass of the structure and we add an extra length of 2 *mm* to the length of the theoretical model of stinger 2, the last antiresonance in the low frequency area will move to 60 Hz (58 Hz in the experiment); for stinger 3, the last antiresonance in the low frequency range will move to 44.5 Hz (45 Hz in the experiment). As a result, the difference between the prediction and the measurement will decrease to less than 3% for stingers 2 and 3. Addition of 2 mm to the length of stinger 4 will improve the prediction of its first elastic antiresonance from 1110 Hz to 1056 Hz which shows 8 Hz (0.7%) difference with the measurement result (1064 Hz).
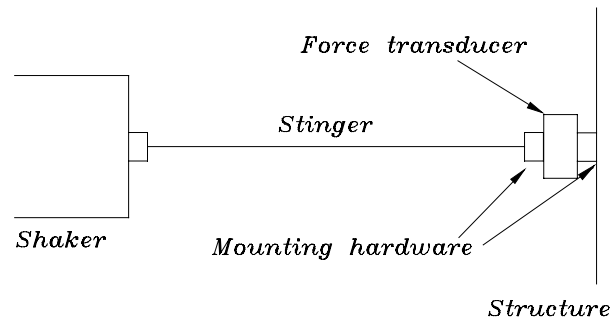
Figure 5-23. Force transducer and mounting hardware in the shaker-stinger-structure system

To examine the effect of misalignment of the stinger on its performance, stinger 4 was chosen and three tests were conducted for three different positions of this stinger. In the first case the equipment was assembled in such a way that the stinger remained straight. In the second case, the suspension spring of the structure was moved downward in such a way that the structure end of the stinger moved 20 *mm* downward with respect to the original position (see Figure 5-26) . In the third case, the suspension spring of the structure was moved downward in such a way that the structure end of the stinger moved 50 *mm* downward with respect to the original position. Figure 5-26 shows the effect of these misalignments on the measured FRFs. The differences between the measured FRFs are considerable but the natural frequencies do not show major differences. Moreover, as the deformation was increased the anti-resonance of the stinger shifted to the lower frequencies, as was predicted by the theoretical model.

The deformation of the stinger biases the results and can be restricted by determining a maximum allowable deformation of the stinger. This can be done by calculating the changes in the first elastic antiresonance of the stinger relating to its deformation which was presented in section 5.3.6. Based on the results of the latter experiment, it is recommended that the deformation of the stinger is restricted so that the changes in the first antiresonance of the theoretical model of the stinger is less than 5 Hz.

Because the deformed stinger is arch-like, it will not exhibit linear behaviour any more. Therefore, when the structure is excited by a deformed stinger, the measured FRFs should be checked for signs of nonlinearity. Figures 5-28 to 5-30 show the results of the measurements for the cases of the straight and deformed stingers (cases 1 and 2 in Figure 5-26) for three different levels of excitation force. For the case of the straight stinger, no sign of nonlinearity was detected while for the cases of the deformed stingers the measured FRFs showed nonlinearity in the areas of antiresonance of the stinger.

The results of this experimental case study show that the shaker-stinger-structure model which has been introduced in this chapter can give us reasonable data for predicting the behaviour of stingers and designing them for special purposes. Moreover, this model can be used for predicting the effect of the misalignment of the stinger on the measured FRFs. It is necessary to define a maximum allowable misalignment for a particular stinger to prevent obtaining biased results.
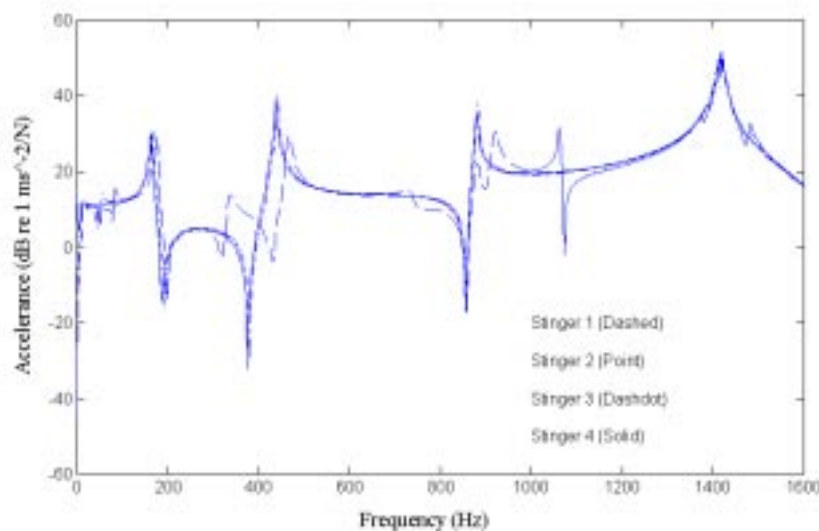
Figure 5-24. The effects of the stingers on the measured FRFs
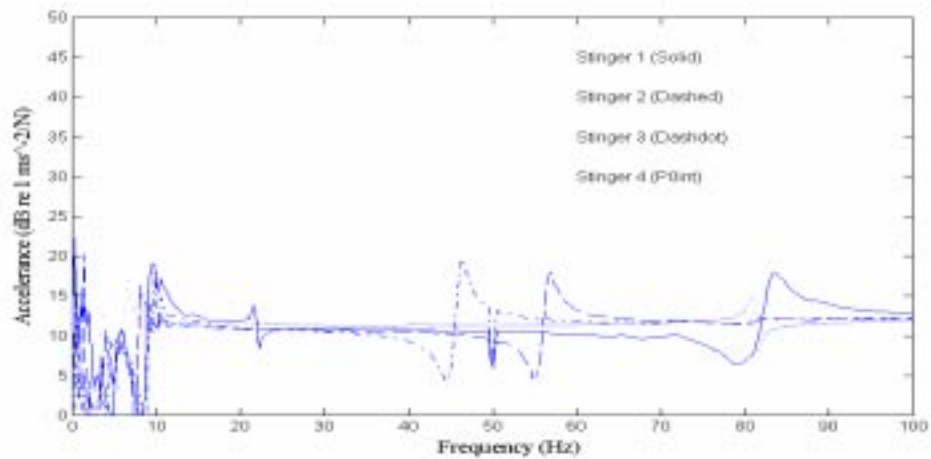
Figure 5-25. The effects of the stingers on the measured FRFs in the low frequency region
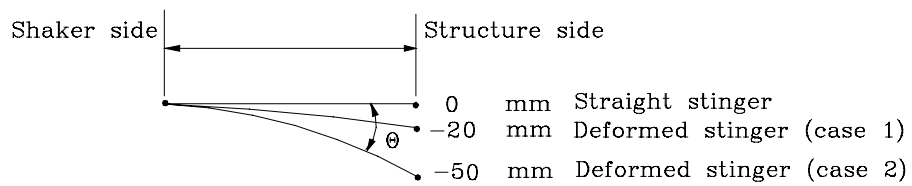
Figure 5-26. Deformed stingers
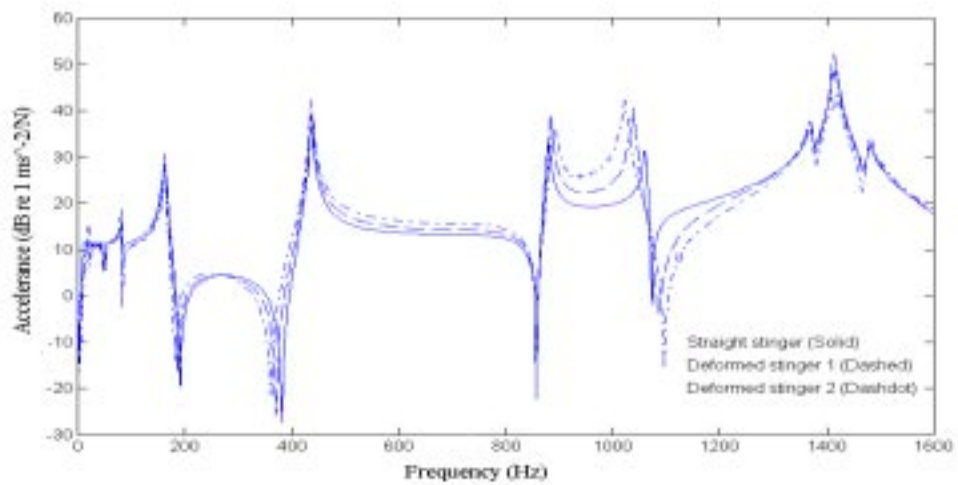
Figure 5-27. The effect of the misalignment of the stinger on its performance
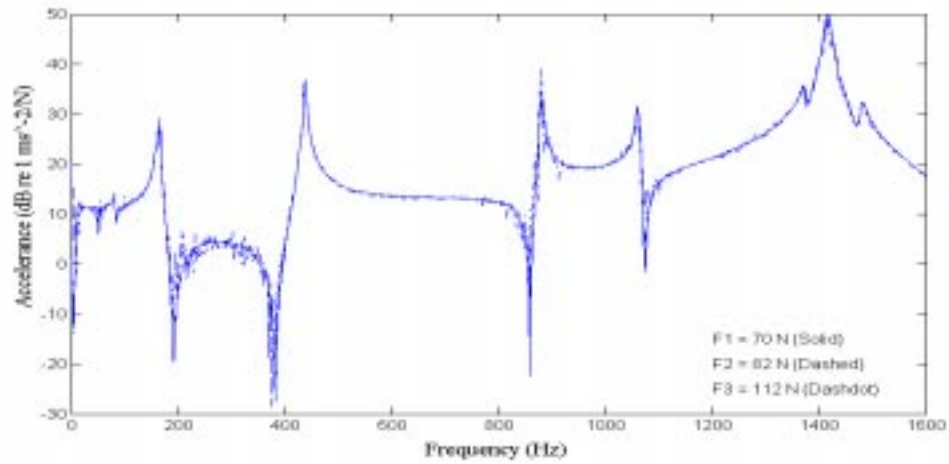
Figure 5-28. Nonlinearity check for the straight stinger

(different lines represent measured FRFs using different levels of excitation force)
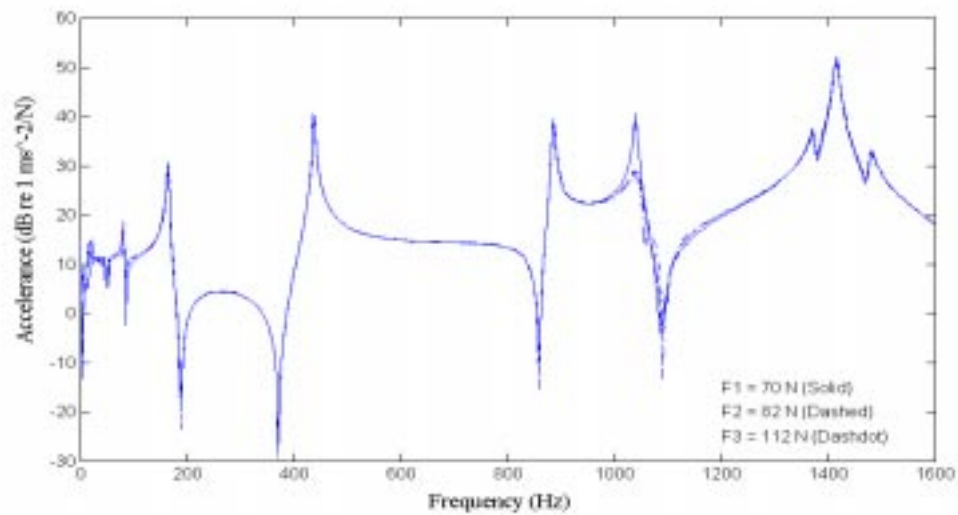
Figure 5-29. Nonlinearity check for the deformed stinger (case 1)

(different lines represent measured FRFs using different levels of excitation force)
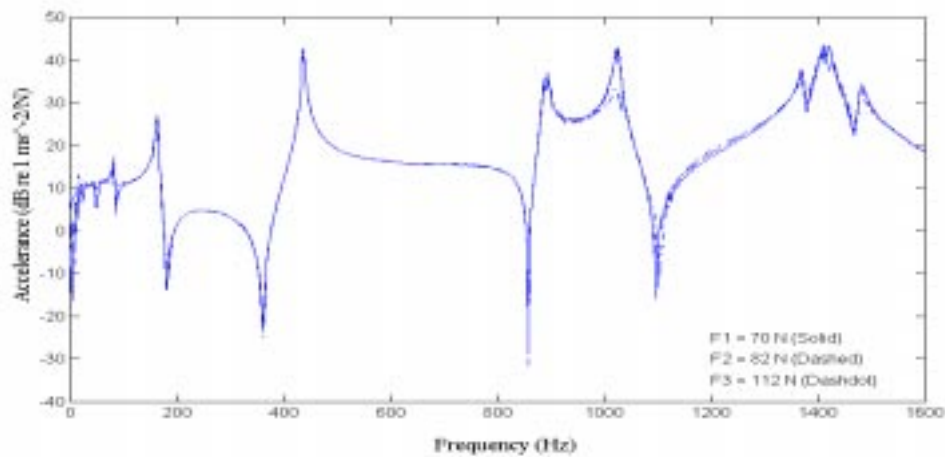
Figure 5-30. Nonlinearity check for the deformed stinger (case 2)

(different lines represent measured FRFs using different levels of excitation force)

5.5 How to design a stinger

The measured FRFs can become so noisy in the low frequency region of the response that it is not possible to determine if the lowest elastic mode of the system is buried in noise. From a signal processing point of view the goal of modal testing is to produce a measurable response such that the ratio of the input and response can be properly calculated. It is therefore necessary to determine the minimum measurable response for the particular application. This depends on the background noise, the transducers' sensitivities, and the minimum resolution of the data acquisition system.

To find the relation between the minimum measurable frequency due to noise and the required input force, suppose that our system is a simple mass and spring system (*m=5 kg, k= 500 KN/m*). Thus, the equation governing the system is :

$$F = X''(\frac{k}{-\omega^2} + m) \tag{5-15}$$

where X'' is the acceleration in the frequency domain. If the sensitivity of the accelerometer is 10 v/g and it is easy to measure 10 millivolts of signal, it is possible

to measure a response of 0.01g. In order to determine how much excitation force is necessary, the minimum frequency of interest should be known. For example, if the minimum frequency is 10 Hz then the required force is :

$$f = \left|(0.01) \times (9.8) \times (\frac{500000}{-(2 \times \pi \times 10)^2} + 5)\right| = 11.92 \quad N$$

If this same test is required to provide reliable data down to 2 Hz, then 309.85 N is needed. For 1 Hz, then 1240.7 N is needed. Conversely, it is the reason that FRFs get more and more noisy as the frequency diminish. Although this discussion holds for sinusoidal excitation, practically, it holds for other excitation method as well.

It can be concluded that reliable FRF data in some part of the low frequency range will be unobtainable. The effect of noise depends on the dynamic behaviour of the structure which is under investigation by the modal test, the level of the background noise and many other parameters. Therefore, there is no straightforward formula to relate the input force and the level of the noise. However, a more powerful shaker will decrease the effect of noise in the low frequency range.

Once the input force and the size of the shaker are chosen the following steps should be followed to design the stinger:

Step 1- Calculate the minimum allowable diameter of the stinger. If the maximum input force is P, and the material endurance stress of stinger is σ_s, then :

$$\sigma_s = \frac{P}{A_s}; A_s = \frac{\pi d_s^2}{4} \tag{5-16}$$

The minimum allowable diameter of the stinger is thus:

$$d_{min} = \sqrt{\frac{4P}{\pi \sigma_s}} \tag{5-17}$$

The diameter of the stinger can be chosen to be greater than the minimum allowable diameter (d_{min}). However, a thinner stinger is more flexible and has less effect on the measured FRFs.

Step 2- Calculate the maximum allowable length of the stinger from Euler formula to avoid the buckling of the stinger:

$$l_{max} = \sqrt{\frac{2\pi^2 E_s I_s}{P}}; I_s = \frac{\pi d_s^4}{64}$$

(5-18)

The length of the stinger cannot be more than l_{max}. However l_{max} is not the optimum length of the stinger.

The most important part of designing a stinger is to choose the optimum length. If the minimum and maximum desirable frequencies (f_{min} and f_{max}) are known, the optimum length of the stinger should be chosen in such a way that the last antiresonance in the low frequency range of the stinger is lower than f_{min} and the first elastic antiresonance of the stinger is higher than f_{max}. This can be done by trial- and-error of different lengths in the theoretical model of the stinger which was presented in section 5.3.1.

Step 3- For a particular length of stinger, compute the antiresonance in the low frequency region, as was discussed in section 5.3.3. For this computation the parameters of the shaker and those of the structure are needed. It is important to add the mass of the force transducer and that of the mounting hardware to the mass of the structure. Moreover, it is necessary to add an additional length to the length of the stinger to compensate for the length of the mounting hardware and that of the force transducer. Based on the experience gained in section 5.4, this additional length is 2~3 *mm.*

Step 4- Calculate the first elastic antiresonance for the stinger of a particular length, as was discussed in section 5.3.4. Table 5.2 shows some of these antiresonances for different lengths and diameters of the steel stingers.

Step 5- Calculate the first antiresonance of the stinger in the axial direction using the ANSYS model as was presented in section 5.3.8. If the first antiresonance of the stinger in the axial direction is lower than that of the stinger in the bending direction then the antiresonance in the axial direction should be more than f_{max}.

Step 6- After trying different lengths for the stinger, the optimum length can be chosen so that the antiresonances of the stinger are not in the frequency range of $f_{\min}$ to $f_{\max}$.

Step 7- Determine a maximum allowable deflection of the stinger. The experimental results of section 5.4 showed that the deformation of the stinger can bias the results unacceptably. Based on the experience gained in section 5.4, it is recommended that the deformation of the stinger should be restricted so that the change in the first antiresonance of the stinger is less than 5 Hz. The procedure to calculate the change in the first antiresonance of the stinger due to its misalignment was explained in section 5.3.6.

5.6 How to check the effects of a stinger on the measured FRFs

In the previous section we presented a procedure to design a stinger for the test so that its effect on the measured FRFs become minimum. However, it is necessary to check the effects of the stinger on the measurements for assessing the quality of the measurement.

In the design of a stinger the main effort is to avoid the stinger's antiresonances. If the length of the stinger is changed slightly, its antiresonances (bending or axial) will shift slightly in the frequency range. As a result, the effects of the antiresonances of the stinger on the measured FRF will shift slightly and this is a sign of error. We present this fact by a numerical example:

A steel beam was tested in a simulated shaker test using two different stingers (Figure 5-32). The parameters of the simulated test were:

<u>Beam</u> : Dimension : $0.02 \times 0.006 \times 0.44$ *m* , Material: Steel.

<u>Shaker</u> : Mass : 10.5 *kg*, Rotary moment of inertia : 0.03 *kg.m²* , Suspension: $k_{sh} =$ 5400 *N/m*, $kr_{sh} = 0$ *N-m/rad*.

<u>Stinger 1</u> : Diameter : 2 *mm* , Length : 0.075 *m*, Material : Steel.

Stinger 2 : Diameter: 2 *mm*, Length: 0.079 *m*, Material : Steel.

Measurement Set up : Excitation : at point 3, Response: at point 7.

Frequency range : 200-2000 Hz

Figure 5-33 shows that the location of the first elastic antiresonance of stinger 1 is at 1645 Hz and that of stinger 2 is at 1480 Hz. Figure 5-34 shows the effects of stingers1 and 2 on the measured FRF. This figure shows that by replacing stinger 2 with stinger 1, the effect of the latter stinger shifts slightly to the lower frequencies while the other parts of the measured FRF remains unchanged. This suggests that by a slight change in the length of the stinger, its effect on the measured FRF can be revealed. Consequently, using this method the effect of a designed stinger on the measured FRF can be checked.
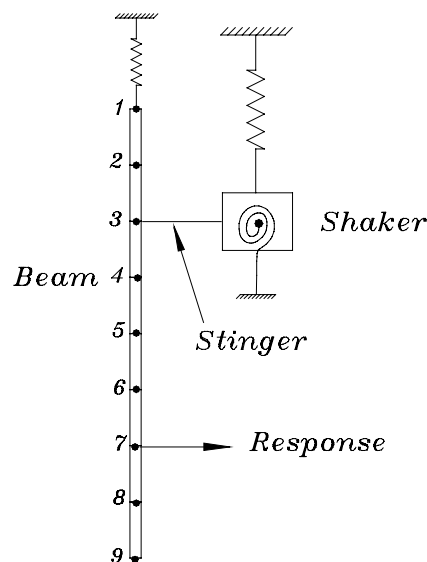
Figure 5-31. Model used for the Simulated shaker test
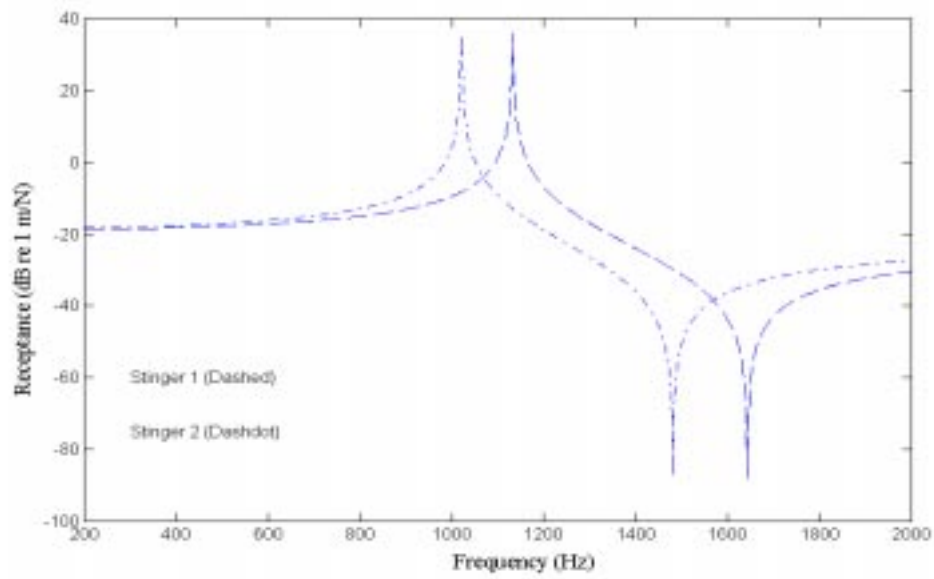
Figure 5-32. Antiresonances of stingers 1 and 2
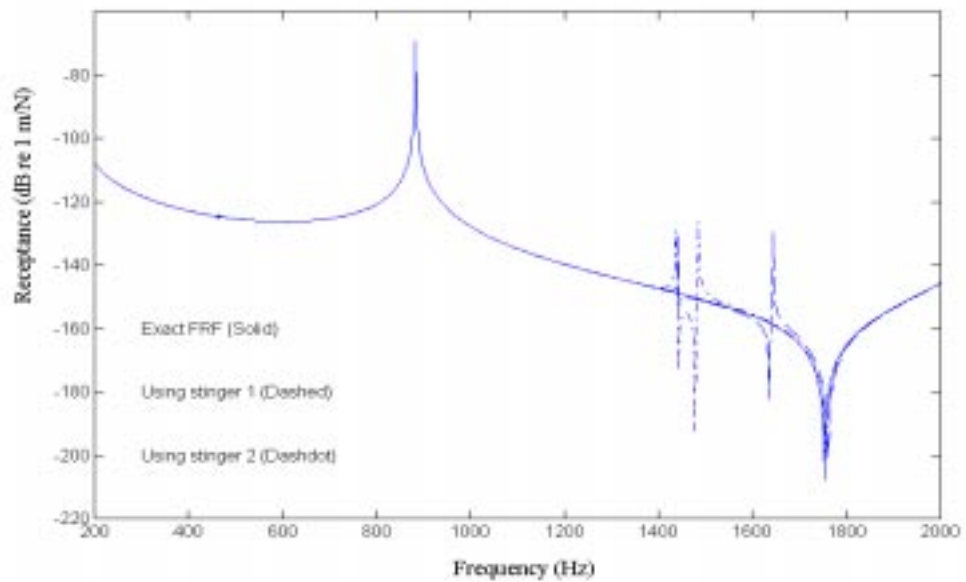
Figure 5-33. The effects of stingers 1 and 2 on the measured FRF

5.7 Design of a stinger in an actual test

A steel beam with a mass of 0.412 *kg* is to be experimentally tested for its dynamic characteristics. The beam is to be suspended vertically with an elastic cord with the stiffness of 410 *N/m*. A 80 *N* electromagnetic shaker is chosen to excite the structure. The mass of the shaker is 10.5 *kg* (the mass of the coil is 0.21 *kg*) and its moment of inertia is 0.03 $Kg.m^2$. The shaker was suspended by a spring with the stiffness of 5400 *N/m*. The mass of the force transducer and that of the mounting hardware is 0.025 *kg*. The required frequency range of the measurement was 80 to 1250 Hz.

In order to find the optimum stinger for this test the procedure is:

The minimum diameter is calculated from equation (5-17) as:

$$d_{min} = \sqrt{\frac{4 \times 80}{\pi \times 345 \times 10^6}} = 5.5 \times 10^{-4} \ m$$

In which $\sigma_s = 345 \times 10^6$ *N/m* is the material endurance stress of the steel. The diameter of the stinger can be chosen to be 1.5 *mm*. It should be mentioned that the diameter of the stinger can be chosen to be greater than the minimum allowable diameter (d_{min}). However, a thinner stinger is more flexible and has less effect on the measured FRFs.

The maximum allowable length of the stinger can be calculated from equation (5-18) as:

$$l_{max} = \sqrt{\frac{2\pi^2 \times 121 \times 10^9 \times \pi \times (1.5 \times 10^{-3})^4}{64 \times 80}} = 0.086 \ m$$

Calculations show that the last antiresonance in the low frequency range for a stinger with the diameter of 1.5 *mm* and length of 25 *mm* is at 44.5 Hz and its first elastic bending antiresonance is at 11080 Hz. The first axial anti resonance of this stinger is at 4239 Hz. Therefore this stinger is suitable for measuring the FRFs of the beam in the frequency range of 80 to 1250 Hz.

Calculations show that for a stinger with the diameter of 1.5 *mm* and length of 25 *mm,* when we have 2.1 *mm* misalignment between two ends of the stinger (Figure 5-31) , the first elastic anti resonance of the stinger (in the axial direction) moves to 4234 Hz (5 Hz difference). As a result the misalignment between two sides of the stinger should not exceed 2.1 *mm*.
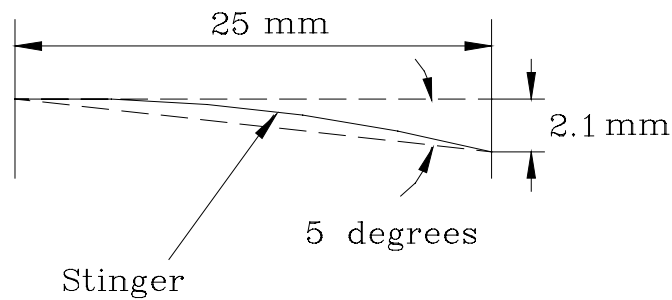
Figure 5-34. Misalignment of the stinger

Figure 5.35 shows the result of the measurement of the beam in the actual test using the stinger designed above with the following parameters:

Stinger 1 : Diameter : 1.5 *mm* , Length : 25 *mm*, Material : Steel.

In order to check the performance of stinger 1 another measurement was conducted using another stinger with the same diameter but slightly different length. The parameters of this stinger were:

Stinger 2 : Diameter : 1.5 *mm* , Length : 27 *mm*, Material : Steel.

Figure 5.35 shows the result of the measurement using stinger 2 which is drawn together with the measured FRF using stinger 1. There is no considerable difference between two measured FRFs. Therefore it can be concluded that stinger 1 (or stinger 2) is suitable for this test.

Figure 5-36 shows the result of the measurement of the beam in the actual test using an unsuitable stinger. The parameters of this stinger are:

Stinger 3 : Diameter : 1.5 *mm* , Length : 82 *mm*, Material : Steel.

Another stinger with the same diameter but slightly different lengths was used to reveal the effect of stinger 3 on the measured FRF (see Figure 5.36). The parameters of this stinger are:

Stinger 4 : Diameter : 1.5 *mm* , Length : 85 *mm*, Material : Steel.

A comparison between two measured FRFs (using stingers 3 and 4) in Figure 5-36 shows that stinger 3 has affected the measured FRF at 1080 Hz and stinger 2 has shift this effect to 1000 Hz. There is no discernible difference between two measured FRFs at all the other frequencies. For comparison purposes the measured FRF using stinger 1 is shown in Figure 5-36. It can be concluded that stinger 3 is not suitable for the measurement of the beam in the frequency range of 80-1250 Hz. Moreover, the result of this test show that the method for assessing the performance of a stinger can show the effects of an unsuitable stinger on the measured FRFs.
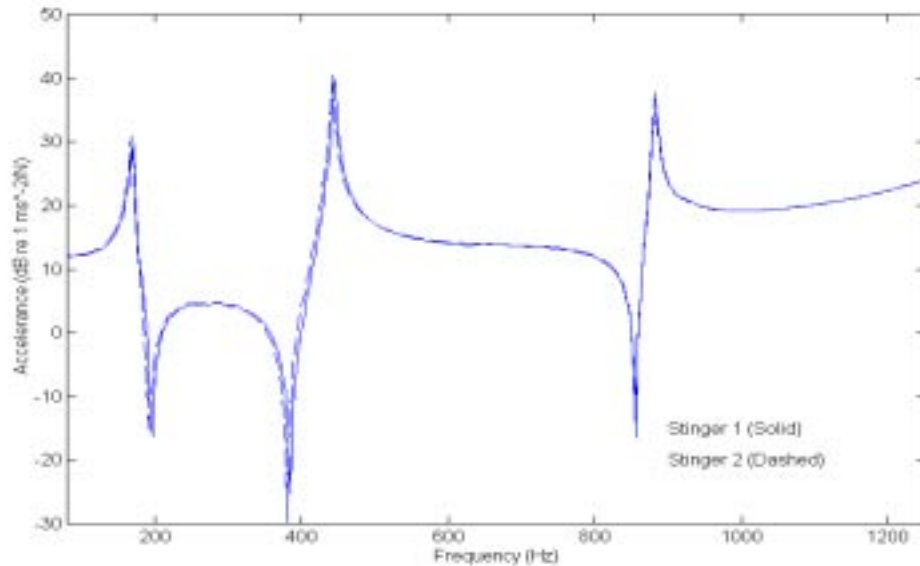
Figure 5-35. Checking of the performance of the designed stinger
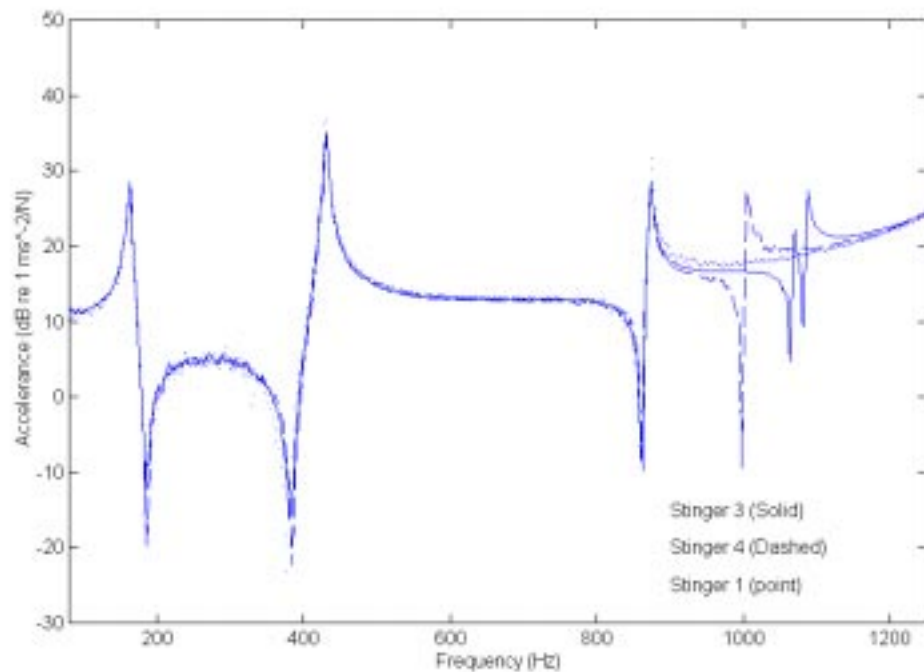
Figure 5-36. Revealing of the effects of an unsuitable stinger on the measured FRF

5.8 Conclusions

- It was proven that the maximum error of the measured FRFs are due to the antiresonances of the rotational driving point receptance of the tip of the stinger.

- In this chapter a new model was presented for the shaker-stinger-structure system. This model allowed us to assess the effect of the misalignment of the stinger on its performance.

- It was shown that when there is a misalignment between two ends of the stinger, the antiresonances of the stinger shift to the lower frequencies and the measured FRFs are biased. Therefore, a maximum allowable deformation of the stinger was introduced based on the changes in the first elastic antiresonance of the stinger.

- The presented model was used for the calculations of the antiresonances of the shaker-stinger-structure system which was successfully validated by the experimental results of a free-free beam.

- Based on this study a design procedure was introduced which was followed by an example.

- It was shown that the effects of the stinger on the measured FRF can be checked by repeating the test with another stinger with the same diameter but slightly different length.

Chapter 6

Correction of mechanical effects in

more than one DOF

Reminder of Nomenclature

α_{ij}^* measured receptance of a modified structure

n number of modification DOFs

n_c number of different configurations

r number of unknowns

$^{(p)}\alpha_{ii}'$ receptance of the attached mechanical element

                            at DOF i for p^{th} configuration

$\left[\alpha_{ii}'\right]$ matrix of the receptances of attached mechanical

                            elements for different configurations

6.1 Introduction

The basic theory for the correction of mass-loading effects of a transducer in one DOF was presented in chapter 3. In chapter 4 a similar method was developed for the correction of the effects of a suspension spring on the test structure. However, the test structure may be affected by mechanical devices in more than one DOF. By mechanical devices we mean suspension springs, transducers and stingers or any other mechanical elements which are used to conduct the modal test. In practice, there are some cases that it is advantageous for us to cancel the effect of the mechanical devices in more than one DOF (see chapters 8 and 9). Therefore, it is imperative to generalise the correction method mathematically before dealing with more complicated practical cases.

In this chapter a general solution for the correction of the effects of mechanical devices on measured FRFs by modifying the test structure at its boundaries will be

presented. It is shown that the FRFs can be corrected if the measurement is repeated in a number of different configuration; each configuration consisting of the system with one or more of its boundary conditions changed. It is also shown that the driving point FRFs related to the degrees of freedom of the attachment of mechanical devices can be computed without actually having to measure them. One of the applications of these correction methods is in chapter 9 where the test structure is modified in two DOFs by the mass and rotational inertia of an attached object in order to generate the rotational FRFs.

6.2 Theory

6.2.1 Modification of the test structure in more than one DOF

Appendix A of this thesis investigates the general case of the changes in measured FRFs due to the attachment of mechanical devices to the test structure. As shown at this appendix, for the general case, when the test structure is modified in n DOFs, the relation between the measured FRF and the exact FRFs is :

$$\alpha_{lk}{}^{*} = \frac{\begin{vmatrix} \alpha_{lk} & \alpha_{l1} & \alpha_{l2} & \cdot & \cdot & \alpha_{ln} \\ \alpha_{1k} & \alpha_{11}+\alpha'_{11} & \alpha_{12} & \cdot & \cdot & \alpha_{1n} \\ \alpha_{2k} & \alpha_{21} & \alpha_{22}+\alpha'_{22} & \cdot & \cdot & \alpha_{2n} \\ \cdot & \cdot & \cdot & \cdot & \cdot & \cdot \\ \cdot & \cdot & \cdot & \cdot & \cdot & \cdot \\ \alpha_{nk} & \alpha_{n1} & \alpha_{n2} & \cdot & \cdot & \alpha_{nn}+\alpha'_{nn} \end{vmatrix}}{\begin{vmatrix} \alpha_{11}+\alpha'_{11} & \alpha_{12} & \cdot & \cdot & \alpha_{1n} \\ \alpha_{21} & \alpha_{22}+\alpha'_{22} & \cdot & \cdot & \alpha_{2n} \\ \cdot & \cdot & \cdot & \cdot & \cdot \\ \cdot & \cdot & \cdot & \cdot & \cdot \\ \alpha_{n1} & \alpha_{n2} & \cdot & \cdot & \alpha_{nn}+\alpha'_{nn} \end{vmatrix}} \tag{6-1}$$

Equation (6-1) can be rewritten as :

$$b = x_{2r+1} - \frac{x_1 a_1 + x_2 a_2 + \cdot \quad \cdot \quad +x_r a_r}{x_{r+1}a_1 + x_{r+2}a_2 + \cdot \quad \cdot \quad +x_{2r}a_r + a_{r+1}} \tag{6-2}$$

where :

$$b = \alpha_{lk}^{*} \tag{6-3}$$

and a_1, a_2, ..., a_{r+1} are the multiplications of α_{ii}''s which are given in Table 6-1. In the first row it is shown that $a_1 = 1$. In the second row it is shown that $a_2 = \alpha_{11}'$, $a_3 = \alpha_{33}'$, ..., $a_{n+2} = \alpha_{nn}'$. In the third row it is shown that $a_{n+3} = \alpha_{11}'\alpha_{22}'$, $a_{n+4} = \alpha_{11}'\alpha_{33}'$ and so on until the last row that $a_{r+1} = \alpha_{11}'\alpha_{22}'\alpha_{33}' \cdot \cdot \cdot \alpha_{nn}'$. The total number of a_i's is $r = 2^n - 1$.

Table 6-1. Parameters of equation (6-2)

a_i		considerations	number of a_i's
a_1	1		1
$a_2,...$	α_{ii}'	$i = 1,2,...,n$	n
a_{n+2},	$\alpha_{ii}'\alpha_{jj}'$	$i, j = 1,2,...,n$ and $i \neq j$	$n \times (n-1)/2$
.	$\alpha_{ii}'\alpha_{jj}'\alpha_{kk}'$	$i, j, k = 1,2,...,n$ and $i \neq j \neq k$	$n \times (n-1) \times (n-2)/3 \times 2$
.	.	. .	.
.	.	. .	.
.	.	. .	.
a_{r+1}	$\alpha_{11}'\alpha_{22}'\alpha_{33}' \cdot \cdot \cdot \alpha_{nn}'$		1
Total number of a_i's $(r+1)$			2^n

x_i's are unknowns and are a combination of α_{ij}'s, x_{2r+1} is :

$$x_{2r+1} = \alpha_{lk} \qquad\qquad (6\text{-}4)$$

x_{r+1}, x_{r+2}, . . . , x_{2r} are a combinations of α_{11}, α_{22}, . . . , α_{nn}. Especially we have :

$$\begin{cases} x_{2r-n+1} = \alpha_{11} \\ x_{2r-n+2} = \alpha_{22} \\ \qquad . \\ \qquad . \\ \qquad . \\ x_{2r} = \alpha_{nn} \end{cases} \qquad\qquad (6\text{-}5)$$

x_1, x_2, . . . , x_r are a combination of α_{11}, α_{22}, . . . , α_{nn}, α_{1k}, α_{2k}, . . . , α_{nk} and α_{l1}, α_{l2}, . . . , α_{ln}.

6.2.2 Correction of the FRFs

Correction of the measured FRFs for the case where a structure is modified in more than one DOF can essentially be accomplished in two main ways :

1. step by step correction : in this approach in each step the effect of one of the mechanical elements corresponding to one DOF is corrected, while the others are constant. An application of this approach for the case of a structure which is modified by two springs in two different DOFs was given in section 4.2.3.(This approach will be used for the generation of rotational FRFs in chapter 9)

2. direct correction : in this approach the structure is tested in a number of different configurations; each configuration consists of the structure with one or more of its boundary conditions changed. Using the data of these tests the effects of the mechanical devices on measured FRFs can be corrected by numerical procedures. The direct correction approach is the main concern of this chapter.

The direct correction method demands more complicated calculations and numerical considerations in order to get realistic results. In equation (6-2), the magnitudes of b's and a's are different in each configuration while the magnitude of x's are a combination of α_{ij}'s and constant. Hence, for each configuration equation (6-2) can be rewritten as :

$$b^{(i)} = x_{2r+1} - \frac{x_1 a_1^{(i)} + x_2 a_2^{(i)} + \cdot \quad \cdot +x_r a_r^{(i)}}{x_{r+1} a_1^{(i)} + x_{r+2} a_2^{(i)} + \cdot \quad \cdot +x_{2r} a_r^{(i)} + a_{r+1}^{(i)}} \qquad \textbf{(6-6)}$$

where i is an indication of a specific configuration. Equation (6-6) can be solved for x_1, x_2, . . . , x_{2r}, x_{2r+1} if the measurement is repeated for enough different configurations. The number of unknowns is $(2r+1)$ in which $r = 2^n - 1$ (n is the number of modification DOFs). Therefore, $2r + 1 = 2^{n+1} - 1$ different configurations are needed to find the unknowns. Equation (6-6) can be rewritten as :

$$x_1 a_1^{(i)} + x_2 a_2^{(i)} + \cdot \quad \cdot +x_r a_r^{(i)} + x_{r+1} a_1^{(i)} b^{(i)} + x_{r+2} a_2^{(i)} b^{(i)} + \cdot \quad \cdot +x_{2r} a_r^{(i)} b^{(i)} \qquad \textbf{(6-7)}$$
$$- x_{2r+1}(x_{r+1} a_1^{(i)} + x_{r+2} a_2^{(i)} + \cdot \quad \cdot +x_{2r} a_r^{(i)}) - a_{r+1}^{(i)} x_{2r+1} = -a_{r+1}^{(i)} b^{(i)}$$

Equation (6-7) is not a linear equation but it can be linearised and solved by the following procedure. For n_c different configurations, the system of equations (6-7) can be written in a shorthand summary as :

$$\begin{vmatrix} x_1 & x_2 & \dots & x_r & x_{r+1} & x_{r+2} & \dots & x_{2r} & x_{2r+1} & x_{2r+1}x_{r+1} & x_{2r+1}x_{r+2} & \dots & x_{2r+1}x_{2r} & cte \\ a_1^{(1)} & a_2^{(1)} & \dots & a_r^{(1)} & a_1^{(1)}b^{(1)} & a_2^{(1)}b^{(1)} & \dots & a_r^{(1)}b^{(i)} & -a_{r+1}^{(1)} & -a_1^{(1)} & -a_2^{(1)} & \dots & -a_r^{(1)} & -a_{r+1}^{(1)}b^{(1)} \\ a_1^{(2)} & a_2^{(2)} & \dots & a_r^{(2)} & a_1^{(2)}b^{(2)} & a_2^{(1)}b^{(1)} & \dots & a_r^{(2)}b^{(2)} & -a_{r+1}^{(2)} & -a_1^{(2)} & -a_2^{(2)} & \dots & -a_r^{(2)} & -a_{r+1}^{(2)}b^{(2)} \\ . & . & \dots & . & . & . & \dots & . & . & . & . & \dots & . & . \\ a_1^{(nc)} & a_2^{(nc)} & \dots & a_r^{(nc)} & a_1^{(nc)}b^{(nc)} & a_2^{(nc)}b^{(nc)} & \dots & a_r^{(nc)}b^{(nc)} & -a_{r+1}^{(nc)} & -a_1^{(nc)} & -a_2^{(nc)} & \dots & -a_r^{(nc)} & -a_{r+1}^{(nc)}b^{(nc)} \end{vmatrix}$$

$$\textbf{(6-8)}$$

To find the solution for the system of equations (6-8), a procedure like the Gauss elimination method can be used [98]. If the elements of the second row of equations (6-8) are multiplied by $a_1^{(2)}$ and the elements of the third row by $a_1^{(1)}$ and the elements of the third row are subtracted from the elements of the second row then x_1 and $x_{2r+1}x_{r+1}$ will be eliminated from the resulted equations. This procedure can be repeated for the second row and other rows of equation (6-8). The resulting equation is :

$$
\begin{vmatrix}
x_2 & \cdots & x_r & x_{r+1} & \cdots & x_{2r} & x_{2r+1} & x_{2r+1}x_{r+2} & \cdots & cte \\
a_2^{(2)}a_1^{(1)}-a_2^{(1)}a_1^{(2)} & \cdots & a_r^{(2)}a_1^{(1)}-a_r^{(1)}a_1^{(2)} & a_1^{(2)}a_1^{(1)}(b^{(2)}-b^{(1)}) & \cdots & \cdot & \cdot & \cdot & \cdots & \cdot \\
a_2^{(3)}a_1^{(1)}-a_2^{(1)}a_1^{(3)} & \cdots & a_r^{(3)}a_1^{(1)}-a_r^{(1)}a_1^{(3)} & a_1^{(3)}a_1^{(1)}(b^{(3)}-b^{(1)}) & \cdots & \cdot & \cdot & \cdot & \cdots & \cdot \\
\cdot & \cdots & \cdot & \cdot & \cdots & \cdot & \cdot & \cdot & \cdots & \cdot \\
a_2^{(nc)}a_1^{(1)}-a_2^{(1)}a_1^{(nc)} & \cdots & a_r^{(nc)}a_1^{(1)}-a_r^{(nc)}a_1^{(nc)} & a_1^{(nc)}a_1^{(1)}(b^{(nc)}-b^{(1)}) & \cdots & \cdot & \cdot & \cdot & \cdots & \cdot
\end{vmatrix}
$$

(6-9)

If the same procedure is followed to eliminate x_2 and $x_{2r+1}x_{r+2}$ from equation (6-9) and the procedure is followed to eliminate x_1, x_2, ..., x_r all nonlinear elements will be eliminated. The final resulting equation is :

$$
\begin{vmatrix}
x_{r+1} & x_{r+2} & \cdots & x_{2r} & x_{2r+1} & & cte \\
q_{11} & q_{12} & \cdots & q_{1r} & q_{1(r+1)} & & p_1 \\
q_{21} & q_{22} & \cdots & q_{2r} & q_{2(r+1)} & & p_2 \\
\cdot & \cdot & \cdot & \cdot & \cdot & & \cdot \\
q_{(nc-r)1} & q_{(nc-r)2} & \cdots & q_{(nc-r)r} & q_{(nc-r)(r+1)} & & p_{(nc-r)}
\end{vmatrix}
$$

(6-10)

Equations (6-10) are a series of linear equations of the form :

$$
\begin{bmatrix}
q_{11} & q_{12} & \cdots & q_{1r} & q_{1(r+1)} \\
q_{21} & q_{22} & \cdots & q_{2r} & q_{2(r+1)} \\
\cdot & \cdot & \cdots & \cdot & \cdot \\
q_{(nc-r)1} & q_{(nc-r)2} & \cdots & q_{(nc-r)r} & q_{(nc-r)(r+1)}
\end{bmatrix}
\begin{Bmatrix}
x_{r+1} \\
x_{r+2} \\
\cdot \\
x_{2r+1}
\end{Bmatrix}
=
\begin{Bmatrix}
p_1 \\
p_2 \\
\cdot \\
p_{(nc-r)}
\end{Bmatrix}
$$

(6-11)

This equation can be summarised as :

$$[q]\{x\}_{r+1}^{2r+1} = \{p\}$$ (6-12)

in which:

$$\{x\}_{r+1}^{2r+1} = \begin{Bmatrix} x_{r+1} \\ x_{r+2} \\ . \\ x_{2r+1} \end{Bmatrix}$$ (6-13)

and the solution is :

$$\{x\}_{r+1}^{2r+1} = [q]^+ \{p\}$$ (6-14)

where $[q]^+$ is the pseudo-inverse of $[q]$. To find $x_1, x_2, \ldots, x_r$ equation (6-14) can be rewritten as :

$$x_1 a_1^{(i)} + x_2 a_2^{(i)} + \cdot \quad \cdot \quad \cdot + x_r a_r^{(i)} = (x_{2r+1} - b^{(i)})(x_{r+1}a_1^{(i)} + x_{r+2}a_2^{(i)} + \cdot \quad \cdot \quad \cdot + x_{2r}a_r^{(i)} + a_{r+1}^{(i)})$$

(6-15)

Knowing $x_{r+1}, x_{r+2}, \ldots, x_{2r}$ from (6-14), the right hand side of equation (6-15) is known. So equations (6-8) can be rearrenged as :

$$\begin{vmatrix} x_1 & x_2 & . & . & x_r & \begin{vmatrix} cte \\ g_{11} & g_{12} & . & . & g_{1r} & v_1 \\ g_{21} & g_{22} & . & . & g_{2r} & v_2 \\ . & . & . & . & . & . \\ g_{nc1} & g_{nc2} & . & . & g_{ncr} & v_{nc} \end{vmatrix} \end{vmatrix}$$ (6-16)

or :

$$[g]\{x\}_r^1 = \{v\}$$ (6-17)

and the solution is :

$$\{x\}_r^1 = [g]^+ \{v\} \tag{6-18}$$

in which $[g]^+$ is the pseudo-inverse of $[g]$. The Pseudo-inverse has been used in equations (6-18) and (6-14) to show that the number of equations can be more than the number of unknowns. In this case $[g]$ or $[q]$ is not square and the pseudo-inverse should be used to find the unknowns. When the data are noisy, increasing the number of equations and using the pseudo-inverse will average the solution and decrease the effect of noise. It should be emphasised that the condition to solve the equations (6-11) is :

$$nc \geq 2^{n+1} - 1 \tag{6-19}$$

By solving equations (6-11) and finding x_1, x_2, . . . , x_{2r}, x_{2r+1} and from equation (6-4), α_{lk}, the exact receptance, can be found. Moreover, from equations (6-5) the correct value of α_{11}, α_{22}, . . . and α_{nn} can be obtained.

The above procedure is a direct method for cancellation of the effects of mechanical devices in more than one DOF. Equation (6-19) show that when the test structure is modified in two DOFs, at least 7 different tests with different configurations are needed to cancel the mechanical effects. In the next section the practical aspects of this method will be studied.

6.3 Demonstration and verification of the method

6.3.1 Programming considerations

In the last section it was shown how a measured FRF of a structure which is modified in *n* DOFs can be corrected using direct approach. To program the method suggested in the last section, the following steps have to be considered:

1- arrange the receptances of the attached mechanical devices in each DOF in a matrix in which each row is for one configuration:

$$[\alpha'] = \begin{bmatrix} {}^{(1)}\alpha'_{11} & {}^{(1)}\alpha'_{22} & \cdot & \cdot & \cdot & {}^{(1)}\alpha'_{nn} \\ {}^{(2)}\alpha'_{11} & {}^{(2)}\alpha'_{22} & \cdot & \cdot & \cdot & {}^{(2)}\alpha'_{nn} \\ \cdot & \cdot & \cdot & \cdot & \cdot & \cdot \\ \cdot & \cdot & \cdot & \cdot & \cdot & \cdot \\ \cdot & \cdot & \cdot & \cdot & \cdot & \cdot \\ {}^{(nc)}\alpha'_{11} & {}^{(nc)}\alpha'_{22} & \cdot & \cdot & \cdot & {}^{(nc)}\alpha'_{nn} \end{bmatrix}$$

(6-20)

2- arrange the measured FRFs in a column matrix $\{b\}$ as :

$$\{b\} = \begin{Bmatrix} {}^{(1)}\alpha^*_{lk} \\ {}^{(2)}\alpha^*_{lk} \\ \cdot \\ \cdot \\ {}^{(nc)}\alpha^*_{lk} \end{Bmatrix}$$

(6-21)

3- To calculate the a's as is shown in table 6-1, all the multiplications of the elements of matrix $[\alpha']$ in each row are needed. Table 6-2 shows a typical example of the procedure which is used to calculate the a's from one row of matrix $[\alpha']$ for the case where $n=5$. Each column can be built from the last column. In the first step *(k=1)*, a_1 to a_5 are equal to α'_{11} to α'_{55}. In the second step *(k=2)*, a_6 is made from the multiplication of a_2 by a_1. Multiplying of a_3 by a_1 and a_2, yields a_7 and a_8 respectively. a_4 is multiplied by a_1, a_2 and a_3 which yields a_9, a_{10} and a_{11} and so on. In the same way all the multiplications of α'_{ii}'s are made as is shown in Table 6-2.

Table 6-2. Programming of the multiplication of a set of α'_{ii}'s

No.		*k=1*		*k=2*		*k=3*		*k=4*		*k=5*
1		$a_1 = \alpha'_{11}$	1	$a_6 = a_1 a_2$	1	$a_{16} = a_6 a_3$	1	$a_{26} = a_{16} a_4$	1	$a_{31} = a_{26} a_5$
2		$a_2 = \alpha'_{22}$		$a_7 = a_1 a_3$		$a_{17} = a_6 a_4$		$a_{27} = a_{16} a_5$		
3		$a_3 = \alpha'_{33}$	2	$a_8 = a_2 a_3$		$a_{18} = a_7 a_4$		$a_{28} = a_{17} a_5$		
4		$a_4 = \alpha'_{44}$		$a_9 = a_1 a_4$	3	$a_{19} = a_8 a_4$		$a_{29} = a_{18} a_5$		
5	5	$a_5 = \alpha'_{55}$		$a_{10} = a_2 a_4$		$a_{20} = a_6 a_5$	4	$a_{30} = a_{19} a_5$		
6			3	$a_{11} = a_3 a_4$		$a_{21} = a_7 a_5$				
7				$a_{12} = a_1 a_5$		$a_{22} = a_8 a_5$				
8				$a_{13} = a_2 a_5$		$a_{23} = a_9 a_5$				
9				$a_{14} = a_3 a_5$		$a_{24} = a_{10} a_5$				
10			4	$a_{15} = a_4 a_5$	6	$a_{25} = a_{11} a_5$				

4. make matrix $[a]$ as:

$$[a] = \begin{bmatrix} 1 & ^{(1)}a_1 & ^{(1)}a_2 & \cdot & \cdot & \cdot & ^{(1)}a_{r+1} \\ 1 & ^{(2)}a_1 & ^{(2)}a_2 & \cdot & \cdot & \cdot & ^{(2)}a_{r+1} \\ 1 & \cdot & \cdot & \cdot & \cdot & \cdot & \cdot \\ 1 & \cdot & \cdot & \cdot & \cdot & \cdot & \cdot \\ 1 & \cdot & \cdot & \cdot & \cdot & \cdot & \cdot \\ 1 & ^{(nc)}a_1 & ^{(nc)}a_2 & \cdot & \cdot & \cdot & ^{(nc)}a_{r+1} \end{bmatrix} \qquad \textbf{(6-22)}$$

where a's were made in the last stage.

5. multiply the last column of matrix $[a]$ by -1.

6.   multiply each row of $[a]$ by the element of $[b]$ in the same row and add the result to matrix $[a]$.

7.   do the elimination procedure explained in section 6.2.2 and find the solution.

6.3.2 Numerical case study

To prove the validity of the method, a beam was considered in a simulated test (Figure 6-1). The beam was modified by the addition of an object which has both mass and rotational inertia properties. The object was attached to the structure at DOFs 3 and 4. The beam was excited at DOF 7 and the response is measured at DOF 9.
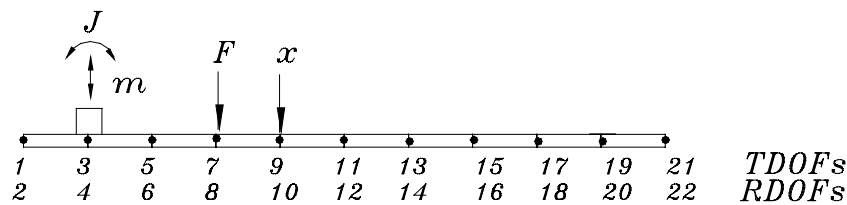
Figure 6-1. A simulated test on a beam

(TDOFs = Translational Degrees of Freedom   ,   RDOFs = Rotational Degrees of Freedom)

The theoretical model of the beam was built using the concept of coupling the free-free beam elements as was explained in chapter 3 .

The attached object modifies the beam by changing the dynamic stiffness matrix of the beam, at DOFs 3 and 4 as :

$$D^{md}(3,3) = D(3,3) - m\omega^2 \qquad\qquad \textbf{(6-23)}$$

and:

$$D^{md}(4,4) = D_b(4,4) - I\omega^2 \qquad\qquad \textbf{(6-24)}$$

The specifications of the beam and those of the attached object are given in Table 6-3.

Table 6-3. Parameters of the theoretical beam

Length of t beam	0.44 (m)
Height of beam	0.02 (m)
Thickness of beam	0.006 (m)
Number of elements in beam	10
Mass of density	7800 (kg / m^3)
Mass	0.412 (kg)
Modulus of elasticity	2e11 (N / m^2)
Mass of the attached object	0.05 kg
Moment of inertia of the attached object	1×10^{-5} ($kg.m^2$)

Once the main effects of the mass and rotational inertia properties of the attached object were included in the model of the beam a simulated experiment was performed in order to determine the effects of the attached object on the measured FRFs of the beam. Figure 6-2 shows the comparison of the affected FRF and the exact FRF.
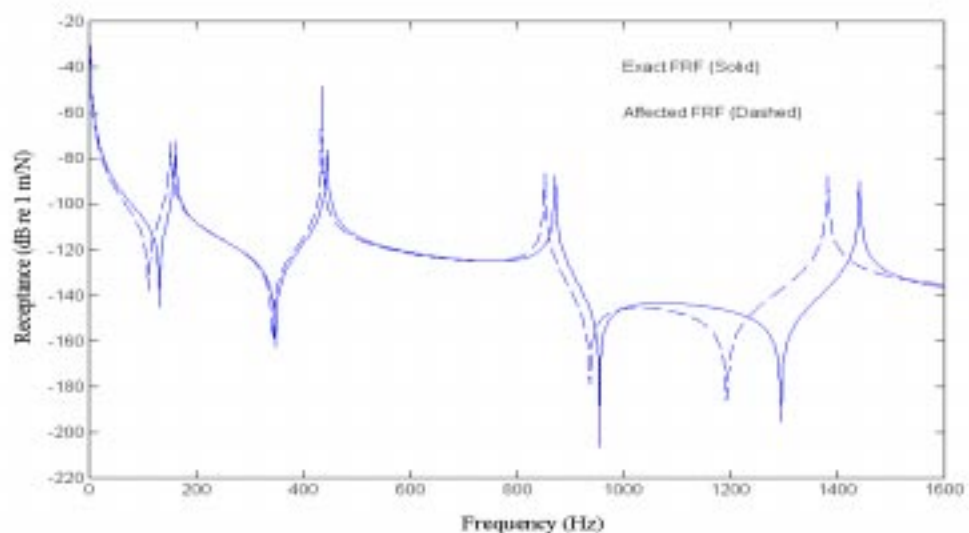
Figure 6-2. The comparison of A_{79} and the affected A_{79} of the beam

According to equation (16) of Appendix A, the receptance of the modified beam is equal to:

$$\alpha_{97}^* = \alpha_{97} - \frac{[\alpha_{47}(\alpha_{33} + \alpha_{33}') - \alpha_{43}\alpha_{37}]\alpha_{94}}{(\alpha_{44} + \alpha_{44}')(\alpha_{33} + \alpha_{33}') - \alpha_{34}\alpha_{43}} \qquad \textbf{(6-25)}$$
$$+ \frac{[\alpha_{47}\alpha_{34} - \alpha_{37}(\alpha_{44} + \alpha_{44}')]\alpha_{93}}{(\alpha_{44} + \alpha_{44}')(\alpha_{33} + \alpha_{33}') - \alpha_{34}\alpha_{43}}$$

From equation (6-2) for the case of $n=2$ and r is equal to $2^n - 1 = 3$ we have :

$$b = x_7 - \frac{x_1 a_1 + x_2 a_2 + x_3 a_3}{x_4 a_1 + x_5 a_2 + x_6 a_3 + a_4} \qquad \textbf{(6-26)}$$

in which:

$$\begin{cases} x_1 = (\alpha_{47}\alpha_{33} - \alpha_{43}\alpha_{37}).\alpha_{94} + (\alpha_{47}\alpha_{34} - \alpha_{37}\alpha_{44}).\alpha_{93} \\ x_2 = \alpha_{47}\alpha_{94} \\ x_3 = -\alpha_{37}\alpha_{93} \\ x_4 = \alpha_{44}\alpha_{33} - \alpha_{34}\alpha_{43} \\ x_5 = \alpha_{44} \\ x_6 = \alpha_{33} \\ x_7 = \alpha_{97} \end{cases} \qquad \textbf{(6-27)}$$

and:

$$\begin{cases} a_1 = 1 \\ a_2 = \alpha_{33}' \\ a_3 = \alpha_{44}' \\ a_4 = \alpha_{33}'\alpha_{44}' \end{cases} , \quad b = \alpha_{97}^* \qquad \textbf{(6-28)}$$

The beam has been modified in 2 DOFs, therefore, according to equation (6-19), at least seven different configurations (mass and rotational inertia of the attached object) are needed to correct the measured FRFs based on the method presented in this

chapter. Equation (6-27) gives the unknown parameters and equation (6-28) gives the known parameters.

Table 6-4 shows different parameters of the attached object for 7 different simulated measurements. Two different sets were considered. Figures 6-3 to 6-5 show the results of applying the correction method using set 1 of Table 6-4. The interesting point of this correction method is that in the simulated measurement the rotational point FRF, α_{44}, is obtained while the translational force and responses were actually measured (Generation of rotational FRFs using correction methods is the subject of chapter 9).

Figures 6-6 to 6-8 show the results of applying the correction method using set 2 of Table 6-4. While the computed transfer FRF matches the exact FRF (Figure 6-6), the computed point FRFs are meaningless (Figures 6-7 and 6-8). This problem arises from the rank deficiency of matrix [*g*] in equation (6-18). The rank of the matrix which is built based on the information of set 1 in Table 6-4 is 4 for all of the frequency points while for the second set it is 3. Thus for set 2, matrix [*g*] is rank deficient and the inverse of this matrix, for some elements, is meaningless.

Here the effect of noise has not been considered. However, in the presence of rank deficiency, using noisy data makes the results more unreliable. The reason for this rank deficiency is choosing of an improper set of objects which modify the test structure. Matrix $[\alpha']$ in equation (6-20), which is the matrix of the receptances of the attached objects, is part of the matrix [*g*] for all of the frequencies. Therefore if the matrix $[\alpha']$ is rank deficient, matrix [*g*] will be rank deficient as well. The rank of matrix $[\alpha']$ for the first set of objects in Table 6-4 is 2 and its condition number is 1.7×10^3. For the second set, the rank of matrix $[\alpha']$ is 1 and its condition number is ∞. As a result, for the second set the results are expected to be unreliable.

Therefore the best way to cope with rank-deficiency is just by choosing a proper set of configurations which creates a matrix of full rank $[\alpha']$ in equation (6-20). This means that the objects which modify the structure need to be selected to avoid numerical difficulties. Fortunately, this design is not case dependent in the sense that

the behaviour of the structure does not have any effect on these numerical problems. For the special case that the test structure is modified in one DOF only (the subject of chapters 3 and 4), matrix $[\alpha']$ is:

$$[\alpha'] = \begin{bmatrix} ^{(1)}\alpha'_{11} \\ ^{(2)}\alpha'_{11} \\ \cdot \\ \cdot \\ ^{(nc)}\alpha'_{11} \end{bmatrix} \qquad \textbf{(6-29)}$$

in which $nc \geq 3$. In this case the rank of the matrix is 1 and may not be made rank-deficient by choosing an improper set of objects.

Table 6-4. Two series of data for the correction

	Set 1		Set 2	
	m (kg)	*I (Kg.m²)*	*m (kg)*	*I (Kg.m²)*
1	0.05	1×10^{-5}	0.05	1×10^{-5}
2	0.06	1.1×10^{-5}	0.055	1.1×10^{-5}
3	0.025	7×10^{-6}	0.045	9×10^{-6}
4	0.033	7.5×10^{-6}	0.06	1.2×10^{-5}
5	0.1	1.5×10^{-5}	0.0425	8.5×10^{-6}
6	0.075	9×10^{-6}	0.0575	1.15×10^{-5}
7	0.038	5×10^{-6}	0.035	7×10^{-6}

6.4 Discussion

The method developed in this chapter provide a mathematical basis for the correction of the mechanical devices effects on the test structure in more than one DOF. However, in practice, applications of these methods are limited. For example when

the test structure is modified in two DOFs by a suspension spring and an accelerometer, 7 different measurements with different configurations are needed to obtain the exact FRF. If the test structure is modified in three DOFs, 15 different measurements with different configurations are needed. In practice, conducting this number of tests with different configurations is not cost efficient. Moreover, the effects of noise and other errors pollute the results of the correction due to the large number of the computation levels.

The application of the methods presented in this chapter is in chapter 9 where the test structure is modified by the mass and rotational inertia of an attached object in two DOFs in order to generate the rotational FRFs.

6.5 Conclusions

- In this chapter a general solution for the correction of the effects of mechanical elements on the measured FRFs was presented.

- It was shown that if the measurement is repeated in a number of different configurations, the exact FRFs are obtainable using two main approaches namely the direct approach and the step-by-step approach. The direct approach was developed in this chapter.

- It was shown that the driving point FRFs of the degree of the freedom of the attachment of mechanical devices can be generated the correction method.

- In the direct approach, numerical errors can be avoided in the calculations due to rank-deficiency of the matrices by selecting proper mechanical elements.
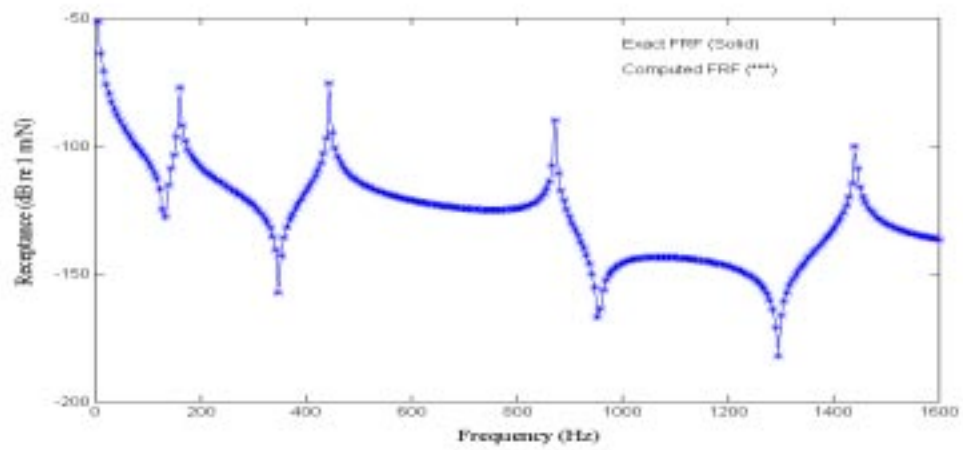
Figure 6-3. Comparison of the Exact FRF, α_{79} ,and the computed FRF (set 1)
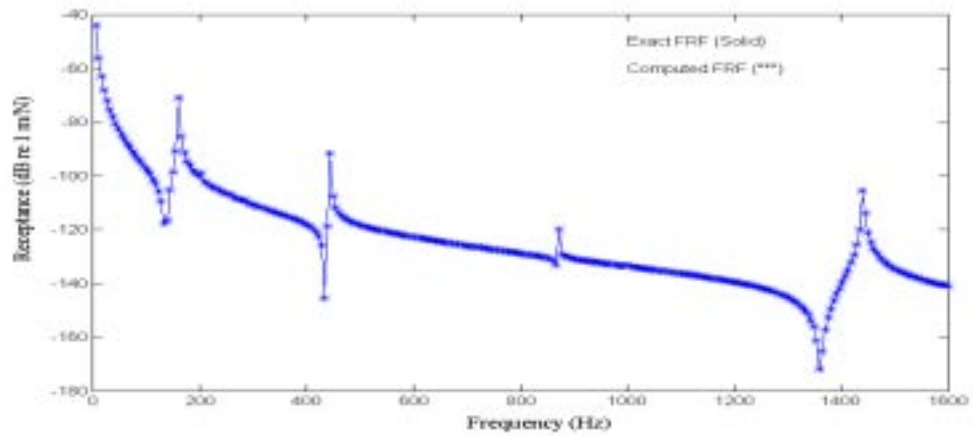
Figure 6-4. Comparison of the Exact FRF, α_{33} ,and the computed FRF (set 1)
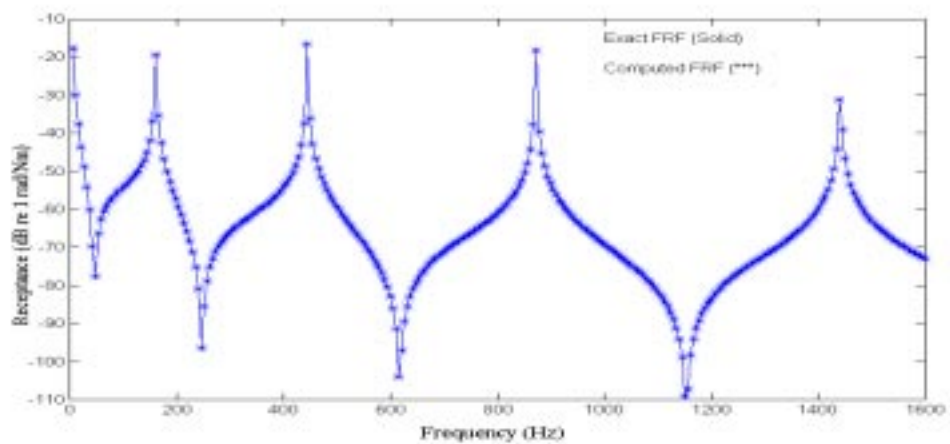
Figure 6-5. Comparison of the Exact FRF, α_{44} ,and the computed FRF (set 1)
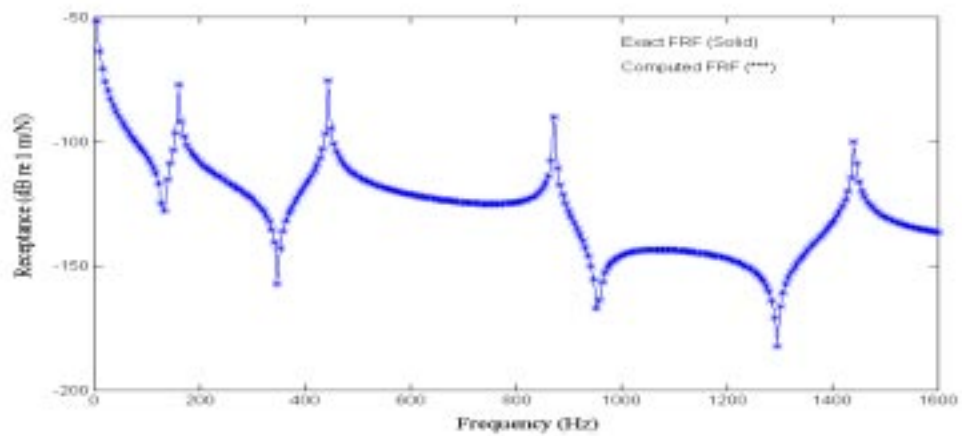
Figure 6-6. Comparison of the Exact FRF, α_{79} ,and the computed FRF (set 2)
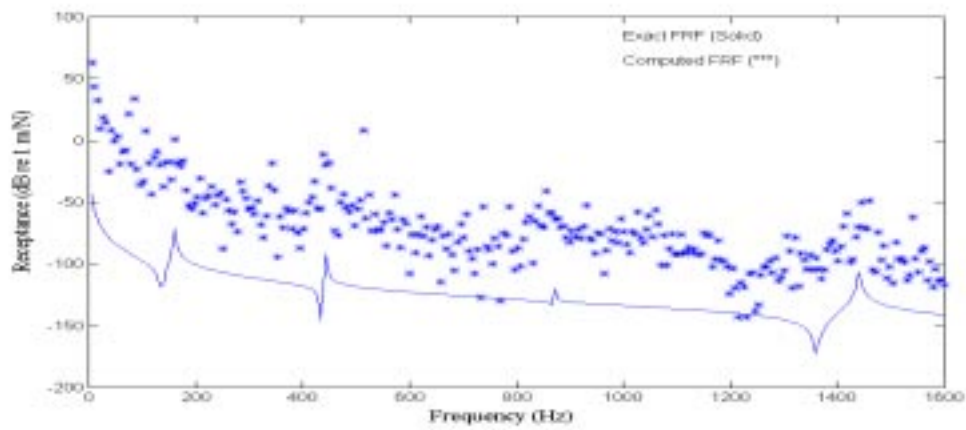
Figure 6-7. Comparison of the Exact FRF, α_{33} ,and the computed FRF (set 2)
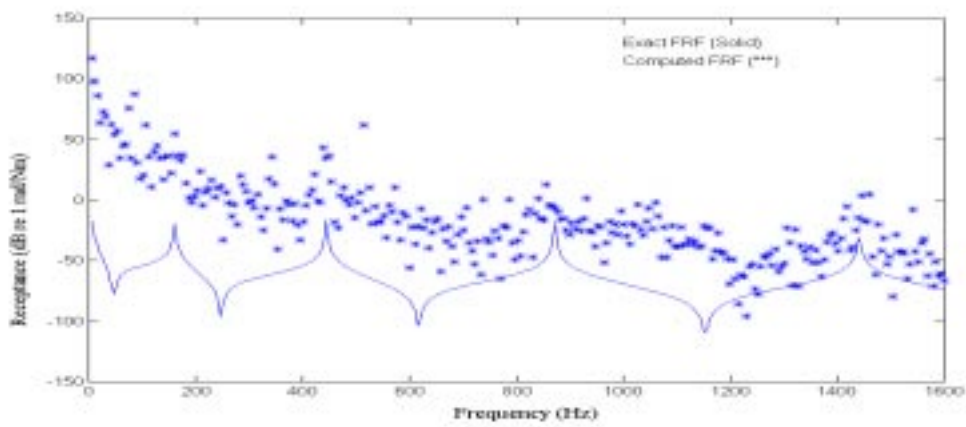
Figure 6-8. Comparison of the Exact FRF, α_{44} ,and the computed FRF (set 2)

Chapter 7

The effect of nonlinearity on the correction methods of mechanical devices

7.1 Introduction

Most of the theory upon which modal testing is founded relies heavily on the assumption that the test structure's behaviour is linear. In practice, real structures are seldom completely linear. In the correction methods presented in the previous chapters, the main assumption was the linear behaviour of the test structure and those of the attached elements. However, if the structure or the attached elements exhibits nonlinear behaviour, the result of the correction is unreliable. In this chapter the effect of nonlinearity on the correction methods which was presented in the previous chapters will be investigated. Application of this study is in chapter 9 where the test structure is modified by an object to generate rotational FRFs.

7.2 The effect of nonlinearity of the test structure

Figure 7-1 indicates a structure which is modified at point l by a mass, m. According to equation (3-12) in chapter 3, accelerance $A_{li}^{(l)}$ can be written with respect to the original FRFs as :

$$A_{li}^{(l)} = \frac{A_{li}}{1 + mA_{ll}} \tag{7-1}$$

It was shown in chapter 3 that when the measurement is repeated with two different masses, m_1 and m_2, the correct values A_{li} and A_{ll} can be computed from:

$$\left\{ \begin{matrix} A_{li} \\ A_{ll} \end{matrix} \right\} = \left(\begin{bmatrix} \dfrac{1}{A_{li}^{(l)}} & -m_1 \\ \dfrac{1}{\overline{A_{li}^{(l)}}} & -m_2 \end{bmatrix} \right)^{-1} \left\{ \begin{matrix} 1 \\ 1 \end{matrix} \right\} \tag{7-2}$$

If the measurement is repeated with another mass, m_3, then A_{li} can be computed again as :

$$\hat{A}_{li} = \frac{\overline{\overline{A}}_{li}^{(l)}}{1 - m_3 A_{ll}} \tag{7-3}$$

in which $\hat{A}_{li}$ is the second computed FRF and A_{ll} is computed from equation (7-2).
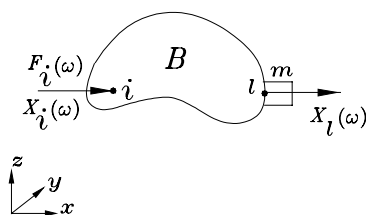
Figure 7-1. Correction of the FRFs for a nonlinear structure

If the assembly of the structure and the modification masses show any nonlinearity, then the amount of A_{li} computed by equation (7-2) is different from $\hat{A}_{li}$ computed by

equation (7-3). In this case, the addition of mass *m* is a kind of passive excitation that changes the effective force which excites the test structure. By attaching mass *m* to the structure, as it acts like a passive force, the level of displacement at the point of attachment can be restricted to a range of motion that produces linear response.

This conclusion applies to general cases where the structure is modified in more than one DOF. If the assembly of the structure and/or the attached objects show any nonlinearity, the results of the correction method is not the same for different sets of data related to different configurations of the test structure.

7.2.1 Numerical example

To demonstrate the effect of the nonlinearity on the corrected FRFs, a simple model of a mass and a hardening spring is considered (Figure 7-2).
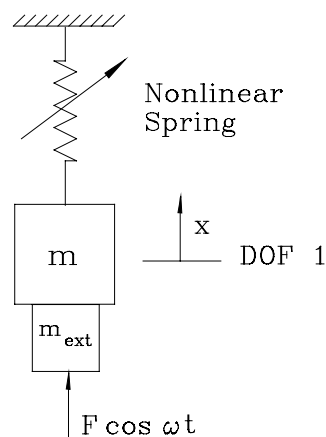
Figure 7-2. One DOF nonlinear system

The equation governing this system is the Duffing equation for cubic hardening stiffness:

$$(m + m_{ext})\ddot{x} + kx + \beta x^3 = F\cos(\omega t) \tag{7-4}$$

The response of this simple system sometimes shows a behaviour which is called the "jump phenomenon". However, depending on different frequency and magnitude of the excitation, different solution can be obtained. Figure 7-3 shows the behaviour of the system shown in Figure 7-2 for three different levels of excitation: *F = 1000 N, F = 5000 N* and *F = 10000 N*.

The parameters of the system are:

m=10 kg , m_{ext} = 0 kg, k=65300 N/m and β = *1000 N / m^3*

The input force is sinusoidal which increases by 0.1 Hz upward. Figure 7-3 shows that by increasing the magnitude of the force, the FRF is more inclined to the right.
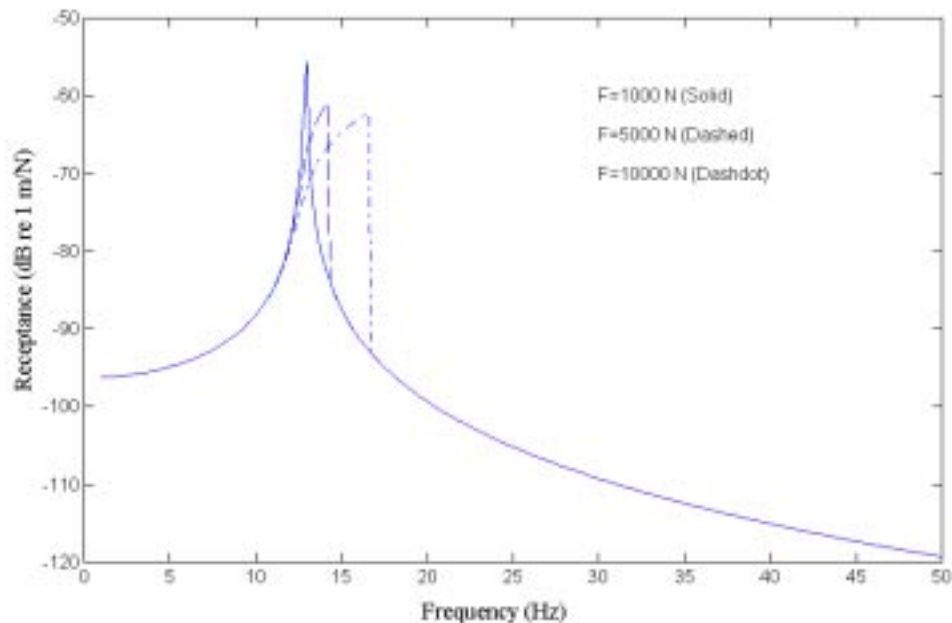
Figure 7-3. The behaviour of a nonlinear system

Figure 7-4 shows the result of the addition of an extra mass to the system shown in Figure 7-2 while the level of the force is constant at 10000 N. If a mass of 5 Kg is added to the system, the peak of the FRF shifts to the left and the system still shows the jump phenomenon. By addition of 40 Kg extra mass to the system, the peak of the FRF shifts even more to the left but the system shows little nonlinear behaviour. Addition of the mass decreases the amplitude of the vibration and this linearises the dynamic behaviour of the system.
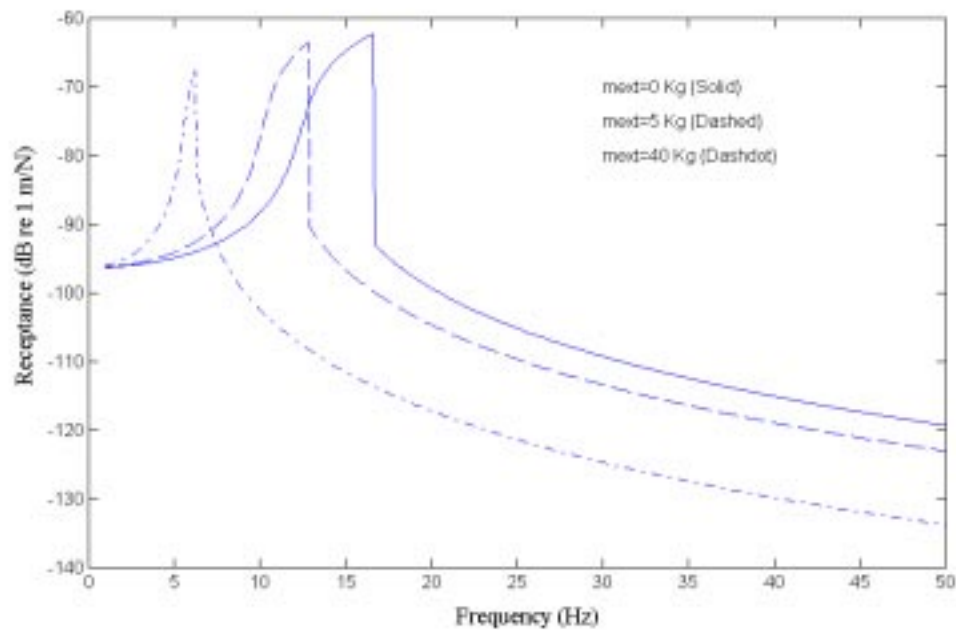
Figure 7-4. Addition of the extra masses to the system while the level of the force is constant (10000 N)

The correction process which was suggested in the previous chapters is based on the linear behaviour of the structure. If the structure is nonlinear, the result of the correction is different for different sets of data corresponding to different configurations. Assuming the linear behaviour for the system shown in Figure 7-2, the measured FRF can be corrected using the equation:

$$\alpha_{11} = \frac{\alpha_{11}^{(1)}}{1 + \omega^2 m_{ext} \alpha_{11}^{(1)}} \qquad \textbf{(7-5)}$$

The result of this correction is shown in Figure 7-5. Because of the nonlinearity, the computed FRFs do not coincide with each other. For comparison purposes, the FRF of the system when $\beta = 0$ in equation (7-4) is shown. In the case where the extra mass is 40 Kg the computed FRF from equation (7-5) coincides with the linear FRF in most of the frequency region. This coincidence proves that by addition of more masses the structure shows more linear behaviour.
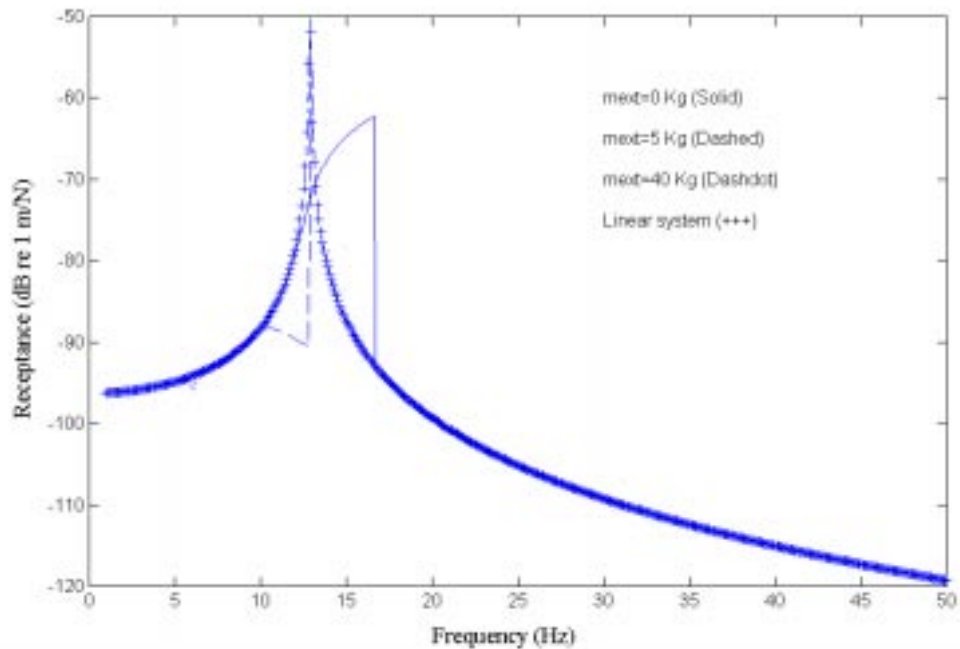
Figure 7-5. The result of the correction for the nonlinear structure

This study implies that the correction methods for nonlinear structures fail to provide a unique solution for different sets of data.

7.3 The effect of nonlinearity of the attached objects

From the practical point of view, the elements which are attached to the test structure may not show linear behaviour in the correction process. Therefore the correction

process may fail to have a unique solution because of the nonlinear behaviour of attached elements.

7.3.1 Numerical example

Figure 7-6 shows a one DOF system of mass and spring which is modified by a nonlinear hardening spring. Two different nonlinear springs used for the correction of the measured FRF. The parameters of the system and those of the nonlinear springs are:

One DOF system: m = 10 *kg* , k = 65300 *N/m*;

Nonlinear spring 1: k_{ext} = 9700 *N/m* , β_{ext} = 1000 N / m^3;

Nonlinear spring 2: k_{ext} = 24700 *N/m* , β_{ext} = 2000 N / m^3;
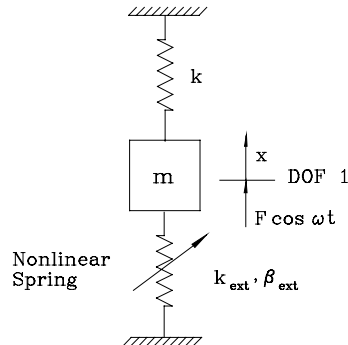
Figure 7-6. Addition of a nonlinear spring

Figure 7-7 shows the receptance of the system when the magnitude of the force is *10000 N.*
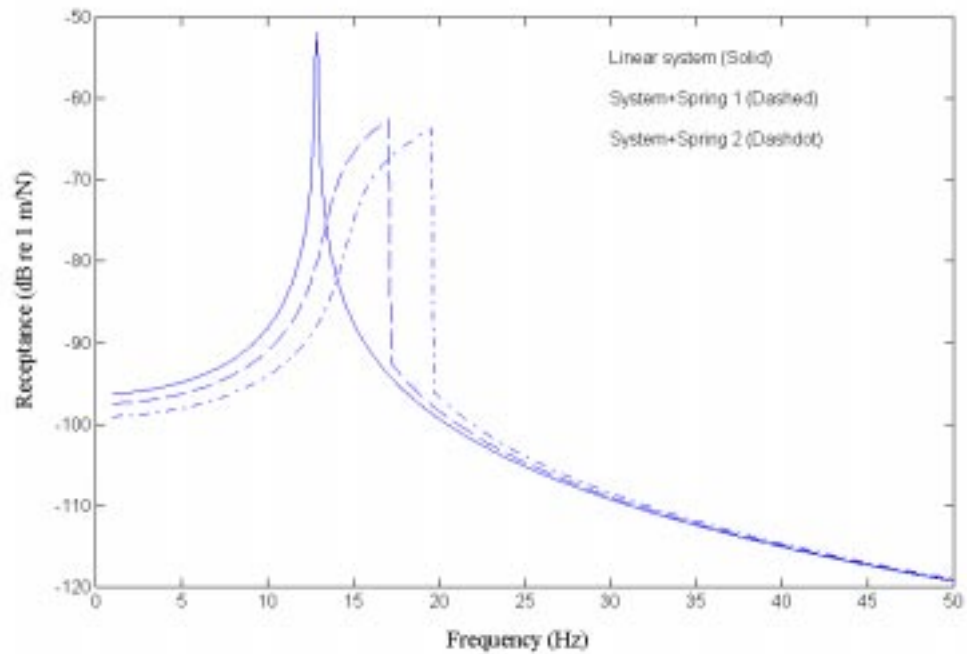
Figure 7-7. The effect of a nonlinear spring on the system

If springs 1 and 2 are considered to be linear ($\beta_{ext} = 0$), the effect of the additional spring on the computed FRF can be removed by equation:

$$\alpha_{11} = \frac{\alpha_{11}^{(1)}}{1 - k_{ext}\alpha_{11}^{(1)}}$$

(7-6)

The result of this correction is shown in Figure 7-8. The receptance of the original linear system is shown for comparison. The FRFs do not coincide in some parts of the frequency region. Therefore the results of the correction is not the same when the attached elements do not show linear behaviour.
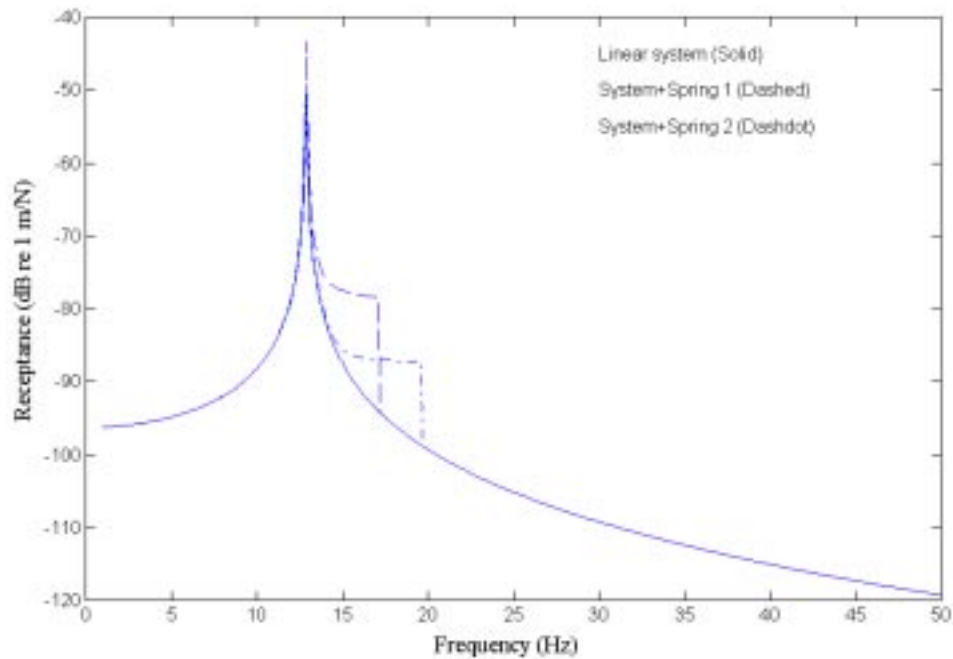
Figure 7-8. Correction of an FRF affected by a nonlinear spring

7.4 The effect of other errors on the correction methods

In previous sections it was shown that in the presence of nonlinearity the results of the correction methods for different sets of data are not the same. However, there are other parameters which may cause the same effects on the correction methods. For example, signal processing errors like leakage or the effect of the window functions may cause the same problem. When a structure is modified by addition of mechanical elements, in the presence of signal processing errors, the response signal of the modified structure may not have the same results in the correction methods. One of the most serious problems which may cause difficulty in the correction methods is the relative phase shift between the force and acceleration signals. This problem was first reported by McConnell in [99]. He showed that large measurement errors occur near resonances in the mass cancellation process when there is a small relative phase shift between the force and acceleration signals. The phase shift between the force and acceleration signals may happen because of the mechanical and electrical effects in each data channel, including amplifiers and anti-aliasing filters. In practice the phase

shift between the force and acceleration signals can not be avoided, so any correction method is subject to these large errors and must be used with caution.

7.5 Conclusions

- if the structure or the attached elements exhibits nonlinear behaviour, the results of the correction methods are not the same using different sets of data corresponding to different configurations.

- As most types of nonlinearity are amplitude-dependent, the attached mechanical elements can be chosen so that the level of the motion of the structure is restricted to a range of motion that produces linear response.

- There are other sources of systematic errors in modal testing which may cause the same effects on the correction methods.

Chapter 8

Generation of the whole matrix of translational FRFs

from measurements of one column

8.1 Introduction

Measurement of the FRFs is a primary objective of modal testing in order to build a mathematical model representing the dynamic behaviour of a structure. When the number of DOFs is large, measuring the whole FRF matrix is difficult and sometimes impossible. However, it is possible to compute the unmeasured FRFs from the measurement and analysis of the FRFs in a single row (Response fixed)or column (Force fixed) of the FRF matrix [5]. The unmeasured FRFs can, in principle, be synthesised from the measured FRFs using the identified modal properties. However, generating the unmeasured FRFs from the measured ones along a single row or column is only theoretically possible when the frequency range covered extends from zero to infinity. In practice, it is necessary to limit the frequency range of measurement for obvious reasons. The remaining part, due to the out of range modes - the residual - is not available and, as a result, estimating the unmeasured FRFs from the measured ones is not accurate unless values for the relevant residual terms can be estimated. In the past, some efforts have been made to relate the residual effects of out-of-range modes between measured and unmeasured FRFs, but without much success. At present, there is no known method to include the residual terms in the calculation exactly.

The idea of evaluating the whole FRF matrix from measurement of some elements by changing the boundary was suggested in [37]. As shown there, it is possible to calculate some FRFs by modifying the structure at the points of interest at its boundaries. New accelerometers were added to the points for each new set of

This work was published in IMAC 1998 [100].

Measurement. Thus, for an *n* DOF system, *n* accelerometers or dummy masses are needed.

The challenge addressed in the present work is to develop a method for generating the whole matrix of translational FRFs based on measurements using one accelerometer and one dummy mass. The theory of the method is based on the direct substructuring technique, Structural Modification Using experimental frequency Response Functions (SMURF). Two different approaches are used to develop the governing equations of a structure modified with two masses. Moreover, it has been shown that in noisy environments, and when the masses of accelerometer and dummy mass are large, the computation is relatively insensitive to noise.

8.2 Theory

In chapter 3, the modification of a structure by an added mass was studied. Figure 8-1 shows a structure which is modified with two different masses at points *i* and *j* .
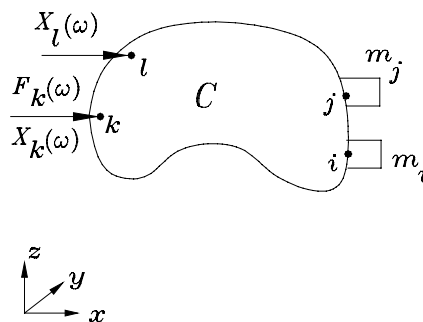
Figure 8-1. Attachment of two masses

Two different approaches can be used to derive equations governing the modified system, as discussed below:

8.2.1 Successive substitution

For the system shown in Figure 8-1, one can consider that mass m_i is attached at point i to the system composed of mass m_j and structure C (Figure 8-2).
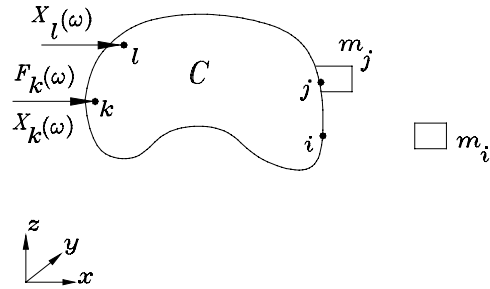
Figure 8-2. Addition of mass m_i to structure C and mass m_j

For this case, we have :

$$A_{lk}^{(i,j)} = A_{lk}^{(j)} - \frac{A_{ik}^{(j)} A_{li}^{(j)}}{\dfrac{1}{m_i} + A_{ii}^{(j)}} \tag{8-1}$$

The accelerances of the modified structure $A_{lk}^{(j)}$, $A_{ik}^{(j)}$, $A_{li}^{(j)}$ and $A_{ii}^{(j)}$ can be written in terms of the accelerances of the basic structure, C. we have :

$$A_{lk}^{(j)} = A_{lk} - \frac{A_{jk} A_{lj}}{\dfrac{1}{m_j} + A_{jj}} \tag{8-2}$$

$$A_{ik}^{(j)} = A_{ik} - \frac{A_{jk} A_{ij}}{\dfrac{1}{m_j} + A_{jj}} \tag{8-3}$$

$$A_{li}^{(j)} = A_{li} - \frac{A_{ji} A_{lj}}{\dfrac{1}{m_j} + A_{jj}} \tag{8-4}$$

$$A_{ii}^{(j)} = A_{ii} - \frac{A_{ji} A_{ij}}{\dfrac{1}{m_j} + A_{jj}} \tag{8-5}$$

Inserting equations (8-2), (8-3), (8-4) and (8-5) in (8-1) results in :

$$A_{lk}^{(i,j)} = A_{lk} - \frac{A_{jk} A_{lj}}{(1/m_j + A_{jj})}$$
$$- \frac{(A_{ik}(1/m_j + A_{jj}) - A_{jk} A_{ij})(A_{li}(1/m_j + A_{jj}) - A_{ji} A_{lj})}{(1/m_j + A_{jj})(1/m_i + A_{ii}) - A_{ji} A_{ij}} \tag{8-6}$$

8.2.2 Direct derivation

Appendix A of this thesis investigates the general case of changes in measured FRFs due to the attachment of mechanical devices to the test structure. As shown at appendix A, for the case that the test structure is modified in two DOFs we have:

$$\alpha_{lk}^{(i,j)} = \alpha_{lk} - \frac{[\alpha_{jk}(\alpha_{ii} + \alpha_{nn}) - \alpha_{ji}\alpha_{ik}]\alpha_{lj}}{(\alpha_{jj} + \alpha_{mm})(\alpha_{ii} + \alpha_{nn}) - \alpha_{ij}\alpha_{ji}}$$
$$+ \frac{[\alpha_{jk}\alpha_{ij} - \alpha_{ik}(\alpha_{jj} + \alpha_{mm})]\alpha_{li}}{(\alpha_{jj} + \alpha_{mm})(\alpha_{ii} + \alpha_{nn}) - \alpha_{ij}\alpha_{ji}} \tag{8-7}$$

Multiplying both sides by $-\omega^2$, and the numerator and denominator of the two fractions on the right hand side of equation (8-7) by ω^4, the relation between accelerances is obtained as:

$$A_{lk}^{(i,j)} = A_{lk} - \frac{[A_{jk}(A_{ii} + A_{nn}) - A_{ji}A_{ik}]A_{lj}}{(A_{jj} + A_{mm})(A_{ii} + A_{nn}) - A_{ij}A_{ji}}$$
$$+ \frac{[A_{jk}A_{ij} - A_{ik}(A_{jj} + A_{mm})]A_{li}}{(A_{jj} + A_{mm})(A_{ii} + A_{nn}) - A_{ij}A_{ji}} \tag{8-8}$$

where :

$$A_{mm} = \frac{1}{m_j} \tag{8-9}$$

and :

177

$$A_{nn} = \frac{1}{m_i} \qquad (8\text{-}10)$$

Inserting equations (8-9) and (8-10) into Equation (8-8) we have :

$$
\begin{aligned}
A_{lk}^{(i,j)} &= A_{lk} - \frac{A_{jk} A_{lj}}{(1/m_j + A_{jj})} \\
&- \frac{(A_{ik}(1/m_j + A_{jj}) - A_{jk} A_{ij})(A_{li}(1/m_j + A_{jj}) - A_{ji} A_{lj})}{(1/m_j + A_{jj})(1/m_i + A_{ii}) - A_{ji} A_{ij}}
\end{aligned}
\qquad (8\text{-}11)
$$

Equation (8-11) is the same as equation (8-6), verifying that both approaches give the same result.

Three special cases can be developed which are applicable for the generation of FRFs in the next sections:

(a) for the case where *l=i,* equation (8-11) can be reduced to :

$$A_{lk}^{(l,j)} = \frac{A_{nn} A_{mm} A_{lk} + A_{nn}(A_{ij} A_{lk} - A_{lj} A_{jk})}{(A_{jj} + A_{mm})(A_{ll} + A_{nn}) - A_{lj} A_{jl}} \qquad (8\text{-}12)$$

(b) when *j=k* and *l=i,* equation (8-12) can be simplified to :

$$A_{lk}^{(l,k)} = \frac{A_{nn} A_{mm} A_{lk}}{(A_{kk} + A_{mm})(A_{ll} + A_{nn}) - A_{lk} A_{kl}} \qquad (8\text{-}13)$$

(c) when *l=k=i,* equation (8-13) can be expressed as :

$$A_{ll}^{(l,j)} = \frac{A_{ll} A_{nn}(A_{jj} + A_{mm}) - A_{nn} A_{jl} A_{lj}}{(A_{jj} + A_{mm})(A_{ll} + A_{nn}) - A_{lj} A_{jl}} \qquad (8\text{-}14)$$

8.3 Generation of the whole matrix of translational FRFs

The method which was developed in [37] for generation of the whole matrix of translational FRFs is difficult to use because the number of accelerometers and dummy masses increases with increasing the number of DOFs. Instead, an alternative

method has been suggested in this section for generating the whole matrix of translational FRFs using one accelerometer and one dummy mass.

8.3.1 Measurement technique

Suppose that a structure is characterised by a model with n DOFs and it is excited with a shaker at DOF 1 and the force and response are measured by a conventional force transducer and accelerometer. The steps needed in order to obtain the whole matrix of translational FRFs are listed in below:

Step 1- attach the accelerometer at point *1*, and measure the driving point FRF, $A_{11}^{(\bar{1})}$;

Step 2- move the accelerometer to point *2* and measure $A_{21}^{(\bar{2})}$, attach the dummy mass at points *1, 3, ..., n* successively and measure $A_{21}^{(1,\bar{2})}$, $A_{21}^{(3,\bar{2})}$, ... , $A_{21}^{(n,\bar{2})}$ on each occasion;

Step 3- move the accelerometer to point *3* and measure $A_{31}^{(\bar{3})}$. Attach the dummy mass at points *1, 2, 4, ..., n* successively and measure $A_{31}^{(1,\bar{3})}$, $A_{31}^{(2,\bar{3})}$, $A_{31}^{(4,\bar{3})}$, ... , $A_{31}^{(n,\bar{3})}$ on each occasion;

Step 4- do the same procedure as step *2* for all other points *4, 5,... , n.*

So the measured FRFs are :

Step 1- $A_{11}^{(\bar{1})}$. (1 measurement)

Step 2- $A_{21}^{(\bar{2})}$, $A_{21}^{(1,\bar{2})}$, $A_{21}^{(3,\bar{2})}$, ... , $A_{21}^{(n,\bar{2})}$. (n measurements)

Step 3- $A_{31}^{(\bar{3})}$, $A_{31}^{(1,\bar{3})}$, $A_{31}^{(2,\bar{3})}$, $A_{31}^{(4,\bar{3})}$, ... , $A_{31}^{(n,\bar{3})}$. (n measurements)

Step 4- $A_{41}^{(\bar{4})}$, $A_{41}^{(1,\bar{4})}$, $A_{41}^{(2,\bar{4})}$, $A_{41}^{(3,\bar{4})}$, $A_{41}^{(5,\bar{4})}$, ... , $A_{41}^{(n,\bar{4})}$. (n measurements)

.

.

Step n- $A_{n1}^{(\bar{n})}$, $A_{n1}^{(1,\bar{n})}$, $A_{n1}^{(2,\bar{n})}$, $A_{n1}^{(3,\bar{n})}$, … , $A_{n1}^{(n-1,\bar{n})}$. (n measurements)

The total number of measurements is :

$$n \times (n-1) + 1 = n^2 - n + 1$$

8.3.2 Generation of the translational FRFs

The procedure to generate the matrix of translational FRFs from the measured FRFs listed in the previous section is as follows:

1- from step 1 we have :

$$A_{11}^{(\bar{1})} = \frac{A_{11}}{1 + m_a A_{11}} \tag{8-15}$$

from which the exact accelerance, A_{11}, can be computed easily :

$$A_{11} = \frac{A_{11}^{(\bar{1})}}{1 - m_a A_{11}^{(\bar{1})}} \tag{8-16}$$

2- from step 2 we have :

$$A_{21}^{(\bar{2})} = \frac{A_{21}}{1 + m_a A_{22}} \tag{8-17}$$

and from equation (8-13) we have :

$$A_{21}^{(1,\bar{2})} = \frac{A_{21}}{(1 + m_d A_{11})(1 + m_a A_{22}) - m_a m_d (A_{21})^2} \tag{8-18}$$

From equations (8-16), (8-17) and (8-18) one can derive A_{21} and A_{22} :

$$A_{21} = \frac{(1 + m_d A_{11})}{m_a m_d} \frac{1}{A_{21}^{(\bar{2})}} - \frac{1}{m_a m_d A_{21}^{(1,\bar{2})}} \tag{8-19}$$

$$A_{22} = \frac{A_{21} - A_{21}^{(\bar{2})}}{m_a} \tag{8-20}$$

The same procedure can be followed for $A_{u1}^{(\bar{u})}$ and $A_{u1}^{(1,\bar{u})}$ to compute A_{u1} and A_{uu}, where $u=2,3,...,n$.

$$A_{u1} = \frac{(1 + m_d A_{11})}{m_a m_d} \frac{1}{A_{u1}^{(\bar{u})}} - \frac{1}{m_a m_d A_{u1}^{(1,\bar{u})}} \tag{8-21}$$

$$A_{uu} = \frac{A_{u1} - A_{u1}^{(\bar{u})}}{m_a} \tag{8-22}$$

3- from step 2, one can compute A_{31} and A_{33} from the measured FRFs $A_{31}^{(\bar{3})}$ and $A_{31}^{(1,\bar{3})}$. From equation (8-12) we have :

$$A_{31}^{(2,\bar{3})} = \frac{A_{31} + m_d(A_{22}A_{31} - A_{32}A_{21})}{(1 + m_d A_{22})(1 + m_a A_{33}) - m_a m_d (A_{23})^2} \tag{8-23}$$

and :

$$A_{21}^{(3,\bar{2})} = \frac{A_{21} + m_d(A_{33}A_{21} - A_{32}A_{31})}{(1 + m_d A_{33})(1 + m_a A_{22}) - m_a m_d (A_{23})^2} \tag{8-24}$$

when $m_a = m_d$ the denominator of the equations (8-23) and (8-24) are equal and one can derive A_{23} :

$$A_{23} = \frac{(A_{31} + m_d A_{22} A_{31}) A_{21}^{(3,\bar{2})} - A_{31}^{(2,\bar{3})} A_{21}(1 + m_d A_{33})}{m_d A_{21} A_{21}^{(3,\bar{2})} - A_{31}^{(2,\bar{3})} m_d A_{31}} \tag{8-25}$$

where A_{21}, A_{22}, A_{31}, A_{33} are known from step 2. The same procedure can be used to find A_{ts} from $A_{t1}^{(s,\bar{t})}$ and $A_{s1}^{(t,\bar{s})}$, where $t \neq s$ and $t \neq 1, s \neq 1$.

$$A_{ts} = \frac{(A_{t1} + m_d A_{ss} A_{t1}) A_{s1}^{(t,\bar{s})} - A_{t1}^{(s,\bar{t})} A_{s1} (1 + m_d A_{tt})}{m_d A_{s1} A_{s1}^{(t,\bar{s})} - A_{t1}^{(s,\bar{t})} m_d A_{t1}}$$

$(8\text{-}26)$

Where A_{t1}, A_{tt}, A_{s1}, A_{ss} are known from step *2*. With this procedure, all of the elements of the matrix of translational FRFs can be generated.

8.3.3 Computation using noisy data

The method suggested in the preceding section is exact, but its application in practical situations may be vulnerable to measurement noise. Equations (8-16), (8-21), (8-22) and (8-26) are used to generate the FRFs. The influence of noise on the computations can be reduced by choosing a proper accelerometer mass. To examine this possibility, another term, ε , is added to the measured FRFs in the above equations. Then the added masses can be chosen in such a way that the computations become less sensitive to ε . From equation (8-16) we have :

$$A_{11} = \frac{A_{11}^{(\bar{1})} + \varepsilon}{1 - m_a (A_{11}^{(\bar{1})} + \varepsilon)}$$

$(8\text{-}27)$

The sensitivity of A_{11} to the changes of ε is :

$$\frac{\partial A_{11}}{\partial \varepsilon} = \frac{1}{(1 - m_a (A_{11}^{(\bar{1})} + \varepsilon))^2}$$

$(8\text{-}28)$

In equation (8-28), for all the frequency points $\dfrac{\partial A_{11}}{\partial \varepsilon}$ decreases with increasing m_a , as a result the effect of ε on A_{11} decreases. A similar analysis can be done for equations (8-21), (8-22) and (8-26). Here we have:

$$A_{u1} = \frac{(1 + m_d A_{11})}{m_a m_d} \frac{1}{(A_{u1}^{(\bar{u})} + \varepsilon_1)} - \frac{1}{m_a m_d (A_{u1}^{(1,\bar{u})} + \varepsilon_2)}$$

$(8\text{-}29)$

The sensitivity of A_{u1} to ε_1 and ε_2 are :

$$\frac{\partial A_{u1}}{\partial \varepsilon_1} = \frac{(1 + m_d A_{11})}{m_a m_d} \frac{-1}{(A_{u1}^{(\bar{u})} + \varepsilon_1)^2} \tag{8-30}$$

$$\frac{\partial A_{u1}}{\partial \varepsilon_2} = \frac{1}{m_a m_d (A_{u1}^{(1,\bar{u})} + \varepsilon_2)^2} \tag{8-31}$$

For equation (8-22) we have :

$$A_{uu} = \frac{A_{u1} - (A_{u1}^{(\bar{u})} + \varepsilon)}{m_a} \tag{8-32}$$

And so the sensitivity of A_{uu} to ε is:

$$\frac{\partial A_{uu}}{\partial \varepsilon} = \frac{-1}{m_a} \tag{8-33}$$

From equations (8-30), (8-31) and (8-33) it can be seen that by increasing the mass of accelerometer (and the dummy mass, $m_a = m_d$) the effects of noise on the computation of the FRFs decrease. A similar discussion holds for equation (8-286)(not shown here).

The general conclusion is that the effect of noise on the computations will decrease by increasing the amount of the mass of accelerometer, m_a, (and the dummy mass, $m_a = m_d$).

8.4 Demonstration and verification of the method

8.4.1 Numerical example

To demonstrate the validity of the method, the simulated system of 12 DOFs which was used in chapter 3 has been considered again here (Figure 8-3). Table 3-1 in chapter 3 shows the full specifications of the system.
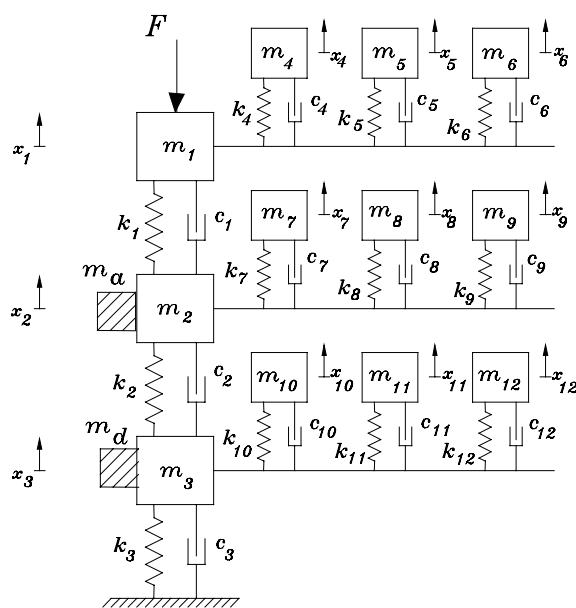
Figure 8-3. A 12 DOF system

The system is excited at DOF 1. One accelerometer and one dummy mass have been used to generate the FRFs. The mass of the accelerometer and that of the dummy mass are each 0.5 kg. The "simulated measurements" are made following the method suggested in this chapter .Then, the true FRFs are generated from equations (8-16), (8-21), (8-22) and (8-26). Figure 8-4 shows the comparison of the exact FRF, A_{23}, (continuous curve) and the generated FRF ($***$ curve).
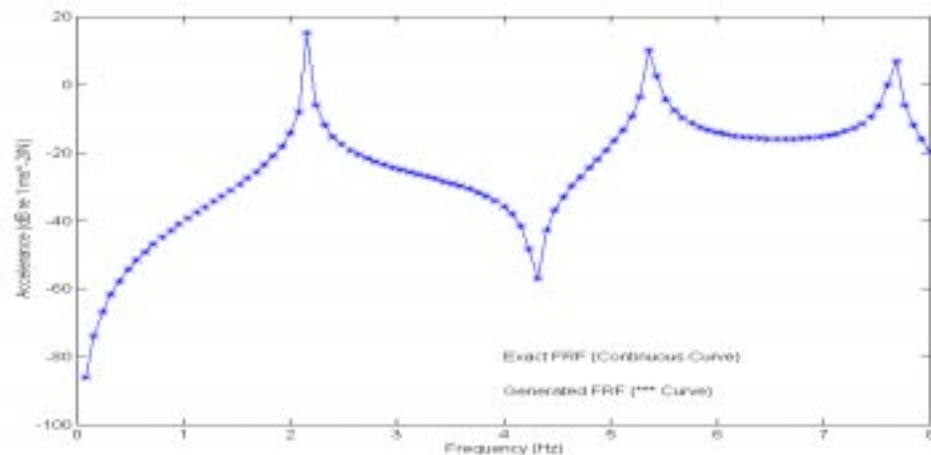
Figure 8-4. comparison of the exact FRF, A_{23} , (continuous curve) and the generated FRF ($\ast\ast\ast$ curve) in the simulated test.

The simulated test was repeated using noisy data. The FRFs were polluted by adding random noise using equation (4-28). Figure 8-5 shows the corresponding computation in the presence of 0.1 % noise. To demonstrate the effect of the size of the accelerometer mass and that of the dummy mass, the same computation was made with a mass of 5 kg for the accelerometer and dummy mass . In this case, the size of the mass has been exaggerated to highlight the results shown in Figure 8-6. Figures 8-7 and 8-8 demonstrate the effect of the size of the accelerometer mass and that of the dummy mass in the presence of 1% noise. Figures 8-9 and 8-10 show this in the presence of 5% noise. As predicted in the theoretical section, the effect of noise on the computations decreases with increasing the mass of the accelerometer and that of the dummy mass. Moreover, these figures show that the generated FRFs are less affected by noise in the resonance area while around antiresonances the results are more vulnerable to noise.

8.4.2 Discussion

It was shown that the effects of noise on the computations decreases by increasing the mass of the accelerometer and that of the dummy mass ($m_a = m_d$). However, these masses cannot be so big that they dominate the dynamics of the structure. In an actual test, there is no structure that behaves like a lumped mass. All structures have a

rotational property that affects the dynamics of the structure (this will be discussed extensively in chapter 9). Therefore in order to apply the method presented in this chapter the size of the accelerometer and that of the dummy mass should be limited so that their rotational effects on the dynamics of the structure become minimum. On this basis, the ratio of the mass of the accelerometer (or that of the dummy mass) to the mass of the structure should definitely be less than one. However, the final judgement of selecting the suitable size for the accelerometer and dummy mass is based on the structure and the computed FRFs.

8.4.3 Experimental case study

The same experimental set up which was used in section 3.3.3 was used again here for the experimental demonstration of the method introduced in this chapter. All the specifications of the test set-up and those of the structure are the same as before (Figure 8-11). To increase the mass of the accelerometer, an extra mass was added to the structure at the response point. The extra mass was a steel cylinder with the weight of 0.026 *kg*. The diameter of the extra mass was 15 *mm* and its length was 20 *mm*. The weight of the accelerometer was 0.004 *kg*. The dummy mass was a steel cylinder with the mass of 0.03 *kg*. The diameter of the dummy mass was15 *mm* and its length was 22 *mm*. Therefore the mass of the accelerometer (and the extra mass) and that of the dummy mass were both equal to 0.03 *kg* ($m_a = m_d = 0.03 kg$). The measurements were conducted and the FRFs were generated following the procedure presented in this chapter. Figure 8-12 show the comparison of the generated FRFs and the measured FRFs. The difference between the natural frequencies of the generated FRFs and those of the measured FRFs are due to the accelerometer mass. The effects of the accelerometer mass and that of the dummy mass have been cancelled through this process, as a result the natural frequencies of the generated FRFs are accurate. Noise has not affected the generated FRFs around the resonance. However, the effect of noise appears in the generated FRFs which were computed in the last stages of the generation process (A_{31}, A_{33} and A_{23}) due to the accumulated errors from the previous stages.
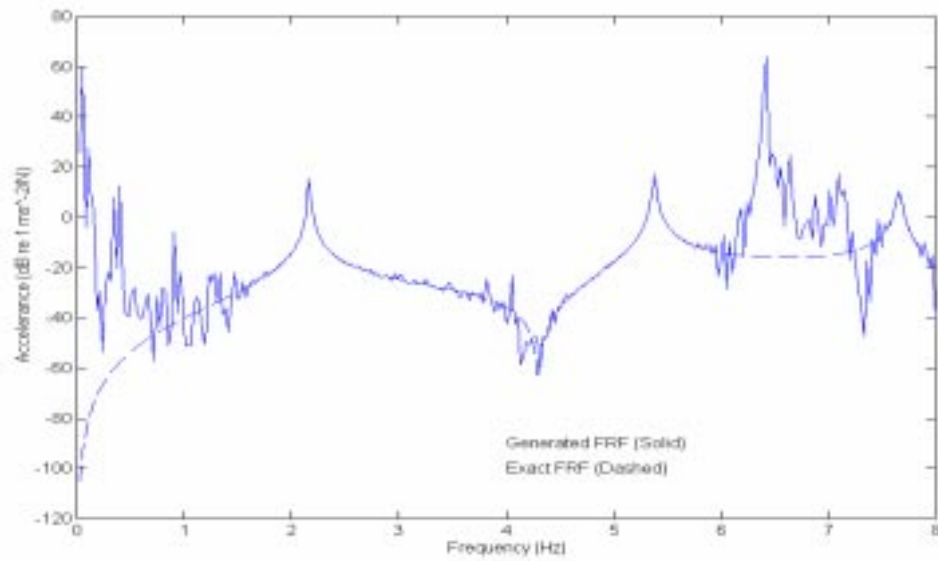
Figure 8-5. comparison of the generated FRF, A_{23} , (solid line) and the exact FRF (dashed line) of the simulated test in the presence of 0.1% noise $(m_a = m_d = 0.5Kg)$.
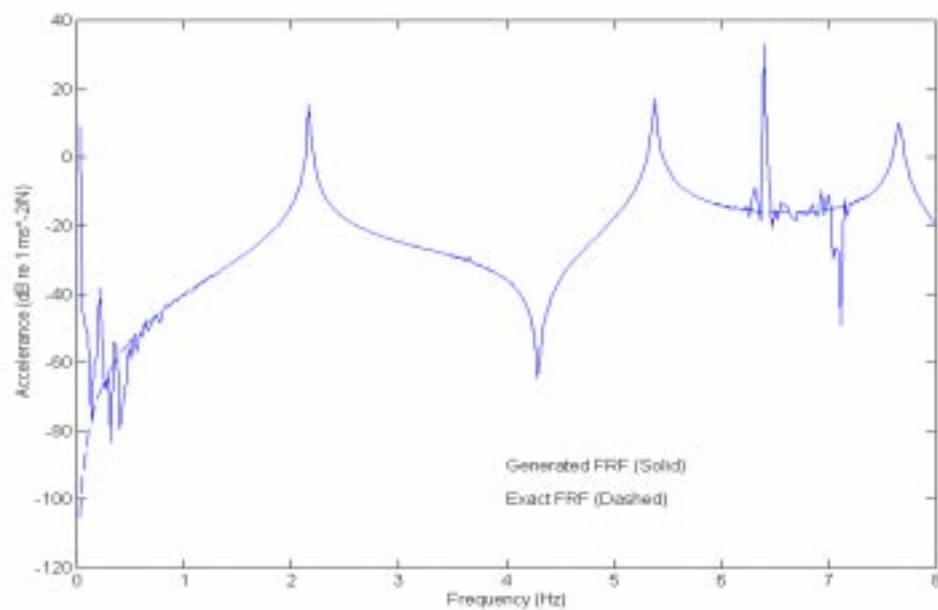
Figure 8-6. comparison of the generated FRF, A_{23} , (solid line) and the exact FRF (dashed line) of the simulated test in the presence of 0.1% noise $(m_a = m_d = 5Kg)$
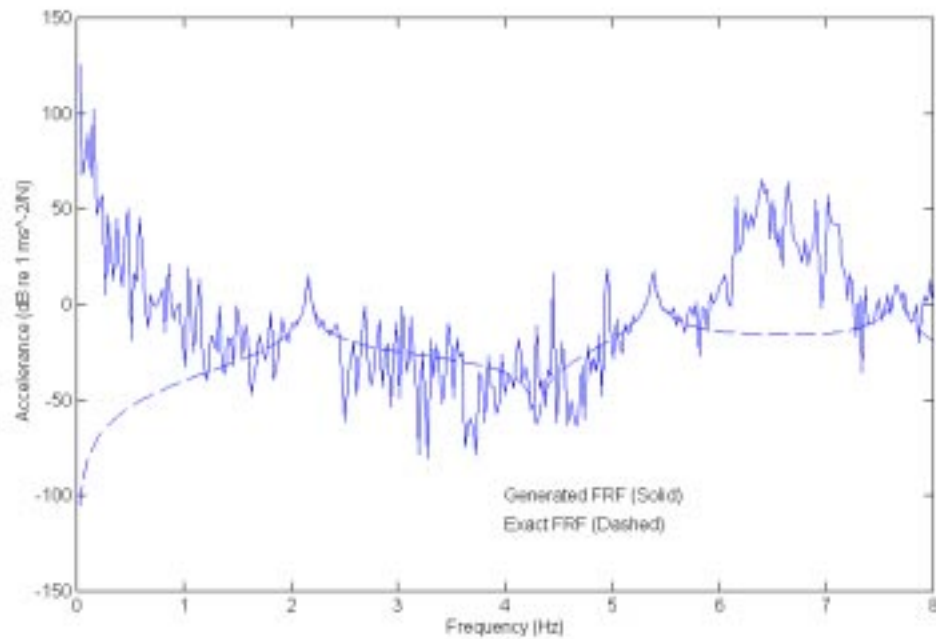
Figure 8-7. comparison of the generated FRF, A_{23} , (solid line) and the exact FRF (dashed line) of the simulated test in the presence of 1% noise $(m_a = m_d = 0.5Kg)$
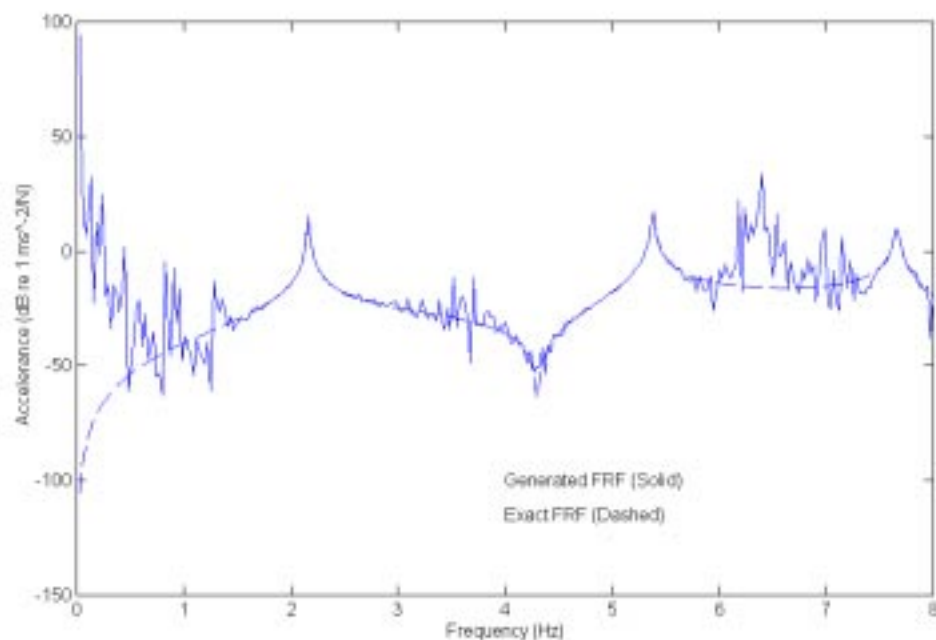
Figure 8-8. comparison of the generated FRF, A_{23} , (solid line) and the exact FRF (dashed line) of the simulated test in the presence of 1% noise $(m_a = m_d = 5Kg)$
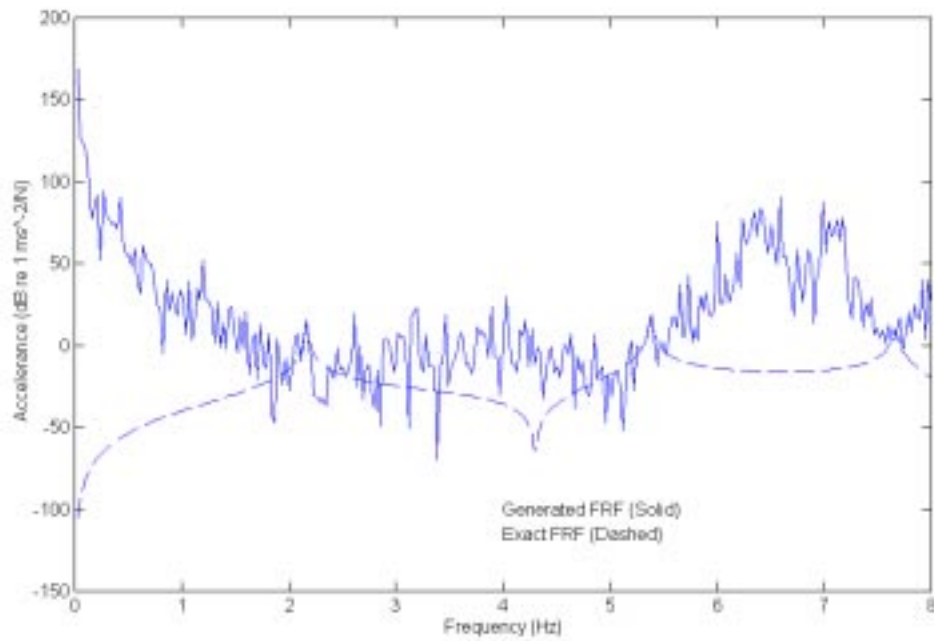
Figure 8-9. comparison of the computed FRF, A_{23} , (solid line) and the correct FRF (dashed line) of the simulated test in the presence of 5% noise $(m_a = m_d = 0.5 Kg)$
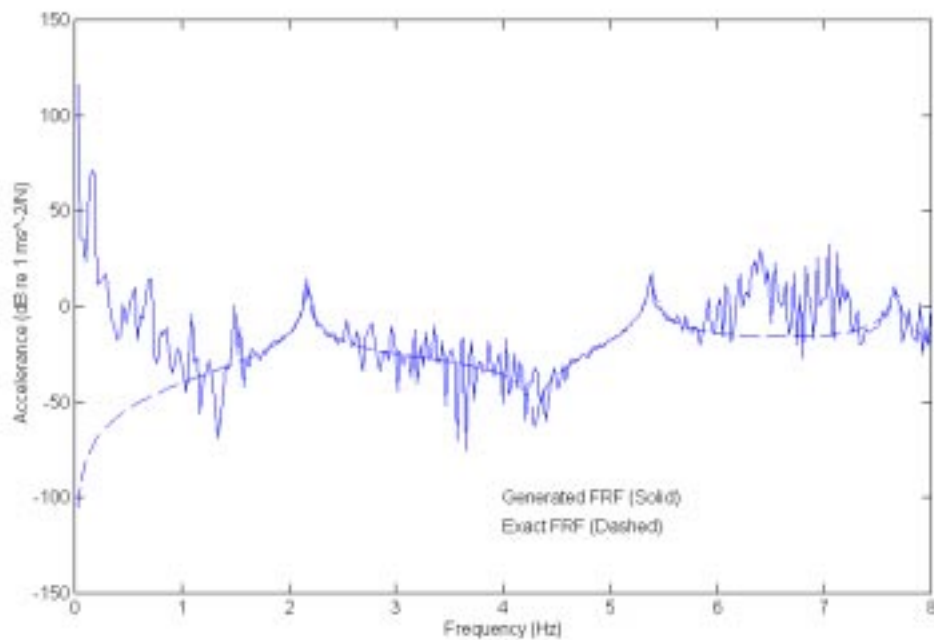
Figure 8-10 comparison of the generated FRF, A_{23} , (solid line) and the exact FRF (dashed line) of the simulated test in the presence of 5% noise $(m_a = m_d = 5 Kg)$.
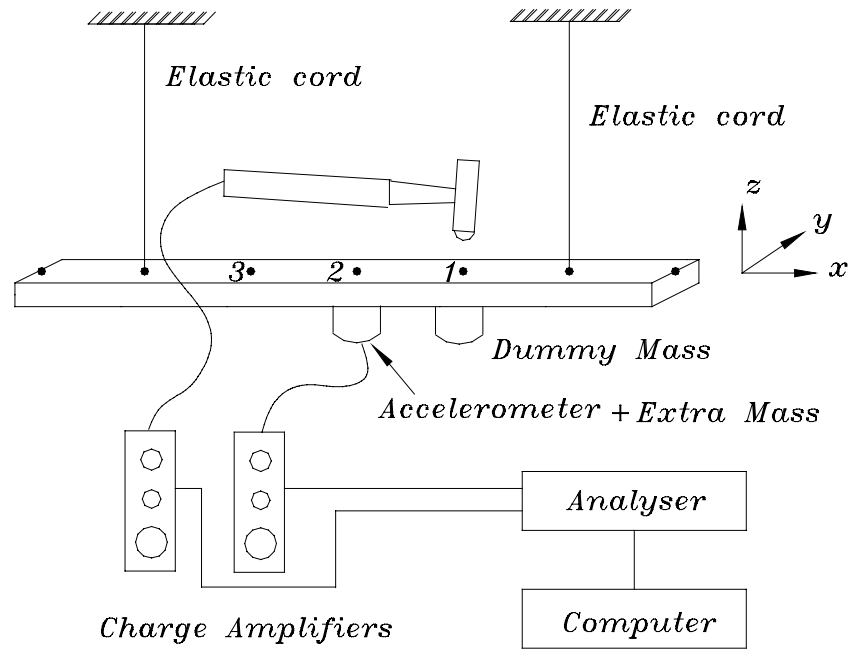
Figure 8-11. Experimental set up for the generation of FRFs
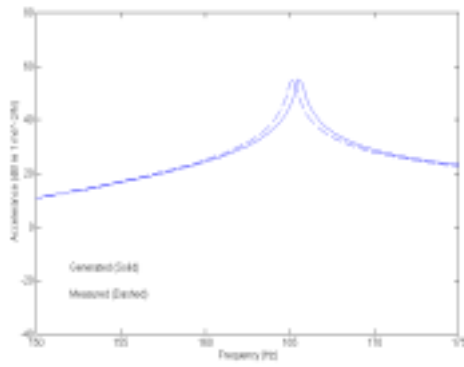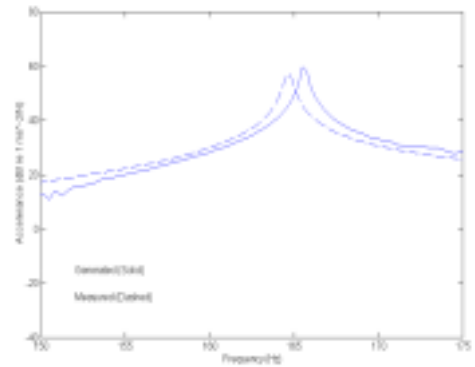
$$A_{11} \qquad\qquad A_{21}$$
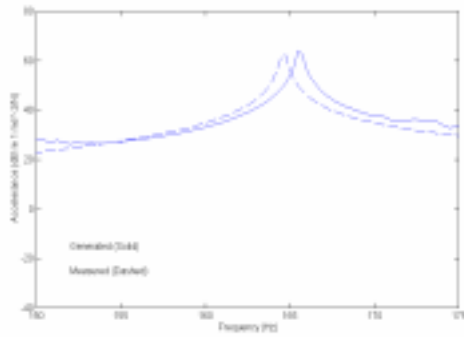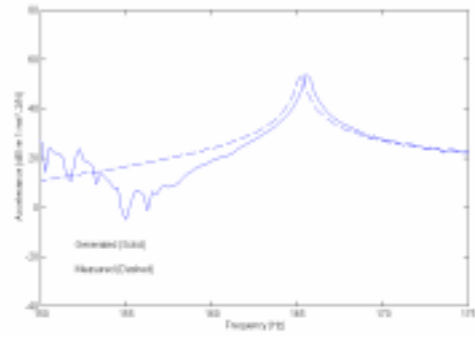
$$A_{22} \qquad\qquad A_{31}$$
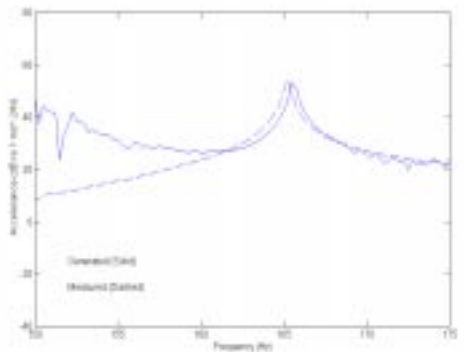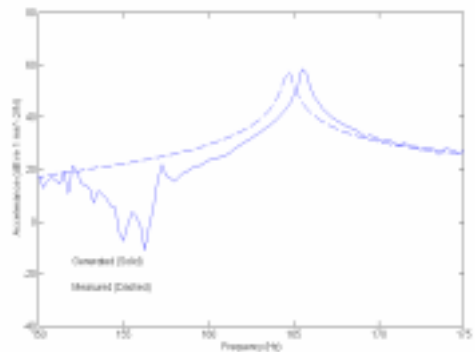
$$A_{33} \qquad\qquad A_{23}$$

Figure 8-12. comparison of the generated FRFs (solid lines) and the measured FRFs (dashed lines) of the beam.

8.5 Conclusions

- In this chapter a method for the correction of the mass-loading effects of an accelerometer and that of a dummy mass and generation of the whole matrix of translational FRFs was presented. The numerical results confirmed the validity of the method.

- In this method an accelerometer and a dummy mass were used to generate the FRFs while the point of excitation is fixed on the structure.

- Two different approaches were used to derive the FRFs of the modified structure, namely, the successive substitution and the direct derivation.

- It was shown that the effect of noise on the computations decreases with increasing the mass of the accelerometer and that of the dummy mass which was confirmed by numerical examples.

- The numerical examples showed that the resonances are less affected by noise while anti-resonances are more vulnerable to noise.

- The method was successfully applied to experimental data from test on a free-free beam.

Chapter 9

Generation of RDOFs by modifying of the

test structure

Reminder of Nomenclature

$A_{iR,jR}$ Accelerance of points i and j and in rotational direction θ_z , here i

and j refer to the points and R refers to the rotational DOF

$_r\mathbf{A}_{jk}$ the modal constant for mode r and DOFs j and k

9.1 Introduction

Rotational FRFs are present in 75% of the whole FRF matrix [5]. Their availability is therefore of extreme importance in the calculations related to the applications of the modal testing such as coupling, structural modification and model updating. However, there are neither practical means of applying moment excitation, nor accurate rotational transducers for measuring the moment and rotational response of the structure. For these reasons most of the modal analysis techniques tend to be developed avoiding as much as possible the knowledge of rotational FRFs, or minimising the effects of not knowing them.

In chapters 3, 4 and 6 correction methods were introduced in order to cancel the effects of the transducers and suspension springs on the measured FRFs. Then, in chapter 8, the same approach was used in order to generate the translational FRFs from measurements on just a single column of the FRF matrix. In this chapter a method is presented for generating the rotational FRFs of the type displacement/moment and rotation/moment by exciting the structure at translational DOFs and by modifying the test structure at particular points.

The problem is that we still need to measure rotational responses. The T-block technique have already been used to generate the rotational FRFs by modifying the test structure for theoretical models [101]. The finite difference technique itself produces rotational FRFs related to a point on the structure. In this chapter we use the finite difference technique and correction methods in order to develop a method for generating the rotational FRFs related to two different points on the structure. The aim is to eliminate the need to apply moment excitation. Instead, the structure is excited at translational DOFs and is modified by the mass and the rotational inertia of the attached objects at desired points.

9.2 Generation of the rotational FRFs by modifying the test structure

When a structure is affected by the mass and the rotational inertia of an attached object, two different degrees of freedom of the test structure are engaged at the same time (Figure 9-1). Although both of these degrees of freedom are at the same point (one translational and one rotational), they are in different directions.
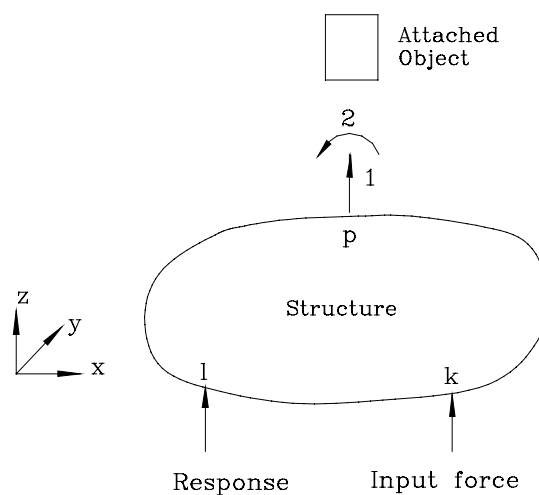
Figure 9-1. Attachment of an object to the test structure

For the correction of the rotational inertia and the mass loading effects of an attached object, two different methods may be used: *(i)* step-by-step correction or *(ii)* direct correction (chapter 6). Here, the step by step correction procedure is considered for the generation of the rotational FRFs, in order to avoid numerical problems.

The first question which may arise is the possibility of generating the rotational FRFs by measuring only translational responses or forces. For the system shown in Figure 9-1 we have:

$$A_{lk}^{(1,2)} = A_{lk}^{(2)} - \frac{A_{l1}^{(2)} . A_{k1}^{(2)}}{A_{11}^{(2)} + A_{11}'} \tag{9-1}$$

where A_{11}' is the accelerance of the attached object at DOF 1. After cancelling the mass-loading effect at DOF 1 (the mathematical procedure has been explained in chapter 4), $A_{lk}^{(2)}$, $A_{11}^{(2)}$ and $A_{l1}^{(2)} . A_{k1}^{(2)}$ are obtainable. The exact FRFs can be found from :

$$A_{lk}^{(2)} = A_{lk} - \frac{A_{l2} . A_{k2}}{A_{22} + A_{22}'} \tag{9-2}$$

$$A_{11}^{(2)} = A_{11} - \frac{(A_{12})^2}{A_{22} + A_{22}'} \tag{9-3}$$

$$A_{l1}^{(2)} . A_{k1}^{(2)} = A_{l1} . A_{k1} - \frac{A_{12} . (A_{l1} . A_{k2} + A_{k1} . A_{l2})}{A_{22} + A_{22}'} + \frac{A_{l2} . A_{k2} . (A_{12})^2}{(A_{22} + A_{22}')^2} \tag{9-4}$$

where A_{22}' is the accelerance of the attached object at DOF 2. After cancelling the rotational inertia effect at DOF 2, A_{lk} A_{11}, A_{22}, $A_{l2} . A_{k2}$, $(A_{12})^2$ and

$A_{l1} . A_{k1} - \dfrac{A_{12} . (A_{l1} . A_{k2} + A_{k1} . A_{l2})}{A_{22} + A_{22}'}$ are obtainable.

Therefore, besides the corrected FRF, A_{lk}, only the point FRFs in the axial and rotational directions, A_{11} and A_{22}, can be obtained from this approach None of the transfer FRFs such as: A_{l2}, A_{k2}, A_{12}, A_{l1} and A_{k1} can be found through this process. Consequently, although it is possible to obtain point rotational FRFs through the correction process it is not possible to obtain rotational transfer FRFs by measuring just translational responses and forces.

There are basically two problems to be resolved: the first is how to measure the rotational responses and the second is how to generate and measure the rotational excitations. In the past, there have been different techniques for measuring the rotational responses (such as the finite difference technique and the T-block technique) but there is no reliable means of applying moment excitations and measuring them. In the next section the finite difference technique is used to develop a method for generating the rotational transfer FRFs by modifying the test structure. The aim is to eliminate the need to produce moment excitations and measure them.

9.2.1 Finite difference technique

In the finite difference method two or three accelerometers (according to the finite-difference formula employed) are placed close to each other, in a constant spacing (*s*). Translational measurements are then made and finite difference formulas are used to derive rotational FRFs. Here , the first-order forward finite difference formula has been considered for estimating rotational FRFs. In figure 9-3 if *c* is a point close to point *a* with the distance *s,* then the rotational FRFs can be estimated from:

$$\begin{cases} A_{12} = (1/s).(A_{15} - A_{11}) \\ A_{22} = (1/s^2).(A_{11} - 2A_{15} + A_{55}) \end{cases} \qquad \textbf{(9-5)}$$

Here, 5 refers to the axial direction at point *c*. Therefore, using this technique the rotational FRFs at point *a* are obtainable. However, the rotational transfer FRFs, such

as: A_{23}, A_{14} and A_{24}, are still not available. To obtain these FRFs the following method is suggested:
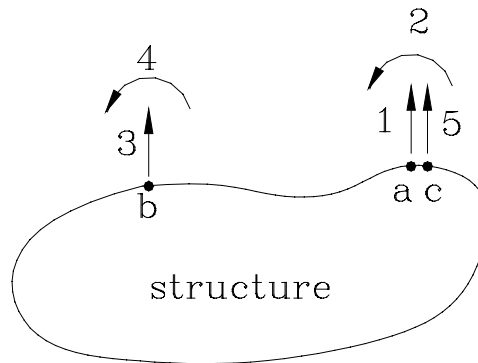
Figure 9-2. Generation of rotational FRFs using the finite difference technique

9.2.2 Measurement technique

Consider the structure shown in Figure 9-2.

1. Obtain A_{11} , A_{21} and A_{22} using the finite difference technique.

2. Obtain A_{33} , A_{43} and A_{44} using the finite difference technique.

3. Measure A_{13}.

4. Attach an object (with a known mass and moment of inertia) at point *b* and obtain $A_{21}^{(3,4)}$ using the finite difference technique. Attach another object (instead of the first object) at point *b* with the same mass as that of the first object but with a different moment of inertia and measure $\overline{A}_{21}^{(3,4)}$ (here $A_{21}^{(3,4)}$ is different from $\overline{A}_{21}^{(3,4)}$).

5. Attach an object (with a known mass and rotational inertia) at point *a* and obtain $A_{43}^{(1,2)}$ using the finite difference technique. Attach another object (instead of the first object) at point *a* with the same mass as that of the first object but with a different moment of inertia and measure $\overline{A}_{43}^{(1,2)}$ (here $A_{43}^{(1,2)}$ is different from $\overline{A}_{43}^{(1,2)}$).

Figure 9-3 shows different stages of the measurement using this measurement technique.
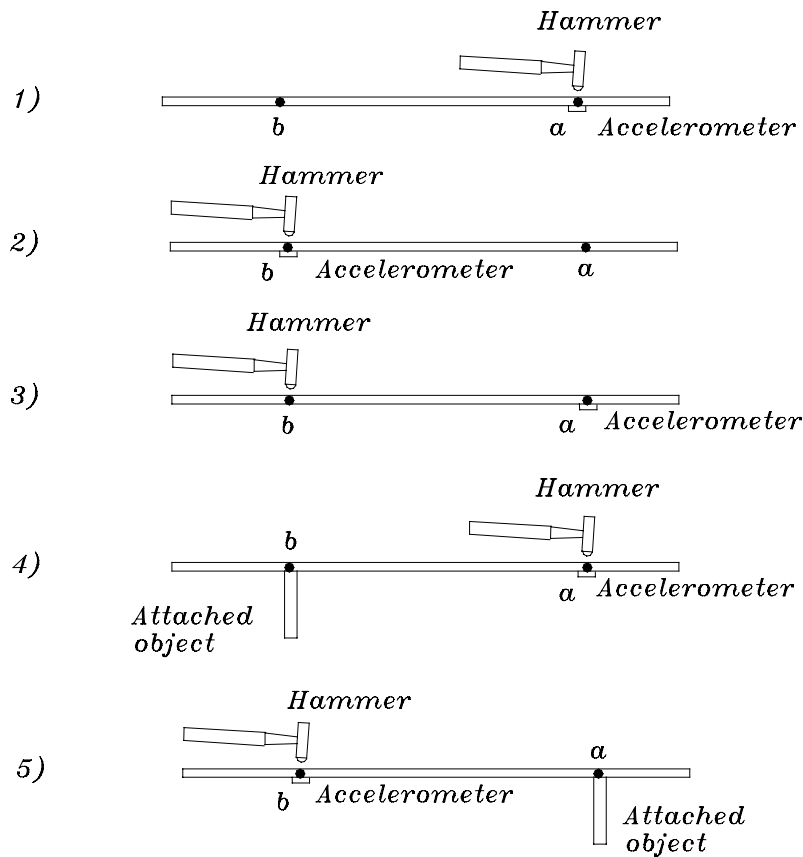
Figure 9-3. Measurement stages for obtaining rotational FRFs

It should be noted that any method of generating the rotational FRFs is more successful the fewer computation stages it has. The reason is that, owing to the presence of noise and other systematic errors in the measurements, the results of the computations in each step become less reliable. Thus, if a FRF can be obtained from direct measurement, the risk of possible errors decreases. Moreover, it is assumed that the attached accelerometer is so light that its mass-loading effect is negligible. The above-mentioned measurement technique is based on the minimum possible number of computation stages, and on the step-by-step correction approach. This means that the masses (m) of the attached objects are the same although their moments of inertia (I) are different.

9.2.3 Generation of the rotational FRFs

The procedure for generating all of the FRFs from the measured FRFs listed in the previous section is:

1. In equation

$$A_{34}^{(1,2)} = A_{34}^{(1)} - \frac{A_{23}^{(1)} . A_{24}^{(1)}}{1 / I + A_{22}^{(1)}}$$

(9-6)

$A_{22}^{(1)}$ is known because A_{11}, A_{12} and A_{22} are known:

$$A_{22}^{(1)} = A_{22} - \frac{(A_{12})^2}{1 / m + A_{11}}$$

(9-7)

For two different objects with the same mass (m) but different moments of inertia: (I_1 and I_2) $A_{34}^{(1)}$ and $A_{23}^{(1)} . A_{24}^{(1)}$ can be obtained from equation (9-6).

Then A_{14} can be obtained from :

$$A_{34}^{(1)} = A_{34} - \frac{A_{13} . A_{14}}{1 / m + A_{11}}$$

(9-8)

A_{34}, A_{13} and A_{11} are known and $A_{34}^{(1)}$ was obtained from the last stage and therefore A_{14} is obtainable.

2. In equation

$$A_{12}^{(3,4)} = A_{12}^{(3)} - \frac{A_{41}^{(3)} . A_{42}^{(3)}}{1 / I + A_{44}^{(3)}}$$

(9-9)

$A_{44}^{(3)}$ is known because A_{33}, A_{34} and A_{44} are known:

$$A_{44}^{(3)} = A_{44} - \frac{(A_{34})^2}{1 / m + A_{33}}$$

(9-10)

For two different objects with the same mass (m) but different moments of inertia: (I_1 and I_2) $A_{12}^{(3)}$ and $A_{41}^{(3)} . A_{42}^{(3)}$ can be obtained from equation (9-9).

Then A_{32} can be obtained from :

$$A_{12}^{(3)} = A_{12} - \frac{A_{31} . A_{32}}{1/m + A_{33}}$$ (9-11)

A_{12}, A_{31} and A_{33} are known and $A_{12}^{(3)}$ was obtained from the last stage and therefore A_{32} is obtainable.

3. To obtain A_{24} we have:

$$A_{23}^{(1)} = A_{23} - \frac{A_{12} . A_{13}}{1/m + A_{11}}$$ (9-12)

A_{23}, A_{12}, A_{13} and A_{11} are known. Therefore $A_{23}^{(1)}$ is obtainable. From step 1 $A_{23}^{(1)} . A_{24}^{(1)}$ was obtained. So $A_{24}^{(1)}$ is obtainable.

$$A_{24}^{(1)} = A_{24} - \frac{A_{12} . A_{14}}{1/m + A_{11}} \rightarrow A_{24} = A_{24}^{(1)} + \frac{A_{12} . A_{14}}{1/m + A_{11}}$$ (9-13)

All of the elements on the right hand side of equation (9-13) are known; therefore A_{24} is obtainable. A_{24} is obtainable from another way. We have:

$$A_{14}^{(3)} = A_{14} - \frac{A_{34} . A_{13}}{1/m + A_{33}}$$ (9-14)

A_{14}, A_{34}, A_{13} and A_{33} are known. Therefore $A_{14}^{(3)}$ is obtainable. From step 2 $A_{14}^{(3)} . A_{24}^{(3)}$ was obtained. So $A_{24}^{(3)}$ is obtainable.

$$A_{24}^{(3)} = A_{24} - \frac{A_{34} . A_{23}}{1/m + A_{33}} \rightarrow A_{24} = A_{24}^{(3)} + \frac{A_{34} . A_{23}}{1/m + A_{33}}$$ (9-15)

Consequently, A_{24} is obtainable in either of two different ways. Comparison of these two derived FRFs of A_{24} can be a way of checking the validity of the method.

9.3 Validation of the method

9.3.1 Practical considerations

Although the method presented in the last section is algebraically correct, in practice it cannot be applied without considering the limitations of the experiment. These considerations are:

1. Selection of the attached objects

The attached objects should influence the structure rotationally and translationally. If the order of the changes of the measured FRFs is the same as the order of the noise present in the experiment then nothing is generated but the noisy results. As most of the information related to the dynamics of a structure is related to its resonances, the additive elements should be designed in such a way that considerable changes happen around the resonance of the structure.

Moreover, the attached objects are assumed to behave as rigid bodies. This means that the behaviour of the attached objects should be checked in the desired frequency range. This can be done by comparing the behaviour of the objects on a known structure.

2. Nodal points:

In order to generate the rotational FRFs it is necessary to choose suitable points on the structure: namely, the location for the addition of the object and the locations for the forcing and measurement of the responses. The selection of these locations has a major influence on the quality of the results. Figure 9-4 shows the first bending mode shape of a free-free beam. In this mode, at point *D* the translational motion is maximum while the rotational motion is zero. If the extra object is added to the beam at point *D* its rotational inertia does not have any effect on the vibration of the beam. As a result, changing the rotational inertia property of the added object does not change the measured FRF. On the other hand, in this mode, at points *A* and *G,* the beam has no translational motion, while the rotational motion is maximum. If

translational receptance is measured at points *A* or *G,* the result is zero. Consequently, if points *A* and *G* are chosen for placing the additive object, only the point rotational FRFs are non-zero. In this case the only equations which are available are:

$$A_{44}^{(2)} = A_{44} - \frac{(A_{24})^2}{1/J + A_{22}}$$
(9-16)

$$A_{22}^{(4)} = A_{22} - \frac{(A_{24})^2}{1/J + A_{44}}$$
(9-17)

which give us only $(A_{24})^2$. Therefore, choosing points *A* or *G* will not simplify the method.
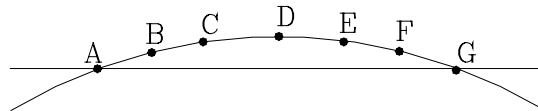
Figure 9-4. First bending mode of a beam

In this mode, if points B and E are chosen for the test the result will be reasonable because each of these points has both rotational and translational motion together.

3. Nonlinearity

The basic assumption of the method presented in this chapter is the linear behaviour of the structure and the attached object. As was shown in chapter 7, if the structure or the additive object shows any nonlinearity, the result of applying the methods such as the one presented in this chapter will not be reliable. Therefore the behaviour of the modified structure should be checked for signs of nonlinearity.

4. Noise

Noise pollutes the results of the computations at each step. One way of avoiding the effects of noise is to regenerate the initial measured FRFs using curve-fitting techniques.

9.3.2 Numerical case study

A theoretical model of a beam was considered for the numerical validation of the method. Table 9-1 shows the parameters of the beam. The model of the beam was made in the same manner as was explained in chapter 3.

Table 9-1. Parameters of the beam

Length	0.7 m
Height	0.0048 m
Thickness	0.0635 m
Number of elements	56
Mass of density	7800 kg/m^3
Mass	2.359 kg
Modulus of elasticity	$2.1 \times 10^{11} (N/m^2)$

Figure 9-5 shows the result of the FEM analysis of the third elastic mode of the beam which is at 274 Hz. Points 9 and 33 were chosen to determine the rotational FRFs using the method presented in this chapter. In order to estimate the rotational responses using the finite difference technique, point 10 was chosen to be close to point 9, and point 34 close to point 33. It should be mentioned that the distance between the points is important in the results of the finite difference technique. However, the aim of this work has not been to find the optimum distance between the points; this distance was chosen based on the work presented in [102].
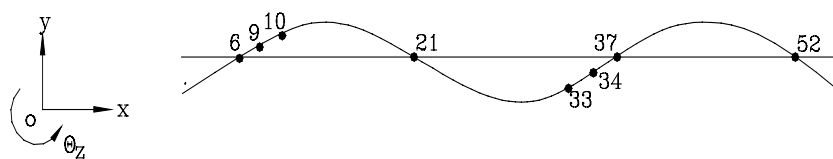
Figure 9-5. Third mode of the free-free beam

Two different additive elements were chosen which have the same masses but different moments of inertia. The parameters of these elements are:

<u>Element 1:</u> mass=0.024 kg, moment of inertia $=5.1304 \times 10^{-5} kg.m^2$;

<u>Element 2:</u> mass=0.024 kg, moment of inertia $=9.4733 \times 10^{-5} kg.m^2$.

Elements 1 and 2 defined above are assumed to behave as rigid bodies. The simulated measurements were conducted by computing the FRFs following the measurement technique stated in section 9.2.2. Figure 9-6 shows the changes in $A_{9,10}$ when elements 1 or 2 are added to the beam at point 33. Figure 9-7 shows the changes in $A_{33,34}$ when elements 1 or 2 are added to the beam at point 9. These figures show that the added elements have made reasonable changes in the FRF around the resonance of the structure.

The FRFs were generated according to the procedure stated in section 9.2.3. Figure 9-8 compares the estimated rotational FRF $A_{9,9R}$ (here "9R" refers to the rotational direction θ_z at point 9) using the finite difference technique and the exact FRF $A_{9,9R}$. Figure 9-9 compares the estimated rotational FRF $A_{33,33R}$ using the finite difference technique and the exact FRF $A_{33,33R}$. Figure 9-10 compares the exact $A_{9,33R}$ and generated $A_{9,33R}$. The two FRFs coincide around the resonance area although some part of the generated FRF shows a considerable difference from the exact FRF at the frequency that the resonance of the modified beam exists. The same situation happens for the FRF $A_{9R,33}$ as shown in Figure 9-11. These differences are due to the approximate nature of the method of the finite difference technique for estimating the rotational FRFs.

Figure 9-12 compares the generated FRFs $A_{33R,9R}$ with the exact FRF. As was shown in section 9.2.3 this FRF can be computed in two different ways. In the resonance region the FRFs coincide, although there is a considerable difference in one part of the FRF. Since the result at the resonance frequency is acceptable, we have most of the necessary information about this mode.
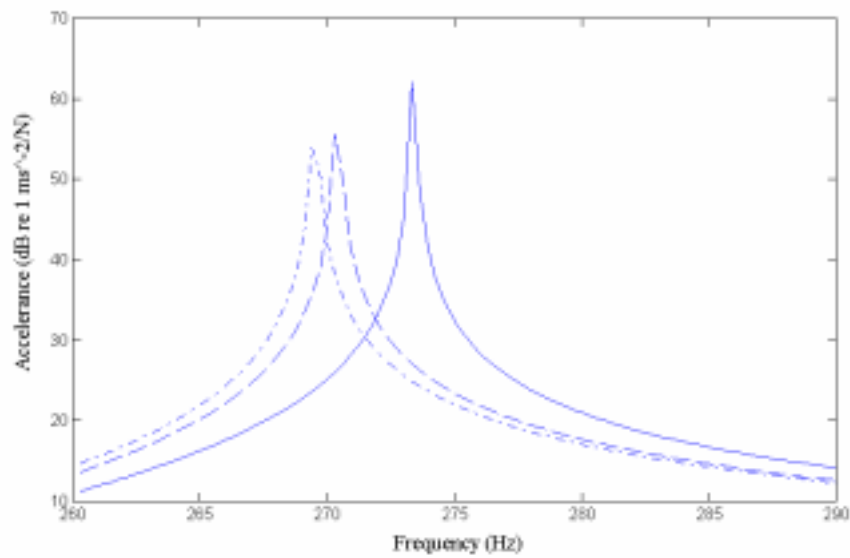
Figure 9-6. Changes in $A_{9,10}$ when Element 1 is added to the structure at point 33 (dashed) and when Element 2 is added to the structure at point 33 (dashdot) compared with the exact FRF (solid)
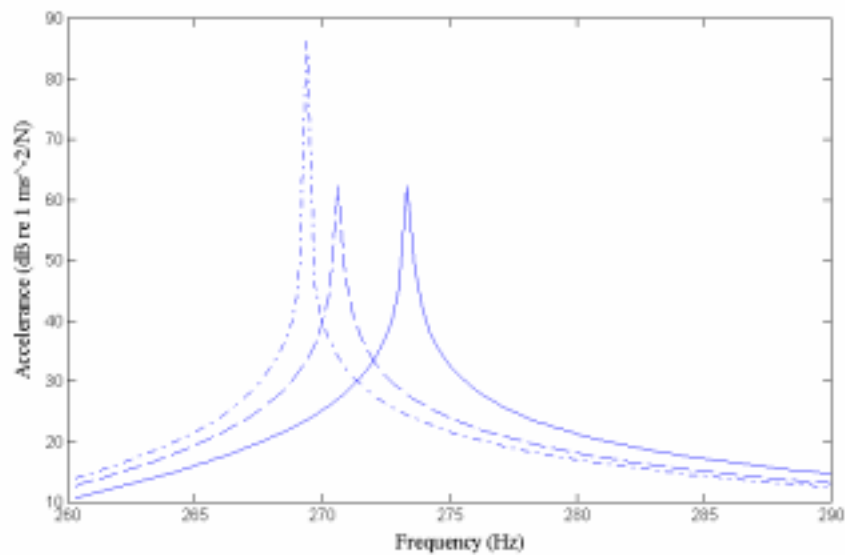
Figure 9-7. Changes in $A_{33,34}$ when Element 1 is added to the structure at point 9 (dashed) and when Element 2 is added to the structure at point 9 (dashdot) compared with the exact FRF (solid).
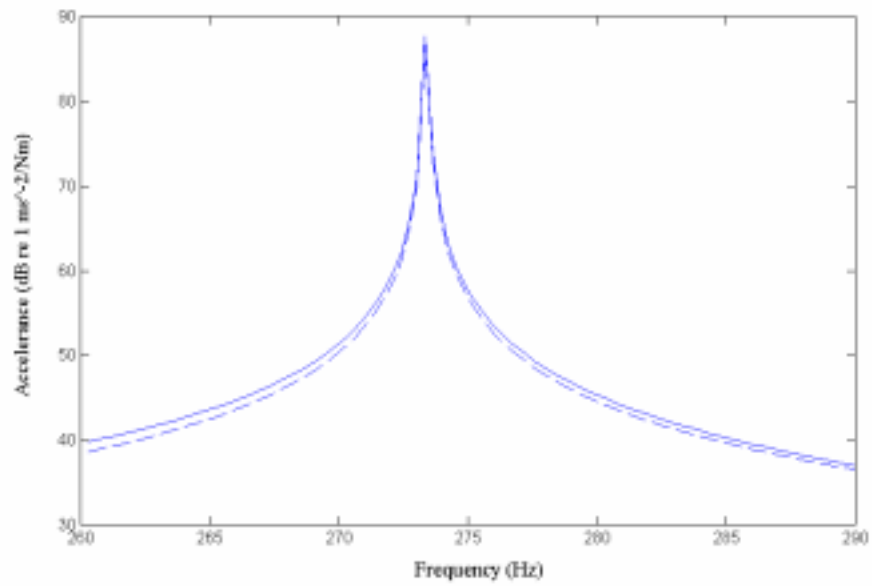
Figure 9-8. Comparison of the exact $A_{9,9R}$ (solid) and estimated $A_{9,9R}$ (dashed) using the finite difference method
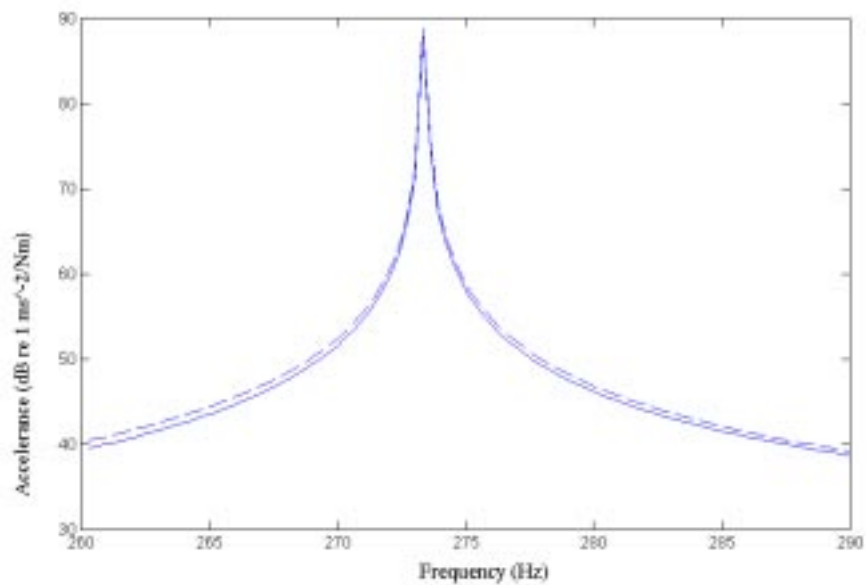
Figure 9-9. Comparison of the exact $A_{33,33R}$ (solid) and estimated $A_{33,33R}$ (dashed) using finite difference method
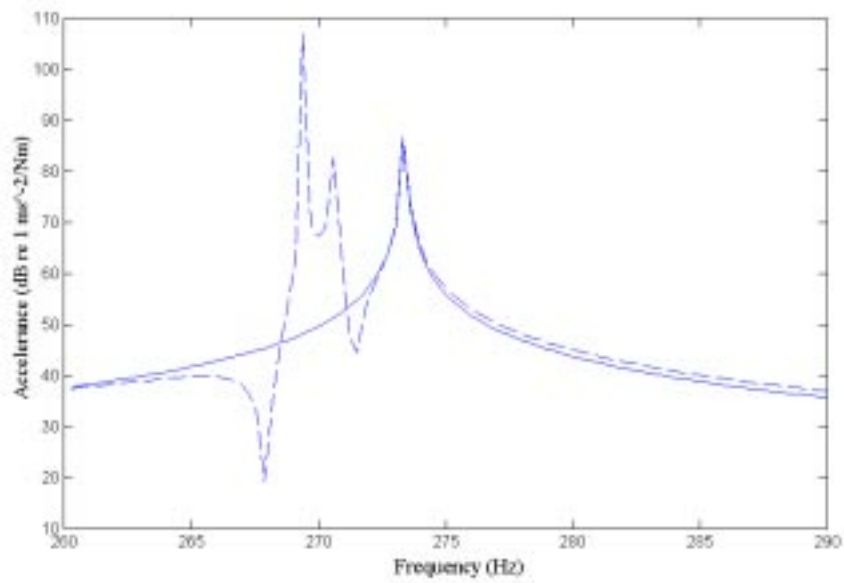
Figure 9-10. Comparison of the exact $A_{9,33R}$ (solid) and generated $A_{9,33R}$ (dashed)
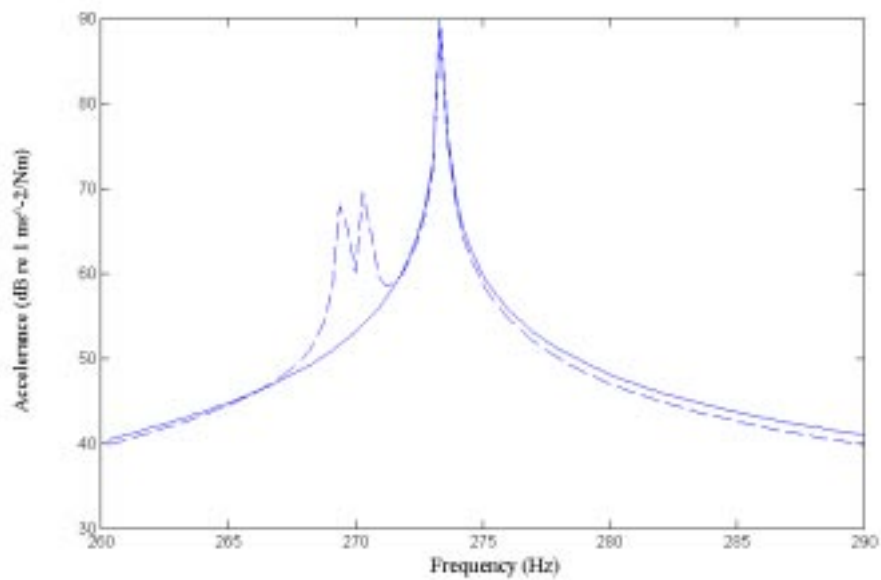
Figure 9-11. Comparison of the exact $A_{33R,9R}$ (solid) and computed $A_{33R,9R}$ (dashed)
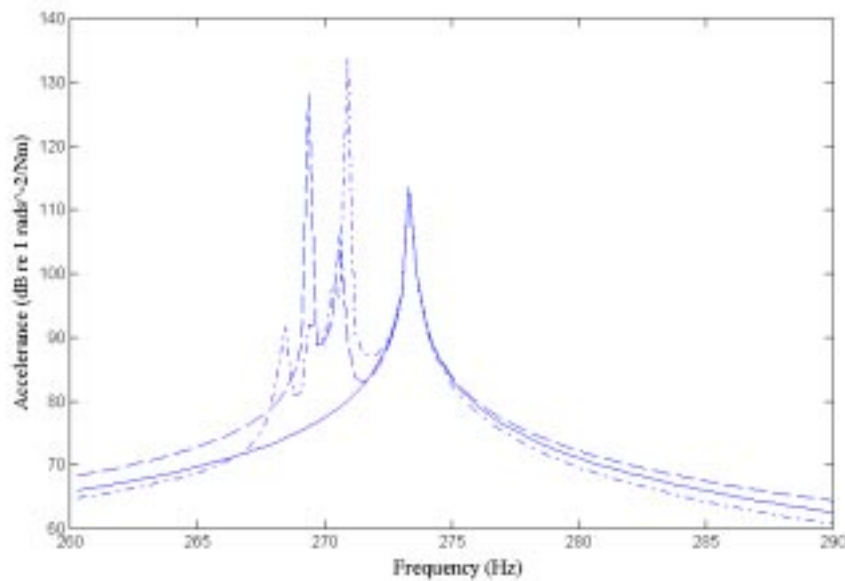
Figure 9-12. Comparison of the exact $A_{33R,9R}$ (solid) and computed $A_{33R,9R}$ (dashed and dashdot)

9.3.3 Experimental case study

A simple beam was used for the experimental validation of the method presented in this chapter. The beam was made of mild steel, and had dimensions $6.35 \times 0.48 \times 70 cm$. Figure 9-13 shows the experimental set-up for the hammer test of the beam. The beam was discretised into 57 points and was tested in a "free-free" configuration, suspended by soft elastic cords with the stiffness of 410 *N/m* attached to the beam at points 6 and 52. Figure 9-5 shows the theoretical mode shape of the third mode of such a beam. As shown in this figure, points 6 and 52 are translational nodes, and as a result are suitable for the attachment of the suspension springs to fulfil the free-free condition in this mode. Moreover, this figure shows that points 9 and 33 are far from nodal points (rotational and translational); and consequently are suitable for applying the method presented in this chapter. Therefore, points 9 and 33 were chosen in order to generate all of the FRFs in the region of the third mode of the beam. To estimate the rotational FRFs using the finite difference technique, points 10 and 34, which are close to points 9 and 33, were considered for the measurement.
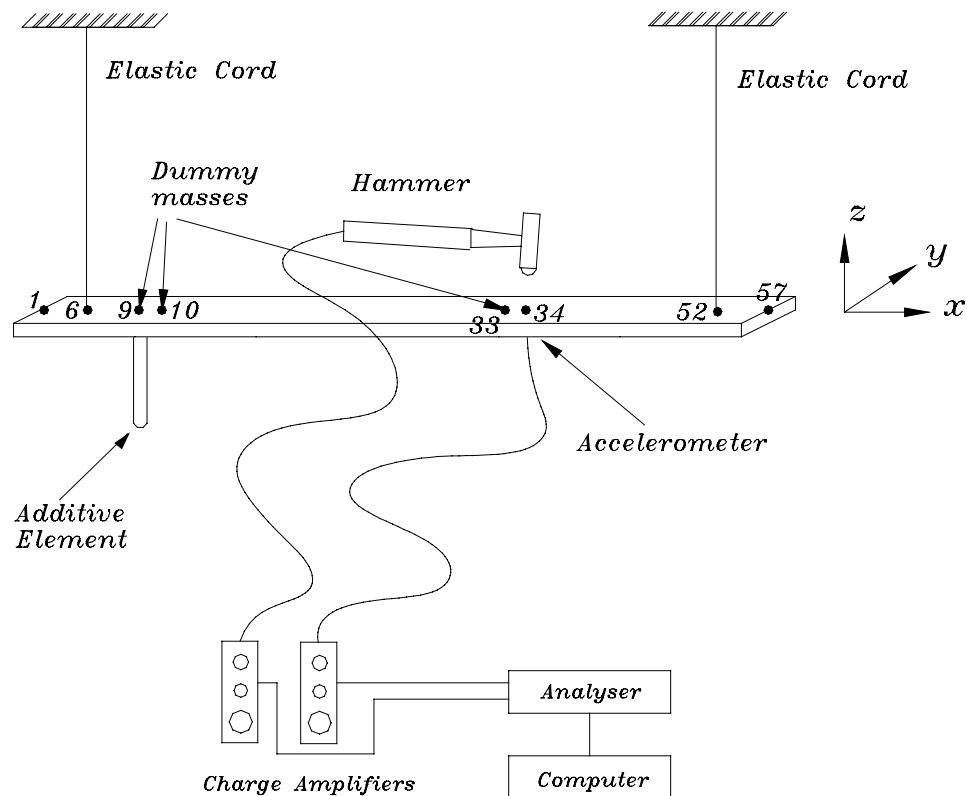
Figure 9-13. Experimental test set-up for the measurement of $A_{34,34}$ when an extra element is added to point 9.

The beam was excited by a hammer at its neutral axis and the response was measured by a light accelerometer of mass 0.004 *kg*. When the response was measured at one of the points 9 or 10 or 33 or 34, three dummy masses, each of 0.004 *kg,* were attached to the beam at three other points to avoid reciprocity problems.

The extra elements which were due to be added to the structure at points 9 and 33 were chosen by trial and error. After trying different elements, two cylindrical elements with the same masses but different moments of inertia were chosen. The properties of these elements are:

Element 1: Shape: Cylinder ; Diameter = 0.007 *m*; Length = 0.08 *m*; Material: Steel; Mass = 0.024 *kg*; Computed moment of inertia = $5.1304 \times 10^{-5} kg.m^2$

Element 2:   Shape: Cylinder ; Diameter = 0.006 *m*; Length = 0.1088 *m*; Material: Steel; Mass = 0.024 *kg*; Computed moment of inertia = $9.4733 \times 10^{-5} kg.m^2$

Here, the second moment of inertia quoted is with respect to the diameter of the cylinder at one of its ends namely the place where it is attached to the structure. Figure 9-14 shows changes in $A_{33,33}$ when these two elements were added to point 9. Figure 9-15 shows changes in A_{99} when the elements were added to point 33. As the elements have the same mass, the difference between the two FRFs of the modified beam is related to the moment of inertia of the added elements. It can thus be concluded that the chosen elements are suitable for the test. Moreover, the measured FRFs show sufficient changes around the resonance of the beam, which is the most important area in the test.

The additive elements are long with respect to their cross section area, as a result of which two problems may arise. Firstly, the elements may not exhibit rigid body behaviour in all of the frequency points. Secondly, the addition of these long elements may result in nonlinear behaviour of the modified structure due to large deflections of the elements. Both of these problems should be checked before applying the method.

Figure 9-16 shows the theoretical result of the point rotational acceleration of one of the ends of the additive elements. This figure indicates that the rotational behaviour of these elements is not constant for all of the frequencies. However, the point rotational acceleration of the additive elements can be approximated at 270 Hz by a constant. The theoretical results of the models of these elements showed that an approximate value of the second moment of inertia of element 1 at 270 Hz was $6 \times 10^{-5} kg.m^2$; for element 2 this value was $2.3 \times 10^{-4} kg.m^2$.

In order to check the possibility of nonlinear behaviour, the coupled structure of the beam and element 2 (which is longer) was tested in a shaker test. The shaker excited the structure at point 9 while element 2 was attached to the beam at point 33. The structure was excited by three different levels of force and A_{99} was measured. Figure 9-17 shows the result of the test. No sign of nonlinearity is present around the third mode of the beam (276 Hz). The test of the nonlinearity at the other points and using

element 1 also showed no sign of nonlinear behaviour; therefore the results of the computations are considered not to be vulnerable to nonlinearity.

As noise pollutes the result of the computations, all of the FRFs present in the computations were regenerated in the frequency range of 260-290 Hz using ICATS program. The result of the regeneration was carefully controlled to match the raw data. Figure 9-18 shows the result of the regeneration of three of these FRFs.
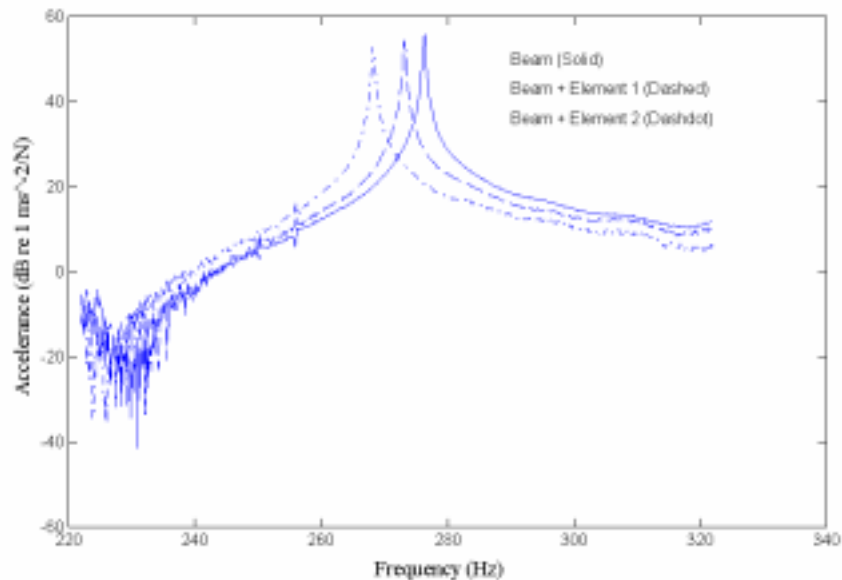
Figure 9-14. Changes in $A_{33,33}$ when an extra element is added to point 9.
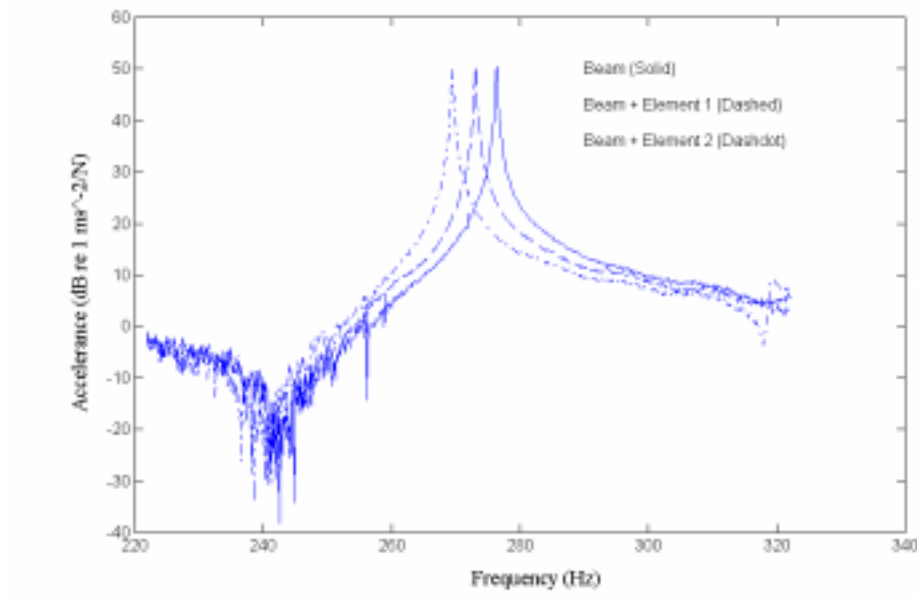
Figure 9-15. Changes in A_{99} when an extra element is added to point 33.
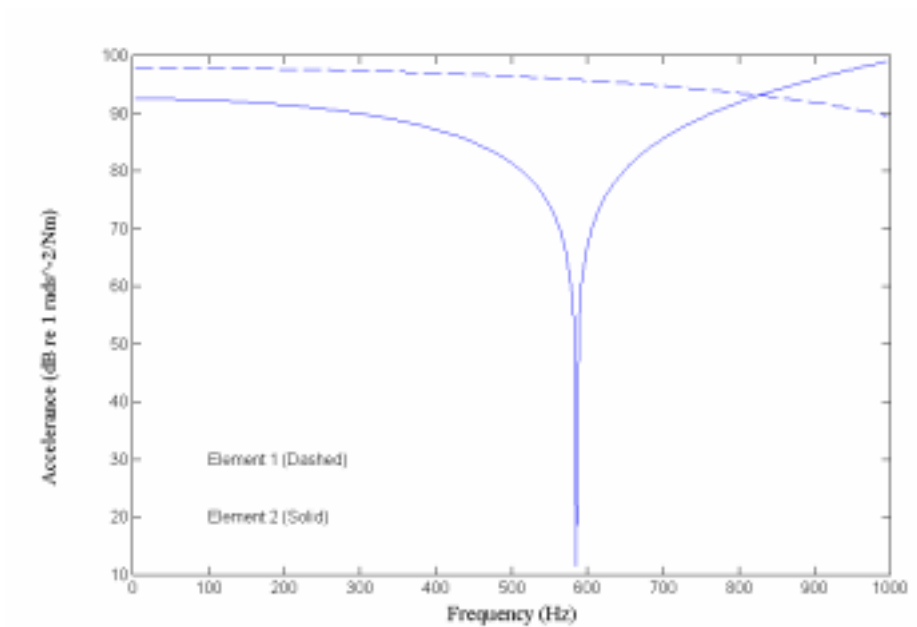
Figure 9-16. Point rotational accelerance of the Elements 1 and 2
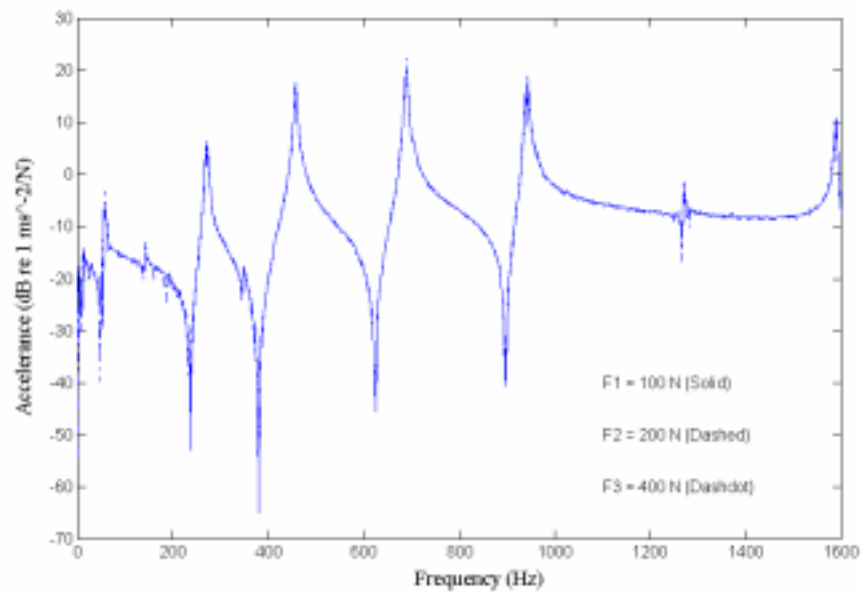
Figure 9-17. The test of nonlinearity in the measurement of A_{99} when Element 2 is attached to point 33 (F_1, F_2 and F_3 are different level of forces).
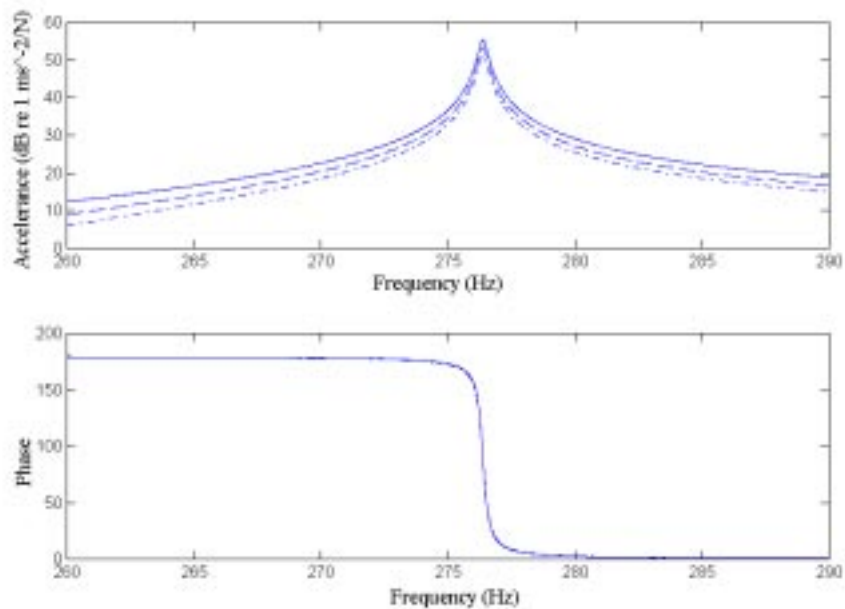
Figure 9-18. Regenerated FRFs of $A_{33,33}$ (solid), $A_{33,34}$ (dashed) and $A_{34,34}$ (dashdot)

All the required FRFs were measured following to the measurement technique stated in section 9.2.2 and the rotational FRFs were generated following to the procedure stated in section 9.2.3. Figure 9-19 shows the two computed rotational FRFs (the FRFs were regenerated using ICATS), $A_{9R,33R}$. As was presented in the method, $A_{9R,33R}$ can be obtained in two different ways which should coincide around 276 Hz. However, a comparison between these two computed FRFs in Figure 9-19 shows a slight difference. One way of assessing the success of the method is to conduct an internal check of the generated FRFs using their modal constants. In principle, the following equations should hold between the modal constants of the measured FRFs of the beam:

$$_3\mathbf{A}_{9R,33R} = \frac{(_3\mathbf{A}_{9,9R}).(_3\mathbf{A}_{9,33R})}{_3\mathbf{A}_{99}} \qquad \qquad (\text{ 9-18})$$

$$_3\mathbf{A}_{9R,33R} = \frac{(_3\mathbf{A}_{9R,33}).(_3\mathbf{A}_{33R,33})}{_3\mathbf{A}_{33,33}} \qquad \qquad (\text{9-19})$$

where $_r\mathbf{A}_{jk}$ is the modal constant for mode r and coordinates j and k. On this basis the required FRFs for equations (9-18) and (9-19) were regenerated and their modal constants derived using the ICATS program. Table 9-2 indicates the modal constants of these FRFs for the third mode of the beam. The result of the calculation for the right hand side of equation (9-18) is 5×10^8 compared with 5.5×10^8 for the left hand side. For equation (9-19) the result of the right hand side of equation is 5.9×10^8 comparing to 5.5×10^8 for the left hand side. The results of this procedure show that the two sides of equations (9-18) and (9-19) above are close together, demonstrating that the method is valid and can be used for estimation of the rotational FRFs around the resonance area of the structure. However, the approximate nature of the finite difference technique and the experimental errors (systematic and random) present in the measurement detract from the reliability of the generated FRFs.
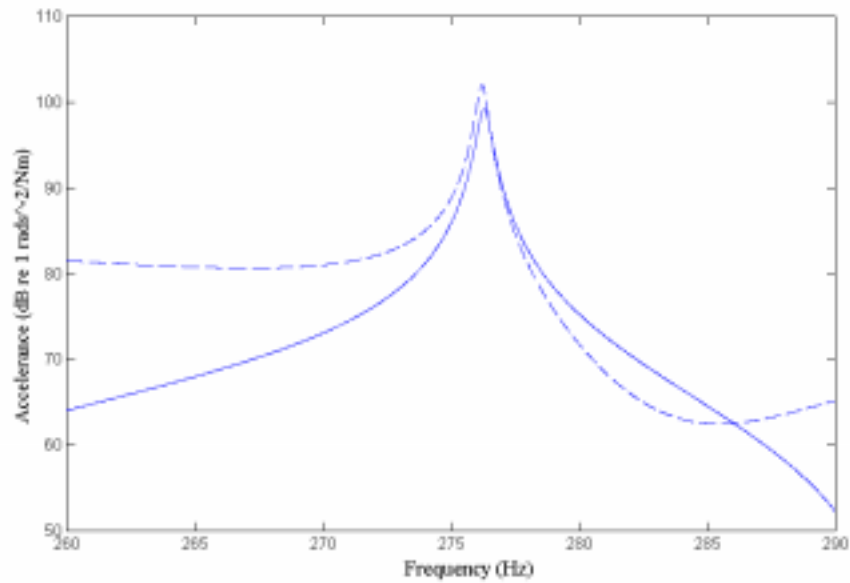
Figure 9-19. Two regenerated FRFs of $A_{9R,33R}$

Table 9-2. Modal constants of the regenerated FRFs

No.	FRF	Frequency (Hz)	Modal Constant
1	A_{99}	276.38	1.1 E 6
2	A_{99R}	276.37	2.5 E 7
3	$A_{33,33}$	276.38	1.9 E 6
4	$A_{33,33R}$	276.38	3.4 E 7
5	$A_{9,33R}$	276.37	2.2 E 7
6	$A_{9R,33}$	276.26	3.3 E 7
7	$A_{9R,33R}$ (1)	276.3	5.5 E 8
8	$A_{9R,33R}$ (2)	276.22	6.1 E 8

9.4 Test strategy

In order to apply the method presented in this chapter for generating the rotational FRFs the following procedure is suggested for the structure shown in Figure 9-20:

1. Obtain the mode shapes of the structure by conducting a conventional modal test on the structure or by using the FE model of the structure.

2. Obtain the nodal points (translational and rotational) of the structure for a particular mode from the corresponding mode shape. It should be noted that rotational nodal points are obtainable using the finite difference technique.

3. Choose two points on the structure which are not close to the nodal points (translational and rotational).

4. Select two additive elements with the same mass but different moments of inertia so that by adding of them to the test structure considerable changes happen around the resonance of the test structure. These additive elements should be chosen by trial and error.

5. Check the behaviour of the modified structure for signs of nonlinearity.

6. Test the structure following the measurement technique stated in section 9.2.2.

7. Regenerate the measured FRFs using curve-fitting techniques to avoid the effects of noise on the computations.

8. Generate the rotational FRFs following the procedure stated in section 9.2.3.

9. Check the results by conducting an internal check of generated FRFs using their modal constants.
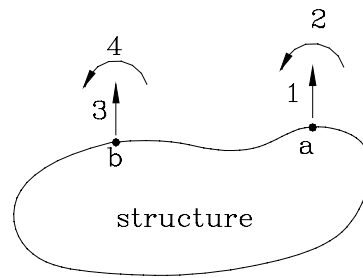
Figure 9-20. Generation of rotational FRFs of a structure

9.5 Conclusions

- In this chapter a method was presented for the generation of the transfer rotational FRFs by modifying the test structure.

- It was shown the problem of the rotational excitation of the structure can be eliminated by adding objects to the structure and using correction methods presented in the previous chapters.

- The results of the theoretical simulation showed that the generated FRFs are acceptable around the resonance area of the structure although some part of the generated FRFs show considerable difference from the exact FRF due to the approximate nature of the finite difference technique.

- The method was successfully applied to experimental data for a free-free beam and the internal check of the generated FRFs demonstrated the validity of the method.

Conclusions and suggestions for future work

10.1 Conclusions

This section presents a summary of the conclusions of the work presented in this thesis.

10.1.1 Introduction

The sources of a lack of precision in modal testing have been categorised in three groups: (i) experimental data acquisition errors (ii) signal processing errors and (iii) modal analysis errors. This research was mostly dedicated to the first category of these sources of errors and particularly on the sources of errors caused by mechanical devices such as: accelerometers, suspension springs and stingers. A detailed literature survey indicated that the current approach used to resolve the problems which these mechanical errors cause is basically "*avoidance*" by choosing suitable test equipment so that the probable errors become minimal.

A new trend to deal with the problem of the mechanical errors is calculating the exact values of the FRFs by repeating the measurement in a number of different configuration; each configuration consisting of the structure with one or more of its boundary conditions changed . The main emphasis in this thesis was to use this trend in order to develop new methods which permit the acquisition of data of high quality and to devise methods to specify the accuracy of the measured data. However, further investigation showed that this new trend is applicable in other fields such as generation of rotational FRFs.

10.1.2 The effects of mechanical devices on the measured FRFs

i) Correction of the mass-loading effects of transducers

A new method was developed for the correction of the mass-loading effects of the transducers. It was shown that if an FRF measurement is repeated using another accelerometer with a different mass, the exact value of the FRF can be obtained using a series of straightforward calculations. Moreover, the driving point FRF at the point of the attachment of the accelerometer is obtainable through this process. The method was successfully applied to analytically-generated test cases and it was shown that, in the presence of noise, this calculation becomes more sensitive to noise when the masses of two accelerometers become closer together. Moreover, the method was successfully applied to experimental data from test on a free-free beam. Based on this approach, a new method was developed for estimating the exact natural frequencies of the structure. A comparison between the exact natural frequencies of the structure and those of the modified structure can show us the quality of the measurement. Moreover, it was shown that the calibration of the measurement set-up can be checked using the method presented for the correction of the mass-loading effects of transducers.

ii) Correction of the suspension effects in modal testing

A method similar to that developed for the correction of the mass-loading effects of the transducers was developed for the correction of the effects of the suspension springs on the measured FRFs. It was shown that for the simplest case where the test structure is suspended from one spring, the FRFs can be corrected if the structure is tested three times using different suspension springs with different stiffness in each test. Moreover, the driving point FRF of the point of the attachment of the spring can be obtained through the correction process. A numerical case study demonstrated the validity of the method. However, in the presence of noise, as the suspension springs become stiffer, the results of the presented correction method become more contaminated. The method was successfully applied to the experimental data from tests on a cantilever beam. Further, an approximate method was introduced to assess the quality of the measurement relating to

the effects of the suspension spring based on the changes in the natural frequencies of the structure.

iii) **The effects of stingers on measured FRFs**

It was proven that in a shaker test, the maximum error on the measured FRFs are associated with the antiresonances of the rotational driving point receptance of the tip of the stinger on the structure side. A new model was presented for the shaker-stinger-structure system in which the test structure was considered as a rigid body that moves in the transverse direction. This new model allowed us to assess the effect of misalignment of the stinger on its performance. It was shown that when there is a misalignment between two ends of the stinger, the antiresonances of the stinger shift to other frequencies and the measured FRFs are biased. As a result, a maximum allowable misalignment of the stinger was introduced based on the changes in the first elastic antiresonance of the stinger. The presented model was used for the calculations of the antiresonances of the shaker-stinger-structure system which was successfully validated by the experimental measurements made on a free-free beam. Based on this study a design procedure was introduced which followed by an example.

Moreover, it was shown that the effects of the stinger on the measured FRF can be checked by repeating the test with another stinger with the same diameter but slightly different length. A comparison between the measured FRFs using these two stingers shows the possible errors due to the antiresonances of the stinger.

10.1.3 **Correction in more than one DOF**

When a test structure is modified in more than one DOF, the measured FRFs can be corrected if the measurement is repeated in a number of different configurations; each configuration consisting of the system with one or more of its boundary conditions changed. Basically, two different approaches can be used for the correction of the effects of the mechanical devices on the test structure in more than one DOF, namely the step by step approach and the direct approach. In these approaches the driving point FRFs related to the degrees of freedom of the attachment of mechanical devices can be

computed without actually having to measure them. However, it was shown that the direct approach produces meaningless results if the matrix which is built based on the receptances of the attached objects is rank deficient.

This study provided a mathematical basis for the correction of the effects of the mechanical elements on the test structure in more than one DOF. However, in practice, applications of these methods are limited. The application of the methods presented in this part of the research was in chapter 9 where the test structure was modified by the mass and rotational inertia of an attached object in two DOFs in order to generate the rotational FRFs.

10.1.4 The effect of nonlinearity on the correction methods of the mechanical devices

The main assumption in the correction methods presented in this work is that the test structure and the attached elements exhibit linear behaviour. In practice, real structures are seldom linear. If the structure or the attached elements exhibits nonlinear behaviour, correction methods show different results using different sets of data corresponding to different configurations of the test structure. When a mechanical element is attached to a structure, the additional mass and/or stiffness of the attached element acts as a passive force. As a result, different mechanical elements produce different passive forces on the nonlinear structures and the results of the correction are different for these mechanical elements.

In practice, there are other sources of systematic errors, such as leakage and phase shift between the force or acceleration signal which may produce the same effects on the correction methods.

10.1.5 Generation of the whole translational FRFs from measurements of one column

When the number of DOFs is large, measuring the whole FRF matrix is difficult. As a result, the elements of one row or one column of the FRF matrix are measured and the

rest of the FRFs are synthesised from the measured ones using the identified modal properties. However, because of the limitation of the frequency range of the measurement, estimation of the unmeasured FRFs is not accurate. Evaluating the whole FRF matrix from measurement of some elements of the FRF matrix by modifying the structure at its boundaries can eliminate the problem of out of range modes. A method was developed to generate the all the translational FRFs using one accelerometer and one dummy mass.

The equations which include the effects of noise on the computed FRFs show that by increasing the mass of the accelerometer and that of the dummy mass, the effects of the noise on the computation of the FRFs decreases. A numerical case study proved the validity of the method. The method was successfully applied to the experimental data of a free-free beam. However, the level of noise was considerable at the frequency points out side the resonance regions.

10.1.6 Generation of the rotational FRFs by modifying the test structure

The aim of this part of the research was to eliminate the need of applying the moment excitation in order to generate rotational FRFs of the type displacement/moment and rotation/moment using the correction methods presented in this work. It was proven that in this procedure we still need to measure rotational responses. Therefore, Finite difference technique and correction methods were used to develop a method in order to generate the rotational FRFs related to two separate points on the structure.

The method was applied to an analytically-generated test case. The results were accurate around the resonances of the analytical model but there were some errors in parts of the frequency range due to the inaccuracy of the finite difference technique. In an actual test, there are some potential problems due to the limitations of the experiment and should be considered cautiously in the test. These problems are: selection of a suitable additive object, nodal points, nonlinearity and noise. Nevertheless, the method was successfully applied to experimental data for a free-free beam. The internal check of the generated FRFs demonstrated that the method is valid and applicable.

10.2 Recommended test strategy

It is usually prudent to carry out a preliminary limited modal test to help judge the quality of the modal test and assess the nature of the structure being tested. Based on the results of this preliminary test the measurement procedure can be planned. In the view of the experience gained during this course of this research, and of the case studies presented in this thesis, the following test strategy for the measurement with respect to the mechanical devices errors is recommended.

i) **Mass-loading effects of transducers on the measured FRFs**

Add an extra mass to the accelerometer and assess the quality of the measurement by estimating the exact natural frequencies of the modified structure as explained in chapter 3. For a mode of the structure, if there is an unacceptable difference between the measured natural frequency and the exact natural frequency of the structure, use the correction method presented in chapter 3 to cancel the effect of the accelerometer on the measured FRFs.

ii) **The effect of the suspension spring on the measured FRFs**

Double the stiffness of the suspension spring and assess the quality of the measurement by estimating the natural frequencies of the structure as explained in chapter 4. If the quality of the measurement is not acceptable, reduce the stiffness of the suspension spring or change the suspension point of the structure to another point or use the correction method presented in chapter 4.

iii) **The effect of the stingers on the measured FRFs**

Design the stinger based on the maximum input force and the minimum and maximum required measurement frequencies as was explained in chapter 5. Determine the maximum allowable deformation of the stinger Test the structure using the designed stinger considering the maximum allowable misalignment of the stinger. Check The quality of the measurement by repeating the measurement using a stinger with the same diameter but slightly different length.

iv) **The effects of the mechanical devices in more than one DOF**

When the test structure is modified in more than one DOF (which is usually the case in modal testing) the abovementioned test strategy for an individual mechanical device should be accomplished for all of the modified DOFs one by one. Clearly when the effect of a mechanical device on the measured FRFs at one DOF is reduced, the total quality of the measurement improves. It is not recommended to use correction methods for more than one DOF because as was shown in chapter 6 when the test structure is modified in two DOFs at least 7 different measurements with different configurations are needed to obtain the exact FRF. In practice, conducting this number of tests with different configurations is not efficient. Moreover, the effects of noise and other errors pollute the results of the correction due to the large number of the computation levels.

Instead, when the structure is affected unacceptably by suspension springs and an accelerometer in more than one DOF, we can reduce the effect of the suspension springs by using softer springs or changing the suspension points to the nodal points of the modes of interest and use the correction method to cancel the mass-loading effect of the accelerometer.

10.3 Summary of contributions of present work

A brief overview of contributions made in this thesis to the subject of ' High quality modal testing methods' is given here.

- A new idea to deal with mechanical errors was introduced and demonstrated using a simple example (section 1.9).

- A detailed literature survey was carried out and all the major sources of a lack of precision in the measurement process related to applied mechanical devices were presented in a consistent notation (chapter 2).

- The problem of the mass-loading effect of transducers was revisited using the SMURF method and a general solution for the correction of these mass-loading effects of the transducers was presented. Based on this method, a new approach for

assessing the quality of the measurement due to the mass-loading effect of the transducers was suggested (chapter 3).

- The method for the correction of the mass-loading effect of transducers was used to develop a new method to check the calibration of the measurement set-up (section 3-4).

- The problem of the suspension effects in modal testing was redefined using the SMURF method and a correction method was developed for this case. Moreover, the effect of noise on the computations was investigated (chapter 4).

- An approximate method was suggested to assess the quality of the measurement for the case that the test structure is affected by one suspension spring (section 4.4).

- A new model was introduced for the shaker-stinger-structure system. This model allowed us to assess the effect of the misalignment of the stinger on its performance (section 5.3).

- A maximum allowable deformation for the stingers was introduced to avoid of biasing the measured FRFs due to the deformation of the stinger (section 5.5).

- A new approach was introduced to assess the quality of the measurement due to the effects of a stinger on the measured FRFs (section 5.6).

- For the case that the test structure is modified in more than one DOF, two different approaches were suggested namely: step by step approach and direct approach. Moreover, it was shown that in direct approach the results can be meaningless due to the rank-deficiency problem (chapter 6).

- The effect of the nonlinearity on the correction methods of the mechanical devices was investigated and it was shown that the results of the correction changes by using different set of data corresponding to different configurations (chapter 7).

- Finite difference technique and the correction methods were applied for the generation of the rotational FRFs and elimination of the need to apply moment excitations (chapter 9).

10.4 Suggestions for future studies

Whereas extensive research work on improving the acquisition of data in high quality of modal testing has been carried out in this thesis, the study undertaken has revealed that some further development may still be necessary and of interest. Areas for possible further studies are summarised below:

- The correction methods can be investigated further to extend their applicability in conventional modal testing.

- The success of the correction methods depends on the level of experimental noise, and hence further developments of experimental equipment to reduce the level of noise are of considerable importance. Development of a smoothing technique to reduce the effect of experimental noise on the FRFs is required.

- Further investigation is necessary on the experimental determination of the displacements (rotational and translational) in other DOFs following the techniques suggested in present work on the experimental determination of rotational properties.

- The suggested correction methods allows us for the measurement of the modes which are normally outside the measurement range. Investigation is necessary on this topic to verify of potentially important out of range modes of the test structure.

- Another interesting topic to be investigated further relates to the determination of the modal properties of the structures possessing close modes. In this case, the close modes can be separated by modifying the test structure and then the measured FRFs can be corrected using correction methods suggested in the present work.

- The correction methods presented in this work can be investigated further to extend its applicability to the Multi-Input-Multi-output (MIMO) techniques.

10.5 Closure

The primary aim of this work was to improve the current measurement techniques and to develop new ones which permit the acquisition of data in high quality and to devise methods to specify the accuracy of the measured data in a conventional modal test. This was achieved by critical investigation of existing methods and by exploring new techniques and a recommended test strategy has been presented in this thesis.

A summary of conclusions and contributions showed the advances made in the measurement techniques. Not surprisingly, however, there is still scope for further study to improve the accuracy of the measured data.

Appendix A

The effects of mechanical devices on the test structure

Reminder of Nomenclature

α_{ij}^{*} measured receptance of a modified structure

α_{ii}' receptance of the attached mechanical element at DOF i

1. Introduction

In this appendix the SMURF method is used to analyse the general case of the modification of a test structure by mechanical devices. By mechanical devices we mean the extraneous objects which are attached to the test structure to conduct the modal test including suspension springs, transducers and stingers.

2. Modification of the test structure by mechanical devices

For the general case, a structure may be modified by addition of the mass and rotational inertia of an attached object, a linear spring or a rotational spring. The connection of these mechanical elements can be at any point on the structure and at any DOF (Three translational DOFs and three rotational DOFs). Figure 1 indicates a typical example of a structure which has been modified by mechanical elements. The boxes are the indications of the extraneous systems which can be an axial spring, a rotational spring, the mass property of an extraneous object , the rotational inertia property of an extraneous object or a combination of them. Only the receptances of the extraneous systems has been shown in the boxes. In Figure 1 numbers 1,2,3,4,5,6 and 7 refer to the number of modification DOFs.

In the system shown in Figure 1 structure C has been modified in the x direction at DOFs 1, 3, 4 and 6. The structure has been modified in the y direction at DOF 5 and in the z direction at DOF 2. At DOF 7, the structure has been modified rotationally in

the θ_y direction. It is important to note that although for example DOFs 5 and 6 are at the same point but they are different in direction. The structure is excited at DOF *l* in the *y* direction and the response is measured at DOF *k* in the *y* direction. We show displacements and rotations in all directions by *X* to derive the general form of the equation of a modified structure.
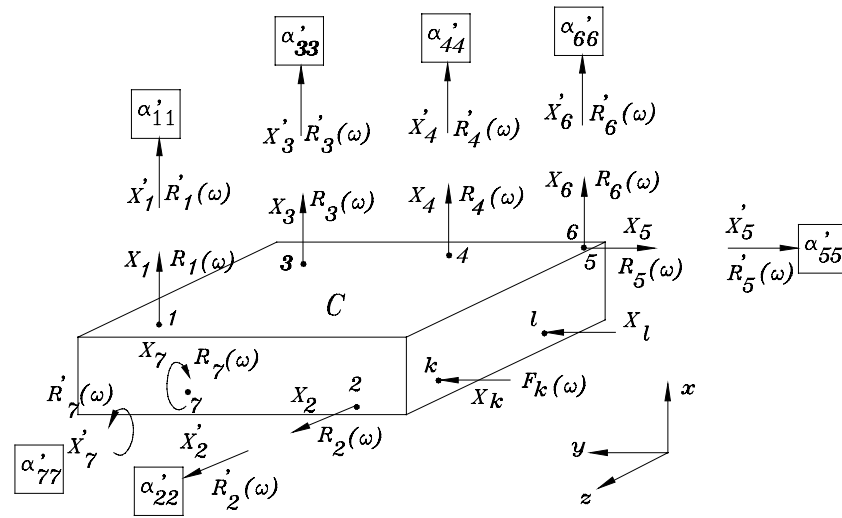
Figure 1. A typical example of a modified structure

As is usually the case in modal testing, the structure and the additional systems are presumed to be linear. For the general case, changes in a Frequency Response Function (FRF) of a structure due to addition of extraneous objects can be computed as follows :

The equations governing the modified system are :

$$
\begin{cases}
X_l = \alpha_{lk} F_k + \alpha_{l1} R_1 + \alpha_{l2} R_2 + \cdots + \alpha_{ln} R_n \\
X_1 = \alpha_{1k} F_k + \alpha_{11} R_1 + \alpha_{12} R_2 + \cdots + \alpha_{1n} R_n \\
X_2 = \alpha_{2k} F_k + \alpha_{21} R_1 + \alpha_{22} R_2 + \cdots + \alpha_{2n} R_n \\
\qquad \cdot \qquad\qquad\qquad \cdot \\
\qquad \cdot \qquad\qquad\qquad \cdot \\
\qquad \cdot \qquad\qquad\qquad \cdot \\
X_n = \alpha_{nk} F_k + \alpha_{n1} R_1 + \alpha_{n2} R_2 + \cdots + \alpha_{nn} R_n
\end{cases}
\qquad (1)
$$

The equations governing the additional systems are :

$$\begin{cases} X_1' = \alpha_{11}' R_1' \\ X_2' = \alpha_{22}' R_2' \\ \quad . \\ \quad . \\ \quad . \\ X_n' = \alpha_{nn}' R_n' \end{cases} \tag{2}$$

The constraining equations are :

$$\begin{cases} X_1' = x_1 \\ X_2' = x_2 \\ \quad . \\ \quad . \\ \quad . \\ X_n' = x_n \end{cases} , \quad \begin{cases} R_1' + R_1 = 0 \\ R_2' + R_2 = 0 \\ \quad . \\ \quad . \\ \quad . \\ R_n' + R_n = 0 \end{cases} \tag{3}$$

where X_1, X_2, …, X_n and X_1', X_2', …, X_n' are unknown displacements or rotations and R_1, R_2, …, R_n and R_1', R_2', …, R_n' are unknown reaction forces. From equations (2), (3) we have :

$$\begin{cases} X_1 = -\alpha_{11}' R_1 \\ X_2 = -\alpha_{22}' R_2 \\ \quad . \\ \quad . \\ \quad . \\ X_n = -\alpha_{nn}' R_n \end{cases} \tag{4}$$

Inserting equations (4) into equation (1) results in :

$$\begin{cases} X_l = \alpha_{lk} F_k + \alpha_{l1} R_1 + \alpha_{l2} R_2 + \cdots + \alpha_{ln} R_n \\ -\alpha'_{11} R_1 = \alpha_{1k} F_k + \alpha_{11} R_1 + \alpha_{12} R_2 + \cdots + \alpha_{1n} R_n \\ -\alpha'_{22} R_2 = \alpha_{2k} F_k + \alpha_{21} R_1 + \alpha_{22} R_2 + \cdots + \alpha_{2n} R_n \\ \qquad\qquad \cdot \qquad\qquad\qquad \cdot \\ \qquad\qquad\quad \cdot \qquad\qquad\qquad\quad \cdot \\ \qquad\qquad \cdot \qquad\qquad\qquad \cdot \\ -\alpha'_{nn} R_n = \alpha_{nk} F_k + \alpha_{n1} R_1 + \alpha_{n2} R_2 + \cdots + \alpha_{nn} R_n \end{cases} \tag{5}$$

or :

$$\begin{cases} X_l = \alpha_{lk} F_k + \alpha_{l1} R_1 + \alpha_{l2} R_2 + \cdots + \alpha_{ln} R_n \\ 0 = \alpha_{1k} F_k + (\alpha_{11} + \alpha'_{11}) R_1 + \alpha_{12} R_2 + \cdots + \alpha_{1n} R_n \\ 0 = \alpha_{2k} F_k + \alpha_{21} R_1 + (\alpha_{22} + \alpha'_{22}) R_2 + \cdots + \alpha_{2n} R_n \\ \qquad\qquad \cdot \qquad\qquad\qquad \cdot \\ \qquad\qquad \cdot \qquad\qquad\qquad \cdot \\ \qquad\qquad \cdot \qquad\qquad\qquad \cdot \\ 0 = \alpha_{nk} F_k + \alpha_{n1} R_1 + \alpha_{n2} R_2 + \cdots + (\alpha_{nn} + \alpha'_{nn}) R_n \end{cases} \tag{6}$$

Equation (6) can be written in matrix form as :

$$\begin{Bmatrix} X_l \\ 0 \\ 0 \\ \cdot \\ \cdot \\ \cdot \\ 0 \end{Bmatrix} = \begin{bmatrix} \alpha_{lk} & \alpha_{l1} & \alpha_{l2} & \cdot & \cdot & \cdot & \alpha_{ln} \\ \alpha_{1k} & \alpha_{11} + \alpha'_{11} & \alpha_{12} & \cdot & \cdot & \cdot & \alpha_{1n} \\ \alpha_{2k} & \alpha_{21} & \alpha_{22} + \alpha'_{22} & \cdot & \cdot & \cdot & \alpha_{2n} \\ \cdot & \cdot & \cdot & \cdot & & & \cdot \\ \cdot & \cdot & \cdot & & \cdot & & \cdot \\ \cdot & \cdot & \cdot & & & \cdot & \cdot \\ \alpha_{nk} & \alpha_{n1} & \alpha_{n2} & \cdot & \cdot & \cdot & \alpha_{nn} + \alpha'_{nn} \end{bmatrix} \begin{Bmatrix} F_k \\ R_1 \\ R_2 \\ \cdot \\ \cdot \\ \cdot \\ R_n \end{Bmatrix} \tag{7}$$

If matrix $[\alpha]$ is defined as :

$$[\alpha] = \begin{bmatrix} \alpha_{lk} & \alpha_{l1} & \alpha_{l2} & \cdot & \cdot & \cdot & \alpha_{ln} \\ \alpha_{1k} & \alpha_{11} + \alpha'_{11} & \alpha_{12} & \cdot & \cdot & \cdot & \alpha_{1n} \\ \alpha_{2k} & \alpha_{21} & \alpha_{22} + \alpha'_{22} & \cdot & \cdot & \cdot & \alpha_{2n} \\ \cdot & \cdot & \cdot & \cdot & & & \cdot \\ \cdot & \cdot & \cdot & & \cdot & & \cdot \\ \cdot & \cdot & \cdot & & & \cdot & \cdot \\ \alpha_{nk} & \alpha_{n1} & \alpha_{n2} & \cdot & \cdot & \cdot & \alpha_{nn} + \alpha'_{nn} \end{bmatrix} \tag{8}$$

then:

$$\begin{Bmatrix} X_l \\ 0 \\ 0 \\ \cdot \\ \cdot \\ \cdot \\ 0 \end{Bmatrix} = [\alpha] \begin{Bmatrix} F_k \\ R_1 \\ R_2 \\ \cdot \\ \cdot \\ \cdot \\ R_n \end{Bmatrix} \tag{9}$$

To find a relation between X_l and F_k, we have:

$$\begin{Bmatrix} F_k \\ R_1 \\ R_2 \\ \cdot \\ \cdot \\ \cdot \\ R_n \end{Bmatrix} = [\alpha]^{-1} \begin{Bmatrix} X_l \\ 0 \\ 0 \\ \cdot \\ \cdot \\ \cdot \\ 0 \end{Bmatrix} \tag{10}$$

The inverse of $[\alpha]$ is :

$$[\alpha]^{-1} = \frac{1}{|\alpha|} \begin{bmatrix} c_{11} & c_{12} & \cdot & \cdot & c_{1n} \\ c_{21} & c_{22} & \cdot & \cdot & c_{2n} \\ \cdot & \cdot & \cdot & \cdot & \cdot \\ \cdot & \cdot & \cdot & \cdot & \cdot \\ c_{n1} & c_{n2} & \cdot & \cdot & c_{nn} \end{bmatrix} \tag{11}$$

Inserting equation (11) in to (10) for the first row of the resulted equation we have:

$$\frac{c_{11}}{|\alpha|} X_l = F_k \tag{12}$$

or :

$$\frac{X_l}{F_k} = \frac{|\alpha|}{c_{11}} \tag{13}$$

$\dfrac{X_l}{F_k}$ is simply α_{lk}^{*}, which is the measured receptance when the structure is modified

by extraneous mechanical devices.

$$\alpha_{lk}^{*} = \frac{|\alpha|}{c_{11}} \tag{14}$$

or :

$$\alpha_{lk}^{*} = \frac{\begin{vmatrix} \alpha_{lk} & \alpha_{l1} & \alpha_{l2} & \cdot & \cdot & \alpha_{1n} \\ \alpha_{1k} & \alpha_{11}+\alpha_{11}' & \alpha_{12} & \cdot & \cdot & \alpha_{1n} \\ \alpha_{2k} & \alpha_{21} & \alpha_{22}+\alpha_{22}' & \cdot & \cdot & \alpha_{2n} \\ \cdot & \cdot & \cdot & \cdot & \cdot & \cdot \\ \cdot & \cdot & \cdot & \cdot & \cdot & \cdot \\ \alpha_{nk} & \alpha_{n1} & \alpha_{n2} & \cdot & \cdot & \alpha_{nn}+\alpha_{nn}' \end{vmatrix}}{\begin{vmatrix} \alpha_{11}+\alpha_{11}' & \alpha_{12} & \cdot & \cdot & \alpha_{1n} \\ \alpha_{21} & \alpha_{22}+\alpha_{22}' & \cdot & \cdot & \alpha_{2n} \\ \cdot & \cdot & \cdot & \cdot & \cdot \\ \cdot & \cdot & \cdot & \cdot & \cdot \\ \alpha_{n1} & \alpha_{n2} & \cdot & \cdot & \alpha_{nn}+\alpha_{nn}' \end{vmatrix}} \tag{15}$$

Equation (15) is the general equation for changes in the FRFs of a structure when it is modified with different mechanical elements connected at different DOFs to the structure.

As an example, when the structure is modified by two mechanical elements, Equation (15) is simplified as [Chapter 4]:

$$\alpha_{lk}^{*} = \alpha_{lk} - \frac{[\alpha_{2k}(\alpha_{11}+\alpha_{11}') - \alpha_{21}\alpha_{1k}]\alpha_{l2}}{(\alpha_{22}+\alpha_{22}')(\alpha_{11}+\alpha_{11}') - \alpha_{12}\alpha_{21}} + \frac{[\alpha_{2k}\alpha_{12} - \alpha_{1k}(\alpha_{22}+\alpha_{22}')]\alpha_{l1}}{(\alpha_{22}+\alpha_{22}')(\alpha_{11}+\alpha_{11}') - \alpha_{12}\alpha_{21}} \tag{16}$$

If these two extraneous elements are two masses the resulting equation is what was driven in chapter 8, and if these elements are the mass and inertia of a T block, the resulting equation is what was driven by Maia, Silva and Ribeiro in [37] using coupling/uncoupling techniques. In both cases the form of the equation is the same as equation (16). Therefore, what is important in this study is the form of the equation and not the type of the extraneous elements.

Appendix B

Estimation of the FRFs of a grounded structure

In chapter 6 it was shown that how the measured FRFs of a structure which is affected by mechanical devices can be corrected by modifying the structure at its boundaries. The solution to this correction method produce FRFs of the structure with free-free boundary condition. However, this solution can be applied for the estimation of other boundary conditions. In this appendix the method suggested in chapter 6 is developed to obtain the FRFs of the structure which is grounded at some of its degrees of freedom.

The example of section 6.3.2 of is considered here again. From equation (6-27) for a structure which is modified in two DOFs we have:

$$\alpha_{79} = x_7 - \frac{x_1 a_1 + x_2 a_2 + x_3 a_3}{x_4 a_1 + x_5 a_2 + x_6 a_3 + a_4} \tag{ 1 }$$

In which x's are unknowns and a's are known parameters.

Figure 1 shows a beam which has been grounded at DOF 3 (transverse direction) or in other words has been pinned at point A.
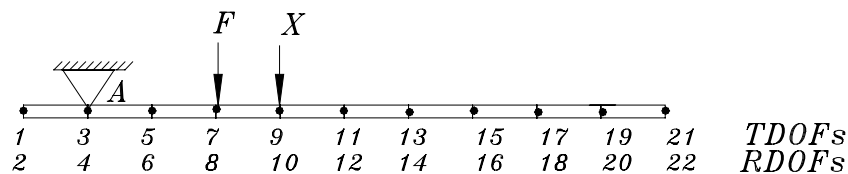
Figure 1. Computation of the FRFs of a pinned beam using correction method

(TDOFs = Translational Degrees of Freedom   , RDOFs = Rotational Degrees of Freedom)

When the receptance of the one of the extraneous elements in a DOF is zero it means that the structure does not have any motion in that DOF or it is grounded on that DOF. Conversely, when the receptance of one of the extraneous elements is ∞ (infinity) it means that the structure is free in that DOF. To ground DOF 3, while DOF 4 is free, the conditions are:

$$
\begin{cases}
\alpha'_{33} = 0 \\
\alpha'_{44} = \infty
\end{cases}
\tag{2}
$$

from equation (6-27) we had:

$$
\begin{cases}
a_1 = 1 \\
a_2 = \alpha'_{33} \\
a_3 = \alpha'_{44} \\
a_4 = \alpha'_{33}\alpha'_{44}
\end{cases}
\tag{3}
$$

Inserting (3) in (1), the result is :

$$
\alpha_{79} = x_7 - \frac{x_1 + x_2(\alpha'_{33}) + x_3(\alpha'_{44})}{x_4 + x_5(\alpha'_{33}) + x_6(\alpha'_{44}) + (\alpha'_{33}\alpha'_{44})}
\tag{4}
$$

Now if conditions (2) is applied in equation (4), we have:

$$
\alpha^{g}_{97} = x_7 - \frac{x_3}{x_6}
\tag{5}
$$

in which α^{g}_{97} refers to the FRF of grounded structure. Figure 2 shows the comparison of the exact FRF of the pinned beam which is computed by the elimination of the DOF 3 in the impedance matrix of the beam and the computed FRF using equation (5) and the answers to the equation (1) in chapter 6.
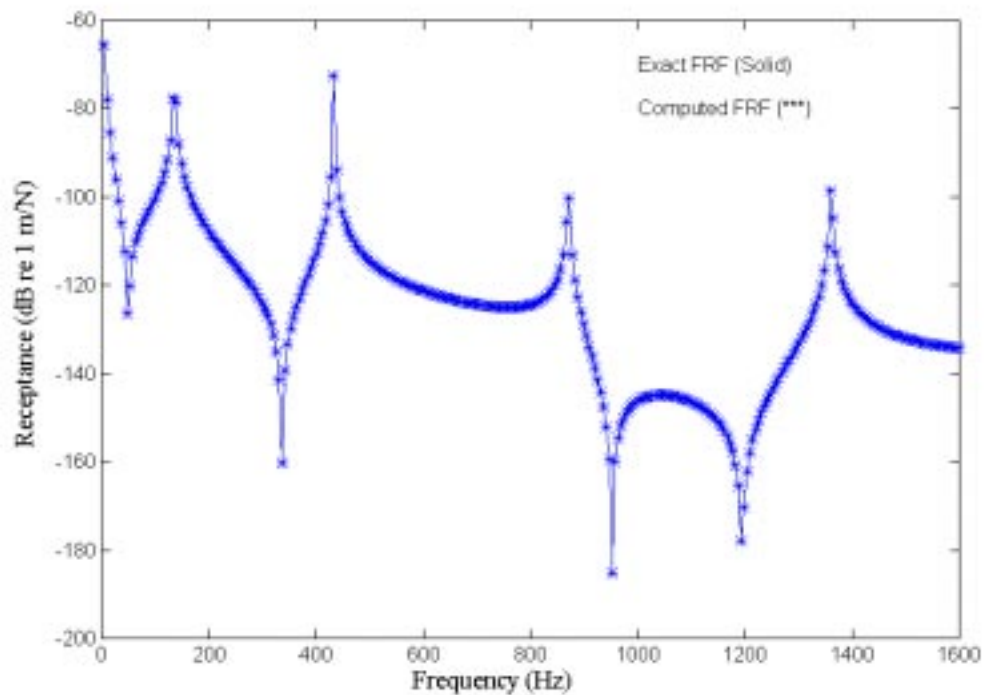
Figure 2. Comparison of the Computed FRF of the grounded
structure and the exact FRF

In this appendix, the correction method suggested in chapter 6 has been developed to produce grounded condition of a test structure by a series of different configurations of the test structure. The method is more reliable than conventional test of a grounded structure because the test structure with the unknown boundary conditions is replaced by a known boundary condition which does not contaminate the modal test results with fixture coupled modes or boundary condition uncertainties.

Matrix Properties

1. Matrix norms

The norm of a matrix is a function of the elements of that matrix which reflects the "size" of the matrix. The most common matrix norms are the Frobenious norms,

$$\|A\|_F = \left[\sum_{i=1}^{M} \sum_{j=1}^{N} |a_{ij}|^2 \right]^{1/2} \tag{1}$$

and

$$\|A\|_F^2 = \sigma_1^2 + \sigma_2^2 + \cdot \quad \cdot \quad \cdot + \sigma_n^2 \tag{2}$$

where σ_i are the singular values of $[A]$.

and the p-norms,

$$\|A\|_p = \sup_{x \neq 0} \frac{\|Ax\|_p}{\|x\|_p} \tag{3}$$

from where,

$$\|A\|_1 = \max_{j} \sum_{i=1}^{M} |a_{ij}| \tag{4}$$

$$\|A\|_\infty = \max_{i} \sum_{j=1}^{N} |a_{ij}| \tag{5}$$

and

$$\|A\|_2 = [\text{max. eigenvalue } [A]^T[A]]^{\frac{1}{2}} = \sigma_1 \tag{6}$$

An important property of the Frobenious norms is that they are invariant with respect to orthogonal transformations. Thus orthogonal transformations just rotate the original matrix without changing its norm.

2. **The rank of a matrix**

The rank of a matrix (r) is the number of linearly independent rows (and columns) in a given matrix. Some of the rank properties of a matrix are:

1. r is a positive integer;

2. when the rank of a square matrix is equal to its number of rows (or columns), then the matrix is non-singular i.e., its inverse exists and is said to have full rank

3. when a matrix is not square, the rank of that matrix equals or is less than the smaller of its number of rows or columns.

4. when the rank of a matrix is not zero, there is at least one square submatrix of that matrix having order of r (rank of the matrix) and is not singular.

2. The Singular Value Decomposition (SVD)

The SVD of an $m \times n$ real matrix [A] is expressed by:

$$[A]_{m\times n} = [U]_{m\times m}[\Sigma]_{m\times n}[V]^T_{n\times n} \tag{7}$$

where [U] and [V] are orthogonal matrices , i.e :

$$[U]^T[U] = [U][U]^T = [V]^T[V] = [V][V]^T = [I] \tag{8}$$

and

$$[U]^T = [U]^{-1} \quad \text{and} \quad [V]^T = [V]^{-1} \tag{9}$$

$[\Sigma]$ is a real matrix with elements $\sigma_{ij} = \sigma_i$ for $i=j$ and $\sigma_{ij} = 0$ for $i \neq j$. The values

σ_i are called singular values of matrix $[A]$. Singular values can be arrenged in decreasing order ($\sigma_1 > \sigma_2 > \cdots > \sigma_N$). Thus:

$$[\Sigma] = \begin{bmatrix} \sigma_1 & 0 & \cdot & 0 \\ 0 & \sigma_2 & \cdot & 0 \\ \cdot & \cdot & \cdot & \cdot \\ 0 & 0 & \cdot & \sigma_n \\ - & - & - & - \\ 0 & 0 & \cdot & 0 \end{bmatrix}_{m \times n} \tag{10}$$

The value of the rank is equal to the number of nonzero singular values. The advantage of using the SVD to calculate the rank is that if a row is not totally linearly dependent instead of zero a small value for the smallest singular value will be obtained and we have to compare this small value with the other singular values. A reasonable criterion for the acceptance or rejection of small singular values is to calculate the consecutive ratios of the singular values, σ_1 / σ_2, σ_2 / σ_3, $\ldots$, σ_{n-1} / σ_n If some of these ratios are very small compared with the others, they are not acceptable.

If $[A]$ is a complex matrix, then equation (7) becomes:

$$[A]_{m \times n} = [U]_{m \times m} [\Sigma]_{m \times n} [V]_{n \times n}^H \tag{11}$$

where the superscript H denotes complex conjugate (hermitian) transpose. Now $[U]$ and $[V]$ are unitary instead of orthogonal, i.e:

$$[U]^H [U] = [U][U]^H = [V]^H [V] = [V][V]^H = [I] \tag{12}$$

$$[U]^H = [U]^{-1} \quad \text{and} \quad [V]^H = [V]^{-1} \tag{13}$$

The singular values of a complex matrix, $[A]$, are the non-negative square-roots of the eigenvalues of the matrix $[A]^H [A]$ and are always real.

3. Condition Number

In general, matrices are not diagonal but using SVD, we have the product of two orthogonal matrices and a diagonal one. As orthogonal matrices preserve norm , the norm of a matrix will be the norm of matrix $[\Sigma]$ in the SVD. So, the matrix of the singular values can give us an indication about ill-conditioning. The ratio of $\sigma_{\min} / \sigma_{\max}$ is an indicator of potential computational problems. The condition number of a matrix is the ratio $\sigma_{\min} / \sigma_{\max}$. where $\sigma_{\max}$ is the largest singular value and $\sigma_{\min}$ is the smallest non-zero singular value of the matrix. A high condition number reflects an ill-conditioned matrix.

4. The Pseudo-inverse of a matrix

The matrix $[A]^+_{n \times m}$ is called pseudo-inverse of the matrix $[A]_{m \times n}$ if the following conditions are satisfied:

1. $[A][A]^+[A] = [A]$

2. $[A]^+[A][A]^+ = [A]^+$

3. $[A][A]^+$ is symmetric

4. $[A]^+[A]$ is symmetric

If $[A]$ is square and non-singular, then $[A]^+ = [A]^{-1}$. The pseudo-inverse is related to the least-square problem , as the value of $\{x\}$ that minimizes $\left\| [A]\{x\} - \{b\} \right\|^2$ in equation $[A]_{m \times n} \{x\}_{n \times 1} = \{b\}_{m \times 1}$. This can be given by $\{x\} = [A]^+ \{b\}$.

The ANSYS model of the stinger

/ The model of the stinger

/FILNAM,beam-b

/TITLE,Stinger

/prep7

/com M1 = mass of the structure

/com J1 = second moment of inertia of the structure

M1=10.5

J1=0

/com M2 = total mass of the shaker for non-axial vibrations

/com   of the stinger and the mass of the coil of the shaker

/com   for the axial vibration

/com J2 = second moment of inertia of the total mass of the shaker for

/com   non-axial vibrations of the stinger and second moment of inertia

/com   of the mass of the coil of the shaker for the axial vibration

M2=0.02

J2=0.001

/com K1 = Suspension stiffness of the structure

/com K2 = Suspension stiffness of the shaker

/com KT2 = Rotational suspension stiffness of the shaker

K1=850

K2=1400

KT2=0.469

/com L = lenght of the stinger

/com A = Cross sectional area of the stinger

/com I = Second moment of inertia of the stinger

/com h = height of the beam

L=.1

A=3.1416E-6

I=7.854E-13

h=.002

KAN,2

KAY,2,50

KAY,3,0

/com EX = modolus of elasticity of the stinger

/com DENS = Mass density of the stinger

ET,1,3

R,1,A,I,h

EX,1,210E9

DENS,1,7800

N,1,0,0,0

N,101,L,0,0

FILL

Appendix   D

243

```
N,102,L,0.3,0

N,103,0,0.3,0

N,104,0,0,0


REAL,1

E,1,2

EGEN,100,1,1


ET,5,21

 KEYOPT,5,3,3

 KEYOPT,5,2,0

 R,8,M1,J1

 TYPE,5

 REAL,8

 E,101


ET,6,21

 KEYOPT,6,3,3

 R,9,M2,J2

 TYPE,6

 REAL,9

 E,1


ET,2,14

 KEYOPT,2,3,2

 R,2,K1
```

```
TYPE,2

REAL,2

E,101,102


R,3,K2

TYPE,2

REAL,3

E,1,103


ET,7,14

KEYOPT,7,2,6

R,4,KT1

TYPE,7

REAL,4

E,1,104


F,101,MZ,1.25


D,103,ALL,0

D,102,ALL,0

D,104,ALL,0


TOTAL,200

ITER,1,1,1

FINISH
```

References

[1] Blevins, R. D. : *"Formulas for Natural Frequency and Mode Shape"*. Van Nostrand Reinfold Company, 1979.

[2] Cook, R. D. : *"Concepts and Applications of Finite Element Analysis"* John Wiley and Sons, 2nd edition, 1981.

[3] Bathe, K-L : *"Finite Element Procedures in Engineering Analysis"* Prentice-Hall, 1982.

[4] Zienkiewicz, O. C. and Taylor, R. L. : *"The Finite Element Method"* MacGraw-Hill 4th edition, 1986.

[5] Ewins, D.J., : *"Modal Testing : Theory and Practice"*. John Willey & Sons, London, 1984.

[6] Ewins, D.J. : *"State-of-the-Art Assessment of mobility Measurement Techniques (SAMM)"*. Journal of Soc. Env. Engrs., pages 1-11, March 1981.

[7] Ewins, D.J. and Imergun, M. : "*State-of-the-Art Assessment of Structural Dynamic Response Analysis Methods (DYNAS)",* Shock and Vibration Bulletin, 56(1), August 1986.

[8] Harwood N. : *"Quality Assurance In Dynamic Testing"*. Proceeding of the !5th Seminar on Modal analysis Leuven, Sep. 1990.

[9] Jung, H. and Ewins, D.J. : *"On the Use of Simulated "Experimental" Data for Evaluation of Modal Analysis Methods"* . Proceeding of the 10th International Modal Analysis Conference, pages 421-429,1992.

[10] Marudachalam, Kannan and Whicks, A.L. :"*An Attempt to Quantify the Errors in the Experimental Modal Analysis Process"*. Proceeding of the 9th International Modal Analysis Conference, pages 1522-1527,1991.

[11] Mitchell, L. D and Randolph, L. S. : *"Modal Tests Methods : Quality, Quantity, and Unobtainable"* NAFEMS, International Conference Structural Dynamics Modelling Test, Analysis and Correlation.

[12] Mitchell, L. D. and Elliot, K. B., : *"Structural Modification Utilizing Beam Elements"*. Proceedings of the International Modal Analysis conference V, IMAC-V, Volume II, Imperial College of Science and Technology, London, England, pp. 956-959, April 6-9, 1987.

[13] Mitchell, L. D. and Elliot, K. B. : *"The effect of Modal Truncation on Modal Modification"*. Proceeding of the International Modal Analysis Conference V, IMAC-V, Volume I, Imperial College of Science and Technology, London, England, pp. 72-78, April 6-9, 1987.

[14] Mitchell, L. D. and LUK Y. W., : *"Implementation of the Dual Modal Space Structural Modification Method"*. Proceeding of the International Modal Analysis Conference II, IMAC II, Orlando, Florida, Published by Union College, Schenectady, NY, PP. 930-936, February 6-9,1984.

[15] DTA Handbook, *"Attachment of Excitation Device : Drive rods"*. ITEM 32.3 M, pp.1-6, 11 Oct, 1994.

[16] Mitchell, L. D.,and Elliott, K. B., : *"How to Design Stingers for Vibration Testing of Structures"*. Sounds and Vibration, pp.14-18, April 1984.

[17] Mitchell, L. D.,and Elliott, K. B., : *"A Method for Designing Stingers for Use in Mobility Testing"*. Proceedings of the 2nd International Modal Analysis Conference, pp. 872-876, 1984.

[18] Hieber, G. M., : *"Non-Toxic Stingers"*. Proceedings of the 6th International Modal Analysis Conference, pp. 1371-1379, 1984.

[19] Chiang Lee, J. and Fang Chou, Y., : *"The Effects of Stingers on Modal Testing"*. Proceedings of the 11th International Modal Analysis Conference, pp. 293-*299*, 1993.

[20] Chiang Lee, J. and Fang Chou, Y., : *"The Effects of Stingers on Recptance Function Measurement"*. Transactions of the ASME, pp. 220-226.

[21] McConnell, K. G., Zander, E., Dong, J. and Thekentattil, S., : *"Effect of Stinger Stiffness on Measured Accelerance"* . Proceedings of the 15th International Modal Analysis Conference, pp. 672-678 , 1997.

[22] Anderson, I.A., : *"Avoiding Stinger Rod Resonance Effects on Small Structures"*. Proceedings of the 8th International Modal Analysis Conference, pp. 673-678, 1990.

[23] Billhart, R. D. & Hunt, D. L. & Pierre, M. S. : *"Advantages of Excitation Using Plastic Stinger Rods"*. Proceedings of the 11th International Modal Analysis Conference, pp. 1217-1220, 1993.

[24] Han, S., : *"Analysis on Natural Frequency Distortion Due to the Attachment of Shaker"*. Proceedings of the 13th International Modal Analysis Conference, pp. 1715-1721, 1995.

[25] Vandepitte, D. V. ,Olbrechts, T. and Sas, P. : *"FRF Measurements Errors Caused by The Use of Inertia Mass Shaker"*. Proceedings of the 15th International Modal Analysis Conference, pp. 188-194 , 1997.

[26] McConnell, K. G. and Hu, X. : *"Stinger mass compensation Part One : Theoretical study & Part Two : Experimental Investigation"*. Modal Analysis: the International Journal of Analytical and Experimental Modal Analysis, V8 & n1, p. 35-44, p. 45-54, Jan 1993.

[27] McConnell, K. G. and Hu, X. : *"An Advanced Model for Stinger Force, Motion and Energy Transmissibilities"*. Modal Analysis: the International Journal of Analytical and Experimental Modal Analysis, V7 & n4, p. 271-283, Oct 1992.

[28] Olsen, N. L., *"Using and Understanding Electrodynamic Shakers in Modal Application"*. Proceedings of the 4th International Modal Analysis Conference, pp. 1160-1167 , 1986.

[29] Peterson, E. L., Mouch, T. A., and Rusen, W. M., : *"Modal Excitation : Force Drop-Off at Resonances".* Proceedings of the 8th International Modal Analysis Conference, pp. 1226-1231 , 1990.

[30] Rao, D. K., *"Electrodynamic Interaction Between a Resonating Structure and an Exciter"* . Proceedings of the 5th International Modal Analysis Conference, pp. 1142-1150 , 1987.

[31] Tomlinson, G. R., *"A Simple Theoretical and Experimental Study of the Force Characteristics from Electrodynamic Exciters on Linear and Non-linear Systems".* Proceedings of the 8th International Modal Analysis Conference, pp. 1479-1486 , 1987.

[32] Synder, V. W., : *"Structural Modifications and Modal Analysis".* Proceedings for Experimental Stress Analysis, 1983.

[33] Avitabile, P. and O'Callahan, J., : *"Understanding Truncation Effects in Structural Dynamic Modification".* Sound and Vibration, June 1990**.**

[34] Ole Dossing, : *"Prediction of Transducer Mass-Loading Effects and Identification of Dynamic Mass".* Proceedings of the 9th International Modal Analysis Conference, pp. 306-312 , 1991.

[35] Decker, J. and Witfeid, H : *"Correction of Transducer-Loading Effects in Experimental Modal Analysis"* . Proceedings of the 13th International Modal Analysis Conference, pp. 1604-1608 , 1995.

[36] Silva, J. M. M., Maia, N. M. M. and Ribeiro, A. M. R., : *"Some Applications of Coupling/Uncoupling Techniques in Structural Dynamics, Part 1 : Solving the Mass Cancellation Problem"* . Proceedings of the 15th International Modal Analysis Conference, pp. 1431-1439 , 1997.

[37] Silva, J. M. M., Maia, N. M. M. and Ribeiro, A. M. R., : *"Some Applications of Coupling/Uncoupling Techniques in Structural Dynamics, Part 1 : Generation of the Whole FRF Matrix from measurements on a Single Column-The Mass Uncoupling*

Method (MUM)" . Proceedings of the 15th International Modal Analysis Conference, pp. 1440-1452 , 1997.

[38] Bisplinghoff, R. L., Ashley, H., & Halfman, R.L., *"Elasticity",* Addison-Wsley Publishing Company, Inc., Cambridge, MA, pp. 771-779.

[39] Strutt, J. W. (Lord Ryleigh), *"The Theory of Sound"* Vol.1, 2nd ed., Dover Publications, Inc., Newyork, 1945.

[40] Wolf Jr., J.A., *"The Influence of Mounting Stiffness on Frequencies Measured in a Vibration Test",* SAE Paper 840480, Society of Automotive Engineers, 1984.

[41] Carne, G.T., & Dohrmann, C. R., : *"Support Conditions, Their Effect on Measured Modal Parameters"* Proceedings of the 16th International Modal Analysis Conference, pp. 477-483 , 1998.

[42] Lindholm,B. E. and West, R. L. : *"Determination of Suspension Effects by Direct Experiments and Comparisons to an Analytical Model"* . Proceedings of the 12th International Modal Analysis Conference, pp. 262-268 , 1994.

[43] Simley, R. G. and Brinkman, B. A. : *"Rotational Degrees-of-Freedom in Structural Modification".* Proceedings of the 2th International Modal Analysis Conference, pp. 937-939 , 1984.

[44] Wade, B., Kuo, C., Glaser, R : *"Extension of Ground-Based Testing for Large Space Structures",* Journal of Spacecraft and Rockets, Vol. 23, No. 2, pp. 184-188, 1986.

[45] Wade, B.,Kuo, C., Glaser, R., : *"Multiple Boundary Condition Test (PBC) Approach to Update Mathematical Models of Large Flexible Structures".* SAE Paper 851933, Oct 14-17,1985.

[46] Kuo, C., Wade, B. : *"More About Multiple-Boundary-Condition Testing"*, Nasa Tech Brief, Vol. 14, NO 1, Item 16,JPL Invention Report NPO-17574/7082, January, 1990.

[47] Glaser, R., Kuo, C., Wade, B., : *"Improvement of Structural Models Using Covariance Analysis and Nonlinear Generalised Least Squares",* AIAA Journal, Vol. 30, No. 1, pp. 226-233, 1992.

[48] Anderson, J. B. & Coleman, A. D. & Driskill, T. C. & Brown, D. L., : *"A Mass Additive Technique for Modal Testing as Applied to the Space Shuttle Atro-1 Payload"* . Proceedings of the 6th International Modal Analysis Conference, pp. 154-159 , 1988.

[49] Gwinn, K., Lauffer, J.and Miller, A. : *"Component Mode Synthesis Using Experimental Modes Enhanced by Mass Loading"* . Proceedings of the 6th International Modal Analysis Conference, pp. 1088-1093 , 1988.

[50] Lammens, S., Sas, P., Brown, D. L. : "Model Updating and Perturbed Boundary Condition Testing", Proceedings of the 17th International Seminar on Modal Analysis, 1992.

[51] Chen, K. N., Brown, D. L., Nicolas, V. T., : *"Perturbed Boundary Condition Model Updating"* . Proceedings of the 11th International Modal Analysis Conference, 1993.

[52] Barney, P., Pierre, M. S., Brown, D. L., : *"Identification of a Modal Model Utilizing a Perturbed Boundary Condition Test Method"* . Proceedings of the 10th International Modal Analysis Conference, pp. 1221-1231 , 1992.

[53] Li, S., Brown, D. and Vold, H., : *"Using the Scaled Total Least Squares Method and Unified Matrix Polynomial Approach for Condensing the Perturbed Boundary Condition Test Data".* Proceedings of the 13th International Modal Analysis Conference, 1995.

[54] Anonymous, Kistler Piezo-Instrumentation, Catalog K2.006, Kistler Instrument Corp., Amherst, NY, p.46, September 1989.

[55] Sainsbury, M. G., : *"Vibration Analysis of Damped Complex Structures"*. PhD Thesis, Imperial College, University of London, 1976.

[56] Silva, J. M. M. : *"Measurement and Applications of Structural Mobility Data for the Vibration Analysis of Complex Structures"* . PhD Thesis, Imperial College, University of London, 1987.

[57] Ewins, D.J. and Sainsbury, M.G. : *"Mobility Measurements for the vibration Analysis of Connected Structures"* Shock and Vibration Bulletin, 42(1), pp.105-122, 1972.

[58] Gleeson, P.T. : *"Identification of Spatial Models"*. PhD Thesis, Imperial College, University of London, 1979.

[59] Skingle, G. W., : *"Structural Dynamic Modification Using Experimental Data"* PhD Thesis, Imperial College, University of London, 1989.

[60] Urgeria, A.P.V., : *"Dynamic Analysis of Coupled Structures Using Experimental Data"*. PhD Thesis, Imperial College, University of London, 1989.

[61] Chen, W. H. ; Cherg, J. S. : *"Modal Synthesis Via Combined Experimental and Finite Element Techniques with Consideration of Rotational Effects"*. Journal of Sound and Vibration, vol 103 (1), 1985.

[62] Sattinger, S.S., : *"A method for Experimentally Determining Rotational Mobilities of Structures"* . Shock and Vibration Bulletin, 50 (1), 1980.

[63] Smiley, R. G. and Brinkman, B. A., : *"Rotational Degrees-of-Freedom in Structural Modification"*. Proceedings of the 2nd International Modal Analysis Conference, pp. 937-939, 1984.

[64] Liorca, F; Gerard, A. and Brenot, D., : *"Improving Interface Conditions in Modal Synthesis Methods. Application to a Bolted Assembly of Rectangular Plates"*. Proceedings of the 12th International Modal Analysis Conference, pp. 411-417, 1994.

[65] O'Callahan, J. C. ; Lieu, I. W. and Chou, C. M. : *"Determination of Rotational Degrees-of-Freedom for Moment Transfers in Structural Modification".* Proceedings of the 3rd International Modal Analysis Conference, pp. 465-470, 1985.

[66] Williams, E. J. and Green, J. S., : *"A Spatial Curve Fitting Technique for Estimation of Rotational Degrees of Freedom".* Proceedings of the 8th International Modal Analysis Conference, pp. 376-381, 1990.

[67] Haisty, B. S., and Springer, W. T., : *"A Simplified Method for Extracting Rotational Degrees-of-Freedom Information from Modal Test Data"* IJAEMA, 1(3), pp. 35-39 (1986).

[68] Ng' andu, A. N., FOX, C. H. J. and Williams, E. J., : *"On the Estimation of Rotational Degrees-of Freedom Using Spline Functions"* . Proceedings of the 13th International Modal Analysis Conference, pp. 791-797, 1995.

[69] Leschiutta, M., Eng, J. A. and Martin, J. K., : *"Dynamic Piston Measurements Using a Laser Range-Finding Technique".* SAE Technical Paper Series, No. 900482, 1990.

[70] wang, W. and Bush-Vishniac, I., *"Four Dimensional Non-contacting Sensing System for Micro-Automation Machines"* . ASME Paper no.90-WA/DSC-23A., 1990.

[71] Cafeo, J. A., Trethewey, M. W., Rieker, J. R. and Sommer, H. J., : "Application of a Three Degree of Freedom Laser Vibrometer for Experimental Modal Analysis" . Proceedings of the 9th International Modal Analysis Conference, pp. 1161-1167, 1991.

[72] Bokelberg, E. H., Sommer, H. J., and Trethewey, M. W., : *"A Six-Degree-of-Freedom Laser Vibrometer. Part I : Theoretical Development & Part II : Experimental Validation"* . Journal of Sound and Vibration 178(5), pp. 643-654, 1994.

[73] Huffaker, R. M., "*Laser Doppler Detection Systems for Gas Velocity Measurement*", Applied Optics, Vol.9, No.5,May 1970.

[74] Donavan, J. B., "*Three-Dimensional Vibrometry via Three Positions of a One-Dimentional Laser Doppler Velocimeter",* Master Thesis, Virginia Polytechnic Institute and State University, Blacksburg, VA, 1991.

[75] Mitchell, L. D. and Abel, J. J., : "*Extraction of In-Plane Velocities Using Laser Doppler Velocimetry*" . Proceedings of the 11th International Modal Analysis Conference, pp. 402-408, 1993.

[76] Mitchell, L. D., and Galaitsis, G. S., : "*Extraction of Drilling-Angular Velocities Using a Nodal-Spatial Array of In-Plane, Translational Laser-Derived Velocities*". ……pp.735-741.

[77] Kochersberger, K., Mitchell, L. D., and Wicks, A. L., : "*Structural Angular Velocity Extraction Using DFT/IDFT Techniques*" . Proceedings of the 9th International Modal Analysis Conference, pp. 657-663, 1991.

[78] Sun, F. P., and Mitchell, L. D., "*Two-Dimensional Velocity Data Smoothing and Structural Angular Velocity Extraction Using a DFT-IDFT Technique*" . Proceedings of the 13th Biennial ASME Conference on Mechanical Vibration and Noise, pp. 303-309, 1991.

[79] Lindoholm, B. E., : "*Three-Dimensional Position Registration of a Scanning Laser-Doppler Vibrometer*" .

[80] Stanbridge, A. B., and Ewins, D. J., : "*Using a Continuously-Scanning Laser Doppler Vibrometer for Modal Testing*" . Proceedings of the 14th International Modal Analysis Conference, 1996.

[81] Stanbridge, A. B., and Ewins, D. J., : "*Modal Testing of Rotating Discs Using a Scanning LDV*" . Proc. ASME Design Engineering Technical Conference, Boston, DE- Vol. 84-2, Vol.3B.

[82] Stanbridge, A. B., and Ewins, D. J., : *"Structural Modal Analysis Using a Scanning Laser Doppler Vibrometer"* . R. Ae. Soc. Forum on Aeroelasticity and Structural Dynamics, Manchester, 1995.

[83] Stanbridge, A. B., and Ewins, D. J., : *"Measurement of Total Vibration at a Point Using a Conical-Scanning LDV"* . Proc. of ANCONA, 1996.

[84] Bendat, J. S., and Piersol, A. G., : *"Random Data : Analysis and Measurement Procedures"* . Jhon Wiley and Sons, Wiley-Interscience, NewYork, NY,pp. 408-409, 1986.

[85] Mitchell, L. D., *"Improved Methods for the Fast Fourier Transform (FFT) Calculation of the Frequency Response Function"* . Journal of Mechanical Design, Transactions of the ASME, pp. 277-279, Vol. 104, April 1982.

[86] Wicks, A. L., and Vold, H., : *"The H_s Frequency Response Function Estimator"* . Proceedings of the 4th International Modal Analysis Conference, 1986.

[87] Wicks, A. L., and Mitchell, L. D., : *"Methods for Estimation of Frequency Response Functions in the Presence of Uncorrelated Noise, A Review"*. International Journal of Analytical and Experimental Modal Analysis, Vol. 2, No.3, pp. 109-112, July 1987.

[88] Wicks, A. L., and Shapton, W. S., *"A Comparison of H_1 and H_2 Frequency Response Functions"* . Society of Experimental Mechanics, Fall Annual Meeting, Milwaukee, WI, November 1984.

[89] Vold, H., Rocklin, G. T., and Crowly, J., *"A comparison of H_1, H_2, H_v Frequency Response Functions"* . International Modal Analysis Conference Proceedings, Orlando,FL, pp. 272-278, November 1984.

[90] Goyder, H. G. D., *"Foolproof Methods for Frequency Response Measurement"* . Proceedings of the Second International Conference on Recent Advances in Structural Dynamics, Southampton, England, 1984.

[91] Cobb, R. E., and Mitchell, L. D., *"Estimates of Variance and Confidence Bands for the three-Channel Frequency Response Function Estimator"* . international Journal of Analytical and Experimental Modal Analysis, Vol. 5., No.3,pp. 185-194, July 1990.

[92] Cobb, R. E., and Mitchell, L. D., *"Estimation of Uncorrelated Content in Experimentally Measured Frequency Response Functions Using Three Measurement Channels"* . Mechanical Systems and Signal Processing, Vol. 4, No.6, pp. 449-461, Nov.-Dec., 1990.

[93] Ashory, M. R. : " *Correction of Mass Loading Effects of Transducers and Suspension Effects in Modal Testing"* Proceeding of the 16th International Modal Analysis Conference, pp. 815-828, 1998.

[94] McConnell, G. M., : *"Vibration Testing : Theory and Practice"* JhonWiley & Sons, Inc., 1995.

[95] Klosterman, A. : *"On the Experimental Determination and Use of Modal Representations of Dynamic Characteristics".* PhD Dissertation, University of Cincinnati, 1971.

[96] Bishop, R. E. D. and Johnson, D. C. : *"The Mechanics of Vibration".* Cambridge at the University Press, 1960.

[97] Blevins, R. : *"Formulas for natural frequency and mode shape"* Krieger Publishing Company, Malabar, Florida.

[98] Fraleigh, J. B. and Beauregard, R. A. : *"Linear Algebra".* Addison-Wesely Publishing Company, 1995.

[99] McConnell, K. G. and Hu, X. : *"Why do Large FRF Errors Result from Small Relative Phase Shifts When Using Force Transducer Mass Compensation Methods?"* Proceedings of the 11th International Modal Analysis Conference, pp. 845-849 , 1993.

[100] Ashory, M. R. and D. J. Ewins : *"Generation of the Whole FRF Matrix from Measurements on One Column "* Proceeding of the 16th International Modal Analysis Conference, pp. 800-814, 1998.

[101] Silva, J. M. M., Maia, N. M. M. and Ribeiro, A. M. R., : *"Some Applications of Coupling/Uncoupling Techniques in Structural Dynamics, Part III : Estimation of Rotational Frequency Response Functions Using MUM)"* . Proceedings of the 15th International Modal Analysis Conference, pp. 1453-1462 , 1997.

[102] Duarte, M. L. M., : *"Experimentally-Derived Structural Models for Use in Further Dynamic Analysis"* PhD Thesis, Imperial College, University of London, 1996.